



UNIVERSITY OF  
BIRMINGHAM

THE PHASE BEHAVIOUR, FLOW BEHAVIOUR, AND  
INTERFACIAL PROPERTIES OF PROTEIN-  
POLYSACCHARIDE AQUEOUS TWO-PHASE SYSTEMS  
WITH SUGAR

by

ASJA PÖRTSCH

A thesis submitted to  
The University of Birmingham  
for the degree of  
DOCTOR OF PHILOSOPHY

School of Chemical Engineering  
College of Engineering and Physical Sciences  
The University of Birmingham

October 2011

UNIVERSITY OF  
BIRMINGHAM

**University of Birmingham Research Archive**

**e-theses repository**

This unpublished thesis/dissertation is copyright of the author and/or third parties. The intellectual property rights of the author or third parties in respect of this work are as defined by The Copyright Designs and Patents Act 1988 or as modified by any successor legislation.

Any use made of information contained in this thesis/dissertation must be in accordance with that legislation and must be properly acknowledged. Further distribution or reproduction in any format is prohibited without the permission of the copyright holder.

## **Abstract**

Aqueous two-phase systems (ATPS) with biopolymers (i.e., proteins and polysaccharides) and sugars give texture and taste to many dairy-emulsion-based convenience foods. Proteins and polysaccharides readily phase separate due to their thermodynamic incompatibility. The biopolymers are affected by sugars, which change their functionality, as well as the solvent quality. Accordingly, the aim of this work is to better understand the importance of most common types of sugars on the solubility of biopolymers, their microstructure, and their flow properties.

Model sodium caseinate-galactomannan aqueous two-phase systems (NaCAS-GM ATPS) differing in GM-type (locust bean gum (LBG), tara gum (TG), guar gum (GG), fenugreek gum (FG)) and added sugar (trehalose, sucrose, glucose and fructose) were studied using the phase-volume ratio method, rheoptics, and the droplet retraction method on phase equilibria, flow behaviour, and interfacial properties, respectively, at pH 5.8 and various temperatures.

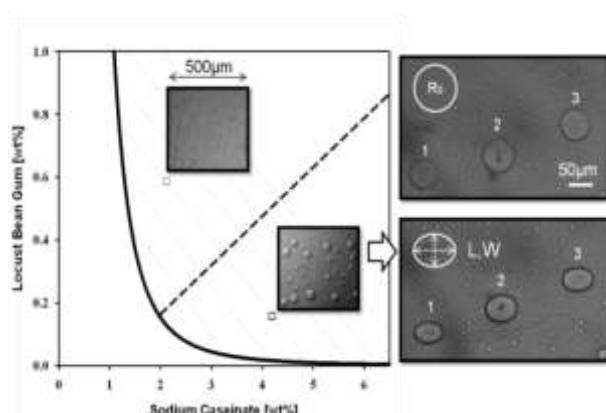
The results revealed that the microstructure of the ATPS depends on the composition of the equilibrium phases (concentration and type of sugar/GM), the physical properties of the phases (viscosity  $\eta$  and interfacial tension  $\sigma$ ), and shear. Sugar (i.e., sucrose) added in concentrations of between 5 and 40 wt% increased cosolubility/mixing of the biopolymers and decreased  $\sigma$  between the equilibrium phases that are rich on either of the biopolymers (NaCAS-rich and GM-rich phases). Sugar concentrations  $> 40$  wt% decreased cosolubility. In polysaccharide-continuous ATPS, the occurrence of a shear-induced phase inversion event was observed at  $< 20$  wt% sugar. A further increase in sugar concentration ( $>20$  wt%) was found to suppress this phenomenon due to decreased viscosity ratio and the formation of thread-like structures in flow. Based on the mannose : galactose ratio of GM and type of sugar (added at a

concentration of 15 wt%) the best cosolubility and corresponding smallest  $\sigma$  was attributed to FG and trehalose, respectively.

This work demonstrates the importance of the steric molecular structures of sugars and GMs as well as of concentration on their solubility in an aqueous medium. Trehalose and fructose, sugars that form the highest number of hydrogen bonds with water molecules, are capable of structuring water, improving biopolymer cosolubility in ATPS, and reducing  $\sigma$  between equilibrium phases in the ATPS to a greater extent than glucose/sucrose. A similar effect is observed when GMs with the highest degree of branching (i.e., GG/FG) are present. Consequently, the ATPS with the abovementioned components are stable over a wider range of biopolymer concentrations compared with ATPS with glucose/sucrose and less-branched GMs (i.e., LBG/TG). Sugars, at constant biopolymer concentration, when added in a large quantity significantly influence the microstructure of the biopolymer systems, especially under flow, as they preferentially bind water and cause a significant increase in overall viscosity of the ATPS.

**Keywords:** *phase equilibria; microstructure; viscometry; phase inversion; interfacial tension; galactomannans; sodium caseinate; sugars.*

#### Graphic abstract:



The figure shows a phase diagram of a sodium caseinate-locust bean gum system on which light micrographs of the protein-continuous and polysaccharide-continuous systems are also shown. The protein-continuous systems are shown in quiescent conditions and under shear.  $R_0$  is the radius of a relaxed droplet,  $L$  is the length of a deformed droplet, and  $W$  is its width.

## **Acknowledgements**

I am very grateful to Professor Ian Norton and Dr. Fotis Spyropoulos for their supervision and guidance throughout this project. I could not have completed it without their support.

I would also like to thank Unilever for generously sponsoring my project, DMV International, Emerald Seeds and Cargill for kindly providing me with the ingredients for my experiments, and the University of Birmingham for allowing me to use the facilities and equipments. I am also grateful to Professor Bettina Wolf and Dr. Valeriy Grinberg for sending their papers relevant to my project.

A heartfelt thank you is also due to researchers, administrators, technicians and organisers of workshop at the University of Birmingham, in particular in the Department of Chemical Engineering. A special thanks goes to: Professor Andrzej W. Pacek and Ourania Gouseti for the use of an optical rheometer. Dr. Adi Utomo for the help on this thesis. Dr. Karin Mehauden-Ural and Dr. Roman Pichot for their help during my PhD. I also thank Steven Hall for proofreading a draft of this thesis.

I would also like to thank the following colleagues for making my life in the lab enjoyable: Aleksandra Pawlik, Sarah Frash-Melnik, Fideline Tchienbou-Magaia, Naeema Abdulrahman, Monica Jaime-Fonseca, Alex Heuer, Sala Odeen, Angel Fernandez, Ricardo Roque, Yan Sim Lee, Nima Niknafs, and Andrea Gabriele.

I am also grateful to my family and friends, in particular my parents Vislava Potočnik and Johann Pörtsch, my grandmother Marija, my aunts Klara, Zvonka and Zdenka Truden, as well as my husband Yujin Nagasawa and his parents Yoko and Yonosuke Nagasawa for their loving support, care and patience. This thesis is dedicated to all of you.

*To my family with love*

# Nomenclature

## Annotations

$D_{self}$	Self diffusion coefficient $D_{self} = kT/6\pi\eta_c R_h$ , [m <sup>2</sup> /s], $D_{self}(H_2O) = 3.2 \times 10^{-9}$
$R_h$	Hydrodynamic radius,
$D_{eff}$	Effective diffusion coefficient ( $D_{eff} \propto \lambda_{eff} \sigma$ ), [m <sup>2</sup> /s]
$R_c$	Critical radius in terms of bending rigidities [ $\mu$ m]
$t_D$	$t_D = (4\pi R_h^3 \eta_0)/kT$
$k$	Boltzman's constant = $R/N_A$
$T$	Absolute temperature [K]
$L_p$	Persistence length/stiffness of a polymer
$I$	Ionic strength [mol/L=M]
$M_w$	Weight average molecular weight [g/mol]
$\Delta G_{mix}$	Gibbs free energy of mixing [J/mol]
$\mu_i$	Chemical potential [J/mol]
$\Delta S_{mix}$	Change of entropy of mixing [J/Kmol]
$\Delta H_{mix}$	Change of enthalpy of mixing [J/kg]
$\mu_i^0$	Standard chemical potential [J/mol]
$m^0$	Standard molal concentration [mol/g]
$m_i$	Molal/molar concentration of the component $i$ [mol/g or mol/L]
$A_{ii}$	Molal second virial coefficient [cm <sup>3</sup> mol/g <sup>2</sup> ]
$A_{ij}$	Molal cross second virial coefficient [cm <sup>3</sup> mol/g <sup>2</sup> ]
$R$	Ideal gas constant [8.314 J/molK]
$N_A$	Avogadro number [ $6.022 \times 10^{23}$ mol <sup>-1</sup> ]
$n_i$	Number of moles of component $i$ [mol]
$N_i$	Number of molecules of component $i$
$\varphi_i$	Volume fraction of the component $i$ =mole fraction
$\chi_{ij}$	Flory-Huggins interaction parameter between different molecular species [J]
$m_i^v$	Molar volume ratio
$N_i$	Number of molecules, $N_i = \varphi_i V_s/V_i$
$V_{overlap}$	Overlap volume [L]
$\Pi$	Osmotic pressure $\Pi = m_i RT$ [J/L]

$V_{\text{excluded}}$	Excluded volume [L]
$P$	Pressure [Pa]
$R_g$	Radius of gyration [nm]
$Ca$	Dimensionless capillary number
$R_0$	Radius of a retracted spherical droplet [nm]
$C_\infty$	Characteristic ratio defines the flexibility of polymer chain
$C_{1-6}$	Scaling parameters/critical exponents
$r^- r^+$	Volume fraction of the bottom phase (-) and top phase (+)
$D, D_0$	Taylor's dimensionless deformation factor, at time $t$ and time $t_0$
$a, b$	Major and minor axis of an ellipsoid [nm]
$y, 1-y$	Apparent mass/weight fraction of sodium caseinate, galactomannans, respectively
[GM]	Weight concentration of galactomanna(s)
$\sim$	Approximately
§	section
$a=L, b=W$	Major and minor axis of the ellipsoid droplet representation.
$c^*$	Critic biopolymer overlap concentration [wt%, % w/v]
$c^{**}$	Second biopolymer critic overlap concentration [wt%, % w/v]
$g$	Earth's gravity, 9.81 m/s <sup>2</sup>
$k$	Consistency constant ( $Ns^n/m^2 = Pa.s^n$ )
$\log C_{\text{biopol}}$	Effective activity of biopolymer in its saturated solution
$m$	Mass [kg]
M:G	Mannose : galactose ratio
$n$	Power law index (flow behaviour index)
$R_{0i}$	Radius of a retracted droplet of number $i$
$R^2$	The coefficient of determination/regression

## Greek letters

$\varphi$	Mass/volume fraction of GM-rich/NaCAS-rich equilibrium phase per weight of solution [wt% or %w/v]
$\eta_{sp}$	Specific viscosity is the fractional enhancement of viscosity ( $\eta$ ) to that of the solvent
$\eta_{rel}$	Relative viscosity = $\eta/\eta_s$
$[\eta]$	Intrinsic viscosity, a measure of the solutes contribution to $\eta$ [L/g]
$c[\eta]$	degree of space occupancy (coil overlap parameter)
$\Theta$	Theta/the ideal solvent
$\dot{\gamma}$	Shear rate [ $s^{-1}$ ]
$\eta$	Apparent viscosity [Pa.s]
$\eta_0$	Extrapolated zero shear viscosity [Pa.s]
$\xi$	Thickness of the interface [nm]
$\theta$	Angle of rotation of an axis of ellipse [rad]
$\pi$	Mathematical constant determining the ratio between perimeter and diameter of a circle, 3.142
$\tau$	Dimensionless characteristic time, $t\sigma/\eta_c R_0$
$R_c$	Critical radius determining the size of the droplet that can't be broken under shear [nm]
$k$	Bending rigidity
$\lambda_{eff}$	Effective permeability
$\lambda_{sym}$	Distance between the critical and threshold points
$\lambda = \eta_d/\eta_c$	Viscosity ratio
$\eta_c, \eta_d$	Viscosity of continuous/dispersed phase [Pa.s]
$\alpha, 1/\alpha$	(Inverse) distance from the characteristic points of the phase diagram to the origin of the Cartesian space
$\Delta$	Difference/change
$\lambda$	Phase viscosity ratio = $\eta_d/\eta_c$
$\rho$	Density [kg/L]
$\sigma$	Interfacial tension [ $\mu\text{N/m}$ ]

**Abbreviations and subscripts**

ATPS	Aqueous two-phase system(s)
avg	Arithmetic average
BP, [BP]	Biopolymer, biopolymer concentration [wt%, w/v%]
BP, TP	Bottom phase (NaCAS-rich equilibrium phase), top phase (GM-rich equilibrium phase)
crit	Critical point
D	Droplet deformation parameter
c	Continuous phase
d	Disperse phase
FG	Fenugreek gum
GG	Guar gum
GM, [GM]	Galactomannan(s), Galactomannan (LBG, TG, GG and FG) concentration [wt%]
I <sub>p</sub>	Isoelectric point of the protein, pH at which
LBG	Locust bean gum
Min, max	Minimum, maximum
NaCAS, [NaCAS]	Sodium caseinate, Concentration of sodium caseinate [wt%]
r	rich
[sugar]	Sugar concentration [wt%]
STL	Slope of the tie-line length(s)
sym	Symmetry
TG	Tara gum
thres	Threshold point
TLL	Tie-line length(s) $\sqrt{(\Delta[NaCAS])^2 + \Delta[GM]^2}$
top, bot	Top, bottom
wt%/%	Percentage of weight of substance per weight of water
wt%=%	Concentration is given as the percentage of weight of sugar over the total weight of the system

## Contents

Abstract.....	i
Acknowledgements.....	iii
Nomenclature.....	v
Contents.....	ix
List of figures.....	xiv
List of tables.....	xxiii

### CHAPTER 1: INTRODUCTION

1.1 BACKGROUND.....	1—1
1.2 AIM AND OBJECTIVES.....	1—5
1.3 LAYOUT OF THE THESIS.....	1—6
1.4 PAPERS AND PRESENTATIONS.....	1—8

### CHAPTER 2: LITERATURE REVIEW

2.1 Introduction.....	2—10
2.2 Phase behaviour of aqueous two-phase systems.....	2—11
2.2.1 Phase separation studies.....	2—11
2.2.2 Thermodynamic approach.....	2—12
2.2.2.1 Gibbs free energy of mixing.....	2—13
2.2.2.2 Partial molar Gibbs energy (chemical potential) and the effect of solvent quality on cosolubility of molecular species.....	2—14
2.2.2.3 Flory-Huggins lattice model and the effect of solvent quality on cosolubility of molecular species.....	2—15
2.2.2.4 Depletion model and the effect of solvent quality on the cosolubility of molecular species.....	2—18
2.2.3 Phase diagrams.....	2—20
2.2.4 Factors influencing phase behaviour.....	2—23
2.2.5 Phase separation microstructures.....	2—24
2.2.5.1 Equilibrium microstructures.....	2—24
2.2.5.2 Non-equilibrium morphologies.....	2—26
2.3 Rheological behaviour.....	2—29
2.3.1 Rheology of pure biopolymer solutions.....	2—30

---

2.3.2	Rheology of aqueous two-phase biopolymer mixtures .....	2—35
2.3.2.1	Comparison of W/W (ATPS) with O/W emulsions .....	2—35
2.3.2.2	The microstructure of ATPS under quiescent conditions and under shear .....	2—36
2.3.2.2.1	Phase inversion in ATPS .....	2—39
2.3.2.2.2	Shear-induced mixing .....	2—42
2.4	Interfacial properties of aqueous two-phase systems .....	2—43
2.4.1	Interfacial region in ATPS .....	2—43
2.4.2	Measurements of the interfacial properties of emulsions .....	2—45
2.4.2.1	Droplet retraction/deformation theory .....	2—47
2.4.2.2	Application of the droplet retraction method for ATPS .....	2—50
2.4.2.2.1	Suitability .....	2—50
2.4.2.2.2	Concerns .....	2—51
2.4.3	Interfacial tensions of various ATPS .....	2—54
2.4.4	Parameters influencing the interfacial tension in ATPS .....	2—56
2.5	Aqueous two-phase model systems .....	2—60
2.5.1	Sodium caseinate .....	2—60
2.5.2	Galactomannans .....	2—63
2.5.3	Effect of sugars on sodium caseinate, galactomannans and their mixtures .....	2—67
2.6	Conclusion .....	2—70

### CHAPTER 3: EXPERIMENTAL SETUP

3.1	Introduction .....	3—72
3.1.1	Model systems .....	3—73
3.2	Materials .....	3—74
3.3	Methods .....	3—76
3.3.1	Phase behaviour of aqueous two-phase systems with sugar .....	3—76
3.3.1.1	Preparation of bulk solutions .....	3—76
3.3.1.2	Preparation of aqueous two-phase binary solutions .....	3—77
3.3.1.3	Phase diagrams and their characteristic points .....	3—81
3.3.1.3.1	Phase-volume ratio method .....	3—81
3.3.1.3.2	Critical and theoretical points .....	3—86
3.3.1.4	Tie-lines determine phase equilibria compositions .....	3—88

3.3.2 Rheology of aqueous two-phase systems, blends and pure biopolymer solutions with and without sugar .....	3-92
3.3.2.1 Preparation of pure biopolymer solutions, aqueous two-phase systems and blends .....	3-92
3.3.2.2 Microstructure of aqueous two-phase binary blends in quiescent conditions .....	3-95
3.3.2.3 Viscometry of pure biopolymer solutions and aqueous two-phase blends .....	3-95
3.3.2.4 Microstructure of aqueous two-phase blends in flow .....	3-97
3.3.2.5 Interfacial rheology .....	3-98
3.3.3 Interfacial properties of aqueous two-phase blends .....	3-100
3.3.3.1 Preparation of aqueous two-phase systems and blends .....	3-100
3.3.3.2 Drop retraction setup and procedure .....	3-103
3.3.3.3 Calculation of interfacial tension .....	3-106

#### **CHAPTER 4: PHASE BEHAVIOUR OF AQUEOUS SODIUM CASEINATE - GALACTOMANNAN - SUGAR MIXTURES**

4.1 Introduction .....	4-109
4.2 Phase behaviour: a general observation .....	4-110
4.2.1 Appearance of the phases .....	4-110
4.2.2 Phase equilibria .....	4-112
4.3 Effect of galactomannan type on the phase behaviour of sodium caseinate-galactomannan mixtures without sugar .....	4-113
4.3.1 Binodals .....	4-113
4.3.2 Asymmetry of the phase diagram: slopes of the tie-lines and characteristic points .....	4-115
4.4 Effect of sugar concentration on the phase behaviour of sodium caseinate-galactomannan mixtures with sucrose .....	4-117
4.4.1 Binodals .....	4-117
4.4.2 Slopes of the tie-lines .....	4-121
4.4.3 Asymmetry of the phase diagrams .....	4-122
4.4.4 Discussion .....	4-124
4.5 Effect of sugar type on the phase behaviour of sodium caseinate-galactomannan mixtures with sugar .....	4-128
4.5.1 Binodals .....	4-128
4.5.2 Slopes of the tie-lines .....	4-130
4.5.3 Asymmetry of the phase diagrams .....	4-131

4.5.4	Discussion .....	4-132
4.6	Conclusion .....	4-136

**CHAPTER 5: RHEOLOGY AND MICROSTRUCTURE OF THE SODIUM CASEINATE - GALACTOMANNAN - SUGAR AQUEOUS TWO - PHASE SYSTEMS**

5.1	Introduction .....	5-138
5.2	Investigated systems .....	5-139
5.3	Quiescent microstructure.....	5-140
5.3.1	Individual equilibrium phases .....	5-141
5.3.2	Blends .....	5-142
5.3.2.1	Without sugar .....	5-142
5.3.2.2	With sugar.....	5-145
5.4	Flow behaviour of the individual equilibrium phases and blends .....	5-147
5.4.1	Without sugar .....	5-147
5.4.2	With sugar.....	5-150
5.5	Complex flow behaviour in polysaccharide-continuous blends.....	5-152
5.5.1	Flow of pure biopolymer solutions and solvents .....	5-152
5.5.2	Effect of blend preparation on flow of the equilibrium phases and blends .....	5-154
5.5.2.1	Centrifugation affects flow properties of the individual equilibrium phases and their blends .....	5-154
5.5.2.2	Direct preparation of blends on the same tie-line .....	5-156
5.5.3	Shear induced phase inversion and the microstructure of blends under shear .....	5-161
5.5.3.1	Complex flow behaviour in polysaccharide-continuous blends.....	5-161
5.5.3.2	Complex flow behaviour in protein-continuous blends and polysaccharide-continuous blends at a high sugar concentration.....	5-164
5.5.4	Rheoptical investigation of blends with and without sugar .....	5-167
5.5.4.1	Protein-continuous blends.....	5-167
5.5.4.2	Polysaccharide-continuous blends .....	5-171
5.5.5	Effect of composition and temperature on the viscometry of ATPS: the equilibrium phases and blends.....	5-174
5.5.5.1	Effect of the biopolymer concentration and galactomannan type on the flow behaviour of individual equilibrium phases.....	5-174
5.5.5.2	Effect of sugar concentration and type on the flow behaviour of the equilibrium phases and blends .....	5-177
5.5.5.3	Effect of temperature on the flow of blends.....	5-180

5.6	Interfacial rheology between the pure sodium caseinate and galactomannan solutions with sucrose .....	5-183
5.7	Conclusions .....	5-186

**CHAPTER 6: INTERFACIAL TENSIONS OF SODIUM CASEINATE - GALACTOMANNAN - SUGAR AQUEOUS TWO - PHASE SYSTEMS**

6.1	Introduction .....	6-188
6.2	Effects of the deformation parameter range and microstructure on interfacial tension.....	6-189
6.2.1	The limits of the deformation parameter range .....	6-189
6.2.2	Effect of phase sense on interfacial tensions.....	6-191
6.2.3	Droplet shapes, sizes and shear .....	6-197
6.3	Interfacial tension in the sodium caseinate-galactomannan aqueous two-phase systems with sugar .....	6-199
6.3.1	Effect of the concentration of sodium caseinate and locust bean gum on the interfacial tension .....	6-199
6.3.2	Effect of sucrose concentration on the interfacial tension .....	6-209
6.3.3	Effect of sugar type on the interfacial tension .....	6-218
6.3.4	Effect of galactomannan type on the interfacial tension .....	6-225
6.3.4.1	Effect of galactomannan type on the interfacial tension of ATPS with 15% trehalose.....	6-230
6.4	Conclusion .....	6-237

**CHAPTER 7: CONCLUSIONS AND FUTURE WORK**

7.1	Phase equilibria.....	7-239
7.2	Microstructure and rheological behaviour .....	7-241
7.3	Interfacial properties .....	7-242
7.4	Future work .....	7-244

<b>CHAPTER 8:</b>	<b>REFERENCES.....</b>	<b>8-246</b>
-------------------	------------------------	--------------

## List of figures

### CHAPTER 2:

- FIGURE 2-1. BINODALS FOR A SOLVENT-POLYMER 1-POLYMER 2 SYSTEM (A)  $m_1 = m_2 = 1000$ ,  $m_s = 1$ ,  $\chi_{12} = 0.004$ , AND  $\chi_{1s}$  AND  $\chi_{2s} =$ (A) 0.1, 0.16, (B) 0.3, 0.36, (C) 0.4, 0.46. (B)  $m_1 = 4000$ ,  $m_2 = 250$ ,  $m_s = 0.02$ , AND  $\chi_{1s}$  AND  $\chi_{2s}$  ARE: (A) 0.1, 0.15, (A') 0.15, 0.1, (B) 0.2, 0.3, (C) 0.3, 0.45, (C') 0.45, 0.3 (SOURCE: HSU AND PRAUSNITZ, 1973, P. 322). ..... 2—18
- FIGURE 2-2. DEPLETION FLOCCULATION FOR A SYSTEM OF COLLOIDAL PARTICLES AND POLYMER COILS.  $\Pi$  IS THE OSMOTIC PRESSURE OF THE SOLUTE. LIGHT GREEN INDICATES THE DEPLETION ZONES (EXCLUDED VOLUME) AND DARK GREEN INDICATES THE OVERLAP VOLUME (ADAPTED BY: DE KRUIF AND TUINIER, 2000, P. 197). ..... 2—19
- FIGURE 2-3. 2D COMPOSITION-COMPOSITION PHASE DIAGRAM. THE BINODAL CURVE OR PHASE CURVE SEPARATES ONE-PHASE REGION (SHADED) FROM TWO-PHASE REGION (UNSHADED). STL=SLOPE OF THE TIE-LINE. LARGE RECTANGLES ARE A SCHEMATIC REPRESENTATION OF THE EQUILIBRIUM BIOPOLYMER MIXTURES; THEIR CONCENTRATIONS ARE MARKED WITH "▲". 2—20
- FIGURE 2-4. PHASE SEPARATED AQUEOUS 5% GELATIN-1% CARRAGEENAN (A) NON-GELLING CA<sup>2+</sup> SENSITIVE  $\iota$ -CARRAGEENAN AND (B) GELLING  $\kappa$ -CARRAGEENAN. CARRAGEENAN IS COVALENTLY LABELLED WITH FLUORESCEIN ISOTHIOCYANATE (GREEN IN IMAGE A) AND GELATINE IS STAINED BY RHODAMINE (RED IN BOTH IMAGES) (SOURCE: TROMP ET AL., 2001, P. 936). ..... 2—24
- FIGURE 2-5. BEHAVIOUR OF PROTEIN-POLYSACCHARIDE MIXTURES (SOURCE: RODRÍGUEZ PATINO AND PHILOSOF, 2011, P. 1926). ..... 2—25
- FIGURE 2-6. LASER SCANNING CONFOCAL IMAGES (1400 × 1400 MM<sup>2</sup>) OF GRAVITY-DRIVEN FLOW IN A PHASE SEPARATING COLLOID-POLYMER MIXTURE. IN (1) (T = 56 S) THE SPINODAL STRUCTURE IS COLLAPSING UNDER ITS OWN WEIGHT LEADING TO STRONG FLOW IN (2), (3) AND (4) (T = 72, 89 AND 106 S, RESPECTIVELY). MINIMAL COARSENING OCCURS. (5) THE ONSET TO A TRANSITION WITH VERTICAL LANES IS OBSERVED. (6) (T = 134 S) INDIVIDUAL DROPLETS BECOME MORE APPARENT. THE WHITE BOX IN (5) MARKS A RAYLEIGH INSTABILITY (SOURCE: AARTS ET AL., 2005, P. 9). ..... 2—27
- FIGURE 2-7. CONFOCAL IMAGES OF (A) DROPLET-LIKE AND (B) INTERCONNECTED MORPHOLOGIES OF PHASE SEPARATED 2.5% GELATINE-2.5% DEXTRAN-0.5 M NaCl TRAPPED UPON (A) SLOW COOLING AND (B) FAST COOLING (SOURCE: TROMP ET AL., 2001, P. 635). ..... 2—28
- FIGURE 2-8. PHASE DIAGRAM OF MICELLAR CASEIN-LBG SYSTEMS AT 5°C AND THE MICROSTRUCTURE (IMAGES OBTAINED BY CONFOCAL MICROSCOPY) OF THESE SYSTEMS DEPENDING ON THE PHASE VOLUME RATIO (PH ≈ 6.8, I ≈ 0.08, IMAGE LENGTH SCALE, 500 μM) (SOURCE: SCHORSCH ET AL., 1999A, P. 321). ..... 2—29
- FIGURE 2-9. CONCENTRATION DEPENDENCE OF POLYSACCHARIDE-SPECIFIC VISCOSITY FOR: POLYSTYRENE IN TOLUENE MARKED WITH "●"; GUAR GUM MARKED WITH "○"; LOCUST BEAN GUM MARKED WITH "□" AND HYALURONATE MARKED WITH "■" (AT PH 2.5 AND 0–15 M NaCl) (ADAPTED BY: MORRIS ET AL., 1981, P. 14). ..... 2—31
- FIGURE 2-10. GENERALISED SHEAR THINNING BEHAVIOUR FOR CONCENTRATED SOLUTIONS OF DISORDERED POLYSACCHARIDES ILLUSTRATED FOR: GUAR GUM MARKED WITH "△"; LAMBDA CARRAGEENAN MARKED WITH "▲"; LOCUST BEAN GUM MARKED WITH "●"; HIGH MANNURONATE ALGINATE MARKED WITH "■", AND HYALURONATE MARKED WITH "○". (SOURCE: MORRIS ET AL., 1981, P. 18). ..... 2—33

- FIGURE 2-11. VARIATION OF THE INTRINSIC VISCOSITY FOR GUAR AND LOCUST BEAN GUM AT DIFFERENT SUCROSE CONCENTRATIONS. "■"=NATIVE LOCUST BEAN GUM, "○"=GUAR, "×"=PURIFIED LOCUST BEAN GUM (SOURCE: RICHARDSON ET AL., 1998, P. 346). ..... 2—34
- FIGURE 2-12. EVOLUTION OF THE MICROSTRUCTURE OF A SODIUM CASEINATE-SODIUM ALGINATE ATPS IN FLOW: (A) BEFORE THE APPLICATION OF A HIGH SHEAR RATE TO CAUSE DROPLET BREAK-UP; (B) THE MOMENT OF INTERRUPTING THE FLOW (3 S AT  $3 \text{ S}^{-1}$ ); (C) 36 S AFTER STOPPING THE FLOW; (D) 76 S AFTER STOPPING THE FLOW (SOURCE: ANTONOV ET AL., 2004, P. 33)..... 2—37
- FIGURE 2-13. THE MICROSTRUCTURE OF PROCESSED 0.75 WT% GELATIN-1 WT% GUAR MIXTURES (WIDTH OF INSERT: 100 MM) (SOURCE: WOLF ET AL., 2000, P. 219)..... 2—39
- FIGURE 2-14. COMPLEX, MULTIPLE DISPERSED STRUCTURES IN THE PHASE INVERSION REGION OF A 54% SODIUM ALGINATE-RICH IN SODIUM CASEINATE-RICH DISPERSION AFTER THE CESSATION OF STIRRING: (A) IN THE VESSEL AFTER 3 MIN; (B) IN A SAMPLE  $\sim 1$  MIN AFTER WITHDRAWAL (SOURCE: PACEK ET AL., 2001, P. 3254). ..... 2—40
- FIGURE 2-15. (A) SHEAR VISCOSITY OF POLYBUTADIENE-POLYISOPRENE BLENDS AT DIFFERENT SHEAR RATES AS A FUNCTION OF THE POLYISOPRENE VOLUME FRACTION, WHERE THE DASHED CURVE IS THE VISCOSITY OF THE HOMOGENISED MIXTURE (SOURCE: JEON AND HOBBIIE, 2001, P. 061403-4). (B) VISCOSITY DATA FOR STRESS-CONTROLLED COOLED GELATINE-GUAR MIXTURES AS A FUNCTION OF TIME AND TEMPERATURE (WOLF ET AL., 2000, P. 220). ..... 2—41
- FIGURE 2-16. EFFECT OF SHEAR FLOW ON THE EVOLUTION OF SMALL ANGLE LIGHT SCATTERING PATTERNS UPON THE INCEPTION OF FLOW FOR A WATER-DEXTRAN-ARABIC GUM SYSTEM: (A) SHEAR RATE OF  $0.02 \text{ S}^{-1}$ , (B) SHEAR RATE OF  $0.1 \text{ S}^{-1}$  AND (C) SHEAR RATE  $1 \text{ S}^{-1}$  (SOURCE: ANTONOV ET AL., 2009, P. 267). ..... 2—42
- FIGURE 2-17. SCHEME OF THE ATTRACTIVE FORCES AMONG THE MOLECULES OF A LIQUID (SOURCE: CARBONI, 2002). ..... 2—44
- FIGURE 2-18. A SCHEMATIC DRAWING OF A DEFORMED DROP SHOWING THE TWO AXES  $A$  AND  $B$  AND THE ANGLE  $\theta$  IN THE PLANE OF SHEAR (SOURCE: GUIDO ET AL., 2002, P. 146). ..... 2—48
- FIGURE 2-19. A SEQUENCE OF IMAGES ACQUIRED AT CONSECUTIVE TIMES SHOWS THE DEFORMATION OF A CASEINATE-RICH PHASE DROPLET IN THE ALGINATE-RICH PHASE (SHEAR RATE:  $0.05 \text{ S}^{-1}$ ): (1) DROPLET AT REST; (2-3) START-UP TRANSIENT; (4) STATIONARY SHAPE; (5-6) RETRACTION (SOURCE: GUIDO ET AL., 2002, P. 148). ..... 2—51
- FIGURE 2-20. CONCENTRATION DEPENDENCE OF THE ZERO-SHEAR VISCOSITY OF CASEINATE SUSPENSIONS AT DIFFERENT TEMPERATURES. THE INSERT SHOWS THE MASTER CURVE OBTAINED BY NORMALISING THE VISCOSITY BY THE SOLVENT VISCOSITY AND THE CONCENTRATION BY  $C^*$  ( $130 \text{ G/L} \approx 13 \text{ WT}\%$ ). THE SOLID LINE IS TO GUIDE THE EYE (SOURCE: PITKOWSKI ET AL., 2008, P. 99). ..... 2—62
- FIGURE 2-21. CONFORMATION OF SIMULATED GALACTOMANNANS OBTAINED WITH DIFFERENT PARAMETER SETTINGS (FROM LEFT TO RIGHT: FENUGREEK GUM, GUAR GUM, TARA GUM AND LOCUST BEAN GUM) (A)  $\text{MIN\_BOND}=3$  AND  $\text{MAX\_BOND}=4$  (B) AT  $\text{MIN\_BOND}=3$  AND THE CUT-OFF DISTANCE= $15 \text{ \AA}$  (SOURCE: WU ET AL., IN PRESS). ..... 2—63
- FIGURE 2-22. (A) FLOW CURVES OF 0.5% GALACTOMANNAN SOLUTIONS. (B) INTERFACIAL ACTIVITIES OF GALACTOMANNANS AT VARIOUS CONCENTRATIONS. FG=FENUGREEK GUM; GG=GUAR GUM; TG=TARA GUM; LBG=LOCUST BEAN GUM (SOURCE: WU ET AL., 2009, P. 1144, 1143). ..... 2—66

**CHAPTER 3:**

FIGURE 3-1. PREPARATION OF BULK GALACTOMANNAN AND SODIUM CASEINATE SOLUTIONS.....3-77

FIGURE 3-2. PREPARATION OF AQUEOUS TWO-PHASE BINARY SOLUTIONS .....3-79

FIGURE 3-3. THE FIRST STEP IN THE PHASE-VOLUME RATIO APPROACH USED FOR THE DETERMINATION OF THE PHASE DIAGRAMS; TYPICAL DEPENDENCIES OF THE PHASE VOLUME RATIO OF SODIUM CASEINATE-RICH EQUILIBRIUM PHASE (R) ON THE MIXTURE COMPOSITION (Y) FOR SODIUM CASEINATE-LOCUST BEAN GUM AQUEOUS TWO-PHASE SYSTEM (USED AS AN EXAMPLE). R=PHASE VOLUME RATIO (I.E., VOLUME FRACTION [%] OF THE SODIUM CASEINATE EQUILIBRIUM PHASE), Y=APPARENT WEIGHT FRACTION (I.E., RATIO OF THE CONCENTRATION OF THE SODIUM CASEINATE ON THE BINODAL AND ITS CONCENTRATION IN THE BULK). .....3-83

FIGURE 3-4. THE SECOND STEP IN THE PHASE-VOLUME RATIO APPROACH USED FOR THE DETERMINATION OF THE PHASE DIAGRAMS; BINODAL (THE CURVE), RECTLINEAR DIAMETER AND  $[NaCAS]^0$  (SODIUM-CASEINATE BULK CONCENTRATIONS) AND  $[GM]^0$  (GALACTOMANNAN BULK CONCENTRATIONS) PAIRS, WHICH ARE CONNECTED WITH DASHED LINES; "○" MARK BINODAL POINTS, "●" MARK RECTLINEAR POINTS.....3-85

FIGURE 3-5. DETERMINATION OF THE CRITICAL POINT IN THE PHASE DIAGRAM ON THE EXAMPLE OF SYSTEM 1 (SODIUM CASEINATE-LOCUST BEAN GUM) WITH NO ADDED SUGAR. CRITICAL POINTS FOR OTHER SYSTEMS AND SUGAR CONCENTRATIONS WERE DETERMINED IN THE SAME WAY. ....3-87

FIGURE 3-6. DETERMINATION OF THE THRESHOLD POINT IN THE PHASE DIAGRAM ON THE EXAMPLE OF SYSTEM 1 (SODIUM CASEINATE-LOCUST BEAN GUM) WITH 15 WT% ADDED SUCROSE. THRESHOLD POINTS FOR OTHER SYSTEMS AND SUGAR CONCENTRATIONS WERE DETERMINED IN THE SAME WAY.....3-87

FIGURE 3-7. TIE-LINE IN THE PHASE DIAGRAM FOR A SODIUM CASEINATE-LOCUST BEAN GUM AQUEOUS TWO-PHASE SYSTEM (ATPS) WITHOUT SUCROSE. A=CONCENTRATION OF LOCUST BEAN GUM BULK SOLUTION, B=CONCENTRATION OF SODIUM CASEINATE BULK SOLUTION, C=CONCENTRATION OF THE ATPS, D=CONCENTRATION OF THE LOCUST BEAN GUM-RICH EQUILIBRIUM PHASE, E=CONCENTRATION OF THE SODIUM CASEINATE-RICH EQUILIBRIUM PHASE.  $[LBG]_0$  IS THE INTERCEPT OF THE TIE-LINE WITH THE Y-AXIS. STL=SLOPE OF THE TIE-LINE. ONE PHASE REGION OF THE PHASE DIAGRAM IS SHADED.....3-89

FIGURE 3-8. PREPARATION OF BLENDS FROM (4) A NACAS-LBG SYSTEM THAT SEPARATES INTO (1) A LBG-RICH EQUILIBRIUM PHASE AND (8) A NACAS-RICH EQUILIBRIUM PHASE). THE EQUILIBRIUM PHASES ARE THEN USED TO PREPARE BLENDS 2, 3, 5, 6 AND 7.....3-94

FIGURE 3-9. A 4° 40 MM CONE-AND-PLATE GEOMETRY (LEFT) AND A 60 MM ACRYLIC PLATE (RIGHT) WERE USED FOR FLOW EXPERIMENTS.....3-96

FIGURE 3-10. 40MM GLASS PLATE-AND-PLATE GEOMETRY USED IN THE STUDY OF THE MICROSTRUCTURE AND INTERFACIAL PROPERTIES OF SODIUM CASEINATE-GALACTOMANANN ATPS.....3-97

FIGURE 3-11. LONG SHAFT 1°, 55 MM BICONAL-RING GEOMETRY USED FOR INTERFACIAL RHEOLOGY (LEFT) AND THE PROCEDURE (RIGHT).....3-98

FIGURE 3-12. SYSTEMS INVESTIGATED ON THEIR INTERFACIAL TENSIONS FOR SODIUM CASEINATE-LOCUST BEAN GUM WITHOUT SUGAR. "■" REFERS TO BLENDS INVESTIGATED FOR INTERFACIAL TENSIONS "●" REFERS TO ATPS WHOSE EQUILIBRIUM PHASES WERE USED TO PREPARE BLENDS. ....3-102

FIGURE 3-13. EXPERIMENTAL SETUP FOR THE INTERFACIAL TENSION MEASUREMENT COMPOSED OF A ROTATIONAL RHEOMETER WITH GLASS PLATE-AND-PLATE GEOMETRY AND VIDEO-MICROSCOPE-COMPUTER SYSTEM: 1-VIDEO AND FLOW RECORDING, 2-BOHLIN GEMINI WITH ROTONETIC DRIVE Z STRESS CONTROLLED ROTATIONAL RHEOMETER (MALVERN INSTRUMENTS), 3-CUSTOM MADE GLASS PLATE-AND-PLATE GEOMETRY (40 MM DIAMETER), 4-STROBE, 5-STEREO MICROSCOPE (110 TIMES MAGNIFICATION), AND 6-C-MOUNTED B/W VIDEO CAMERA (AVT DOLPHIN)..... 3-103

FIGURE 3-14. RETRACTING DROP AT VARIOUS TIMES WITH CORRESPONDING DROP DEFORMATION PARAMETERS (D) AFTER THE CESSATION OF SHEAR. THE SIZE OF THE RETRACTED DROP (MICROGRAPH ON THE RIGHT) IS 60  $\mu$ M..... 3-105

FIGURE 3-15. THE CALCULATION OF THE DROP PARAMETERS IN ELLIPSOID (LEFT) AND SPHERICAL (RIGHT) DROPLETS. L=LENGTH OF THE DROP, W=WIDTH OF THE DROPLET,  $R_0$ =RADIUS OF A RETRACTED (SPHERICAL) DROPLET. DURING THE RETRACTION PROCESS, THE DROP ROTATES ROUND ITS CENTRE. .... 3-107

**CHAPTER 4:**

FIGURE 4-1. LIGHT MICROGRAPHS OF A 95 WT% LOCUST BEAN GUM-RICH BLEND AT 50 TIMES, 100 TIMES, 400 TIMES AND 1000 TIMES MAGNIFICATION. THE PROTEIN-RICH PHASE IS DYED WITH DIRECT RED. .... 4-110

FIGURE 4-2. PHASE SEPARATION KINETICS IN 95 WT% LOCUST BEAN GUM-RICH BLEND 100 TIMES MAGNIFIED. THE PROTEIN-RICH PHASE IS DYED WITH WATER BLUE..... 4-111

FIGURE 4-3. PHASE DIAGRAM OF SODIUM CASEINATE-LOCUST BEN GUM (NACAS-LBG) REFERENCE SYSTEM WITH THE IMAGES OF THE SYSTEMS OF THREE DISTINCT VOLUME FRACTIONS: NACAS-CONTINUOUS (RIGHT), BICONTINUOUS (MIDDLE) AND LBG-CONTINUOUS (LEFT). TOP PHASE IS RICH IN LBG AND BOTTOM PHASE IS RICH IN NACAS. THE MICROGRAPHS ARE A REPRESENTATION OF THE GM-RICH (TOP) AND NACAS-RICH PHASES..... 4-111

FIGURE 4-4. SCANNING ELECTRON MICROGRAPHS OF THE (LEFT) 15 WT% LOCUST BEAN GUM-RICH BLEND, AND (RIGHT) 75 WT% LOCUST BEAN GUM-RICH BLEND..... 4-112

FIGURE 4-5. PHASE DIAGRAMS OF SYSTEMS 1-4 WITHOUT ADDED SUGAR..... 4-114

FIGURE 4-6. DISTANCES BETWEEN CRITICAL AND THRESHOLD POINTS ( $\lambda_{sym}$ ) FOR SYSTEMS 1-4. THE DEGREE OF BRANCHING PROGRESSES FROM SYSTEM 1 WITH LBG TO SYSTEM 4 WITH FG..... 4-116

FIGURE 4-7. INVERSE DISTANCES ( $1/\alpha_{crit}$ ,  $1/\alpha_{thres}$ ) FOR SYSTEMS 1-4. THE DEGREE OF BRANCHING PROGRESSES FROM SYSTEM 1 WITH LBG TO SYSTEM 4 WITH FG..... 4-116

FIGURE 4-8. PHASE DIAGRAMS OF SYSTEM 1 (LEFT) AND SYSTEM 3 (RIGHT) WITH VARIOUS SUCROSE CONCENTRATIONS. .... 4-118

FIGURE 4-9. DISTANCES BETWEEN THE PAIRS OF CRITICAL AND THRESHOLD POINTS ( $\lambda_{sym}$ ) AS A FUNCTION OF SUCROSE CONCENTRATION. DOTTED LINE IS TO GUIDE THE EYE. .... 4-123

FIGURE 4-10. INVERSE DISTANCES AS A FUNCTION  $1/\alpha_{crit}$  (LEFT) AND  $1/\alpha_{thres}$  (RIGHT) AS A FUNCTION OF SUCROSE CONCENTRATION. DOTTED LINE IS TO GUIDE THE EYE. .... 4-124

FIGURE 5-1. (A, B) LOCUST BEAN GUM/LBG-RICH AND (C, D) SODIUM CASEINATE/NACAS-RICH EQUILIBRIUM PHASES OBTAINED FROM 3 WT% NACAS-0.2 WT% LBG ATPS AT 20°C. THE WIDTH OF THE LIGHT MICROGRAPHS A AND C IS 1.3 MM. THE WIDTH OF THE CONFOCAL MICROGRAPHS B AND D IS 0.375 MM. THE RADIUS OF DROPLETS IN MICROGRAPH B IS < 5  $\mu$ M. .... 5-141

FIGURE 5-2. CONFOCAL MICROGRAPHS FOR ATPS 4 (4 WT% NACAS-0.6 WT% LBG WITHOUT SUGAR) AT DIFFERENT PHASE VOLUMES OF THE LBG-RICH PHASE ( $\Phi_{\text{LBG}}$ ) AND AT QUIESCENT CONDITIONS. NACAS-RICH PHASE IS STAINED AND IS THE LIGHTER PHASE. GREEN SQUARE MARKS THE BI-CONTINUOUS SYSTEMS. THE MICROGRAPHS ARE 1.5 MM WIDE.....	5-143
FIGURE 5-3. 3D CONFOCAL MICROGRAPHS FOR ATPS 4 SHOW THREE DISTINCT MICROSTRUCTURES. THE WIDTH OF THE MICROGRAPHS IS 0.882 MM AND THEIR DEPTH IS 165 MM. CROSS SECTIONS WERE SCANNED IN 1.3 MM STEPS.....	5-144
FIGURE 5-4. LIGHT MICROGRAPHS ILLUSTRATE THE INSTABILITY OF BLENDS PREPARED FROM 4 WT% SODIUM CASEINATE-0.6 WT% LOCUST BEAN GUM ATPS WITH $\Phi_{\text{LBG}}=95\%$ MIXED WITH SILVERSON (3 MIN AND 3000 RPM).....	5-145
FIGURE 5-5. CONFOCAL MICROGRAPHS (SUM OF 130 SCANS) OF 1.5 MM WIDTH FOR ATPS "4" (4 WT% NACAS-0.6 WT% LBG WITH AND WITHOUT SUGAR) AT DIFFERENT PHASE VOLUMES OF THE LBG-RICH PHASE ( $\Phi_{\text{LBG}}$ ) AND AT QUIESCENT CONDITIONS. NACAS-RICH PHASE IS THE LIGHTER PHASE. ....	5-145
FIGURE 5-6. CONFOCAL MICROGRAPHS OF ATPS 8. ON LEFT NACAS-RICH PHASE IS SHOWN AS LIGHTER. ON THE RIGHT MICROGRAPH THE MARKING IS INVERTED.....	5-146
FIGURE 5-7. ASCENDING FLOW CURVES OF BLENDS FOR (A) SYSTEM 1 AND (B) SYSTEM 3 IN THE ABSENCE OF SUGAR AND AS THE VOLUME FRACTION OF THE GALACTOMANNAN-RICH PHASE ( $\phi = \phi_{\text{GM}}$ , LBG-RICH, GG-RICH) IS PROGRESSIVELY INCREASED FROM 0% ("PURE" PROTEIN-RICH PHASE) TO 95% (SYSTEM 1) OR 75% (SYSTEM 3).....	5-148
FIGURE 5-8. (A) ASCENDING AND (B) DESCENDING FLOW CURVES OF THE EQUILIBRIUM PHASES AND BLENDS FOR SYSTEM 1 (4 WT% NACAS-0.6 WT% LBG) AS THE VOLUME FRACTIONS ARE PROGRESSIVELY INCREASED FROM 0 ("PURE" PROTEIN-RICH PHASE) TO 100% ("PURE" GALACTOMANNAN-RICH PHASE). ....	5-149
FIGURE 5-9. THE EFFECT OF SHEAR CYCLES ON ATPS 3 ( $\phi_{\text{GM}}=80$ WT% BLEND OF 4 WT%NACAS-0.2 WT% LBG). ....	5-150
FIGURE 5-10. ASCENDING (LEFT) AND DESCENDING (RIGHT) FLOW CURVES OF THE EQUILIBRIUM PHASES AND BLENDS FOR SYSTEM 1 (NACAS-LBG SYSTEM) AT (A) 5, (B) 15, (C) 20, AND (D) 40 WT% OF SUCROSE, AND AS THE VOLUME FRACTIONS OF THE LBG-RICH PHASE IS PROGRESSIVELY INCREASED FROM 0 ("PURE" PROTEIN-RICH PHASE) TO 100% ("PURE" GALACTOMANNAN-RICH PHASE).....	5-151
FIGURE 5-11. FLOW CURVES OF THE SODIUM CASEINATE SOLUTIONS WITH VARIOUS AMOUNTS OF SUCROSE. ....	5-153
FIGURE 5-12. FLOW CURVES FOR (A) VARIOUS CONCENTRATIONS OF GUAR GUM AND FOR (B) VARIOUS TYPES OF GALACTOMANNANS IN THE ABSENCE OF SUGAR. ....	5-153
FIGURE 5-13. FLOW CURVES OF (A) LOCUST BEAN GUM-RICH (LBG-RICH) AND OF (B) SODIUM CASEINATE-RICH (NACAS-RICH) EQUILIBRIUM PHASES FOR 4 WT% NACAS-0.6 WT% LBG SYSTEMS AFTER CENTRIFUGATION AT 4000 RPM AND 20°C. ....	5-155
FIGURE 5-14. FLOW CURVES OF LBG-RICH PHASES THAT WERE CENTRIFUGED FOR VARIOUS PERIODS AND PRESHEARED TO 1000 S <sup>-1</sup> . ....	5-156
FIGURE 5-15. ASCENDING FLOW CURVES FOR BLENDS WITH 25, 50 AND 75 WT% OF LBG-RICH PHASE AND 0-40 WT% SUCROSE, PREPARED BY DISSOLVING OF THE POWDERED INGREDIENTS (LEFT) AND BY BLENDING OF THE EQUILIBRIUM PHASES FROM A PRIMARY ATPS (RIGHT).....	5-159
FIGURE 5-16. DESCENDING FLOW CURVES FOR BLENDS WITH 25, 50 AND 75 WT% OF LBG-RICH PHASE AND 0-40 WT% SUCROSE, PREPARED BY DISSOLVING OF THE POWDERED INGREDIENTS (LEFT) AND BY BLENDING OF THE EQUILIBRIUM PHASES FROM A PRIMARY ATPS (RIGHT).....	5-160

FIGURE 5-17. SHEAR VISCOSITY-COMPOSITION DEPENDENCE FOR SYSTEM 1 (NACAS-LBG) WITH 0, 5, 15, 20 AND 40% SUCROSE. THE NUMBER NEXT TO PHASE VOLUME OF THE LBG-RICH PHASE ( $\phi = \phi_{LBG}$ ) CORRESPONDS TO THE NUMERING FOR THE SYSTEMS USED LATER IN TABLE 5-2 (P. 5-165).....5-163

FIGURE 5-18. MICROSTRUCTURES UNDER SHEAR AND FLOW CURVES OF ATPS 3 (4 WT% NACAS-0.2 WT% LBG) AT  $\Phi_{LBG}=1$  WT%. THE WIDTH OF VIEW IS 1.7 MM. ....5-168

FIGURE 5-19. MICROSTRUCTURES OF ATPS 3 (4 WT% NACAS-0.2 WT% LBG) AT  $\phi_{GM}=5$  WT%, 5% SUCROSE AND AT 18 TIMES MAGNIFICATION UNDER SHEAR. THE WIDTH OF VIEW PER MICROGRAPH IS 5 MM. ....5-169

FIGURE 5-20. MICROSTRUCTURES OF ATPS 3 (4 WT% NACAS-0.2 WT% LBG) AT  $\phi_{GM}=40$  WT%, 5% SUCROSE AND AT 18 TIMES MAGNIFICATION UNDER SHEAR. THE WIDTH OF VIEW PER MICROGRAPH IS 5 MM. ....5-169

FIGURE 5-21. A FORMATION OF THE THREAD-LIKE OR TUBULAR STRUCTURES FROM THE PROTEIN-CONTINUOUS BLENDS FOR ATPS 3 AT  $\phi_{GM}=40$  WT% AFTER SHEAR. THE WIDTH OF VIEW IS 1.186 MM. ....5-170

FIGURE 5-22. MICROSTRUCTURES UNDER SHEAR AND FLOW CURVES OF ATPS 3 (4 WT% NACAS-0.2 WT% LBG) AT  $\Phi_{LBG}=20$  WT%. THE WIDTH OF VIEW IS 1.7 MM. ....5-171

FIGURE 5-23. MICROSTRUCTURES UNDER FLOW AND FLOW CURVES FOR ATPS 3 (4 WT% NACAS-0.2 WT% LBG) AT  $\phi_{GM}=80$  WT% AND 110 TIMES MAGNIFICATION. THE WIDTH OF VIEW PER MICROGRAPHS IS 1.7 MM. ....5-172

FIGURE 5-24. MICROSTRUCTURES UNDER FLOW AND FLOW CURVES FOR ATPS 3 (4 WT% NACAS-0.2 WT% LBG) AT  $\phi_{GM}=80$  WT% AND 30% SUCROSE. THE WIDTH OF VIEW PER MICROGRAPHS IS 0.85 MM. ....5-173

FIGURE 5-25. PURE LBG-RICH PHASE OF ATPS 3 AT 18 TIMES MAGNIFICATION. THE WIDTH OF VIEW IS 5 MM. ....5-174

FIGURE 5-26. EFFECT OF THE TOTAL BIOPOLYMER CONCENTRATION ON THE VISCOSITY OF (A) LBG-RICH AND (B) NACAS-RICH EQUILIBRIUM PHASES FOR SODIUM CASEINATE-LOCUST BEAN GUM (NACAS-LBG) ATPS.....5-175

FIGURE 5-27. EFFECT OF THE GALACTOMANNAN TYPE ON THE VISCOSITY OF (A) LBG-RICH AND (B) NACAS-RICH EQUILIBRIUM PHASES FOR SODIUM CASEINATE-LOCUST BEAN GUM (NACAS-LBG) ATPS.....5-176

FIGURE 5-28. EFFECT OF THE SUCROSE CONCENTRATION ON THE VISCOSITY OF (A) LBG-RICH AND (B) NACAS-RICH EQUILIBRIUM PHASES FOR SODIUM CASEINATE-LOCUST BEAN GUM (NACAS-LBG) ATPS .....5-177

FIGURE 5-29. EFFECT OF THE SUGAR TYPE ON THE VISCOSITY OF (A) LBG-RICH AND (B) NACAS-RICH EQUILIBRIUM PHASES FOR SODIUM CASEINATE-LOCUST BEAN GUM (NACAS-LBG) ATPS .....5-178

FIGURE 5-30. COMPARISON OF SYSTEMS 1 (NACAS-LBG) AND 3 (NACAS-GG) BASED ON THE SUGAR TYPE.....5-179

FIGURE 5-31. EFFECTS OF SHEAR, TEMPERATURE AND SUGAR TYPE ON BLENDS OF SYSTEM 3 WITH 25, 50 AND 75% OF THE GG-RICH PHASE. THE BLENDS AT 0 AND 15% OF SUCROSE ARE POSITIONED ON THE LEFT HAND SIDE, AND THE BLENDS WITH 15% GLUCOSE ON THE RIGHT HAND SIDE.....5-181

FIGURE 5-32. EFFECTS OF SHEAR, TEMPERATURE AND SUGAR TYPE ON BLENDS OF SYSTEM 1 WITH 25, 50 AND 75% OF THE LBG-RICH PHASE. THE BLENDS AT 0 AND 15% OF SUCROSE ARE POSITIONED ON THE LEFT HAND SIDE, AND THE BLENDS WITH 15% GLUCOSE ON THE RIGHT HAND SIDE.....5-182

FIGURE 5-33. LOG-LOG PLOTS OF THE INTERFACIAL MODULI WITH TIME FOR SODIUM CASEINATE, GUAR GUM, AND AIR INTERFACES, AT (A) 0, (B) 5, (C) 15, AND (D) 50 WT% OF SUCROSE..... 5-184

## CHAPTER 6:

FIGURE 6-1. DROPLET DEFORMATION PARAMETER ( $D$ ) AGAINST TIME FOR A 4 %WT SODIUM CASEINATE-0.2 %WT LOCUST BEAN GUM AQUEOUS-TWO-PHASE SYSTEM WITH  $\Lambda$  ( $0.001 \text{ S}^{-1}$ )=15.3. THREE STAGES IN THE DROPLET RETRACTION METHODS ARE SHOWN WITH THREE LIGHT MICROGRAPHS, THE RADIUS OF THE RETRACTED DROPLET,  $R_0 = 54 \text{ MM}$ . THE LEFT GRAPH ( $R^2=0.98$ ) SHOWS LINEAR AND THE RIGHT GRAPH ( $R^2=0.95$ ) EXPONENTIAL DECAY CHANGE OF  $D$  VS. TIME. .... 6-190

FIGURE 6-2. LIGHT MICROGRAPHS FOR (A) A SODIUM CASEINATE-CONTINUOUS AND (B-D) A LOCUST BEAN GUM-CONTINUOUS SYSTEMS AFTER SHEAR. SYSTEMS SHOWN IN MICROGRAPHS A-C WERE PREPARED FROM THE EQUILIBRIUM PHASES OF A 4 WT% SODIUM CASEINATE-0.2 WT% LOCUST BEAN GUM ATPS, AND SYSTEM SHOWN IN MICROGRAPH D WERE PREPARED FROM THE EQUILIBRIUM PHASES OF A 4 WT% SODIUM CASEINATE-0.2 WT% LOCUST BEAN GUM-30% SUCROSE. .... 6-193

FIGURE 6-3. DIFFERENCES IN CHARACTERISTIC RETRACTION TIMES ( $T$ ) FOR TWO DISTINCT MICROSTRUCTURES. GRAPH (A) SHOWS A SYSTEM WITHOUT SUCROSE, AND GRAPH (B) SHOWS A SYSTEM AT 30 WT% SUCROSE. FOR EACH SYSTEM, TWO DROPS WERE CHOSEN: ONE DROPLET WAS CHOSEN TO SHOW RETRACTION IN A SODIUM CASEINATE-CONTINUOUS BLEND ( $\varphi_{GM} = 20 \text{ WT\%}$ ) AND THE OTHER IN A LOCUST BEAN GUM-CONTINUOUS BLEND ( $\varphi_{GM} = 80 \text{ WT\%}$ ). ..... 6-194

FIGURE 6-4. TWO DISTINCT MICROSTRUCTURES SHOWN ON THE PHASE DIAGRAM OF A SODIUM CASEINATE-LOCUST BEAN GUM SYSTEM WITHOUT SUGAR..... 6-195

FIGURE 6-5. DROPLET SHAPES OBSERVED IN SHEAR FOR VARIOUS AQUEOUS TWO-PHASE SYSTEMS. THE CONCENTRATION OF THE BIOPOLYMERS IS IN WEIGHT PERCENT..... 6-198

FIGURE 6-6. PHASE DIAGRAM FOR A SODIUM CASEINATE-LOCUST BEAN GUM SYSTEMS. SYSTEMS INSPECTED FOR INTERFACIAL TENSIONS ARE MARKED WITH "●". A CRITICAL POINT IS MARKED WITH "✕", A TIE-LINE AND ITS SLOPE ( $STL$ ) IS GIVEN FOR EACH OF THE SYSTEMS. THE AVERAGE SLOPE OF THE TIE-LINE IS  $0.25 \pm 0.02$ ..... 6-200

FIGURE 6-7. LOG-LOG APPARENT VISCOSITIES OF THE TOP (TP) AND BOTTOM (BP) EQUILIBRIUM PHASES FOR SODIUM CASEINATE-LOCUST BEAN GUM (NACAS-LBG) ATPS INVESTIGATED FOR THE EFFECT OF THE CONCENTRATION OF BIOPOLYMERS ON THE INTERFACIAL TENSION. ... 6-202

FIGURE 6-8. SEMI LOGARITHMIC PLOT OF THE DEFORMATION PARAMETER ( $D$ ) AS A FUNCTION OF TIME WITH LINEAR REGRESSION FOR A 4 WT% SODIUM CASEINATE-0.2 WT% LOCUST BEAN GUM ATPS AT  $\Phi=1 \text{ WT\%}$ .  $R_0$ =RADIUS OF A RETRACTED DROPLET.  $\Phi$ = VOLUME FRACTION OF THE LOCUST BEAN GUM-RICH PHASE. .... 6-203

FIGURE 6-9. DEFORMATION PARAMETER ( $D$ ) AS A FUNCTION OF  $T/R_0$  FOR A 4 WT% SODIUM CASEINATE-0.2 WT% LOCUST BEAN GUM ATPS. .... 6-204

FIGURE 6-10. INTERFACIAL TENSIONS IN SODIUM CASEINATE-LOCUST BEAN GUM ATPS AS A FUNCTION OF THE TIE-LINE LENGTH ( $A$ ). THE LOG-LOG PLOT (B) GIVES A STRAIGHT LINE... 6-206

FIGURE 6-11. INTERFACIAL TENSIONS IN SODIUM-CASEINATE AND LOCUST BEAN GUM (NACAS-LBG) ATPS OF VARIED CONCENTRATIONS AS A FUNCTION OF NACAS ( $\Delta[\text{NACAS}]$ , MARKED WITH "●") AND LBG ( $\Delta[\text{LBG}]$ , MARKED WITH "○") CONCENTRATION DIFFERENCES BETWEEN THE PHASES. THE CONCENTRATIONS OF THE ATPS ARE GIVEN IN WEIGHT %. .... 6-207

FIGURE 6-12. PHASE DIAGRAMS OF SODIUM CASEINATE-LOCUST BEAN GUM-SUCROSE SYSTEMS. SYSTEMS INSPECTED FOR INTERFACIAL TENSIONS ARE MARKED WITH "●" AND CRITICAL POINTS WITH "✕", A TIE-LINE AS WELL AS ITS SLOPE (STL) IS CALCULATED FOR EACH OF THE ATPS.  $STL_{AVG} = -0.24 \pm 0.02$ ..... 6-210

FIGURE 6-13. LOG-LOG PLOTS OF APPARENT VISCOSITIES OF THE TOP (TP, LBG-RICH=LOCUST BEAN GUM-RICH) AND BOTTOM (BP, NACAS-RICH=SODIUM CASEINATE-RICH) PHASES OF THE ATPS INVESTIGATED FOR THE EFFECTS OF SUCROSE CONCENTRATION..... 6-210

FIGURE 6-14. SEMI-LOGARITHMIC PLOT OF THE DEFORMATION PARAMETER (D) AS A FUNCTION OF TIME WITH LINEAR REGRESSION FOR A 4 WT% SODIUM-CASEINATE-0.2 WT% LOCUST BEAN GUM-5% SUCROSE ATPS AT  $\Phi = 1$  WT%.  $R_0$ =RADIUS OF A RETRACTED DROPLET;  $\Phi$ =VOLUME FRACTION OF THE LOCUST BEAN GUM-RICH PHASE..... 6-212

FIGURE 6-15. INTERFACIAL TENSION FOR A SODIUM CASEINATE-LOCUST BEAN GUM-SUCROSE ATPS AS A FUNCTION OF THE TIE-LINE LENGTH (A). THE LOG-LOG PLOT (B) GIVES A STRAIGHT LINE .... 6-215

FIGURE 6-16. INTERFACIAL TENSION FOR A 4 WT% SODIUM CASEINATE-0.2 WT% LOCUST BEAN GUM-SUCROSE (NACAS-LBG-SUCROSE) ATPS AS A FUNCTION OF THE NACAS ( $\Delta[NACAS]$ , MARKED WITH "●") AND LBG ( $\Delta[LBG]$ , MARKED WITH "○") CONCENTRATION DIFFERENCE BETWEEN THE PHASES..... 6-215

FIGURE 6-17. PHASE DIAGRAM OF A SODIUM CASEINATE-LOCUST BEAN GUM ATPS AT 15 WT% OF SUCROSE, TREHALOSE, GLUCOSE AND FRUCTOSE. SYSTEMS INSPECTED FOR INTERFACIAL TENSIONS ARE MARKED WITH "●" AND A CRITICAL POINT "✕", A TIE-LINE, AS WELL AS ITS SLOPE (STL) IS GIVEN FOR EACH OF THE SYSTEMS. THE CURVES FOR GLUCOSE AND TREHALOSE ALMOST OVERLAP.  $STL_{AVG} = -0.22 \pm 0.02$ ..... 6-218

FIGURE 6-18. LOG-LOG APPARENT VISCOSITIES OF TOP (TP) AND BOTTOM (BP) PHASES OF A SODIUM CASEINATE-LOCUST BEAN GUM (NACAS-LBG) ATPS INVESTIGATED FOR THE EFFECTS OF SUGAR-TYPE (SUCROSE, TREHALOSE, GLUCOSE AND FRUCTOSE) ON INTERFACIAL TENSIONS..... 6-219

FIGURE 6-19. INTERFACIAL TENSION FOR SODIUM CASEINATE-LOCUST BEAN GUM ATPS FOR VARIOUS SUGAR TYPES AS A FUNCTION OF THE TIE-LINE LENGTH (A). THE LOG-LOG PLOT (B) GIVES A STRAIGHT LINE..... 6-222

FIGURE 6-20. INTERFACIAL TENSIONS FOR SODIUM-CASEINATE AND LOCUST BEAN GUM (NACAS-LBG) ATPS WITH DIFFERENT SUGAR TYPES AS A FUNCTION OF NACAS ( $\Delta[NACAS]$ , MARKED WITH "●") AND LBG ( $\Delta[LBG]$ , MARKED WITH "○") CONCENTRATION DIFFERENCES BETWEEN THE PHASES..... 6-223

FIGURE 6-21. PHASE DIAGRAM OF SODIUM CASEINATE-GALACTOMANNAN SYSTEMS WITHOUT SUGAR. THE SAME AMOUNTS OF SODIUM CASEINATE AND GALACTOMANNANS: LOCUST BEAN GUM (LBG), TARA GUM (TG), GUAR GUM (GG) AND FENUGREEK GUM (FG) WERE ADDED TO MAKE THE ATPS. SYSTEMS INSPECTED FOR INTERFACIAL TENSIONS ARE MARKED WITH "●" AND A CRITICAL POINT MARKED WITH "✕", A TIE-LINE, AS WELL AS ITS SLOPE (STL) IS GIVEN FOR EACH OF THE ATPS.  $STL_{AVG} = -0.23 \pm 0.01$ ..... 6-225

FIGURE 6-22. LOG-LOG PLOTS OF APPARENT VISCOSITIES FOR THE TOP (TP) AND BOTTOM (BP) PHASES OF A SODIUM CASEINATE-GALACTOMANNAN (NACAS-GM) ATPS INVESTIGATED FOR THE EFFECT OF GALACTOMANNAN TYPE ON INTERFACIAL TENSION. GM=GALACTOMANNAN, LBG=LOCUST BEAN GUM, GG=GUAR GUM, FG=FENUGREEK GUM..... 6-226

FIGURE 6-23. INTERFACIAL TENSION FOR THE SODIUM CASEINATE-GALACTOMANNAN ATPS AS A FUNCTION OF THE TIE-LINE LENGTH (A). THE LOG-LOG PLOT (B) GIVES A STRAIGHT LINE. LBG=LOCUST BEAN GUM, TG=TARA GUM, GG=GUAR GUM, AND FG=FENUGREEK GUM..... 6-229

FIGURE 6-24. INTERFACIAL TENSIONS IN THE 4 WT% SODIUM CASEINATE-0.2 WT% GALACTOMANNAN (NACAS-GM) ATPS AS A FUNCTION OF NACAS ( $\Delta$ [NACAS], MARKED WITH "●") AND GM ( $\Delta$ [GM], MARKED WITH "○") CONCENTRATION DIFFERENCES BETWEEN THE EQUILIBRIUM PHASES. ....	6-229
FIGURE 6-25. PHASE DIAGRAM OF THE SODIUM CASEINATE-LOCUST BEAN GUM (NACAS-LBG) AND SODIUM CASEINATE-FENUGREEK GUM (NACAS-FG) ATPS WITH 15% TREHALOSE AND WITHOUT TREHALOSE. SYSTEMS INVESTIGATED ON INTERFACIAL TENSIONS ARE MARKED WITH "●". CRITICAL POINTS ARE MARKED WITH "x". A TIE-LINE AND ITS SLOPE (STL) IS GIVEN FOR EACH OF THE INVESTIGATED SYSTEMS. $STL_{AVG} = -0.23 \pm 0.02$ . ....	6-231
FIGURE 6-26. LOG-LOG APPARENT VISCOSITIES OF THE TOP (TP) AND BOTTOM (BP) PHASES OF THE SODIUM CASEINATE-GALACTOMANNAN (NACAS-GM) ATPS INVESTIGATED FOR THE EFFECTS OF GALACTOMANNAN TYPE AND SUGAR TYPE ON THE INTERFACIAL TENSION. LBG=LOCUST BEAN GUM, FG=FENUGREEK GUM. ....	6-231
FIGURE 6-27. INTERFACIAL TENSION FOR THE SODIUM CASEINATE-LOCUST BEAN GUM/FENUGREEK GUM (NACAS-LBG/FG) ATPS WITH AND WITHOUT TREHALOSE AS A FUNCTION OF THE TIE-LINE LENGTH (A). THE LOG-LOG PLOT GIVES A STRAIGHT LINE (B). GALACTOMANNANS ARE COMPARED AT THE SAME TREHALOSE CONCENTRATION. ....	6-233
FIGURE 6-28. INTERFACIAL TENSION FOR THE SODIUM CASEINATE-LOCUST BEAN GUM/FENUGREEK GUM ATPS (NACAS-LBG/FG) WITH AND WITHOUT TREHALOSE AS A FUNCTION OF THE TIE-LINE LENGTH (A). THE LOG-LOG PLOT (B) GIVES A STRAIGHT LINE. ATPS ARE COMPARED BY THE INDIVIDUAL GALACTOMANNAN TYPE AT DIFFERENT TREHALOSE CONCENTRATIONS. ....	6-234
FIGURE 6-29. INTERFACIAL TENSIONS IN THE SODIUM CASEINATE-LOCUST BEAN GUM/FENUGREEK GUM (NACAS-LBG/FG) ATPS AS A FUNCTION OF A NACAS AND LBG/FG CONCENTRATION DIFFERENCES IN THE EQUILIBRIUM PHASES. ATPS ARE COMPARED AT DIFFERENT TREHALOSE CONCENTRATIONS. ....	6-235
FIGURE 6-30. INTERFACIAL TENSIONS IN THE SODIUM CASEINATE-LOCUST BEAN/FENUGREEK GUM (NACAS-LBG/FG) ATPS AS A FUNCTION OF A NACAS AND LBG/FG CONCENTRATION DIFFERENCES IN THE EQUILIBRIUM PHASES. THE ATPS ARE COMPARED FOR THE GALACTOMANNAN TYPES. ....	6-236

## List of tables

### CHAPTER 2:

TABLE 2-1. INTERFACIAL TENSION VALUES OF PROTEIN-POLYSACCHARIDE AND SURFACTANT-POLYSACCHARIDE ATPS. * IF NOT STATED OTHERWISE, THE INTERFACIAL TENSION IS GIVEN AT ROOM TEMPERATURE.....	2—55
TABLE 2-2. APPROXIMATE MANNOSE : GALACTOSE RATIO ( $M : G_{approx}$ ), MOLECULAR WEIGHT ( $M_w$ ), INTRINSIC VISCOSITY ( $[\eta]$ ), PERSISTENCE LENGTH ( $L_p$ ), CHARACTERISTIC RATIO ( $C_\infty$ ) AND RADIUS OF GYRATION ( $R_g$ ).....	2—64
TABLE 2-3. STUDIES ON THE EFFECT OF SUGAR ON INDIVIDUAL PROTEINS/NACAS AND GALACTOMANNANS.....	2—68
TABLE 2-4. STUDIES ON THE EFFECT OF SUCROSE IN ATPS. ....	2—69

### CHAPTER 3:

TABLE 3-1. THE AQUEOUS TWO-PHASE SYSTEMS INVESTIGATED ON THEIR PHASE BEHAVIOUR. ....	3-78
TABLE 3-2. SODIUM CASEINATE-GALACTOMANNAN-SUGAR ATPS, BLENDS (1-3) AND PURE SOLUTIONS (4-6) INVESTIGATED ON FLOW. [NACAS], [GM] AND [SUGAR] ARE THE WEIGHT CONCENTRATIONS OF SODIUM CASEINATE, GALACTOMANNANS (LBG, TG, GG OR FG) AND SUGAR, RESPECTIVELY.....	3-93
TABLE 3-3. CALIBRATION OF THE OLYMPUS CZ-CTV MICROSCOPE WITHOUT 10 TIMES MAGNIFYING EYEPIECE AT VARIOUS MAGNIFICATION SCALES (PERSONAL COMMUNICATION WITH OURANIA GOUSETI).....	3-98
TABLE 3-4. AQUEOUS TWO-PHASE SYSTEMS INVESTIGATED ON THEIR INTERFACIAL PROPERTIES.....	3-100

### CHAPTER 4:

TABLE 4-1. PARAMETERS $A$ AND $B$ IN EQ. [3-3] AND THE SLOPES OF THE TIE-LINES (STL) FOR SYSTEMS 1-4. THE EQUATION OF THE PHASE CURVE IS $[GM] = a[NaCAS]^{-b}$ .....	4-114
TABLE 4-2. SYSTEMS INVESTIGATED ON THE EFFECT OF SUCROSE CONCENTRATIONS.....	4-117
TABLE 4-3. PARAMETERS $A$ AND $B$ OF THE PHASE CURVES WITH STANDARD FITTING ERRORS FOR SYSTEMS 1-4 WITH VARIOUS AMOUNTS OF SUCROSE. COEFFICIENTS OF DETERMINATION FOR BINODALS ARE $> 0.92$ . THE EQUATION OF THE PHASE CURVE IS $[GM] = a[NaCAS]^{-b}$ .....	4-118
TABLE 4-4. THE SLOPES OF THE TIE-LINES (STL) FOR SYSTEMS 1-4 WITH SUCROSE.....	4-121

TABLE 4-5. PARAMETERS *A* AND *B* WITH STANDARD FITTING ERRORS FOR THE PHASE CURVES OF SYSTEMS 1-4 WITH VARIOUS AMOUNTS OF TREHALOSE, GLUCOSE AND FRUCTOSE. COEFFICIENTS OF DETERMINATION FOR BINODALS ARE > 0.92. THE EQUATION OF THE PHASE CURVE IS  $[GM] = a[NaCAS]^{-b}$  ..... 4-129

TABLE 4-6. THE SLOPES OF THE TIE-LINES (STL) WITH STANDARD ERROR FOR SYSTEMS 1-4 WITH TREHALOSE, GLUCOSE AND FRUCTOSE..... 4-130

TABLE 4-7. DISTANCES BETWEEN THE CORRESPONDENT CRITICAL AND THRESHOLD POINTS FOR THE SYSTEMS OF LOCUST BEAN GUM/SODIUM-CASEINATE, AND GUAR GUM/SODIUM-CASEINATE. THE FOLLOWING EQUATION WAS USED IN THEIR CALCULATION  $\lambda_{sym} = \sqrt{([GM]_{crit} - [GM]_{thres})^2 + ([NaCAS]_{crit} - [NaCAS]_{thres})^2}$  ..... 4-131

TABLE 4-8. INVERSE DISTANCES BETWEEN THE CRITICAL AND THRESHOLD POINTS AND THE ORIGIN OF THE 2D SYSTEM FOR SYSTEMS 1-4 WITH TREHALOSE, GLUCOSE AND FRUCTOSE. THE FOLLOWING TWO EQUATIONS WERE USED IN THEIR CALCULATION  $\alpha_{crit} = \sqrt{[GM]_{crit}^2 + [NaCAS]_{crit}^2}$  AND  $\alpha_{thres} = \sqrt{[GM]_{thres}^2 + [NaCAS]_{thres}^2}$  ..... 4-132

**CHAPTER 5:**

TABLE 5-1. AQUEOUS TWO-PHASE SYSTEMS (ATPS) FROM WHICH EQUILIBRIUM PHASES WERE HARVESTED AND BLENDS WERE PREPARED. NACAS=SODIUM CASEINATE; GM=GALACTOMANNAN; LBG=LOCUST BEAN GUM; TG=TARA GUM; GG=GUAR GUM; FG=FENUGREEK GUM; R=RICH..... 5-139

TABLE 5-2. AQUEOUS TWO-PHASE SYSTEMS (ATPS) INVESTIGATED ON THEIR MICROSTRUCTURE AT QUIESCENT CONDITIONS AND UNDER SHEAR. ABSOLUTE VISCOSITIES OF THE EQUILIBRIUM PHASES OF THESE SYSTEMS ARE ALSO SHOWN..... 5-165

TABLE 5-3. POWER LAW PARAMETERS FOR THE RELATIONSHIP BETWEEN THE TOTAL BIOPOLYMER CONCENTRATIONS OF THE EQUILIBRIUM PHASES WITH THEIR APPARENT VISCOSITIES. .... 5-175

**CHAPTER 6:**

TABLE 6-1. INTERFACIAL TENSIONS OF DIFFERENT BLENDS ( $\phi_{GM} = \Phi = 20, 60$  AND  $80\%$ ) FOR A 4 WT% SODIUM CASEINATE-0.2 WT% LOCUST BEAN GUM SYSTEM AT 0% AND 30% OF SUCROSE. THE TABLE SHOWS THE VISCOSITIES OF THE EQUILIBRIUM PHASES AT THE SHEAR RATE OF  $0.001 \text{ S}^{-1}$  AND THEIR VISCOSITY RATIOS ( $\Lambda$ ).  $H_c$ = VISCOSITY OF THE CONTINUOUS PHASE,  $H_d$ =VISCOSITY OF THE DISPERSED PHASE,  $R_0$ =RADIUS OF A RETRACTED DROP,  $\Sigma$ =INTERFACIAL TENSION, AND  $T$ =AVERAGE RETRACTION TIME..... 6-196

TABLE 6-2. COMPOSITIONS OF THE SYSTEMS INVESTIGATED AT 20°C ON THE EFFECTS OF INDIVIDUAL BIOPOLYMER CONCENTRATIONS ON INTERFACIAL TENSIONS. THE TABLE ALSO SHOWS: VOLUME FRACTIONS ( $\Phi$ ), DENSITIES ( $\rho$ ), CONSISTENCY CONSTANTS ( $K$ ), POWER LAW INDEX ( $N$ ), AND AVERAGE VISCOSITIES ( $H_{AVG}$ ) OF THE INDIVIDUAL EQUILIBRIUM PHASES OF INVESTIGATED ATPS. .... 6-200

TABLE 6-3. CALCULATED INTERFACIAL TENSIONS ( $\Sigma$ ) AND THEIR AVERAGED VALUES FOR THE SODIUM CASEINATE-LOCUST BEAN GUM (NACAS-LBG) ATPS OF VARIOUS CONCENTRATIONS. THE TABLE ALSO GIVES THE RADII OF THE DROPLETS ( $R_0$ ) FROM WHICH THE INTERFACIAL TENSIONS WERE CALCULATED, THE APPARENT VISCOSITIES ( $H$ ) OF THE EQUILIBRIUM PHASES GIVEN FOR A SHEAR RATE OF  $0.001 \text{ S}^{-1}$  AND A TEMPERATURE OF 20°C, AS WELL AS THE CORRESPONDING VISCOSITY RATIOS ( $\Lambda$ ). ..... 6-205

TABLE 6-4. CALCULATED INTERFACIAL TENSIONS ( $\Sigma$ ) AND THEIR AVERAGED VALUES FOR THE SODIUM CASEINATE-LOCUST BEAN GUM (NACAS-LBG) ATPS OF VARIOUS CONCENTRATIONS. THE TABLE ALSO GIVES THE RADII OF THE DROPLETS ( $R_0$ ) FROM WHICH THE INTERFACIAL TENSIONS WERE CALCULATED, THE APPARENT VISCOSITIES (H) OF THE EQUILIBRIUM PHASES GIVEN FOR A SHEAR RATE OF 0.5 S <sup>-1</sup> AND A TEMPERATURE OF 20°C, AS WELL AS THE CORRESPONDING VISCOSITY RATIOS ( $\Lambda$ ). .....	6-205
TABLE 6-5. COMPOSITIONS OF A 4 WT% SODIUM CASEINATE-0.2 WT% LOCUST BEAN GUM-SUCROSE ATPS INVESTIGATED AT 20°C FOR THE EFFECTS OF SUCROSE CONCENTRATIONS ON THE INTERFACIAL TENSION. THE TABLE SHOWS: VOLUME FRACTIONS ( $\Phi$ ), DENSITIES (P), CONSISTENCY CONSTANTS (K), THE POWER LAW INDEX (N) AND AVERAGE VISCOSITIES ( $H_{AVG}$ ) OF THE INDIVIDUAL EQUILIBRIUM PHASES OF THE INVESTIGATED ATPS.....	6-211
TABLE 6-6. CALCULATED INTERFACIAL TENSIONS FOR THE 4 WT% SODIUM CASEINATE-0.2 WT% LOCUST BEAN GUM (NACAS-LBG) ATPS AT DIFFERENT SUCROSE CONCENTRATIONS. THE TABLE ALSO GIVES THE RADII OF THE DROPLETS ( $R_0$ ) FROM WHICH THE INTERFACIAL TENSIONS WERE CALCULATED, THE APPARENT VISCOSITY OF THE EQUILIBRIUM PHASES AT THE SHEAR RATE OF 0.001 S <sup>-1</sup> AND 20°C(H), AS WELL AS THE VISCOSITY RATIO ( $\Lambda$ ). .....	6-214
TABLE 6-7. CALCULATED INTERFACIAL TENSIONS FOR THE 4 WT% SODIUM CASEINATE-0.2 WT% LOCUST BEAN GUM (NACAS-LBG) ATPS WITH DIFFERENT SUCROSE CONCENTRATIONS. THE TABLE ALSO GIVES THE RADII OF THE DROPLETS ( $R_0$ ) FROM WHICH THE INTERFACIAL TENSIONS WERE CALCULATED, THE APPARENT VISCOSITY OF THE EQUILIBRIUM PHASES AT THE SHEAR RATE OF 0.5 S <sup>-1</sup> AND 20°C(H), AS WELL AS THE VISCOSITY RATIO ( $\Lambda$ ).....	6-214
TABLE 6-8. COMPOSITIONS OF SYSTEMS INVESTIGATED AT 20°C ON THE EFFECTS OF SUGAR TYPE ON INTERFACIAL TENSION. THE TABLE ALSO SHOWS: VOLUME FRACTIONS ( $\Phi$ ), DENSITIES (P), CONSISTENCY CONSTANTS (K), POWER LAW INDEX (N) AND AVERAGE VISCOSITIES ( $H_{AVG}$ ) OF THE INDIVIDUAL EQUILIBRIUM PHASES.....	6-219
TABLE 6-9. CALCULATED INTERFACIAL TENSIONS ( $\Sigma$ ) AND THEIR AVERAGES FOR THE SODIUM CASEINATE-LOCUST BEAN GUM (NACAS-LBG) ATPS WITH VARIOUS SUGARS. THE TABLE ALSO GIVES THE RADII OF THE DROPLETS ( $R_0$ ), THE APPARENT VISCOSITIES (H) OF THE EQUILIBRIUM PHASES AT THE SHEAR RATE OF 0.001 S <sup>-1</sup> AND TEMPERATURE OF 20°C, AS WELL AS THE VISCOSITY RATIOS ( $\Lambda$ ). .....	6-221
TABLE 6-10. CALCULATED INTERFACIAL TENSIONS ( $\Sigma$ ) AND THEIR AVERAGES FOR THE SODIUM CASEINATE-LOCUST BEAN GUM (NACAS-LBG) ATPS WITH VARIOUS SUGARS. THE TABLE ALSO GIVES THE RADII OF THE DROPLETS ( $R_0$ ), THE APPARENT VISCOSITIES (H) OF THE EQUILIBRIUM PHASES AT THE SHEAR RATE OF 0.5 S <sup>-1</sup> AND TEMPERATURE OF 20°C, AS WELL AS THE VISCOSITY RATIOS ( $\Lambda$ ). .....	6-221
TABLE 6-11. COMPOSITIONS OF SYSTEMS INVESTIGATED AT 20°C ON THE EFFECTS OF GALACTOMANNAN-TYPE ON INTERFACIAL TENSIONS. THE TABLE SHOWS: VOLUME FRACTIONS ( $\Phi$ ), DENSITIES (P), CONSISTENCY CONSTANTS (K), POWER LAW INDEX (N) AND AVERAGE VISCOSITIES ( $H_{AVG}$ ) OF THE INDIVIDUAL EQUILIBRIUM PHASES. LBG=LOCUST BEAN GUM, TG=TARA GUM, GG=GUAR GUM AND FG=FENUGREEK GUM.....	6-227
TABLE 6-12. CALCULATED INTERFACIAL TENSIONS ( $\Sigma$ ) AND THEIR AVERAGES ( $\Sigma_{AVG}$ ) FOR THE SODIUM CASEINATE-GALACTOMANNAN (NACAS-GM) ATPS. THE TABLE ALSO GIVES RADII OF DROPLETS ( $R^0$ ), APPARENT VISCOSITIES (H) OF THE EQUILIBRIUM PHASES AT THE SHEAR RATE OF 0.001 S <sup>-1</sup> AND TEMPERATURE OF 20°C AND VISCOSITY RATIOS ( $\Lambda$ ). LBG=LOCUST BEAN GUM, TG=TARA GUM, GG=GUAR GUM; FG=FENUGREEK GUM. ....	6-227
TABLE 6-13. CALCULATED INTERFACIAL TENSIONS ( $\Sigma$ ) AND THEIR AVERAGES ( $\Sigma_{AVG}$ ) FOR THE SODIUM CASEINATE-GALACTOMANNAN (NACAS-GM) ATPS. THE TABLE ALSO GIVES RADII OF DROPLETS ( $R^0$ ), APPARENT VISCOSITIES (H) OF THE EQUILIBRIUM PHASES AT THE SHEAR RATE OF 0.5 S <sup>-1</sup> AND TEMPERATURE OF 20°C AND VISCOSITY RATIOS ( $\Lambda$ ). LBG=LOCUST BEAN GUM, TG=TARA GUM, GG=GUAR GUM; FG=FENUGREEK GUM. ....	6-228

TABLE 6-14. CALCULATED INTERFACIAL TENSIONS FOR THE 4 WT% SODIUM CASEINATE-0.2 WT% LOCUST BEAN GUM/FENUGREEK GUM ATPS WITHOUT SUGAR AND AT 15% TREHALOSE. THE TABLE ALSO GIVES THE RADII OF THE RETRACTED DROPLETS ( $R_0$ ), THE APPARENT VISCOSITIES (H) OF THE EQUILIBRIUM PHASES FOR THE SHEAR RATE OF  $0.001\text{S}^{-1}$  AND  $20^\circ\text{C}$ , AS WELL AS THE VISCOSITY RATIOS ( $\Lambda$ ) ..... 6-232

TABLE 6-15. CALCULATED INTERFACIAL TENSIONS FOR THE 4 WT% SODIUM CASEINATE-0.2 WT% LOCUST BEAN GUM/FENUGREEK GUM ATPS WITHOUT AND WITH 15% TREHALOSE. THE TABLE ALSO GIVES THE RADII OF THE RETRACTED DROPLETS ( $R_0$ ) , THE APPARENT VISCOSITIES (H) OF THE EQUILIBRIUM PHASES FOR THE SHEAR RATE OF  $0.5\text{ S}^{-1}$  AND  $20^\circ\text{C}$ , AS WELL AS THE VISCOSITY RATIOS ( $\Lambda$ ) ..... 6-232

# CHAPTER 1: INTRODUCTION

## 1.1 BACKGROUND

The food industry continually increases the demand for novel products by means of innovation and advertising. New textures are explored daily by thermal and mechanical treatments of various formulations, which are commonly mixtures of biopolymers, taste additives and oils (Jourdain et al., 2008; Perrechil and Cunha, 2011). In order to produce novel textures, increase ingredient flexibility and cater for consumer needs, the industry requires an understanding of the structure building mechanisms, the ingredients and their interactions during processing (Norton and Frith, 2001; Granger et al., 2005). The research covered in this work aims to provide a better understanding of the role of cosolutes, namely common sugars, in the microstructure evolution of mixed nongelling biopolymer mixtures in quiescent conditions and under shear.

Phase separation—demixing of components—is a basic thermal and mechanical process of texturisation during food processing and food digestion. It is inherent to all foods that contain mixtures of biopolymers and it occurs in three stages, which are:

- (i) liquid-liquid phase separation that typically concludes in the formation of a two-phase system or a water-in-water (W/W) emulsion<sup>1</sup>;
- (ii) deformation of the W/W emulsions under shear, which concludes in formation of a plethora of structures, which can be fixed to produce novel textures; and

---

<sup>1</sup> Emulsions are mixtures of immiscible liquids with droplets of one phase dispersed in the other.

(iii) adsorption of other components (fats and small molecular solutes) to the interfaces between the immiscible aqueous phases; the extent and strength of which is controlled by the interactions between the components (Tolstoguzov, 2006).

Upon mixing, proteins and polysaccharides form two distinct microstructures: (i) a homogenous system or (ii) a heterogeneous phase separated system. The type of microstructure formed depends on the thermodynamic compatibility of the components—the strength of intermolecular association, and the concentration and size of each of the ingredients (Tolstoguzov, 1999). In a heterogeneous system, the type of phase separation is determined by the difference in distribution of the macromolecules between the phases (Rodríguez Patino and Pilosof, 2011). For example, uncharged or similarly charged molecules associate minimally and—similar to the basic incompatible system of oil and water—readily demix into equilibrium phases, where one of the phases is enriched in one biopolymer and depleted of the other, and vice versa (Piculell and Lindman, 1992). These systems are referred to as aqueous two-phase systems (ATPS).

The properties of the equilibrium phases in ATPS are determined by their major component. In the case of different average molecular weights ( $M_w$ ) of the biopolymers in ATPS, the phase containing the biopolymer of a greater  $M_w$  is more concentrated, and hence more viscous. The component found in the largest quantity in both equilibrium phases is water, which gives the phases very similar densities and refractive indices, no problems with sedimentation and creaming, and makes the phases impossible to be

completely separated without ultracentrifugation (Frith, 2010).

The structural characteristics of ATPS—an example of which are mixtures of proteins and polysaccharides—are also determined by applied shear and their interfacial properties. In the past two decades, advances in rheoptics have made it possible to observe directly the microstructure evolution in flow (Pacek et al., 1994; Stokes et al., 2001; Wolf and Frith, 2003) and to measure the interfacial properties based on dynamic observation of the interfaces (Guido and Villone, 1999; Van Puyvelde et al., 2002; Antonov et al., 2004). These studies give a better understanding of these systems.

Although different in many aspects, the flow behaviour of ATPS is commonly equated to oil-in-water (O/W) emulsions. Under shear, previously spherical droplets of the dispersed phase deform and break. If the continuous phase is more viscous than the dispersed phase, droplet deformation evolves like “spinneret-less spinning” and concludes in the formation of a variety of typically thread-like structures. These flow differently from conventional emulsions (Wolf and Frith, 2003; Tolstoguzov, 2006).

Under certain conditions the phase sense of the system changes—that is the dispersed phase inverts and becomes continuous. Inversion happens either when the volume fraction of one of the phases is increased sufficiently, or when the system with a more viscous continuous phase is sufficiently sheared (Efthimiadu and Moore, 1994; Spyropoulos et al., 2010). Phase inversion in ATPS or W/W emulsions is—compared to O/W emulsions—slow (Pacek et al., 2001).

Interfacial tension is an important parameter in processing of ATPS and its quantification is vital for controlled structuring at the microscale, by which the product's performance can be manipulated and designed. The interfacial layer in ATPS is permeable, depleted of biopolymers (it is composed of water) and decreases in thickness with an increase in the total biopolymer concentration (Scholten et al., 2006b). The characteristics of the interface influence both the process of liquid-liquid phase separation (the equilibrium state) and the evolution of structures under flow (easy deformation and coalescence). The inherently low interfacial tension of ATPS also enables the adsorption of interfacially active substances, such as lipids (e.g., oils) to these interfaces, or allows the changes in interfacial thickness to occur through bulk interactions (in the case of sugars) (Tolstoguzov, 2006).

Dairy food formulations, such as ice cream mixes, usually contain the following ingredients: a ubiquitous dairy protein—sodium caseinate (NaCAS)—a stabiliser—typically one of the galactomannans (GM, Petkowicz et al., 1998), sugar—added in substantial amounts for taste—and fat. Similarly, to the mixture containing NaCAS and GM, the mixture of NaCAS, GM and fat would have an inherent tendency to phase separate into distinct bulk equilibrium phases. The mechanisms by which the coarsening would occur, the structures formed at the fat-water interface as well as the compositions of the equilibrium phases would be however, different (Goff, 2002). In our work, however, we exclude fat for the sake of simplicity and in order to study the effect of sugars on a NaCAS-GM ATPS, which is principally responsible for the structure of dairy mixes. Sugar (namely sucrose) causes a change in the solvent property and affects both NaCAS and GM individually (Richardson et al., 1998; Antipova et al., 1999;

Belyakova et al., 2003). Besides sucrose, other commonly used sugars (trehalose, glucose and fructose) also affect the individual macromolecular mechanisms, change the thermal stability, conformation, self-association properties, surface activity and alter the associations between proteins and polysaccharides in the bulk in a similar way, but to a different extent (Semenova et al., 2002; Doyle et al., 2006). The effect of sucrose on phase behaviour and rheological behaviour was confirmed previously for several other model protein-polysaccharide ATPS (Schorsch et al. 1999a, 1999b, 2000a, 2000b, Capron et al., 2001), but was not studied on NaCAS-GM ATPS.

## **1.2 AIM AND OBJECTIVES**

The overall aim of this work is to gain a better understanding of the process of texturisation in model NaCAS-GM mixtures in the presence of high levels of sugar using visual assessment, microscopy and optical rheometry. Four model ATPS: NaCAS-LBG (System 1, LBG=locust bean gum), NaCAS-TG (System 2, TG=tara gum), NaCAS-GG (System 3, GG=guar gum) and NaCAS-FG (System 4, FG=fenugreek gum) were studied on the effects of sugar concentrations (up to 60 wt%) and types (sucrose, trehalose, glucose and fructose).

To achieve the aims of this work, the following tasks were formulated:

- (i) Characterise the effect of sucrose, trehalose, glucose and fructose concentration on the phase equilibria of the model systems at 20°C and pH 5.8 (Chapter 4).
- (ii) Establish the rheology and structure/composition dependence in the

model system containing sugars, and study the effect of temperature, sugar concentration, type of sugar and type of galactomannan on the flow of ATPS (Chapter 5).

(iii) Determine the interfacial properties of the model systems as a function of concentration and type of biopolymers and sugars (Chapter 6).

### 1.3 LAYOUT OF THE THESIS

The thesis consists of seven chapters: Chapter 1, briefly introduces the research topic and lays out the thesis structure. Chapter 2 reviews the relevant literature on the topics of phase equilibria, rheology and interfacial properties of ATPS and reviews the individual components of the model systems. Chapter 3 explains the experimental setup. The latter chapter focuses on the studies of: (i) phase behaviour, (ii) rheological behaviour with microstructure, and (iii) interfacial properties.

Chapters 4–6 are experimental chapters; Chapter 4 reviews and discusses the phase equilibria results of Systems 1–4 with the addition of sucrose, trehalose, glucose and fructose. Phase diagrams were obtained, and tie-lines and characteristic theoretical points of the phase diagrams were used to evaluate the effect of sugars on the molecular compatibility of the systems. Chapter 5 reviews the flow properties of the equilibrium phases, pure solutions and their blends, and investigates how they are affected by temperature, biopolymer concentration, sugar concentration and sugar type. This chapter also reviews the microstructure of the ATPS under quiescent conditions and under shear. Chapter 6 reports the interfacial tensions of the systems as a function of

biopolymer concentration, galactomannan type, sugar concentration and sugar type, calculated by the drop retraction method. Each experimental chapter ends with a conclusion.

Finally, Chapter 7 sums up the conclusions drawn on the basis of the experimental work, recommends future improvements and proposes possible application of the findings.

## 1.4 PAPERS AND PRESENTATIONS

The results of this study have been published as follows:

1. Portschi, A., Spyropoulos, F. and Norton, I.T., Phase equilibria and rheological behaviour of polysaccharide/protein mixtures in the presence of sugars. Proceedings of the 5<sup>th</sup> International Symposium on Food Rheology and Structure 2009, Pages 302–305.
2. Portschi, A., Spyropoulos, F. and Norton, I. T., Phase equilibria and rheological behaviour of polysaccharide-protein aqueous solutions with sugar. In: Gums and Stabilisers for the Food Industry 15, Eds: P. A. Williams and G. O Philips, RSC Publishing, 2010, Pages 293–246.
3. Spyropoulos, F., Portschi, A. and Norton, I.T., Effect of sucrose on the phase and flow behaviour of polysaccharide/protein aqueous two-phase systems, Food Hydrocolloids, Volume 24, Issues 2–3, March–May 2010, Pages 217–226.
4. Spyropoulos, F., Portschi, A. and Norton, I.T., Effect of sugars on the phase and flow behaviour of polysaccharide/protein aqueous two-phase systems, 5<sup>th</sup> World Congress of Emulsions conference proceeding (digital copy 0134, 6 pgs.), 2010, Lyon.
5. Portschi, A., Spyropoulos, F. and Norton, I.T., Effect of sugars on the phase behaviour, flow and interfacial properties of protein/polysaccharide aqueous two-phase systems, 11th Congress on Engineering and Food conference proceeding (digital copy, 6 pgs.), 2011, Athens.

Finally, the results of this study have been presented as follows:

1. Portschi, A., Spyropoulos, F. and Norton, I.T., Phase equilibria and flow behaviour of aqueous protein-polysaccharide mixes in the presence of sucrose. Presented at: First European food conference: food production, nutrition, healthy consumers, Ljubljana, Slovenia, 6/11/2008.
2. Portschi, A., Spyropoulos, F. and Norton, I.T., Phase equilibria and rheological behaviour of protein-polysaccharide solutions with sugars. Presented at: The 5th International symposium on rheology and food structure, Zurich, Switzerland, 17/6/2009.
3. Portschi, A., Spyropoulos, F. and Norton, I.T., Phase equilibria and rheological behaviour of protein-polysaccharide solutions with sugars. Presented at: 15th Gums and stabilisers for the food industry conference, Wrexham, UK, 23/06/2009.
4. Portschi, A., Spyropoulos, F. and Norton, I.T., Effect of sugars on the phase and flow behaviour of polysaccharide-protein aqueous two-phase systems. Poster presentation at: The 5th World Congress on Emulsions, Lyon, France, 14/10/2010.
5. Spyropoulos, F., Portschi, A. and Norton, I.T., Effect of sugars on the phase behaviour, flow and interfacial properties of protein/polysaccharide aqueous two-phase systems. Presented at: 11th Congress on Engineering and Food, Athens, Greece, 22–26/05/2011.

## CHAPTER 2: LITERATURE REVIEW

### 2.1 Introduction

Dairy convenience emulsion-based foods are composed mainly of proteins, polysaccharides and sugars, which give them nutrition, structure and taste. Depending on the concentration of these components, these foods can be either homogenous or phase separated. In the latter, two separate phases are formed due to the thermodynamic incompatibility of the constituent proteins and polysaccharides, and such systems are called aqueous two-phase systems (ATPS). Sugars added to the ATPS affect the functional properties of the macromolecules contained in the system, and in turn change the phase behaviour, rheological behaviour and interfacial properties of these systems, which determine the phase morphology and overall structure of ATPS.

Accordingly, the following literature review covers the topics of:

1. Phase separation: the thermodynamic approach, description of a phase diagram, a brief overview of the factors influencing phase behaviour and various phase separation morphologies;
2. Rheological behaviour of pure and multicomponent biopolymer systems, with special emphasis on (i) comparison of water-in-water (W/W or ATPS) emulsions to conventional oil-in-water (O/W) emulsions and (ii) various shear-induced morphologies and events in these ATPS;

3. Interfacial properties of ATPS as well as the techniques and drop deformation models applied in the measurement and calculation of very low interfacial tensions;
4. An introduction to the structural and functional properties of the individual ingredients, GM and NaCAS, and how they are affected by sugars, either individually or when in ATPS.

## **2.2 Phase behaviour of aqueous two-phase systems**

### **2.2.1 Phase separation studies**

Biopolymers have been characterised by their low cosolubility (Beijerink, 1910) and readiness to separate into phases (Tolstoguzov, 1996). The process of phase separation is applied in bioseparation (Albertsson and Frick, 1960) and is important for the creation of structures in formulated foods. These structures determine characteristics such as texture, consistency, stability, flavour release, mouthfeel and/or spreadability (Polyakov et al., 1986; Norton and Frith, 2001; Tolstoguzov, 2003).

The phase behaviour of ATPS has been extensively investigated both experimentally and theoretically. Experimentally, it has been studied in model biopolymer mixtures and real foods such as extrudates, dough, ice cream mixes, low-fat spreads and beverages (Tolstoguzov, 2002). Many authors have studied phase separation equilibria under various environmental conditions (Antonov et al., 1977; Tolstoguzov, 1999). Only few, however, have assessed the kinetics of phase separation, which gives an understanding of the timescales and lengthscales of molecular ordering

and enables the creation of new structures by means of applied shear and temperature (Lorén, 2001; Norton and Frith, 2001; Wolf and Frith, 2003; Tolstoguzov, 2006; Dickinson, 2008). Theoretically, a thermodynamic approach and computer modelling are used to further quantify phase equilibria and to understand the underlying physical processes of macromolecular ordering (Semenova and Dickinson, 2010).

Research on the phase behaviour of ATPS has shown that phase separation occurs due to the thermodynamic instability of mixed biopolymers through the processes of coalescence caused by depletion flocculation and Brownian motion of protein aggregates (Bourriot et al., 1999). Various types of phase separation morphologies are formed based on the compatibility of the mixed biopolymers, i.e., the type of biopolymer A-biopolymer B, biopolymer A (B)-biopolymer-A (B) and biopolymer A (B)-solvent interactions. The compatibility of the mixed biopolymers is altered further by cosolutes, which interact with water and the biopolymers, thus changing biopolymer-solvent interactions. Moreover, the biopolymer concentration, the  $M_w$  of the biopolymers, and their hydrophilicity determine the degree to which they compete for water and the way in which water is redistributed between the phases (Polyakov et al., 1985b).

### **2.2.2 Thermodynamic approach**

The thermodynamic approach studies the behaviour of molecules in solution. It quantitatively explains molecular interactions such as solubility, self-association, phase separation, adsorption to interfaces and surface interactions by applying the ideas of

energy transformation and dynamic equilibrium. This approach is, however, unable to predict accurately the behaviour of the biopolymer mixtures due to their intrinsic complexity and difficulties in obtaining the experimental data needed for the calculations (Semenova and Dickinson, 2010). The following subsections introduce the general ideas of the free energy of mixing,  $\Delta G_{mix}$  (§ 2.2.2.1), chemical potential,  $\mu_i$  (§ 2.2.2.2) and the theoretical models most commonly applied in studies on phase behaviour (§ 2.2.2.2, § 2.2.2.3 and § 2.2.2.3).

### 2.2.2.1 Gibbs free energy of mixing

The Gibbs free energy of mixing ( $\Delta G_{mix}$ ) is a thermodynamic variable that determines the miscibility of biopolymers in solution.  $\Delta G_{mix}$  of a closed system is a measure of the internally stored available energy of the system to perform a change and represents a balance between the changes in entropy ( $\Delta S_{mix}$ ) and enthalpy ( $\Delta H_{mix}$ ):

$$\Delta G_{mix} = \Delta H_{mix} - T\Delta S_{mix} \quad [2-1]$$

$\Delta G_{mix}$  is determined by the meeting point of the growing  $\Delta H_{mix}$  and falling  $\Delta S_{mix}$ . If  $\Delta G_{mix} \leq 0$ , the system will mix, but if  $\Delta G_{mix} > 0$ , the system will phase separate.  $\Delta H_{mix}$ , a measure of the total energy of the system, is positive and favours demixing; hence,  $\Delta S_{mix}$  is more important in the determination of the overall free energy of the system (Semenova and Dickinson, 2010).

In a mixed biopolymer solution,  $\Delta S_{mix}$  is a measure of the molecular disorder and either remains constant or increases. The third law of thermodynamics provides the

zero reference point for its calculation (the so-called quasi-crystalline approach claiming that  $\Delta S_{mix}$  of the system at absolute zero is zero). In non-ideal irregular biopolymer systems (e.g., biopolymer-solvent solutions),  $\Delta S_{mix}$  is smaller than in an ideal system due to presence of larger molecules and as a result of a reduction in the number of possible arrangements between the molecular species of different sizes and different affinities for the solvent.  $\Delta H_{mix}$  dominates. Hence, it is more common for such systems to demix. Consequently, in the non-ideal irregular polymer solutions— $\Delta S_{mix}$  and  $\Delta H_{mix}$  deviate from ideal behaviour— $\Delta G_{mix}$  depends on  $T\Delta S_{mix}$  term and  $\Delta H_{mix}$ , which differs from 0. In ideal small molecular solutions (e.g., cosolute-solvent solutions),  $\Delta S_{mix}$  is large and positive, hence  $\Delta G_{mix}$  is negative and the solutes mix (Çengel and Boles, 2007; Frith, 2010; Semenova and Dickinson, 2010).

### **2.2.2.2 Partial molar Gibbs energy (chemical potential) and the effect of solvent quality on cosolubility of molecular species**

Chemical potential is a thermodynamic variable expressed as a sum of functions dependant on temperature (T) and pressure (p) on one hand, and composition ( $m_i$ ) on the other. It describes a change in the energy of a system when an increment of a molecular species is introduced to this system (Semenova and Dickinson, 2010).

The chemical potential of a biopolymer mixture of two biopolymer species and a solvent is determined by a second virial coefficient as follows:

$$\mu_i = \mu_i^0 + RT(\ln(m_i / m^0) + (A_{11}m_1 + A_{12}m_2)) \quad [2-2]$$

$$\mu_2 = \mu_2^0 + RT(\ln(m_2 / m^0) + (A_{22}m_2 + A_{12}m_2)) \quad [2-3]$$

$$\mu_s = \mu_s^0 - (RT/m_s)(m_1 + m_2 + 1/2(A_{11}m_1^2 + A_{22}m_2^2) + A_{12}m_1m_2) \quad [2-4]$$

where subscript 1 belongs to "biopolymer A", 2 to "biopolymer B" and s to the solvent.  $\mu_i^0$  is a standard chemical potential,  $m^0$  is the standard molal concentration,  $m_i$  is the molal concentration of the component  $i$ ,  $A_{11}$  and  $A_{22}$  are the molal second virial coefficients characterising interactions between the molecules of the same molecular species and  $A_{12}$  is the cross second virial coefficient that characterises the interactions between different molecular species (Antipova et al., 1999).

The second virial coefficients  $A_{12}$ ,  $A_{11}$ , and  $A_{22}$  can be measured experimentally. They largely determine the outcome of mixing of the biopolymers in the solution. Under  $\Theta$  solvent conditions the biopolymer chains act like an ideal random walk. Under these conditions biopolymer segments do not interact and no heat is either emitted or absorbed upon mixing of the biopolymers, which makes the system stable,  $A_{12} = 0$ , and the solution miscible (Richardson et al., 1998). If the solvent conditions deviate from the ideal, however,  $A_{12}$  deviates from 0 and phase separation occurs: at  $A_{12} > 0$ , systems phase separate by segregation and at  $A_{12} < 0$  by association. The same goes for  $A_{11}$  and  $A_{22}$  (Antipova et al., 1999).

### **2.2.2.3 Flory-Huggins lattice model and the effect of solvent quality on cosolubility of molecular species**

The Flory-Huggins lattice model explains the general features of phase separation in ATPS. It is especially effective in offering a solid qualitative explanation of uncharged

biopolymer mixtures, but it fails to sufficiently describe highly polydisperse systems with different  $M_w$ , high charges and pronounced secondary and tertiary molecular structures with limited flexibility of movement (Schorsch et al., 2000a; Dickinson, 2010).

The model makes the following assumptions: (i) the composition of the bulk and the local compositions are the same, (ii) molecules are flexible uncharged “random walks”, where each molecular segment is free to move in a 2D lattice, (iii) either solvent molecule or a biopolymer molecule occupies each lattice site and (iv) molecules interact only with the nearest neighbour pair.

The first version of a model that provides a thermodynamic description of the behaviour of one polymer in solution was later extended to describe the behaviour of more than one polymer in solution. The Flory-Huggins model expands the usual thermodynamic  $\Delta G_{mix}$  equation [2-1] by taking into account the difference in the molecular size of the biopolymers as the driving force for phase separation, which results in the following expression of the Gibbs free energy of mixing:

$$\Delta G_{mix} = RT((n_1 \ln \varphi_1 + n_2 \ln \varphi_2 + n_s \ln \varphi_s) + (\chi_{12}\varphi_1\varphi_2 + \chi_{1s}\varphi_1\varphi_s + \chi_{2s}\varphi_2\varphi_s)(m_1^v n_1 + m_2^v n_2 + m_s^v n_s)) \quad [2-5]$$

where  $R$  is the gas constant (reciprocal of the Boltzmann constant  $kN_A$ ),  $n_i$  is the number of moles of the component,  $\varphi_i$  is the volume fraction of the component,  $\chi_{ij}$ <sup>2</sup> is the Flory-Huggins interaction parameter between the components,  $m_i^v$  is the ratio of the molar volume:  $m_1^v + m_2^v + m_s^v = V_1/V_s + V_2/V_s + V_s/V_s = 1$ , where 1 is biopolymer A, 2 is biopolymer B

---

<sup>2</sup>  $\chi_{ij}$  represents free energy for the formation of contacts between segments of the components/molecules.

and *s* is the solvent (Flory, 1953; Hsu and Prausnitz, 1974).

The theory assumes that two polymers of a different nature and size in the absence of solvent demix and that if sufficient quantity of solvent is provided they always mix. The equation [2-5] shows that  $\Delta G_{mix} \propto \chi_{ij}, N_i, \varphi_i^2, (T, p) - \Delta S_{mix} \propto N_i, \varphi_i$  and  $\Delta H_{mix} \propto N_i, \varphi_i, \chi_{ij}$ —where  $N_i$  is the number of molecules and equals to  $\varphi_i V_s / V_i$ .  $\Delta G_{mix}$  therefore depends on the number, size and the space (size of lattice) available for the molecules to move in ( $N_i$  and  $\varphi_i$ ) and also on the interactions between the segments of the biopolymers, and the biopolymers and the solvent.

An example of the use of this model is provided by theoretical work by Scott and Tompa (1949, cited by Zeman and Patterson, 1972, p. 513) who attribute the incompatibility of the polymers to the unfavourable interactions among them ( $\chi_{12} > 0$ ). Their prediction was later corrected by Zeman and Patterson (1972) who found that phase separation is strongly promoted by any asymmetry in the polymer-solvent interaction ( $\chi_{1s} \neq \chi_{2s}$ ) to the extent that even a solution where  $\chi_{12} = 0$  phase separates. Hsu and Prausnitz (1974), in their theoretical work, also showed the effect of interaction parameters and  $M_w$  on polymer compatibility. For example, Figure 2-1, taken from their work, is a mathematical representation of the phase separation of a ternary mixture for polymer components of: (a) equal  $M_w$  and (b) disparate  $M_w$ , both at changing polymer-solvent interaction parameters  $\chi_{is}$ .

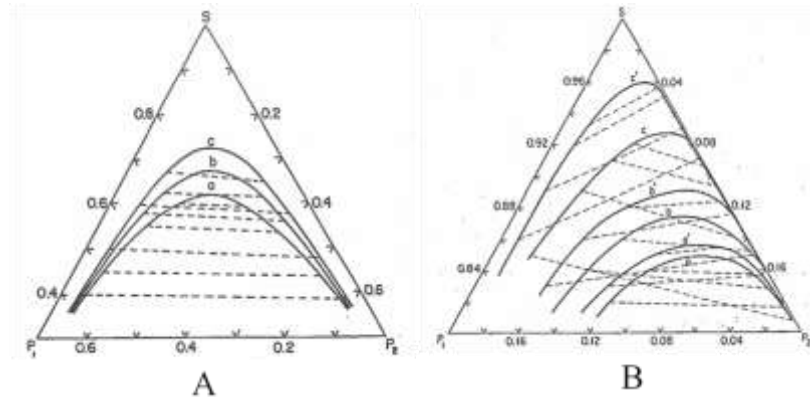


**Figure 2–1. Binodals for a solvent-polymer 1-polymer 2 system (A)  $m_1 = m_2 = 1000$ ,  $m_s = 1$ ,  $\chi_{12} = 0.004$ , and  $\chi_{1s}$  and  $\chi_{2s} =$  (a) 0.1, 0.16, (b) 0.3, 0.36, (c) 0.4, 0.46. (B)  $m_1 = 4000$ ,  $m_2 = 250$ ,  $m_s = 0.02$ , and  $\chi_{1s}$  and  $\chi_{2s}$  are: (a) 0.1, 0.15, (a') 0.15, 0.1, (b) 0.2, 0.3, (c) 0.3, 0.45, (c') 0.45, 0.3 (Source: Hsu and Prausnitz, 1973, p. 322).**

The polymer-solvent interaction parameter  $\chi_{is}$  by Flory determines the quality of the solvent.  $\chi_{is} > 0.5$  defines a good solvent. At  $\chi_{is} = 0.5$  (in so-called  $\Theta$  conditions<sup>3</sup>) the solvent and segments of the polymer chain are thermodynamically stable, but when  $\chi_{is} < 0.5$ , polymer segments attract each other; under these conditions, polymers aggregate and precipitate and systems are unstable (Richardson et al., 1998).

#### **2.2.2.4 Depletion model and the effect of solvent quality on the cosolubility of molecular species**

The depletion model is another model that adequately explains the phase separation of systems of non-adsorbing polymers and colloidal particles (Hoskins et al., 1996; Jenkins and Snowden, 1996; Tuinier et al., 2003; Radford et al., 2004). The model is based on Pauli's exclusion principle and is applied to molecules. The model

<sup>3</sup> A polymer chain dissolved in the  $\Theta$  (theta) solvent behaves like an ideal chain. The ideal chain is modelled as a random walk chain. The model neglects any kind of interaction between the segments of that chain.

determines the depletion potential by the existence of the excluded volume<sup>4</sup> of a polymer coil/segment, which is greatly affected by solvent quality (Wang et al., 2001). Brownian motion causes dispersed molecules of one species surrounded with depletion zones to approach and the solvent to migrate from the overlap zones ( $V_{overlap}$ ) to the bulk of the solution due to the difference in osmotic pressure ( $\Pi$ ), shown in Figure 2-2 (de Kruif and Tuinier, 2000; McClements, 2000). In this way, the system minimises the excluded volume ( $V_{excluded}$ ) and becomes more stable.  $V_{excluded}$  is decreased by molecular compaction, flocculation and aggregation. A reduction of steric freedom and the repulsion of molecules increases  $\Delta S_{mix}$  and decreases  $\Delta H_{mix}$ . Consequently,  $\Delta G_{mix}$  is minimised, which makes the system stable (Rivas et al., 2004). By depletion flocculation,  $\Delta G_{mix}$  is reduced by the factor that equals the product of the osmotic pressure and the overlap volume of the depletion zones,  $\Pi V_{overlap}$  (Wang et al., 2001). As such,  $\Delta G_{mix}$  can be lowered by an increase in  $V_{overlap}$ ,  $V_{excluded}$  and  $\Pi \propto T, p, m_i$ , where  $m_i$  is the molar concentration of the solute in solution. Both variables can be obtained experimentally.

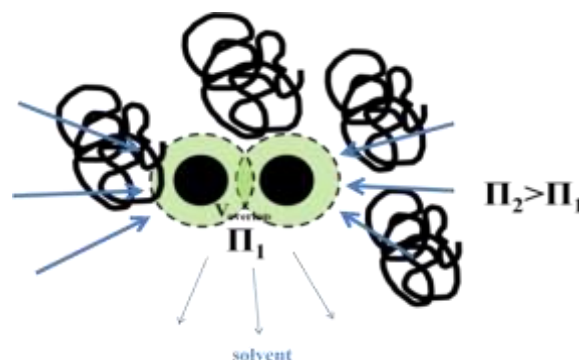


**Figure 2-2. Depletion flocculation for a system of colloidal particles and polymer coils.  $\Pi$  is the osmotic pressure of the solute. Light green indicates the depletion zones (excluded volume) and dark green indicates the overlap volume (Addapted by: de Kruif and Tuinier, 2000, p. 197).**

<sup>4</sup> The excluded volume of a molecule or a segment is the volume unavailable to the centre of mass of any other molecule or segment.

### 2.2.3 Phase diagrams

Phase separation phenomena are quantified by phase diagrams, which for various thermodynamically incompatible biopolymer systems, show miscible and immiscible regions (Koningsveld et al., 2001). For ATPS, typically two-dimensional composition phase diagrams are used. Figure 2-3 provides a schematic of a phase diagram.

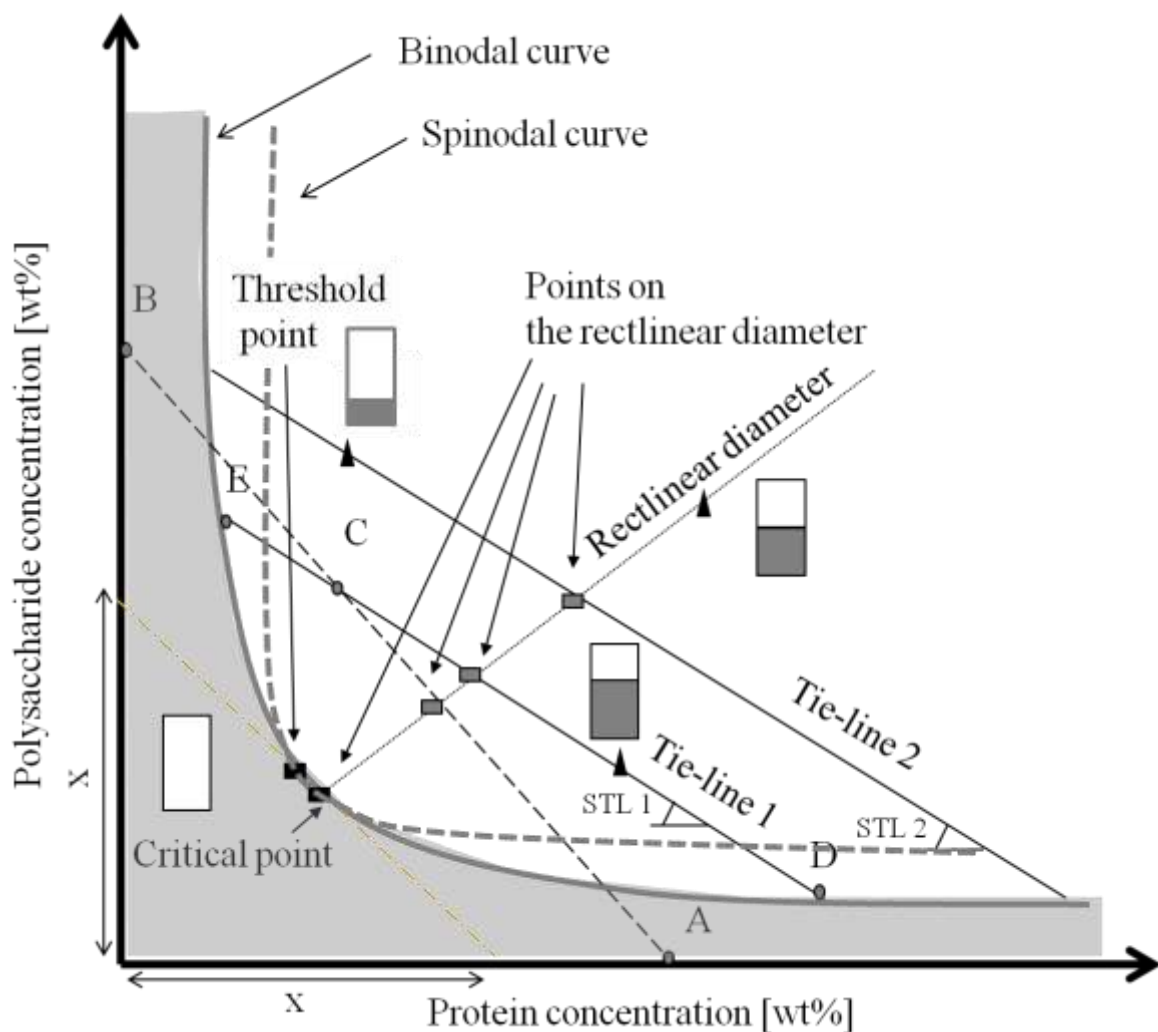


Figure 2-3. 2D composition-composition phase diagram. The binodal curve or phase curve separates one-phase region (shaded) from two-phase region (unshaded). STL=slope of the tie-line. Large rectangles are a schematic representation of the equilibrium biopolymer mixtures; their concentrations are marked with "▲".

In the following section, the above phase diagram is explained in detail. A point in the phase diagram corresponds to the weight/volume concentrations of the two biopolymers in the biopolymer mixture,  $([BP]_1, [BP]_2)$ , where the solvent makes up the remainder, i.e.,  $[BP]_1 + [BP]_2 + [solvent] = 100\%$ . Depending on external conditions such as shear, temperature and biopolymer concentration, the biopolymer mixture either falls in a one-phase region or a two-phase region of the phase diagram. A binodal curve divides the two regions (Koningsveld et al., 2001; Antonov et al., 2009). In Figure 2-3, one phase region is shaded and the mixtures found there are homogeneous. The mixtures in the two-phase region and above the binodal curve phase separate into two coexisting equilibrium phases. They lie on the binodal curve and on the tie-line—a straight line that passes through the concentrations of the primary ATPS and that of its equilibrium phases. The compositions of the equilibrium phases can be determined directly by chemical or physical analysis of the separated phases or indirectly by calculations, such as the phase volume fraction ratio method (Polyakov et al., 1980; Polyakov et al., 1985a). The binodal curve is usually close to the axes, hence the equilibrium phases are composed mainly of either of the two biopolymers and are typically referred to as protein-rich (the part of the binodal curve close to the x-axis) and polysaccharide-rich (the part of the binodal curve closer to the y-axis). The x-axis belongs to the biopolymer that is concentrated in the bottom phase, e.g., protein, and the y-axis to the biopolymer that is concentrated in the top phase, e.g., polysaccharide.

Two characteristic theoretical points lie on the binodal curve: the critical point and the threshold point (marked with "■" in Figure 2-3). The threshold of the phase

separation is the point of contact between the binodal curve and the tangential line cutting off equal segments of the x- and y-axes (Figure 3-6, p. 3-87). The critical point is the intersection between the rectilinear diameter and the curve (Figure 3-5, p. 3-87). The rectilinear diameter connects the middle points of the tie-lines, where the mixture phase separates into equivolumetric equilibrium phases. The position of the characteristic points relative to the bisectrix of the right angle of the Cartesian coordinate space is determined by  $M_w$  and the hydrophilicity of the biopolymers.

The tie-lines are straight lines that characterise any point inside the two-phase region of the phase diagram. Theoretically, for an idealised system, they are parallel to each other and decrease in length as they approach the critical point of the phase diagram. They show how the biopolymers partition themselves between the top and bottom phases. For example, in Figure 2-3, the mixture of the effective bulk concentration C, phase separates into the top phase with concentration E, and the bottom phase with the concentration D, hence the lengths of the lines  $\overline{CE}$  and  $\overline{CD}$  correspond to the volume fractions of the bottom and top phases, respectively. Theoretically, on the same tie-line, the compositions of both equilibrium phases are unchanged and only their volume fractions and total effective/bulk concentration of the mixtures change.

Inside the binodal curve<sup>5</sup> lies a spinodal<sup>6</sup> curve that separates mixtures which phase separate spontaneously from mixtures that phase separate via the process of

---

<sup>5</sup> A phase curve/boundary that separates a stable region from the metastable and unstable regions.

<sup>6</sup> A phase curve/boundary that encloses the unstable region.

nucleation and growth. Mixtures inside the metastable region—the region between the curves—phase separate via a lengthier process of nucleation and growth whereas mixtures inside the spinodal region (deeper in the two-phase region) phase separate more rapidly (Dickinson, 1982).

#### **2.2.4 Factors influencing phase behaviour**

Various internal and external factors control phase separation behaviour. The concentration of the biopolymer mixture determines the occurrence and its speed. For example, the closer a mixture is to the binodal curve, the slower (hours or even weeks) the phase separation will be (Dickinson, 1982). The phase separation can be stopped by kinetically trapping the structures. Besides  $T$ ,  $p$  and shear can also modify phase behaviour (Antonov et al., 2003; Frith, 2010). On the molecular level the phase separation is controlled in two ways: (i) by changing the electrostatic interactions between the charged biopolymers with added salt, acid or base and (ii) by changing the solvent quality by adding sugars or alcohols (Dickinson and Woskett, 1988; Schorsch et al., 1999a; Schorsch et al., 1999b; Spyropoulos, 2006; Semenova, 2007). In addition, the charge size of the molecules is also a determining factor for their phase behaviour. For example, the components with higher  $M_w$  in a polydisperse system will phase separate at lower concentrations and concentrate in one of the phases, which is also a basis for fractionation in the process of bioseparation (van Heukelum et al., 2003).

### 2.2.5 Phase separation microstructures

The type, mechanism and kinetics of phase separation and shear, influence the microstructure of ATPS. Most commonly, ATPS are liquids and their structure is emulsion-like<sup>7</sup> (Figure 2–4), but in terms of size and appearance, various types of equilibrium and non-equilibrium phase separation microstructures can form through molecular arrangements.

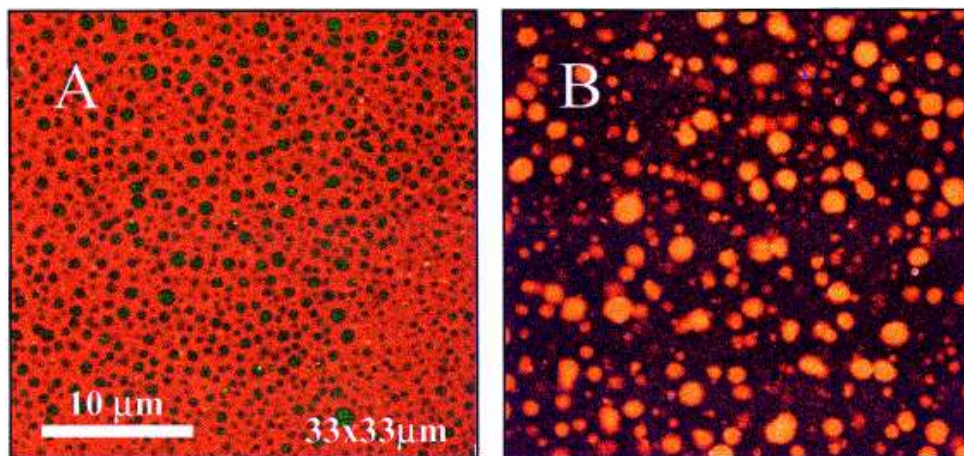


**Figure 2–4.** Phase separated aqueous 5% gelatin-1% carrageenan (A) non-gelling  $\text{Ca}^{2+}$  sensitive  $\iota$ -carrageenan and (B) gelling  $\kappa$ -carrageenan. Carrageenan is covalently labelled with fluorescein isothiocyanate (green in image A) and gelatine is stained by rhodamine (red in both images) (Source: Tromp et al., 2001, p. 936).

#### 2.2.5.1 Equilibrium microstructures

Three types of equilibrium microstructures can form when proteins and polysaccharides are mixed (Figure 2–5). The types depend on the concentration and electrostatic potential of the macromolecules.

<sup>7</sup> An emulsion-like structure is a droplet-like structure, in which a phase present in a smaller volume fraction assumes the role of a dispersed phase and the phase of a larger volume that of a continuous phase. Unstable aqueous emulsions can be stabilised by kinetically trapping the structures (i.e., gelation and cooling).

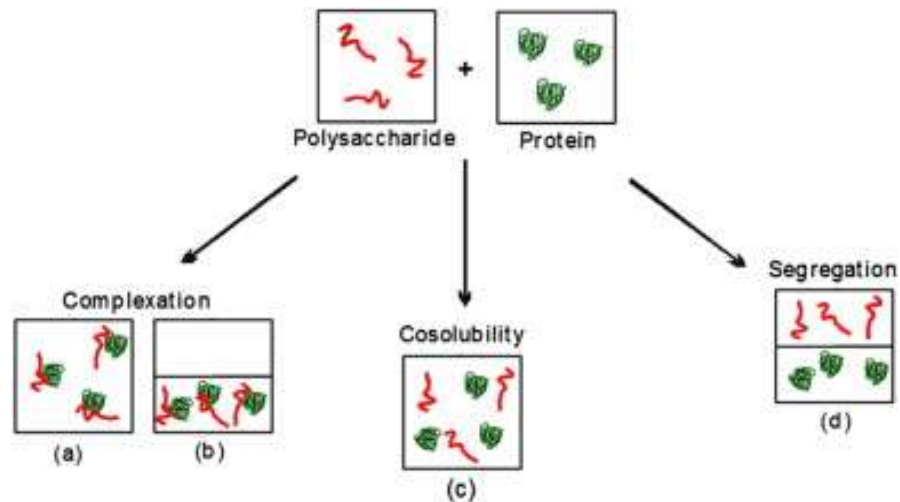


**Figure 2–5. Behaviour of protein–polysaccharide mixtures (Source: Rodríguez Patino and Philosof, 2011, p. 1926).**

In dilute systems, the macromolecules are cosoluble and systems are homogenous. In concentrated systems, however, emulsion-like structures form. They can, depending on the sign and charge, result in two additional types of phase separation morphologies: associative complexation and segregative phase separation (Piculell and Lindman, 1992; Tolstoguzov, 1998; Frith, 2010; Rodríguez Patino and Pilosof, 2011). Sometimes, deviations from the above morphologies can occur. At certain ionic strengths, both associative and segregative phase separation morphologies coexist (Zaslavsky, 1995; Turgeon and Laneuville, 2009), but complete separation of biopolymers is rarely observed (Tromp et al., 1995).

Associative complexation occurs between oppositely charged biopolymers (e.g., proteins and charged polysaccharides, such as pectins, carrageenans, gum Arabic, xanthan and acacia gum). Due to mutual attraction, they form an insoluble biopolymer complex, which concentrates in a single phase or in a precipitate (see Figure 2–5 a and b). On the other hand, the repulsion between uncharged or similarly charged

biopolymers results in the segregative type of phase separation, which leads to the formation of two equilibrium phases where one phase is concentrated in one biopolymer and depleted in the other (Rodríguez Patino and Pilosof, 2011). The latter is also of interest in this work.

Segregative phase separation may be desired when it is applied for aqueous partitioning (membraneless osmosis/concentrating proteins (Dickinson, 2008)), or undesired when homogeneous shelf-stable solutions are produced. Either way, it is an important structure-making process that has been studied extensively (Antonov et al., 1982; Tolstoguzov, 1988).

#### **2.2.5.2 Non-equilibrium morphologies**

Non-equilibrium morphologies are formed (i) during the process of phase separation, (ii) by blending of the equilibrium phases and (iii) shear.

The non-equilibrium morphologies related to phase separation kinetics were revealed during real-time studies of the kinetics of phase separation (Figure 2-6) and by kinetically trapping the phase separated structures by gelation (Figure 2-7). Depending on the concentration of the system, phase separation occurs in different ways. Inside the metastable region<sup>8</sup> of the phase diagram (Figure 2-3), phase separation occurs via a slower mechanism of nucleation and growth while deep inside the two-phase region,

---

<sup>8</sup> The metastable region is the region between the spinodal and binodal curves.

systems separate via the faster mechanism of spinodal decomposition<sup>9</sup> (Koningsveld et al., 2001; Clark, 2006). Differently sized morphologies depend on which stage of the coarsening of the domains the phase separation is stopped. Droplets of the dispersed phase formed by spinodal decomposition are of similar sizes, whereas droplets formed by nucleation and growth have a wider size distribution (Norton and Frith, 2001). As shown in Figure 2–6, spinodal decomposition is spontaneously perpetuated by fluctuations in the concentration of both polymers with the purpose of minimising  $\Delta G_{mix}$  (see § 2.2.2.1, p. 2–13).

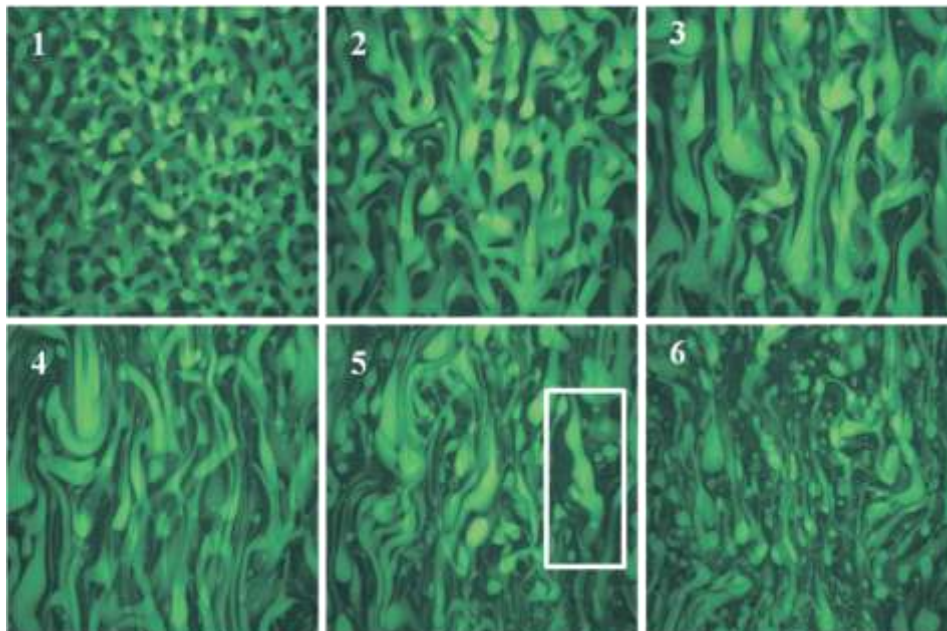


**Figure 2–6.** Laser scanning confocal images ( $1400 \times 1400 \mu\text{m}^2$ ) of gravity-driven flow in a phase separating colloid–polymer mixture. In (1) ( $t = 56 \text{ s}$ ) the spinodal structure is collapsing under its own weight leading to strong flow in (2), (3) and (4) ( $t = 72, 89$  and  $106 \text{ s}$ , respectively). Minimal coarsening occurs. (5) The onset to a transition with vertical lanes is observed. (6) ( $t = 134 \text{ s}$ ) individual droplets become more apparent. The white box in (5) marks a Rayleigh instability (Source: Aarts et al., 2005, p. 9).

Because of the slow diffusion rates characteristic of polymers, spinodal decomposition in both phases generates a fine granulated mixture of the phases (Lorén,

<sup>9</sup> Spinodal decomposition is a type of phase separation that occurs uniformly across the material and not only at nucleation sites.

2001; Norton and Frith, 2001; Clark, 2006; Fang et al., 2006; Frith, 2010). If the system is kinetically trapped at this stage, it looks like the system in Figure 2-7 b, but if trapped later, it looks like a polydisperse emulsion as shown in Figure 2-7 a.

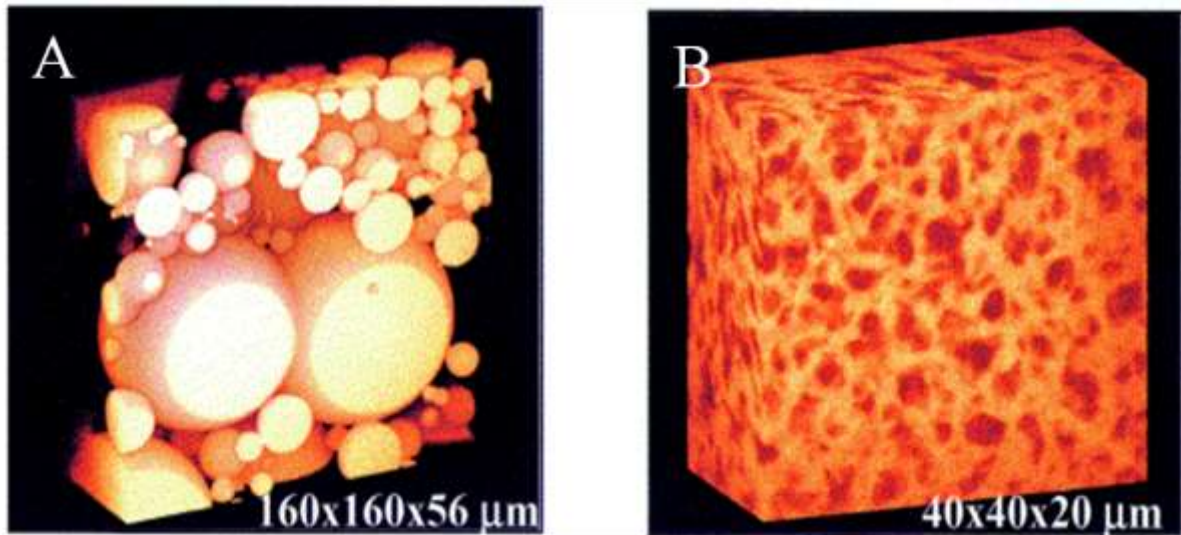


**Figure 2-7. Confocal images of (A) droplet-like and (B) interconnected morphologies of phase separated 2.5% gelatine-2.5% dextran-0.5 M NaCl trapped upon (A) slow cooling and (B) fast cooling (Source: Tromp et al., 2001, p. 635).**

Another structure-forming mechanism in ATPS depends on the volume fraction of the equilibrium phases ( $\phi$ ). The equilibrium phases in mixed biopolymer systems show no specific preferences to whether they want to assume the role of a dispersed or continuous phase. Under quiescent conditions, therefore, the microstructure of the system depends only on the volume fraction of the equilibrium phases (Figure 2-8). If the volume fraction of one of the biopolymers is increased, the biopolymer gradually stops being the included phase and becomes a continuous phase, i.e., the system phase inverts (Schorsch et al., 1999 a; Frith, 2010).

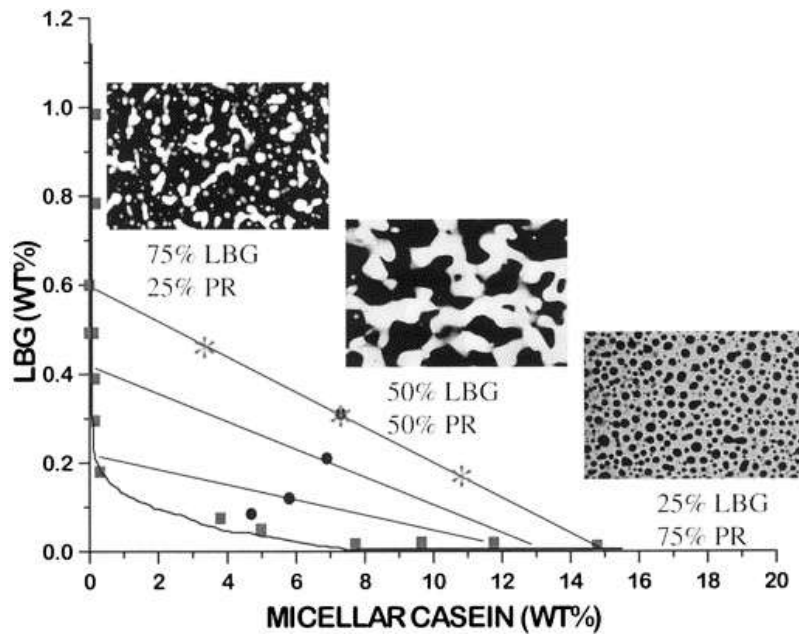


**Figure 2–8.** Phase diagram of micellar casein–LBG systems at 5°C and the microstructure (images obtained by confocal microscopy) of these systems depending on the phase volume ratio (pH≈6.8,  $I \approx 0.08$ , image length scale, 500  $\mu\text{m}$ ) (Source: Schorsch et al., 1999a, p. 321).

The phase sense of the created blend can be altered additionally by shear and/or gelation (Schorsch et al., 1999a; Schorsch et al., 1999b; Wolf and Frith, 2003). Under shear, a low viscosity phase, though present in a lower volume fraction, can become continuous and shear-induced phase inversion can occur. A review of shear-induced phenomena on the microstructure of ATPS continues in § 2.3.2.2, p. 2–36.

### 2.3 Rheological behaviour

Studies on the rheological behaviour of pure biopolymer solutions and multicomponent ATPS can simulate thermal and mechanical processes that govern the phase state and texturisation of emulsion-based foods (Tolstoguzov, 2006) and provide an understanding of these systems on various lengthscales (molecular, supramolecular and macroscopic) (Tolstoguzov, 2002).

### 2.3.1 Rheology of pure biopolymer solutions

Biopolymers, namely polysaccharides, are used in a wide range of food applications, mainly for their thickening properties. The dissolution of a single biopolymer at concentration  $\sim 1\%$  w/v or less in water elevates its viscosity significantly (Tolstoguzov, 2002). It has been shown that the mechanism of thickening relates to the number, size and conformational properties of the molecules in the solvent, as well as the temperature. Therefore, the viscosity of such a system is influenced by the amount of aqueous space (Jeon et al., 2001; Wolf and Frith, 2003).

The rheological behaviour of biopolymers shows great dependence on the concentration, shear and solvent environment. These topics are shown for polysaccharides in the following paragraphs. The flow of NaCAS is covered in § 2.5.1, p. 2-60-62.

Depending on the concentration and molecular conformation of the biopolymer, two distinct flow regimes are observed: dilute and concentrated (Figure 2-9). These are not observed for solutions of small molecules, such as sugars with a fixed viscosity over a wide range of shears.

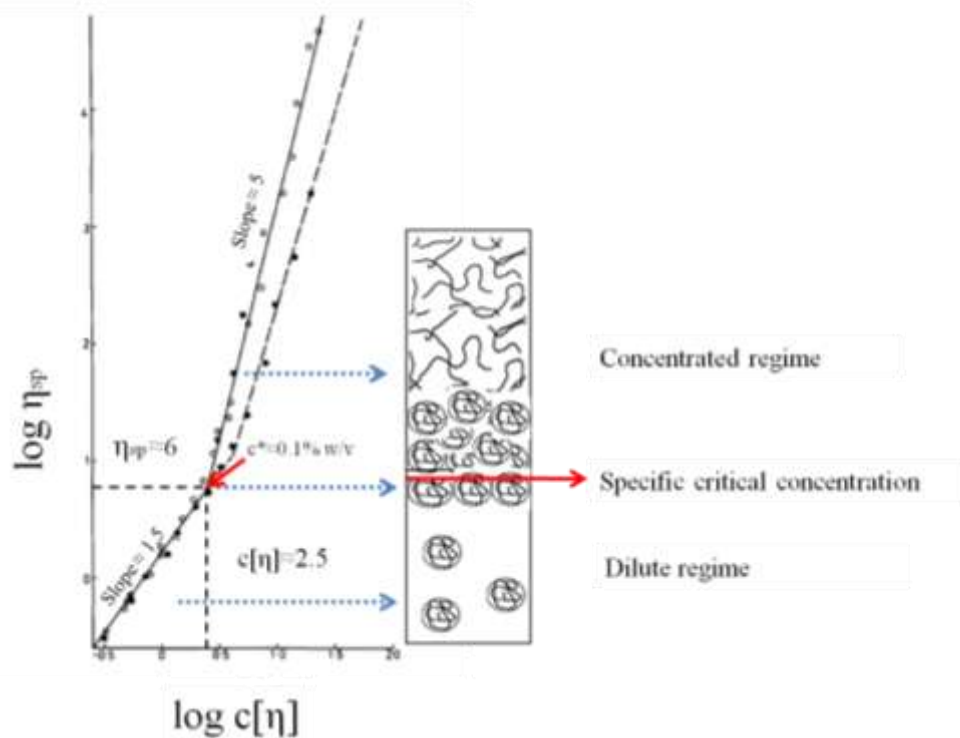


**Figure 2–9. Concentration dependence of polysaccharide-specific viscosity for: polystyrene in toluene marked with "●"; guar gum marked with "○"; locust bean gum marked with "□" and hyaluronate marked with "■" (at pH 2.5 and 0–15 M NaCl) (Adapted by: Morris et al., 1981, p. 14).**

Biopolymers below a critical biopolymer concentration<sup>10</sup> ( $c^*$ ) exhibit Newtonian behaviour—their viscosities are shear independent—and they appear in the solution as molecular particles surrounded by the solvent. Their size is characterised by the radius of gyration ( $R_g$ ). At  $c^*$ , the packing density of these particles reaches a maximum value and they touch. For the majority of disordered random coil polysaccharides (e.g., dextran, carrageenan and alginate), the transition to a concentrated system occurs at the space occupancy  $c[\eta] \approx 4$ , but for GMs (e.g., LBG, TG, GG and FG), the polysaccharides relevant to this work, the transition occurs sooner at  $c[\eta] \approx 2.5$  (Morris et al., 1981; Doyle et al., 2009).

<sup>10</sup> Critical biopolymer concentration  $c^*$  is the concentration of the biopolymer below which the flow behaviour of the system is near-Newtonian. For the majority of random coil polysaccharides, it is described by the equations  $c^* = 4/[\eta]$  and  $\eta_{sp} \approx 10$ .

In the concentrated regime above  $c^*$ , the flow of all polysaccharides is non-Newtonian shear-thinning<sup>11</sup>. The flow no longer depends solely on the molecular structure but rather on the size of the network blobs formed by molecular overlapping. Compared to other random coil polysaccharides, GMs show greater concentration dependence (a slope of 5 compared to a slope of 3.3 as seen with other random coil polysaccharides). This is attributed to the existence of hyperentanglements among galactose chains in GMs (for details on GM structure, see § 2.5.2, p. 2–63) added to the effect of overlapping, which is characteristic of other random coil polysaccharides (Morris et al., 1981; Doyle et al., 2009).

It has been noted, however, that transition of GMs from dilute to concentrated regions via a semi-dilute region, is positioned between  $c^*$  and  $c^{**}$  (i.e., second biopolymer overlap critic concentration). The values of  $c^*$  and  $c^{**}$  depend on the molecular characteristics and vary with solvent quality (Richardson et al., 1998).

Sufficiently concentrated pure random coil polysaccharide solutions show shear/frequency dependence. Similarities are observed when comparing their flow and oscillation data. The data show Newtonian regions, where structure formation and breakup are balanced, and shear thinning regions, where increased shear breaks structures faster than they can form. Critical shear rates/frequencies, which mark the border between the regions, move to lower shears with increased concentrations. For many polysaccharides, the rheology data from flow and oscillation can be correlated by

---

<sup>11</sup> Shear thinning behaviour exhibits a logarithmic decrease in viscosity at increasing shear rates. The flow diagram of shear stress ( $\sigma$ ) vs. shear rate ( $\dot{\gamma}$ ) produces an exponential curve.

the Cox-Merz rule<sup>12</sup>, but GMs fail to obey it (especially at low shears/low frequencies) due to the existence of non-covalent hydrogen bonds (Morris et al., 1981; Williams, 2006).

As shown in Figure 2–10, the curve  $\eta/\eta_0$  vs.  $\dot{\gamma}/\dot{\gamma}_{0.1}$ , where  $\eta$  and  $\eta_0$  are viscosity and zero shear viscosity, and  $\dot{\gamma}_{0.1}$  is the shear rate at which  $\eta = \eta_0/10$ , the shear thinning profile of any concentrated random coil biopolymer solution can be superimposed on the same curve. As such, the viscosity at any shear rate is characterised by the values of  $\eta_0$  and  $\dot{\gamma}_{0.1}$ . When sheared, biopolymers orient in the direction of the shear field; changes in polydispersity can therefore contribute to differences in shear thinning (Morris et al., 1981).

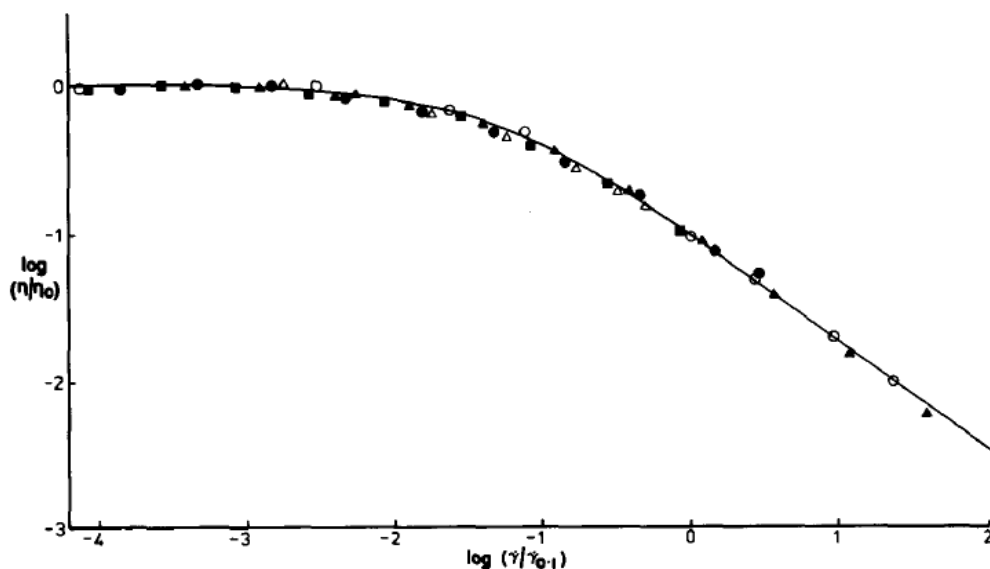


**Figure 2–10. Generalised shear thinning behaviour for concentrated solutions of disordered polysaccharides illustrated for: guar gum marked with "△"; lambda carrageenan marked with "▲"; locust bean gum marked with "●"; high mannuronate alginate marked with "■", and hyaluronate marked with "○". (Source: Morris et al., 1981, p. 18).**

<sup>12</sup> Model that provides a correlation between the viscometric and linear viscoelastic functions.

The flow of pure biopolymer solutions can be used to study the molecular characteristics of polysaccharides. The molecular characteristics are determined by the following parameters: (i) the zero shear viscosity  $\eta_0$  that determines the molecular size and interactions and (ii) the intrinsic viscosity  $[\eta]$  that measures the hydrodynamic volume. The value of  $[\eta]$  is derived through the Flory-Fox relationship and is related to  $M_w$ ,  $R_g$ , chain length and chain stiffness, and if multiplied by the critical concentration  $c^*$  determines the critical degree of coil overlap (Morris et al., 1981). For example, Richardson et al. (1998) conducted a study on the effect of sucrose on dilute solutions of LBG and GG and found that sugar affects  $[\eta]$  in a manner shown in Figure 2-11. The authors supported their findings by changes in the molecular behaviour of GMs, i.e., changes in molecular self-associations and expansion. For a comparison of  $[\eta]$  between GMs in the absence of sucrose, see § 2.5.2, Table 2-2, p. 2-64.

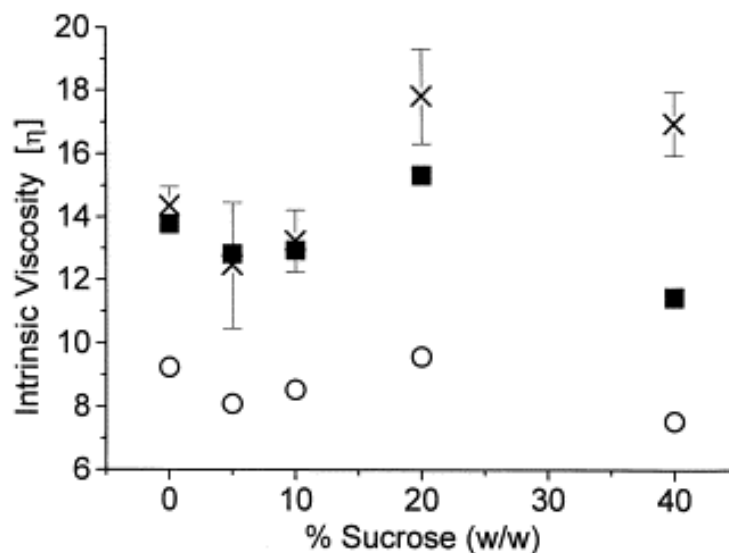


**Figure 2-11.** Variation of the intrinsic viscosity for guar and locust bean gum at different sucrose concentrations. "■"=native locust bean gum, "○"=guar, "×"=purified locust bean gum (Source: Richardson et al., 1998, p. 346).

### 2.3.2 Rheology of aqueous two-phase biopolymer mixtures

The rheological properties of pairs of equilibrium phases that form in the process of phase separation are decided by the biopolymer present in the larger volume fraction (Frith, 2010). The phases can be mixed together in different volume fractions to produce blends (Schorsch et al., 1999a), which appear and flow much like conventional O/W emulsions. They are called W/W emulsions and similar mathematical models are typically used to explain the flow behaviour of both emulsion types (Stokes et al., 2001).

#### 2.3.2.1 Comparison of W/W (ATPS) with O/W emulsions

This section summarises the similarities and differences of W/W and O/W emulsions in terms of their flow behaviour and microstructure evolution under flow.

Similar to O/W emulsions, the structure of W/W emulsions forms in shear through the competing processes of droplet breakage and coalescence that conclude in the formation of multicomponent/droplet-like morphologies. Under certain conditions, both types of emulsion can phase invert. The flow behaviour of the emulsion types is influenced by factors such as (i) the viscosity of the continuous phase ( $\eta_c$ ), (ii) the viscosity ratio ( $\lambda$ ), (iii) the phase volume fractions of the dispersed ( $\varphi_d$ ) and continuous phases ( $\varphi_c$ ), (iv) their phase sense, and (v) the chemical compositions of the phases (Pacek et al., 2001; Wolf and Frith, 2003; Simeone et al., 2004; Caserta et al., 2005).

The microstructure of W/W emulsions undergoing shear flow differs from the

microstructure of the conventional O/W emulsions because of the partial miscibility and very low interfacial tensions characteristic of W/W emulsions (Guido et al., 1999b; Wolf et al., 2000). The differences are the following: (i) the microstructure of the W/W emulsions depends more on its phase sense, i.e., the viscosities and volume fractions of the dispersed and continuous phases ( $\eta_{d,c}$ ,  $\varphi_{d,c}$ ), and to a lesser degree on the hydrodynamic conditions (Simeone et al., 2004; Spyropoulos, 2006); (ii) droplet breakup in ATPS is faster (i.e., it occurs within less than a second) and (iii) the phase inversion region in ATPS is significantly wider and less abrupt than that in O/W emulsions and involves the formation of thread-like structures as opposed to spherical and ellipsoid droplets in O/W emulsions (Pacek et al., 1994a; Jeon and Hobbie, 2001a).

### **2.3.2.2      *The microstructure of ATPS under quiescent conditions and under shear***

The microstructure of ATPS is greatly controlled by the forces of the flow field, which determine the final shape and size of droplets (Wolf et al., 2000; Stokes et al., 2001; Wolf and Frith, 2003). It is, however, also affected by the factors that influence phase separation, such as biopolymer-biopolymer and biopolymer-solvent interactions, active on a nanometre scale, which determine the properties of the separate phases (Richardson et al., 1998; Lorén, 2001; Ding et al., 2005). The droplets created and the way they interact in turn determine the flow properties of these systems and also determine the properties of formulated foods, such as colour, creaminess, spreadability and fat mimicry (Wolf et al., 2000).

The relationship between structure and composition has been studied under quiescent conditions and under shear (Wolf et al., 2000; Wolf and Frith, 2003; Spyropoulos et al., 2008b). Figure 2–12 is an example of the ATPS microstructure under quiescent conditions, during flow and after the cessation of flow.

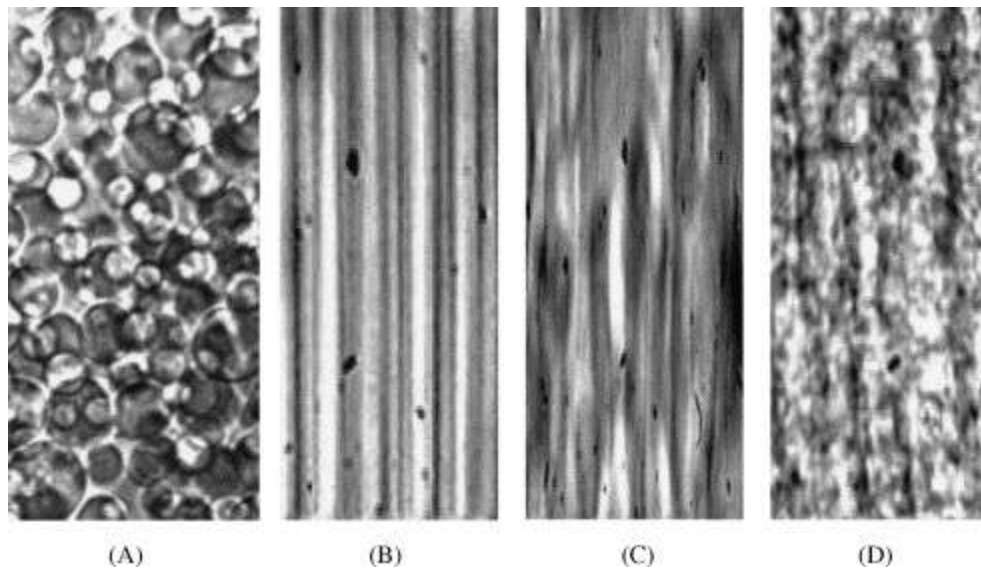


**Figure 2–12. Evolution of the microstructure of a sodium caseinate-sodium alginate ATPS in flow: (A) before the application of a high shear rate to cause droplet break-up; (B) the moment of interrupting the flow (3 s at  $3 \text{ s}^{-1}$ ); (C) 36 s after stopping the flow; (D) 76 s after stopping the flow (Source: Antonov et al., 2004, p. 33).**

Under quiescent conditions, various microstructures of ATPS are formed by blending together the equilibrium phases (see § 2.2.5.2, Figure 2–8, p. 2–29) or alternatively, by preparing ATPS of a corresponding concentration from scratch. In such a way, three distinct microstructures can be produced. If for example, an ATPS is composed of a protein and a polysaccharide, the systems will be (i) protein dispersed, (ii) bicontinuous and (iii) polysaccharide dispersed. The microstructure of a quiescent ATPS is that of an emulsion, where the dispersed phase assumes the shape of spherical drops and the continuous phase surrounds it (Figure 2–12 a) (Simeone et al., 2004; Spyropoulos et al., 2008b; Frith, 2010).

Under shear, the microstructure of an ATPS blend is formed because of the balance between the processes of droplet deformation and break-up on one hand and coalescence on the other. The studies conducted in extrusion devices (Antonov et al., 1980), stirred vessels (Pacek et al., 1994b; Pacek et al., 2001) and rheometers (Wolf et al., 2000; Caserta et al., 2005; Spyropoulos et al., 2008b) that related the microstructure of an ATPS blend to flow, show that the size and shape of droplets produced under shear depends on many factors. These are (i) the shear rate ( $\dot{\gamma}$ ), (ii) the phase sense, (iii) the viscosity ratio ( $\lambda$ ), with the phase volume of the dispersed phase ( $\varphi_d$ ) and (iv) the presence of a gelling polysaccharide. The morphology of an ATPS is sensitive to shear, and higher shears typically produce smaller droplets than lower shears, where coalescence is much faster due to shorter drainage times (Wolf et al., 2000; Stokes et al., 2001; Caserta et al., 2005). The phase sense, i.e., the volume fraction of the dispersed phase, also influences microstructure under shear. A system of low volume fractions of the dispersed phase ( $\varphi_d < 30$  wt%) forms under medium and high shear ellipsoid droplets. If the system is initially bicontinuous ( $40$  wt%  $< \varphi_d < 75$  wt%), the shapes of droplets become irregular, long and extended (Figure 2-12 b). The structures narrow at high shears, and after the shear is stopped, typically break up into small droplets (Figure 2-12 c, d). The formation of thread-like structures is preferred at low viscosity ratios ( $\lambda \approx 0.01$ ), which also favour shear-induced phase inversion, as discussed further in § 2.3.2.2.1, next page. If the disperse phase gels and the structures are quenched while under shear, they appear as those seen in Figure 2-13. When the volume fraction of the dispersed phase is large ( $\varphi_d > 90$  wt%), systems under shear form uniform spherical droplets (Pacek et al., 1994b; Wolf et al., 2000; Jeon and Hobbie, 2001a).

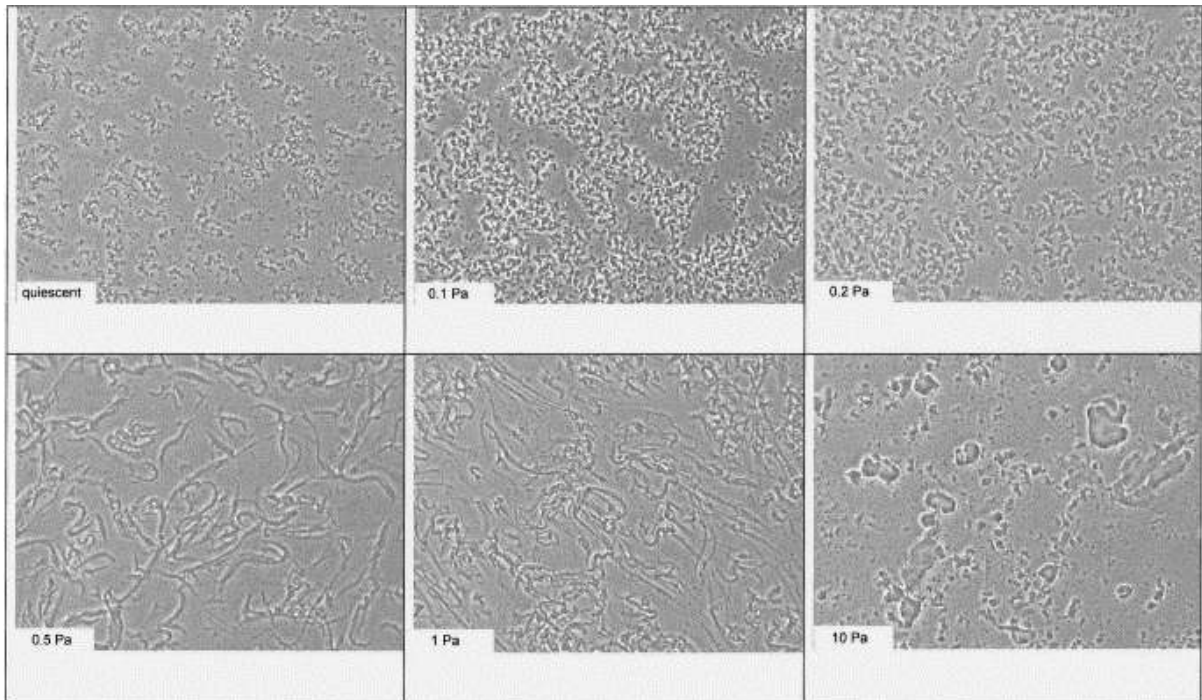


**Figure 2–13. The microstructure of processed 0.75 wt% gelatin–1 wt% guar mixtures (width of insert: 100  $\mu\text{m}$ ) (Source: Wolf et al., 2000, p. 219).**

#### 2.3.2.2.1 Phase inversion in ATPS

The phase inversion event in a dispersed ATPS is characterised by a change in its phase sense. Phase inversion is controlled differently under quiescent conditions and under shear. Under quiescent conditions, ATPS phase invert when the volume fraction of one of the phases is increased. The ATPS transits from a biopolymer A-in-biopolymer B-emulsion, via a bicontinuous system, to a biopolymer B-in-biopolymer A-emulsion (Spyropoulos et al., 2008b). Under shear, however, the onset of phase inversion is more complex. Phase separation can be triggered by events: (i) changes in the composition of the system induced by temperature or gelation, which alter the viscosities ( $\eta$ ), densities ( $\rho$ ) and the interfacial tension ( $\sigma$ ) of the equilibrium phases and (ii) shear and various geometrical factors such as impellers, pipes, vessels and flow geometries with

different wetting characteristics (Efthimiadu and Moore, 1994; Foster et al., 1996; Yeo et al., 2000; Wolf et al., 2000).

Phase inversion occurs after a delay because of the enhanced coalescence of the dispersed phase compared to droplet break-up. The delay in the onset of phase inversion is longer for systems with low interfacial tension, high viscosity of the dispersed phase and a low density difference between the equilibrium phases. During the phase inversion event, the polydispersity of the system increases. The continuous phase breaks up and folds into parts of the dispersed phase. The event concludes with the formation of bicontinuous structures (Figure 2 -14). In quiescent and sheared systems, bicontinuous systems exist over a wide range of  $\varphi_d$ , hence phase inversion is not an abrupt process. For example, in a NaCAS-sodium alginate system, bicontinuous systems exist in the range of  $40 \text{ wt}\% < \varphi_d < 75 \text{ wt}\%$  (Pacek et al., 2001).

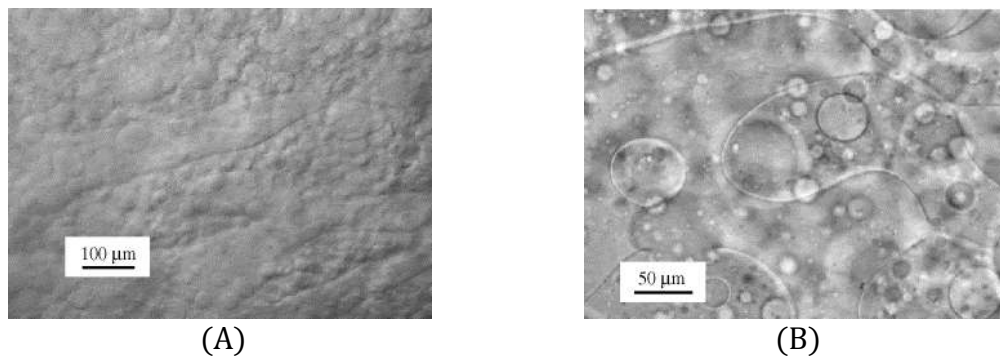


**Figure 2–14. Complex, multiple dispersed structures in the phase inversion region of a 54% sodium alginate-rich in sodium caseinate-rich dispersion after the cessation of stirring: (A) in the vessel after 3 min; (B) in a sample ~1 min after withdrawal (Source: Pacek et al., 2001, p. 3254).**

The phase inversion event can cause the material changes of the system. These can be seen as (i) changes in the viscosity of a system ( $\eta_{ATPS}$ ), (ii) changes in the phase

viscosity ratio ( $\lambda$ ), (iii) phase separation time and (iv) droplet deformation and size (Wolf et al., 2000; Jeon and Hobbie, 2001b).

Figure 2-15 gives two examples of viscosity changes observed when a phase inversion event takes place.

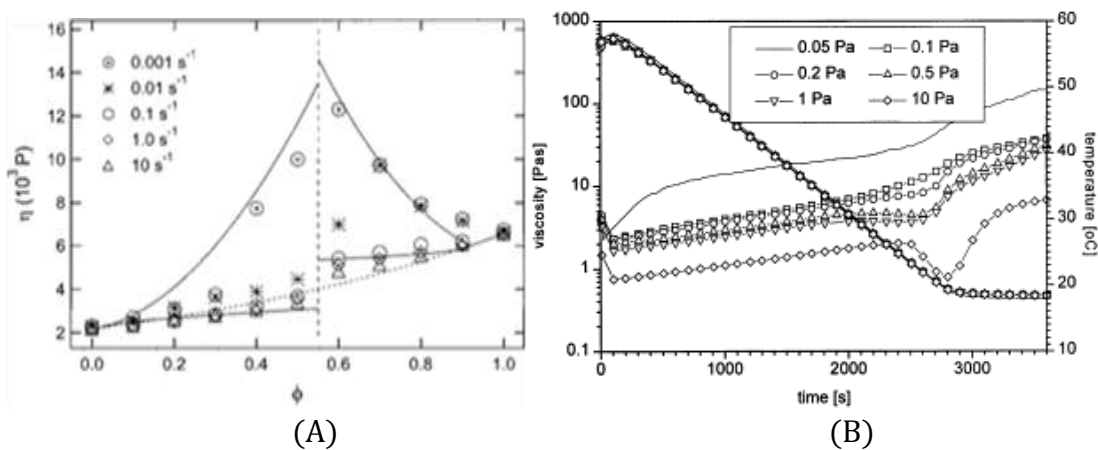


**Figure 2-15. (A) Shear viscosity of polybutadiene-polyisoprene blends at different shear rates as a function of the polyisoprene volume fraction, where the dashed curve is the viscosity of the homogenised mixture (Source: Jeon and Hobbie, 2001, p. 061403-4). (B) Viscosity data for stress-controlled cooled gelatine-guar mixtures as a function of time and temperature (Wolf et al., 2000, p. 220).**

The methods applied in the determination of the phase inversion region in ATPS are not as straightforward as in O/W emulsions. Nevertheless, phase inversion can be measured by (i) rheo-optical experiments (Spyropoulos et al., 2008b) where changes in the viscosity of ATPS and in the size, shape and deformation of the dispersed droplets are observed, (ii) confocal micrographs (Wolf and Frith, 2003) and (iii) various mathematical models, which are particularly useful in the determination of the phase inversion compositions of equiviscous systems ( $\lambda \approx 1$ ) where optical methods fail (Foster et al., 1996; Wolf and Frith, 2003). Furthermore, a combination of the abovementioned methods can be used (Wolf and Frith, 2003; Spyropoulos et al., 2008b).

### 2.3.2.2.2 Shear-induced mixing

Shear also has the ability to change the phase behaviour of biopolymer ATPS. Under quiescent conditions, a two-phase system can become homogeneous under critical shear. The homogenisation process is typically preceded by the formation of threads. Homogenisation/shear-induced mixing takes place when hydrodynamic forces exceed intermolecular forces, hence the factors that determine it are (i) biopolymer concentration, (ii)  $M_w$ , macromolecular structure (branching, ordering), (iii) solvent quality, pH and ionic strength, (iv) interfacial properties and (v) the viscosity ratio ( $\lambda$ ) (Antonov et al., 2003; Antonov et al., 2009; Antonov et al., in press).

In their work, Antonov et al. (2003; 2009) studied the onset of homogenisation in an ATPS under shear ( $0.1\text{--}200\text{ s}^{-1}$ ) by employing small angle light scattering. The scattering patterns enabled the determination of droplet size and shape, and the absence of a signal was a sign of complete mixing (Figure 2–16).

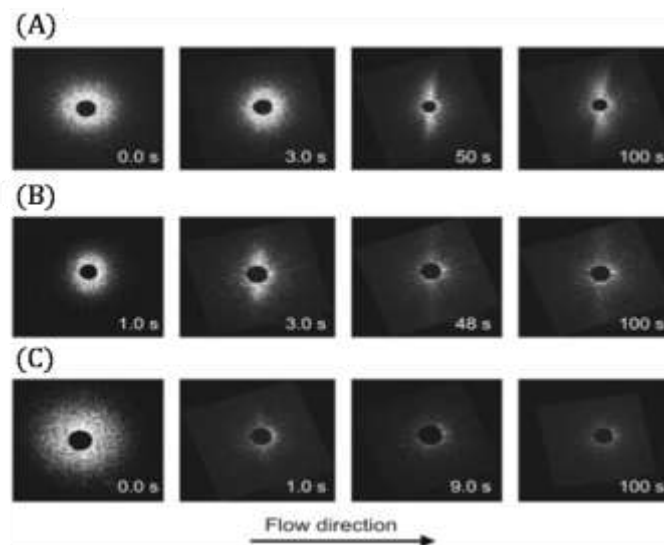


**Figure 2–16.** Effect of shear flow on the evolution of small angle light scattering patterns upon the inception of flow for a water–dextran–arabic gum system: (A) shear rate of  $0.02\text{ s}^{-1}$ , (B) shear rate of  $0.1\text{ s}^{-1}$  and (C) shear rate  $1\text{ s}^{-1}$  (Source: Antonov et al., 2009, p. 267).

They found a correlation between solvent quality and the sensitivity of the system to homogenisation. They assessed the solvent quality thermodynamically by calculating the molar second virial coefficient ( $A_{ij}$ ) and the thermodynamic activity of biopolymers in concentrated solutions ( $\log C_{biopol}$ ). While the homogenisation took place when  $A_{12} < \sqrt{A_{11}A_{22}}$ , the systems with low  $\log C_{biopol}$  (e.g., NaCAS-sodium alginate systems) did not homogenise under shear.

## 2.4 Interfacial properties of aqueous two-phase systems

### 2.4.1 Interfacial region in ATPS

The interfacial region is a film of highly concentrated solvent that separates the two immiscible equilibrium phases in ATPS. For example, Scholten et al. (2004a) calculated its thickness ( $\xi$ ) close to the critical point to be  $\sim 340$  nm. The region is visible because of the difference in the optical densities of the phases in contact. It affects the shape and size of dispersed droplets in a W/W emulsion and controls the product's performance and processing characteristics (Tolstoguzov, 2006).

The interfacial region is much wider in systems composed of smaller molecules. Its absolute thickness ( $\xi$ ) depends on many factors, such as (i) the biopolymer concentration, such that the thickness of the interface increases with a reduction in the difference in concentrations of the phases and (ii) external factors including pH, ionic strength, shear and the presence of small molecular ingredients, such as sugars, salts and surfactants, which can either be redistributed in the bulk or adsorbed to the

interfacial region (Scholten et al., 2004a; Scholten et al., 2006b).

Scholten et al. (2006a) have shown that the interface is permeable and open to diffusion of the ingredients. Depending on the concentration of the surrounding media and forces exerted on the dispersed droplet, the diffusing components are either (i) both biopolymers and solvent or (ii) only solvent. Overall, because of the permeable interface, W/W emulsions look like molecular sponges.

The mechanical strength of the interface/interfacial tension can be both measured and calculated. Its quantification can be approached from a thermodynamic or mechanic point of view. The interfacial tension ( $\sigma$ , Figure 2–17) is a surface phenomenon caused by intermolecular forces expressed as force (N) per unit length (m) at the interface between two phases. It is a force required to create a new unit area of the interface and is numerically equal to the interfacial free energy (the energy difference between the molecules in the bulk, which are in a favourable energy state and molecules on the surface, which are in an unfavourable energy state). The system tends to reduce the interfacial energy by creating interfaces with the lowest area per volume; therefore, their most favourable shape is spherical (Ding et al., 2002; Semenova and Dickinson, 2010).

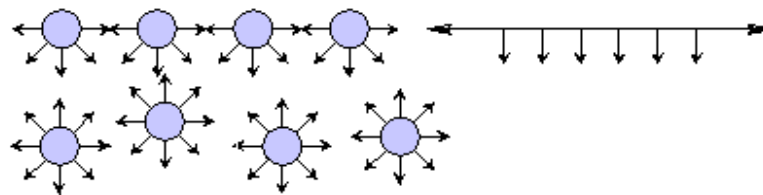


**Figure 2–17. Scheme of the attractive forces among the molecules of a liquid (Source: Carboni, 2002).**

The properties of the interface, such as thickness, permeability, mechanical strength, surface coverage and surface charge density in the absorbed layers and interactions within and among these absorbed layers are important characteristics of a system and determine the stability of an emulsion (Sigillo et al., 1997; Dickinson, 2010; Semenova and Dickinson, 2010).

#### **2.4.2 Measurements of the interfacial properties of emulsions**

Many experimental methods have been used for measuring the interfacial tensions of emulsions; however, not all are equally suitable for W/W emulsions. Accordingly, the following two paragraphs of this section overview, first, the variety of methods used in emulsions and, second, the reasoning behind the selection of the best method for ATPS or W/W emulsions.

Many methods have been used to measure interfacial properties of emulsions. Semenova and Dickinson (2010) have reported the use of the following experimental methods for emulsions: static and dynamic interfacial tensiometry, shear and dilatational interfacial rheology, zeta potentiometry, ellipsometry, infrared reflection-adsorption spectroscopy, atomic force spectroscopy, Brewster angle microscopy, fluorescence microscopy and neutron X-ray reflectivity. They also reported on the importance of modelling and computer simulation for providing an understanding of these systems. Holmberg (2001), on the other hand, has grouped the techniques into (i) force methods (capillary rise, Wilhelmy plate and Du Noüy Ring methods), (ii) shape methods (pendant drop, sessile drop and spinning drop methods) and (iii) pressure

methods (maximum bubble pressure method). Likewise, Ding et al. (2002) have grouped these methods into (i) force and (ii) shape methods, and added another group including (iii) dynamic methods. Dynamic methods study (i) drop deformation and breakage in shear, (ii) the steady state shape of droplets in shear and (iii) droplet retraction methods after shear is stopped. In the abovementioned classifications, the division between static and dynamic tensiometry is not clear-cut, as these methods can be, depending on the time frame in which the measurements are taken, considered as either dynamic or static (Holmberg, 2001).

The selection of the optimal experimental method for ATPS depends on their chemical and physical properties (i.e., viscosity and density), and on the accessibility and ease of use of the method itself. ATPS, e.g., mixtures of proteins and non-ionic polysaccharides, reach equilibrium slowly, in a matter of hours or even days. Their individual phases are composed mainly of water, which gives them similar densities and very low interfacial tensions. However, since one phase is typically concentrated in one biopolymer and depleted in the other, the viscosities and optical densities of the individual phases are very different (Ding et al., 2002; Spyropoulos et al., 2008a). When considering the classification of methods by Ding et al. (2002), this eliminates force and equilibrium shape methods and leaves the group of dynamic methods as those most suitable for ATPS. The following subsections will discuss in detail the simplest among the dynamic methods, the drop retraction method.

### 2.4.2.1 Droplet retraction/deformation theory

This section is an overview of several mathematical models relating interfacial tension with droplet shape. The methods assume that the shape of the interface is balanced by a combination of the internal interfacial and external viscous forces that are generated by flow. All models were initially developed for ideal dilute Newtonian systems where fluid flow far from the droplet is undisturbed and both phases flow independently of the shear rate. They were, however, later also proven to work well for dilute non-Newtonian W/W systems (Guido et al., 2002).

Taylor (1934) proposed the first theoretical droplet deformation model. He assumed that the flow viscous stress and velocity components are balanced with the interfacial tension ( $\sigma$ ) through changes in the curvature of the droplet. The famous Taylor correlation is given as:

$$D = Ca \frac{19\lambda + 16}{16\lambda + 16} \quad [2-6]$$

where  $\lambda$  is the viscosity ratio and  $D$  is Taylor's dimensionless deformation factor:

$$D = \frac{(a-b)}{(a+b)} \quad [2-7]$$

$a$  and  $b$  are the major and minor axes of a widely used ellipsoidal droplet representation (Figure 2-18),  $Ca$  is the dimensionless capillary number (i.e., a balance of deforming stresses and restoring stresses):

$$Ca = \frac{\eta_c \dot{\gamma} R_0}{\sigma} \quad [2-8]$$

where the parameters  $\eta_c$ ,  $\dot{\gamma}$  and  $R_0$  are the viscosity of the continuous phase, the shear

rate and the radius of the retracted spherical droplet, respectively.  $Ca$  and  $\lambda$  determine the type of deformation and breakage under shear. Torza et al. (1972) showed that Taylor's equation works well for Newtonian systems of equal viscosities and small deformations. Taylor's model was later expanded by Cox (1969, cited Guido and Villone, 1999, p. 247), Torza et al. (1972) and other authors (Guido et al., 2002) and experimentally reevaluated in a number of systems with various droplets sizes and velocity gradients.

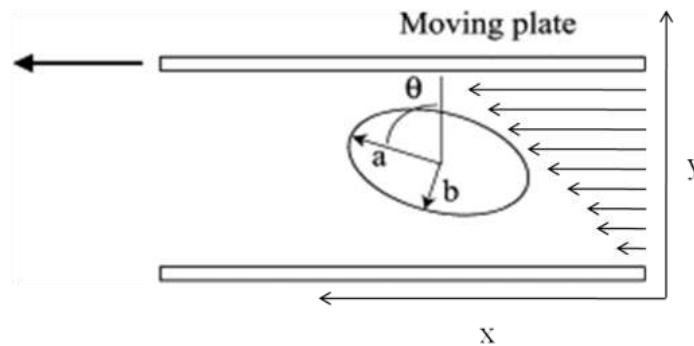


**Figure 2–18.** A schematic drawing of a deformed drop showing the two axes  $a$  and  $b$  and the angle  $\theta$  in the plane of shear (Source: Guido et al., 2002, p. 146).

Cerf (1951) and Cox (1969) developed models that provide the expression of (i) angle of rotation  $\theta$  (see Figure 2–18) or (ii) both,  $\theta$  and  $D$ , with  $Ca$  and  $\lambda$  (Guido et al., 2002). The small deformation model (eq. [2-9]) initially developed by Cerf (1951) and later corrected and expanded by Roscoe (1967) and Chaffey and Brenner (1967, cited by Guido et al., 2002, p. 146) provides a good fit to experimental data and can be used to calculate  $\lambda$  when combined with eq. [2-6] (from the slope of the linear plot of  $\theta$  vs.  $D$ ). Nevertheless,  $\theta$  is difficult to measure for small deformations.

$$\theta = \frac{\pi}{4} + \frac{(19\lambda + 16)(2\lambda + 3)}{80(1 + \lambda)} Ca \quad [2-9]$$

On the other hand, Cox (1969) reported the following two theoretical models for  $D$  and

$\theta$  for the droplet deformed in a steady state flow:

$$D = \frac{5(19\lambda + 16)}{4(1 + \lambda)\sqrt{(19\lambda)^2 + (20/Ca)^2}} \text{ or } \theta = \frac{\pi}{4} + \frac{1}{2} \tan^{-1} \left( \frac{19Ca\lambda}{20} \right) \quad [2-10]$$

His theory was later evaluated by Torza et al. (1972) who concluded that the Cox theory is correct only for  $\lambda \gg 1$  (Guido and Villone, 1999; Guido et al., 2002).

Later models for the calculation of  $\sigma$  from droplet deformation were developed and modified by Rallison et al. (1984), Carriere and Cohen (1989, 1991), Tjahjadi et al. (1994) (cited by Guido and Villone, 1999, p. 247) and Sigillo et al. (1997). Guido and Villone (1999) assessed the performance of the abovementioned models (by Rallison, Sigillo et al. and Carriere and Cohen; the model by Tjahjadi et al. was dismissed as it is better suited for highly deformed droplets) by plotting the non-dimensional axis  $a$  during retraction. They reported that all three models provide good estimates. While the model by Rallison had the best fit with the experimental data, the models by Sigillo et al. and Carriere and Cohen predicted the retraction as being slightly faster or slower, respectively. The polynomial model by Rallison, shown in eq. [2-11], describes the time evolution of the parameter of distortion from a spherical shape ( $\alpha A$ ).

$$I(\alpha_i) = \int_{\alpha_0}^{\alpha_i} \frac{1}{\alpha} \frac{1 + \frac{2}{5(\lambda-1)\alpha^2}}{\alpha \left( \left( \frac{1 + \frac{2}{5\lambda}}{\lambda} \right) \alpha \right)^{0.125} (1-\alpha)} d\alpha = \frac{1}{\tau} (t - t_0); \tau = \frac{\eta_c R_0}{0.465\sigma}; \alpha = \frac{b}{a} \quad [2-11]$$

where  $\alpha$  is the distortion from a spherical shape. The equation was solved by Guido and Villone (1998; 1999) for  $Ca \ll 1$  with steady state droplet deformation. Furthermore, the authors assumed the absence of flow during droplet retraction and hence neglected the vorticity and strain tensors. They obtained the following exponential decay function for  $D$ :

$$D = D_0^{-\frac{40(\lambda+1)}{(2\lambda+3)(19\lambda+16)}\tau} \quad [2-12]$$

where  $D_0$  is  $D$  at the start of retraction and  $\tau$  is the dimensionless characteristic time equal to  $t\sigma/\eta_c R_0$  where  $t$  is time. The above equation is usually used in its linear logarithmic form ( $\ln(D/D_0)$  vs.  $t$ ) and is valid for  $D \ll 1$  (or  $Ca \ll 1$ ):

$$\ln\left(\frac{D}{D_0}\right) = -\frac{1}{\tau} \Rightarrow \tau = \frac{\eta_c R_0}{\sigma} \frac{(19\lambda+16)(2\lambda+3)}{40(\lambda+1)} \quad [2-13]$$

#### 2.4.2.2 Application of the droplet retraction method for ATPS

In the following two subsections, the droplet retraction model presented by Guido and Villone (1998) is assessed for its suitability as the best of methods for measuring interfacial tension.

##### 2.4.2.2.1 Suitability

The droplet retraction method of Guido and Villone (1998) is a simple and accurate dynamic in situ method for the measurement of very low interfacial tensions ( $\sigma$ ,  $\sim 10^{-6}$  N/m) characteristic for ATPS. For the calculation of  $\sigma$ , the method requires experimental measurements of the viscosities of the individual phases ( $\eta_c$  and  $\eta_d$ ) and the time evolution of  $D$  of a droplet. The viscosities of the individual phases are obtained by viscometry and  $D$  by direct observation of a (sequence of images) deformed droplet restoring its shape after the shear is removed (Figure 2–19).

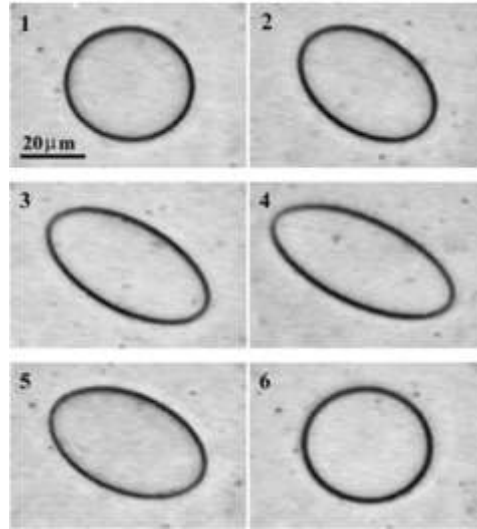


**Figure 2–19.** A sequence of images acquired at consecutive times shows the deformation of a caseinate-rich phase droplet in the alginate-rich phase (shear rate:  $0.05 \text{ s}^{-1}$ ): (1) droplet at rest; (2–3) start-up transient; (4) stationary shape; (5–6) retraction (Source: Guido et al., 2002, p. 148).

Guido et al. (2002) have confirmed for an aqueous system of NaCAS-sodium alginate that their modified droplet retraction model gives results that are in good agreement ( $\pm 10\%$ ) with the classical droplet deformation models mentioned in the previous section. Finally, they managed to obtain reproducible values of  $\sigma$  for both protein-continuous and polysaccharide-continuous systems.

#### 2.4.2.2.2 Concerns

There are also concerns regarding the use of the droplet retraction method.

First, the droplet retraction method was designed for equiviscous ( $\lambda \approx 1$ ) model Newtonian systems and not ATPS, which are more complex and characterised by disparate viscosities and various degrees of non-Newtonian shear thinning behaviour. Various authors (Guido et al., 2002; Ding et al., 2002; Spyropoulos et al., 2008a), however, justify the use of the method on ATPS in two ways: (i) by keeping the shear

rates of their experiments inside the zero-shear Newtonian plateau of the flow of the individual phases and (ii) by the fact that droplet retraction is monitored in the absence of shear, hence neither the degree of the non-Newtonian behaviour at higher shears nor the shear history should matter.

Second, the degree of the separation between the phases in an ATPS is very sensitive to time, temperature and shear (Guido et al., 2002; Antonov et al., 2003; Ding et al., 2005), which can cause changes in droplet size and composition. Ding et al. (2002) also confirmed that shear affects the accuracy of the measurements through its effect on droplet size and shape. This can cause errors in experiments where the phases are dispersed/“homogenised” and not injected into one another, as in the experiments performed by Guido et al. (2002). These undesired changes can be avoided by timely execution of the experiments, the use of equilibrated phases (not ultracentrifuged) and by conducting experiments at a constant temperature and shear. The existence of secondary phase separation inside polysaccharide-rich droplets during experiments, however, cannot be avoided, but is believed to not have an effect on the interfacial properties as the droplets of the low viscous phase are stabilised by the high viscosity medium.

Third, more recently, Shi et al. (2004) and Scholten et al. (2004a; 2005; 2006a) have brought attention to additional concerns regarding the use of the droplet retraction method in ATPS, such as the effects of (i) polydispersity, (ii) interfacial rigidity and (iii) interfacial permeability of ATPS. The biopolymers composing the equilibrium

phases are typically polydisperse. Shi et al. (2004) studied the kinetics by which the stationary value of  $\sigma$  ( $\sigma_s$ ) is affected by polydispersity,  $M_w$  ( $\sigma \propto M_w^{-3.5}$ ). Typically, systems with a narrow distribution of  $M_w$  reach  $\sigma_s$  faster and give higher  $\sigma$  than more polydisperse systems with wider  $M_w$  distributions. The authors also acknowledged the importance of droplet size, i.e., the size of the reservoir holding the polydisperse components, on the speed by which  $\sigma_s$  was obtained. They concluded that  $\sigma_s$  in shear experiments was reached in less than one second, which was  $3.3 \times 10^{-5}$  times faster than in pendant drop experiments ( $\sim 10$ – $100$  min) where droplet volumes were up to 30,000 times greater. It was further concluded that the effects of polydispersity can be dismissed in shear experiments. Similarly, Scholten et al. (2005) also dismissed, after some consideration, the effect of bending rigidities ( $k$ ) on the retraction of droplets. They calculated, taking into account realistic values for  $k$  and  $\sigma$ , that bending rigidities become important only for droplets of a critical radius ( $R_c$ ) of  $\sim 2$   $\mu\text{m}$ , which is much smaller than the 20–80  $\mu\text{m}$  sized droplets produced in measurements of  $\sigma$  with the drop retraction method. On the other hand, interfacial permeability has proven to be an important trait of ATPS influencing measurements of  $\sigma$  in close proximity to the critical point where it can contribute to an overestimation of its value. For example, the  $\sigma$  in an ATPS of  $\sim 10^{-8}$  N/m can be overestimated by  $\sim 90\%$ , and in ATPS with  $\sim 9.2$   $\mu\text{N/m}$  by  $\sim 10$ – $20\%$ . For systems close to the critical point, Scholten et al. (2005) have proposed a modification to the droplet deformation model:

$$\tau = \frac{\eta_c R_0}{\sigma} \left( \frac{40(\lambda + 1)}{(19\lambda + 16)(2\lambda + 3)} + \frac{\lambda_{\text{eff}} \eta_c}{R_0} \right)^{-1} \quad [2-14]$$

where  $\lambda_{\text{eff}}$  is the effective permeability of the ATPS.  $\lambda_{\text{eff}}$  was found to be inversely

proportional to  $\sigma$  ( $\lambda_{eff} \propto 1/\sigma$ ) and proportional to the square of the interfacial thickness  $\xi$  ( $\lambda_{eff} \propto \xi^2$ ). Hence, in systems with a relatively thick interfacial region, interfacial permeability needs to be considered in measurements of  $\sigma$ , but for systems of higher  $\sigma$ , further from critical point,  $\lambda_{eff}$  is of a size of an estimated error, i.e.,  $\sim 10\%$ .

Finally, in terms of the experimental setup, one must also consider (i) the effect of buoyancy ( $\Delta\rho g R_0 / \eta_c \dot{\gamma}$ ) and (ii) wall effects. The effects are negligible when buoyancy is  $< 0.3$  (Philips et al., 1980, cited by Guido et al., 2002, p. 146; Guido et al. assessed the buoyancy of NaCAS-sodium alginate ATPS  $< 0.01$ ) and the gap is  $> 5$  times larger than the size of the droplets (Kennedy et al., 1995, cited Guido et al., 2002, p. 145).

### 2.4.3 Interfacial tensions of various ATPS

Although much research has been carried out on ATPS in terms of their phase behaviour and rheological behaviour, the interfacial tensions of the systems have not been measured as extensively. The reason for the relative scarcity of these data lies in the experimental difficulties involved in  $\sigma$  measurements.

Table 2–1 shows a few studies in which interfacial tensions of ATPS were measured with the intent of giving an indication of the range of absolute values obtained.

**Table 2–1. Interfacial tension values of protein-polysaccharide and surfactant-polysaccharide ATPS. \* if not stated otherwise, the interfacial tension is given at room temperature.**

System	Physical characteristics	Method	Interfacial tension *	Source
Sodium alginate (NaA)-sodium caseinate	NaA=0.25 Pa.s; NaCAS=0.022 Pa.s	Drop retraction method	1.178–1.102 $\mu\text{N/m}$	(Pacek et al., 2001)
Sodium alginate-sodium caseinate	NaA=2.5 Pa.s; NaCAS=0.25 Pa.s	Drop retraction method	8.15-8.41 $\mu\text{N/m}$	(Guido et al., 2002)
Gellan- $\kappa$ -carrageenan	Gellan=0.4 Pa.s $\kappa$ -carrageenan=1.1 Pa.s	Drop retraction method	7.5 $\pm$ 1.4 $\mu\text{N/m}$ at 60°C	(Wolf et al., 2000)
Gelatine-maltodextrin	Gelatine $\approx$ 0.08 Pa.s Maltodextrin $\approx$ 0.12 Pa.s	Drop retraction method	50 $\mu\text{N/m}$ at 60°C	(Stokes et al., 2001)
Gelatine-dextran	Gelatine $\approx$ 0.04-0.16 Pa.s Dextran $\approx$ 0.01-0.06 Pa.s	Drop retraction method	9.14–30.02 $\mu\text{N/m}$	(Ding et al., 2002)
Sodium dodecyl sulphate (SDS)-pullulan with NaCl	SDS=0.006-9.5 Pullulan-rich=0.1-1.1	Drop retraction method	8.26–35.18 $\mu\text{N/m}$	(Spyropoulos et al., 2008a)
Fish gelatine-dextran	$\sim$ 0.005-0.03 Pa.s (average viscosity of the system)	Drop spinning method	$\sim$ 3–8 $\mu\text{N/m}$	(Scholten et al., 2005)
Fish gelatine-dextran	Gelatine=7.3-26 mPa.s Dextran=6.8-34.8 mPa.s	Drop retraction method	0.15–9.2 $\mu\text{N/m}$	(Scholten et al., 2005)
cetyltrimethylammonium bromide,1,3-propanediyl-bis(dodecyldimethylammonium bromide)-sodium dodecyl sulphonate (CTAB,AS-12-3-12, AS) with and without NaBr	12-3-12-AS $\sim$ 50 mPa.s CTAB-AS $\sim$ 10 mPa.s	Spinning drop method	0.06–21 $\mu\text{N/m}$	(Nan et al., 2006)
Sodium alginate-sodium caseinate	NA=0.025–1.34 Pa.s NaCAS=0.088–1.92 Pa.s	Tomotika's theory of fibril break-up	0.01–5.2 $\mu\text{N/m}$	(Van Puyvelde et al., 2002)
Gelatine-dextran	Gelatine $\approx$ 0.02-0.4 Pa.s Dextran $\approx$ 0.08–0.2 Pa.s	Fibril break-up and drop retraction method	19 $\pm$ 2 $\mu\text{N/m}$ (break-up method) 21 $\pm$ 3 $\mu\text{N/m}$ (drop retraction)	(Antonov et al., 2004)

Two types of experiments are reported in the literature: (i) experiments that either evaluate a method or compare methods on a given system (for example Guido et al., 1999a; Van Puyvelde et al., 2002) and (ii) experiments that study the effects of external parameters on the  $\sigma$  of a system (for example Forciniti et al., 1990; Ding et al., 2002; Ding et al., 2005; Spyropoulos et al., 2008a; discussed further in § 2.4.4, p. 2–56). The review of the literature shows that the drop retraction method is most commonly

used in measurements of  $\sigma$ . Other methods, including the improved drop deformation method (Son and Migler, 2002), the spinning drop method (de Hoog and Lekkerkerker, 1999; Scholten et al., 2006a; Nan et al., 2006) and drop break-up method (Van Puyvelde et al., 2002; Antonov et al., 2004) are less common. The work by Scholten et al. (2006a) also provides evidence against the use of the spinning drop method for the measurement of the equilibrium  $\sigma$ . Under conditions that are characteristic of the method (i.e., centrifugal force acting on the suspended drop within a cylindrical container), all components are free to diffuse out from the dispersed drop to the continuous medium until equilibrium is reached. The equilibrium reached during the measurement differs from the equilibrium reached under static conditions.

In drop retraction experiments, various authors used various experimental setups (geometries and microscope-video systems). Drops were sheared either by a custom-made square glass parallel plate apparatus (Wolf et al., 2000, four roll mill; Guido et al., 2002, 100x5x5 mm and 0.5 mm gap) or commercial rheometers with the use of in-house built transparent geometries, such as a glass Couette device ( $d_i = 80$  mm and  $d_o = 85$  mm; Ding et al., 2002; Antonov et al., 2004; Spyropoulos et al., 2008) or glass cone and plate geometries (Tromp and de Hoog, 2008; 40 mm 4° counter-rotating cone and plate geometry) coupled to a microscope and video camera.

#### **2.4.4 Parameters influencing the interfacial tension in ATPS**

The interfacial properties of ATPS have been studied in terms of the effects of (i) concentration, (ii) polydispersity,  $M_w$  and solubility, (iii) temperature and (iv)

additives. Accordingly, the following paragraphs discuss the effects one by one.

The concentration of ATPS affects the interfacial properties in a power law fashion (eq. [2-15]). This was shown by a correlation of the experimental data for  $\sigma$  with the length of the tie-line (TLL):

$$\sigma = C_1 \times TLL^{C_2} \quad [2-15]$$

A similar relationship was found when  $\sigma$  was correlated with (i) the difference in concentration of the biopolymer in either of the separate phases ( $\Delta[BP_i]$ , where  $i=1$  for biopolymer A and 2 for biopolymer B) and (ii) the density difference between the phases, ( $\Delta\rho$ ):

$$\sigma = C_3 \times \Delta[BP_i]^{C_4} \quad [2-16]$$

$$\sigma = C_5 \times \Delta\rho^{C_6} \quad [2-17]$$

$C_{1-6}$  in eq. [2-15] to [2-17] are the scaling parameters/critical exponents. Their values are ATPS-specific and hence depend on the types of biopolymers, their  $M_w$  and environmental parameters. The determination of the scaling parameters of a system makes it possible to calculate  $\sigma$  from the  $TLL$ ,  $\rho_{d/c}$  and  $[BP_i]_{d/c}$  of this system (Forciniti et al., 1990; Ding et al., 2002; Antonov et al., 2004; Nan et al., 2006; Spyropoulos et al., 2008a). Based on these parameters, the system can also be considered as near-critical, if  $C_4$  is 1.3–1.5 and  $C_6/C_5$  is 3–3.9, depending on the model used in the calculation, or off-critical. Consequently, these parameters can also give information on the type of interface (i.e., narrow or diffuse) (Scholten et al., 2004b).

Polydispersity ( $M_w/M_n$ ), molecular weight ( $M_w$ ) and molecular miscibility also affect the  $\sigma$  of an ATPS. The polydispersity of the system (mentioned in different context on p. 2—53) affects the kinetics by which  $\sigma_s$  is reached and also its finite value. A polydisperse system reaches a lower value of  $\sigma_s$  more slowly than a less polydisperse system of the same  $M_w$  (Shi et al., 2004). Studies have shown that increased  $M_w$  of ATPS components increases the  $\sigma$ . For example, Bamberger et al. (1984) reported a 50% increase in measured  $\sigma$  for a 10-fold increase in the  $M_w$  of dextran in a polyethylene glycol-dextran ATPS. Forciniti et al. (1990) further investigated the effect in the same system and concluded that an increase in the  $M_w$  of polyethylene glycol has a more pronounced effect on the  $\sigma$  than dextran, which is also in tune with their difference in  $M_w$ . In a different system (i.e., poly(dimethylsiloxane)-poly(tetramethyldisiloxanylene) with oligodimethylsiloxane of various  $M_w$ ), Sakane et al. (2001) showed that the  $M_w$  of the additive and its miscibility with either of the coexisting phases determines the degree of adsorption of the additive to the interface. They concluded that additives with higher  $M_w$  and lower miscibility adsorb to the interface most effectively and hence cause a large reduction in the  $\sigma$  of the system.

The effect of temperature on the  $\sigma$  of an ATPS is not clear-cut. For example, Van Puyvelde (2002) found that the  $\sigma$  in a gelatine-dextran system increased rapidly when the system approached the gelation temperature of the gelatine-rich phase (32°C), but it stayed virtually unchanged at other temperatures (35–55°C). Ding et al. (2005) confirmed for a gelatine-pullulan system that above the melting point of gelatine

(>32°C), the  $\sigma$  did not change. Nevertheless, they observed a decrease in the  $\sigma$  at the temperature of gelation. Contradictory data also exists for non-gelling ATPS. For example, Bamberger et al. (1984) stated that the  $\sigma$  in a dextran-polyethylene glycol ATPS increased with a decrease in the temperature of the system, which may be explained by the changes in the density of the system. On the other hand, Forciniti et al. (1990), for the same ATPS, did not find any significant correlation between  $\sigma$  and temperature. The kinetics by which a stationary value of  $\sigma$  is obtained is however, clearly dependant on the temperature and is much faster, almost instantaneous, at high temperatures (Shi et al., 2004). Elevated temperatures can also cause denaturation of ATPS components. When a protein, for example, is heated, non-covalent bonds that maintain its secondary and tertiary structures weaken and, at a high enough temperature, break. In the early stages of thermal denaturation, most protein molecules begin to unfold. The unfolding often leads to a slight increase in water tightly bound to the protein. However, if proteins interact to form of a three-dimensional network capable of entraining water, a gel can form (Dickinson and Casanova, 1999).

The solutes (salts, bases, acids and sugars that change the ionic strength, pH and solvent properties of the systems) have been shown to affect the  $\sigma$  of ATPS, aerated ATPS and aerated protein solutions in a system specific way. An increase in salt, for example, NaCl added to a pullulan-sodium dodecyl sulphate ATPS, increased the  $\sigma$  (Spyropoulos et al., 2008a), but when NaCl was added to a different polyethylene glycol-dextran ATPS, no significant effect on its  $\sigma$  was observed. Instead, in this system, an increase in  $\sigma$  was observed upon the addition of PO<sub>4</sub> (Bamberger et al., 1984). To the best of our knowledge, the effect of pH and sugars in unaerated ATPS has not been

studied, but instead these effects can be inferred to from the interfacial/surface studies of aerated ATPS (Miquelim et al., 2010) and aerated protein solutions (Antipova et al., 1999). The  $\sigma$  depends directly on the amount of ionic interactions between the biopolymers, which in turn depends on the amount of charge (controlled by pH) and non-covalent interactions (controlled by the addition of sugars) between the components in ATPS. For example, proteins near the isoelectric point ( $I_p$ ) become hydrophobic by dissociation/aggregation, which causes a decrease in association with other components and a decrease in  $\sigma$ .

## **2.5 Aqueous two-phase model systems**

The physical and chemical properties of the ingredients in ATPS determine its phase behaviour, rheological behaviour and interfacial properties. Accordingly, the following subsections overview the structural and functional characteristics of NaCAS and GM, and how they are affected by sugars, either individually or when they are mixed with other biopolymers. The effects of sugars on the biopolymers is inferred from studies of similar protein-polysaccharide ATPS.

### **2.5.1 Sodium caseinate**

Sodium caseinate is a dissociated native micellar casein, a major protein of mammalian milk (Belyakova et al., 2003), which appears in solution in the form of small ( $R_g = 11 \text{ nm} - 22 \text{ nm}$ ) dissolved molecular blocks of different fractions and functionalities (Tolstoguzov, 1991; Farrer and Lips, 1999; Lucey et al., 2000). Above its isoelectric point ( $I_p = 4.6$ ), the molecules are negatively charged (Antipova et al., 1999).

Although NaCAS loses its micellar structure during the production process, it can, depending on the solvent environment, form submicelles. These submicelles are formed and destroyed in a reversible and competing process of molecular association and dissociation (Pitkowski et al., 2008). They have a hydrophobic centre and a hydrophilic outer surface (see insert in Figure 2-20) and their size/aggregation number and related functional properties (i.e., dissolution, flow, interfacial properties and proneness to association) depend on factors such as (i) ionic strength, (ii) pH, (iii) temperature and (iv) the addition of low molecular weight ingredients (e.g., sugars, alcohols and surfactants). At high ionic strength,  $I > 100$  mM, the activity of NaCAS molecules to react with other molecular species in the mixture is reduced on the account of their self-association and the screening of charges by added salt, commonly demonstrated by an increase in  $[\eta]$ , e.g., from 0.009 to 0.016 L/g (Belyakova et al., 2003; Pitkowski et al., 2008). At low ionic strength, on the other hand, NaCAS dissociates and forms smaller aggregates (Pitkowski et al., 2008). At constant ionic strength and pH above its  $I_p$ , NaCAS also dissociates (the aggregates reduce in size) and consequently its reactivity increases (Jourdain et al., 2008). The size of the aggregates, however, increases upon a decrease in pH (acid-induced aggregation) and increase in temperature (5–50°C). Aggregation is faster at low temperatures and depends greatly on the type of chelant used in the manufacture of NaCAS. Above 50°C, aggregation is temperature independent (Schorsch et al., 2000a; Pitkowski et al., 2008). Besides temperature, small molecular additives also affect NaCAS aggregation in specific ways (Radford et al., 2004). For example, sugars (namely sucrose), also relevant to this project, determine aggregation in a concentration related way through the formation of non-covalent hydrogen bonds

with NaCAS and the solvent (Antipova et al., 1999; Belyakova et al., 2003). All the above mentioned parameters influence both the bulk and surface properties of NaCAS.

The rheological characteristics of NaCAS suspensions are those of multi-arm star polymers. NaCAS shows concentration and temperature dependence. Under flow, similar to other biopolymers, NaCAS molecules behave like soft spheres that jam at a critical biopolymer concentration ( $c^*$ ) (Figure 2–20).

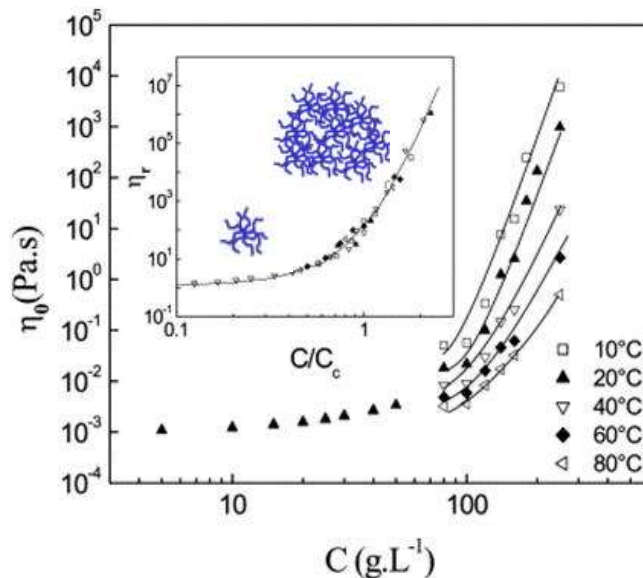


**Figure 2–20. Concentration dependence of the zero-shear viscosity of caseinate suspensions at different temperatures. The insert shows the master curve obtained by normalising the viscosity by the solvent viscosity and the concentration by  $c^*$  (130 g/L  $\approx$  13 wt%). The solid line is to guide the eye (Source: Pitkowski et al., 2008, p. 99).**

At concentrations  $< c^*$ , their viscosities are shear independent (also see § 2.3.1, p. 2–30). The viscosity of NaCAS ( $\eta_{NaCAS}$ ) decreases sharply and reversibly with an increase in temperature. If the temperature ramp is fast, a hysteresis effect is observed. Solutions with a high concentration of NaCAS depend more strongly on temperature than more dilute solutions. With a decrease in temperature, NaCAS solutions gel and the storage ( $G'$ ) and loss ( $G''$ ) moduli increase (Pitkowski et al., 2008).

### 2.5.2 Galactomannans

Galactomannans are rod-shaped, non-ionic random coil polysaccharides with a high degree of polymerisation and polydispersity (Buckeridge et al., 2000). They are widely used in the food industry for their thickening and stabilising effects (Richardson and Norton, 1998). GMs are non-ionic hence they are not affected by the presence of salts. Although not overly sensitive to pH they will degrade at pH extremes and at high temperatures (Kök et al., 1999; Mandala et al., 2007). Their structure differs by plant source, the extraction procedure and in the degree to which they are enzymatically engineered. Common Latin plant names are used to better distinguish galactomannans from each other; several examples are given for the galactomannans that are of interest in this project: *Ceratonia siliqua* (LBG), *Cyamopsis tetragonolobus* (GG), *Caesalpinia spinosa* (TG) and *Trigonella foenum-graecum* (FG) (Srivastava and Kapoor, 2005; Figure 2–21).

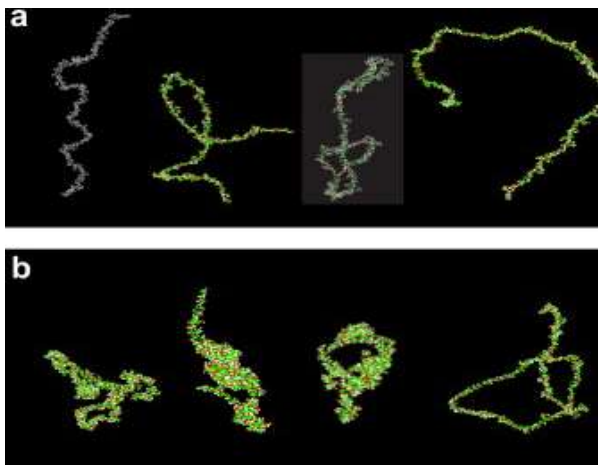


**Figure 2–21. Conformation of simulated galactomannans obtained with different parameter settings (from left to right: fenugreek gum, guar gum, tara gum and locust bean gum) (a) Min\_Bond=3 and Max\_Bond=4 (b) at Min\_Bond=3 and the Cut-Off distance=15 Å (Source: Wu et al., in press).**

The primary and secondary structures of GMs determine their functional properties. The primary molecular structure is common for all GMs; they are comprised of 1,4- $\beta$ -D-mannan linear regions with branches from position 6 of the mannan molecule

to a single  $\alpha$ -D-galactopyranosyl residue. Their finer secondary structure differs and is determined by (i) the galactose content, (ii) the distribution of galactose and (iii) galactose polydispersity in the molecule (Dea et al., 1986a; Dea et al., 1986b; Richardson et al., 1998). The secondary structure determines the character of the molecule, such as size, excluded volume (flexibility), stiffness and elasticity, an example of which is given in Table 2–2 for four GMs relevant to this work.

**Table 2–2. Approximate mannose : galactose ratio ( $M : G_{approx}$ ), molecular weight ( $M_w$ ), intrinsic viscosity ( $[\eta]$ ), persistence length ( $L_p$ ), characteristic ratio ( $C_\infty$ ) and radius of gyration ( $R_g$ ).**

Sample	Fenugreek gum	Guar gum	Tara gum	Locust bean gum
$M : G_{approx}$	1:1	2:1	3:1	4:1
$M_w / M_n$	/	#1.15	/	#1.21
$M_w$ [g/mol]*	##1.4; ###3.2 $10^6$	#1.22; ##1.2; ###2.9 $10^6$	###2.2 $10^6$	#0.81; ##1; ###2 $10^6$
$[\eta]$ [dl/g]*	##9.61; ###15.10	#9.25; ##10.5; ###15.8	###14.5	#13.79; ##14.4; ###14.2
$L_p$ ** [nm]	2.18	4.86	3.10	18.46
$C_\infty$ ** [nm]	2.35	6.27	4.66	18.24
$R_g$ ** [nm]	42.13	31.05	29.61	59.18

\* Average  $M_w / M_n$ ,  $M_w$  and  $[\eta]$  values for various galactomannans are cited from: #Richardson et al. (1999), ##(Brummer et al., 2003) and ###(Wu et al., 2009). \*\* Conformational parameters data are cited from (Wu et al., in press).

The data show that LBG and TG have, in comparison to GG and FG, fewer galactose branches and longer mannan regions ( $M : G_{approx}$ ) and a smaller  $M_w$ . However, the  $[\eta]$  (a measure of the excluded volume and molecular permeability) and the conformational parameters ( $L_p$ ,  $C_\infty$  and  $R_g$ ) show LBG to be the stiffest and largest among the four GMs, with the largest excluded volume. FG, on the other hand, is shown to have the smallest excluded volume and the highest flexibility among the GMs.

The functional properties arising from the GM structure are (i) solubility, dispersiveness and flow, (ii) interfacial properties, (iii) proneness to association and (iv) retardation of ice crystallisation. These functional properties will be addressed in the following four paragraphs. If available, an example will be given for the GMs relevant to this work.

Higher substitution gives GMs improved solubility and dispersiveness. For example, GG readily dissolves at room temperature, whereas LBG requires heat to be dissolved. After dissolution above  $c^*$ , all GMs give highly viscous non-Newtonian solutions (see § 2.3.1, p. 2–30). Highly branched GMs (e.g., GG and FG) show a greater degree of low shear thinning behaviour ( $\eta < 20 \text{ s}^{-1}$ ) and a lesser degree of high shear thinning behaviour than less branched GMs (Figure 2-22 a). A correlation between  $\eta_0$  and  $M_w$  has been observed. The degree of shear thinning is also influenced by the concentration of the GM (i.e., GM solutions of low concentration are more Newtonian). The storage modulus ( $G'$ ), a measure of molecular rigidity, follows: GG>FG>TG>LBG (Wu et al., 2009).

The latest study of the interfacial properties of LBG, TG, GG and FG by Wu et al. (2009) confirms that GMs are inherently surface active. The authors showed that highly branched GMs are most surface active and that interfacial activity increases with the GM concentration. As seen in Figure 2-22 b, FG is the most surface active GM, i.e., measurements are carried out at the air-water interface. At the liquid interface, GG is the best emulsifier, followed by FG, TG and LBG.

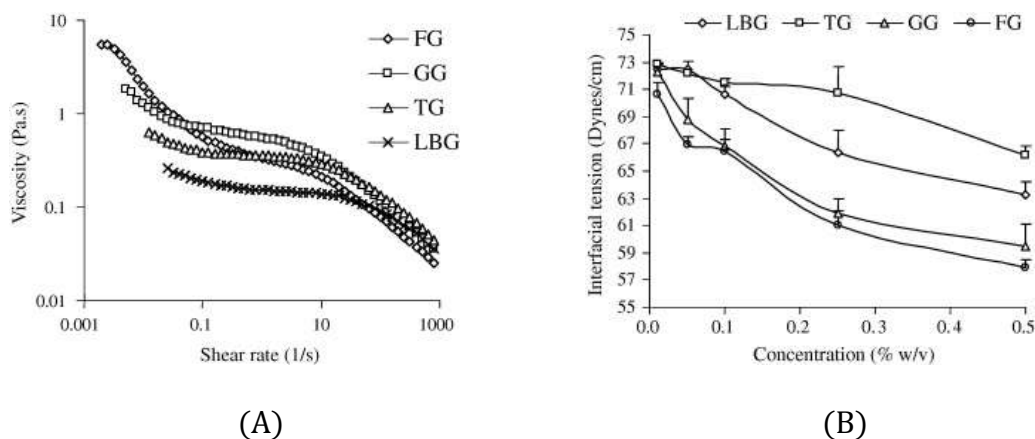


**Figure 2-22. (A) Flow curves of 0.5% galactomannan solutions. (B) Interfacial activities of galactomannans at various concentrations. FG=fenugreek gum; GG=guar gum; TG=tara gum; LBG=locust bean gum (Source: Wu et al., 2009, p. 1144, 1143).**

Despite having an irregular linear structure, GMs can (i) self-associate and (ii) associate with other polysaccharides. This is determined by their fine molecular structure. Different structural characteristics control the two association processes. In terms of self-association, a threshold of the mannan backbone of  $\sim 6$  residues long has been found to be limiting. For example, if GMs have  $> 6$  residues long mannan regions, their interactive properties are controlled by structural characteristics of the unsubstituted region, while if GMs have mannan regions of  $< 6$  residues long, the interactive properties are controlled by the unsubstituted side of the D-mannan region (Dea et al., 1986b). Self-association occurs by binding of the D-mannan backbone with D-galactose via unsubstituted sides in the ordered two-fold ribbon conformation (BeMiller and Whistler, 1996, Figure 2-21, p. 2-63). The association of GMs with other polysaccharides (e.g., xanthan and cellulose), on the other hand, is controlled by the degree of branching and by how  $\alpha$ -D-galactopyranosyl groups are distributed and positioned along the backbone. A higher frequency of midway unsubstituted mannan regions and a higher frequency of exactly alternating regions in the  $\beta$ -D-mannan chain

result in greater activity of GMs with < 30% (e.g., LBG, TG) and > 40% D-galactose (e.g., GG, FG), respectively. This means that even highly branched GMs (i.e., GG) are capable of association with other polysaccharides (Dea et al., 1986a). How the GMs (self) associate also determines their other functional properties.

In frozen solutions, GMs limit the rate of ice crystal growth during recrystallisation. While weakly gelling GMs (i.e., LBG) slow down ice crystal growth by gel formation at the interface of these crystals, other GMs (such as GG, FG and partially TG) slow down crystallisation through increased viscosity of the solution at the interface and hence decreased diffusion of water and solutes. They work best when accompanied with proteins because they form phase-separated protein regions, i.e., extra barrier (Goff et al., 1999).

### **2.5.3 Effect of sugars on sodium caseinate, galactomannans and their mixtures**

Sugars affect the conformational properties of NaCAS and GMs when they are found alone or as a component of a ternary mixture. Studies investigating the effect of sugar/sucrose on the individual components (Table 2-3) and their ternary mixtures (Table 2-4) are summarised on the next two pages. They illustrate the importance of the solvent environment on the stability/functionality of proteins/NaCAS and GMs.

Studies on individual macromolecules have revealed that their solubility depends on factors, such as (i) the molecular structure of the species, (ii) the sugar concentration, and, especially in the case of charged molecules like proteins/NaCAS,

(iii) the environment, such as pH, ionic strength and temperature (Richardson et al., 1998; Semenova et al., 2002). Sugars affect the stability of NaCAS and GMs in two ways: (i) they physically react with the macromolecules and/or (ii) they order the solvent by creating a sugar-water network in which macromolecules surrounded with hydration layer are suspended (Kasapis and Al-Marhoobi, 2000; Semenova et al., 2002; Kaushik and Bhat, 2003).

**Table 2–3. Studies on the effect of sugar on individual proteins/NaCAS and galactomannans.**

System	Conditions	Authors
<b>Proteins</b>		
11 S globulin-sucrose 11 S globulin-glucose 11 S globulin + 0.05% w/v dextran 11 S globulin + 2% w/v dextran 11 S globulin + 0.05% w/v maltodextrin	0.01 mol/dm <sup>3</sup> pH 7.0, 25°C	(Antipova and Semenova, 1997a)
Ovalbumin-sucrose Sodium caseinate-sucrose	pHs (7.0 and 5.5) 20, 35, 45°C 0.005 mol dm <sup>-3</sup> 0.25-1 wt% protein 0.05-1 wt% sucrose and 25 wt%	(Antipova et al., 1999)
Casein-sucrose	2-5 wt% NaCAS 0-40 wt% sucrose 5°C, pH=6.8; I=0.08	(Schorsch et al., 2000a)
Sodium caseinate-sucrose	10 to 78 w/v% sucrose and pH= 7.0 to 3.5	(Belyakova et al., 2003)
RNase A, lysozyme, $\alpha$ -CTgen, cytochrome c with trehalose	pH=2.5, 4, 7 T= 10 to 80°C 1.5-2 M trehalose	(Kaushik and Bhat, 2003)
<b>Galactomannans</b>		
Locust bean gum-sucrose Guar gum-sucrose	0.02-0.1 wt% galactomannan 0-40 wt% sucrose	(Richardson et al., 1998)
rhodamine isothiocyanate locust bean gum (guar gum)-sucrose, etc.	0.42 wt% labelled galactomannans 40 wt% sucrose -50 < T < -10°C	(Goff et al., 1999)
Locust bean gum-glucose Guar gum-glucose K <sup>-</sup> -carrageenan-glucose	0.5- 1 wt% polysaccharide in 82- 82.5 wt% glucose syrup; T=-45 to 20°C	(Kasapis et al., 2000)
Guar gum-sugars	50 wt% fructose, glucose, fructose+glucose and sucrose; 1 wt% guar gum	(Ptaszek et al., 2007)

Although the effect of sugar on macromolecular species as a whole is similar, slight differences have been observed in relation to the type of sugar (Antipova and

Semenova, 1997a; Ptaszek, 2007) and the type of macromolecular species (the type of protein, as shown by Antipova et al. (1999) and the type of GM as shown by Richardson et al., (1998)).

**Table 2–4. Studies on the effect of sucrose in ATPS.**

<b>System</b>	<b>Conditions</b>	<b>Authors</b>
Sodium caseinate-ovalbumin 11S globulin from vicia faba-ovalbumin Sodium caseinate-sodium alginate	0-50% sucrose; pH=7; *I=0.1 mol/L; 25°C	(Antipova and Semenova, 1995)
11S globulin-dextran	0 and 50 w/v% sucrose; pH 7.0, I = 0.1 mol/L; 25°C	(Antipova and Semenova, 1997b)
skim milk powder-with rhodamine isothiocyanate labelled locust bean gum or guar gum, etc.	18.3 wt% skim milk powder; 0.42 wt% labelled galactomannans; 23.3 wt% sucrose; -50 < T < -10°C	(Goff et al., 1999)
Micellar casein-locust bean gum	0-40 wt% sucrose; 5°C; pH=6.8; I=0.08 mol/L	(Schorsch et al., 1999a)
Skimmed milk protein-locust bean gum Native phosphocaseinate-locust bean gum	0-40 wt% sucrose 5°C pH=6.8; I=0.08 mol/L	(Schorsch et al., 1999b)
Skimmed milk protein-locust bean gum Micellar casein-locust bean gum	0-40 wt% sucrose 5°C pH=6.8; I=0.08 mol/L	(Schorsch et al., 2000a)

\*I=ionic strength.

The effects of sugars on the systems have been studied experimentally. The thermodynamic approach has been applied in the studies on the effects of sugar on individual macromolecules (Table 2–3) and on ATPS (Table 2–4) (Antipova and Semenova, 1995; Antipova and Semenova, 1997b). The approach for ATPS is also complemented by studies on the phase behaviour, quiescent microstructure and rheological behaviour of these systems (Schorsch et al., 1999a; 1999b; 2000a).

For protein-polysaccharide ATPS with and without sugar (namely sucrose), low compatibility of the macromolecular ingredients was observed (Table 2–4). While

Antipova and Semenova (1995) on one hand showed a great increase in the cosolubility of macromolecular species in ATPS, Schorsch et al. (1999a; 1999b; 2000) showed that sucrose affected the thermodynamic compatibility of these systems only slightly. Both, however, attributed the increase in cosolubility to the effect of sucrose on the protein component of the ATPS.

## 2.6 Conclusion

Binary and ternary model systems are commonly used to better understand a microstructure formation of the inherently more complex real emulsion-based foods. Studies on the model systems show that the microstructure is controlled by (i) the thermodynamic compatibility of its major components, proteins and polysaccharides, (ii) shear and (iii) interfacial properties, which are controlled by the degree of physical adsorption of the molecules to the interfaces. In dairy food formulations, sugars are typically added in large quantities for taste. Sugars also influence the thermodynamic compatibility of proteins and polysaccharides by changing the solvent properties of these systems.

The reviewed literature also shows that binary solutions of sucrose-NaCAS and sucrose-GMs, all three ubiquitous components of dairy food formulations, have been studied in terms of their bulk and surface properties individually, but not as a ternary NaCAS-GM-sucrose system. Other protein-polysaccharide-sucrose systems have been, however, studied previously, first by Antipova and Semenova (1995; 1997b), and later by Schorsch et al. (1999a; 1999b; 2000). However, the latter studies did not assess the

interfacial properties, nor how they were affected by other common sugars such as glucose, fructose and trehalose. Consequently, and for the added reason that the (co)solubility is system-specific, there is a need for more fundamental research in the area. This research, which is a systematic study on the effect of the four most commonly used sugars on the phase equilibria, flow and interfacial properties of model NaCAS-GM systems, partially fills this gap.

## CHAPTER 3: EXPERIMENTAL SETUP

### 3.1 Introduction

In this study, visual assessment, optical rotational viscometry, light microscopy and confocal laser microscopy were used to characterise four model protein-polysaccharide ATPS: (i) NaCAS-LBG (System 1), (ii) NaCAS-TG (System 2), (iii) NaCAS-GG (System 3) and (iv) NaCAS-FG (System 4) either with or without sugar. Special attention was given to the type and concentration of the GM and sugar present in the model system.

This chapter explains in detail materials and procedures applied in the investigation of the behaviour of these aqueous protein-polysaccharide-sugar systems. Four types of experiments were undertaken to investigate:

- phase behaviour of protein-polysaccharide-sugar aqueous systems;
- rheological behaviour of equilibrium (i.e., protein-rich and polysaccharide-rich) phases, their blends and pure solutions;
- microstructure of these systems in relation to flow;
- and interfacial properties of the aqueous protein-polysaccharide-sugar systems.

### 3.1.1 Model systems

Sodium caseinate-galactomannan model systems are selected because they closely resemble real dairy emulsions or represent their major components. These ATPS are found in ice-creams, low fat spreads, beverages, sauces, dressings and many other foods, where they typically assume a role of a water continuous phase (Tolstoguzov, 2002).

A first component is NaCAS. It is used as a milk protein in all model systems, in order to avoid greater complexity of other biological milk protein solutions, such as skimmed milk and whey. NaCAS is also most commonly used emulsifier, stabiliser, whipping agent, and protein enricher in dietetic formulas, health food products, dairy products, toppings and spray-dried emulsions. NaCAS is a derivate of skimmed milk of high nutritional quality. It is composed of small dissolved molecules or 50 nm stable particles, which are capable of forming micelles (Lucey et al., 2000).

A second component—like NaCAS also a random coiled biopolymer—in the model systems is one of four GMs: LBG, TG, GG, and FG. The GMs are used in the model systems because they are also found as emulsifiers, stabilisers and thickeners (i.e., texture modifiers) in foods, especially in dairy formulations, and have weak gelling properties. As previously mentioned in § 2.5.2, p 2–63, their basic structure is similar—alternating “smooth” regions, to which substituted regions are attached so that they form branches. The GMs, however, differ in the overall degree of branching expressed by the mannuronat : guluronate acid ratio (M:G). LBG (~4:1) is the least branched, followed by more branched TG (~3:1) and GG (~2:1). Most branched, thus most stable

and rigid, is FG (~1:1), where each mannose unit has its own galactose unit. In GMs of lower degree of branching galactose units cluster together in blocks, which are unevenly distributed.

Finally, one of four sugars is added to the model systems to alter its solvent properties. A selection between three most commonly used sweeteners (non-reducing disaccharide sucrose, and reducing monosaccharides: fructose and glucose) and trehalose (also non-reducing disaccharide), was made. Although trehalose is more expensive and not as commonly used as sucrose, it is interesting because of its functional properties (mild sweetness, low browning, high stability and low hygroscopicity), which give the sugar a variety of uses as protein-stabiliser, moisture barrier, flavour-enhancer and cryoprotectant in a variety of foods and even drugs. Besides, it is not as cariogenic and induces a lower insulin response to glucose, which gives trehalose health benefits over the other three sugars. Even though the above sugars are added mainly for taste, they are assessed in this study for their structuring role.

## **3.2 Materials**

Sodium caseinate S<sup>®</sup> (90% protein, 5% moisture, 4% ash, 0.8% fat, and 0.2% lactose, [Na]=1.4g/100g, particle size < 500 μm, bulk ρ=380 g/L), courtesy of DMV International, was first dispersed in a citrate buffer of pH 5.8 at room temperature and was later heated to 60°C for 2 h.

Citrate buffer was prepared from analytical grade trisodium citrate dihydrate (3SC,  $\text{Na}_3\text{C}_6\text{H}_5\text{O}_7 \cdot 2\text{H}_2\text{O}$ ,  $M_w = 294.10$  g/mol, CAS 6132-04-3, code S/3320/53) and citric acid monohydrate (CA,  $\text{C}_6\text{H}_8\text{O}_7 \cdot \text{H}_2\text{O}$ ;  $M_w = 210.14$  g/mol, CAS 5949-29-1, code C/6200/53) both purchased from Fisher Scientific, Loughborough, UK. The citrate buffer was prepared by diluting 0.1 M CA (95 ml  $\text{CA}_{(\text{aq})}$  containing 21.01 g  $\text{CA}_{(\text{s})}/\text{L H}_2\text{O}$ ) and 0.1M 3SC (415 ml of  $3\text{SC}_{(\text{aq})}$  containing 29.41 g  $3\text{SC}_{(\text{s})}/\text{L H}_2\text{O}$ ) to a volume of 1 L. A food grade preservative, potassium sorbate (0.1 wt%,  $\text{C}_6\text{H}_7\text{KO}_2$ ;  $M_w = 150.22$  g/mol, CAS 24634-61-5, Fluka 85520, Sigma–Aldrich, Dorset, UK), was used to inhibit microbial activity during experiments.

The four galactomannans: LBG (E410, LBG Grinstead® 246, 2% > 150  $\mu\text{m}$ ,  $\eta_{\text{min}} = 2.400$  mPa.s, 2% particle size > 150  $\mu\text{m}$ , Danisco, Denmark), donated by Unilever Research Labs, Colworth, UK; TG (E417, CEROTA Tara Gum Type 5000®, loss on drying  $\leq 15\%$ , ash  $\leq 1.5\%$ , protein  $\leq 3.5\%$ ,  $\eta$  (1%) =  $\geq 5.000$  mPas at 87°C, particle size  $\geq 80\%$  < 100  $\mu\text{m}$ ), donated by Roeper, Hamburg, Germany; GG (E412, G4129, CAS 9000-3-0, purchased from Sigma-Aldrich, Dorset, UK); and FG (Canafen Gum®, < 15% moisture, < 5% protein, < 3% ash, < 1% fat, particle size 99% < 420  $\mu\text{m}$ ) donated by Emerald Seed Products, Avonlea, Canada, were also dissolved in the citrate buffer at the slightly higher temperature of 70–80°C.

The sucrose used in this study was a “Tate + Lyle” commercially available sugar. D-(+)-glucose ( $\text{C}_6\text{H}_{12}\text{O}_6$ ,  $M_w = 180.16$  g/mol, CAS 50-99-7, code G/0500/53) and D-(-)-fructose ( $\text{C}_6\text{H}_{12}\text{O}_6$ ,  $M_w = 180.16$  g/mol, solubility=18 g/L, CAS 50-99-7, code F0127-5kg)

were purchased from Sigma-Aldrich, Dorset, UK. Trehalose (Treha 16400®, 98% pure, loss on drying 1.7%, 11.5% moisture, CAS 6138-23-4, CN code 2940-00-0) was donated by Cargill, Manchester, UK.

The Nile blue sulphate ( $2 \cdot C_{20}H_{20}N_{30} \cdot SO_4$ , CAS 3625-57-8,  $M_w = 732.85$  D, 51180, CN code 222-832-5, N0766-5G) and Rhodamine B ( $C_{28}H_{31}CN_2O_3$ ,  $M_w = 479.02$  D, 83689-1G, CAS 81-88-9, CN 201-383-9) dyes used (0.01 wt%) for the confocal microscopy observations were purchased from Sigma-Aldrich (Dorset, UK). All materials were used with no further purification or modification of their properties.

### 3.3 Methods

#### 3.3.1 Phase behaviour of aqueous two-phase systems with sugar

The following paragraphs explain the experimental setup for the study of phase behaviour in NaCAS-GM-sugar ATPS.

##### 3.3.1.1 Preparation of bulk solutions

Bulk solutions of NaCAS (4, 5, 6, 8, 10 wt%), LBG, TG, GG and FG (all 0.3, 0.4, 0.5, 0.6 wt%) were prepared by dissolution of the powders in citrate buffer at pH 5.8 (Figure 3-1). The bulk solutions were mixed with a digital dual range mixer IKA® RW 20 (IKA®-Werke GmbH & Co. KG, Staufen, Germany) and 6-blade (50 mm diameter) impeller at a rotation speed of ~650 rpm. To aid the dissolution, the bulk solutions were mixed at a high temperature ( $60 \pm 5^\circ\text{C}$  for NaCAS and  $80 \pm 5^\circ\text{C}$  for GM). After the biopolymers were dissolved, KS (0.1 wt%) and sugar—glucose, fructose, sucrose and

trehalose; 0–60 wt% (sucrose) or 0–30 wt% (glucose, fructose, trehalose)—were added to the warm bulk solution. The solutions were then cooled to 25°C and the evaporated water was replaced. Finally, the bulk solutions were mixed for a further ~1 min with a Silverson L4RT high-shear mixer (50 mm diameter general purpose mixing head, Silverson Machines Ltd., Chesham Bucks, UK) at 1000 rpm and were later stored overnight in the fridge (~5°C) to enable complete rehydration of the individual hydrocollids. The bulk solutions were used without further purification in preparation of the aqueous two-phase binary solutions.

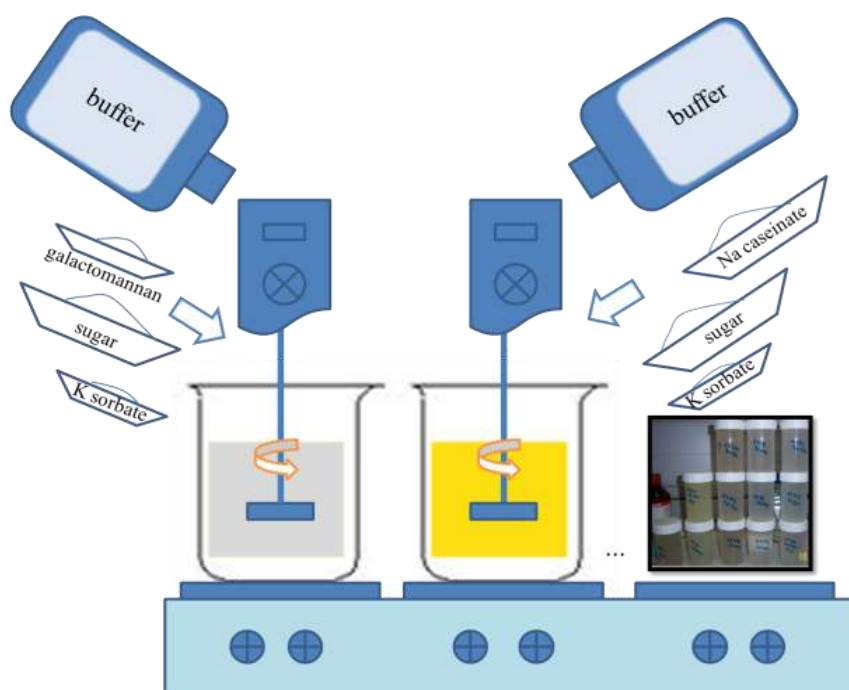


**Figure 3–1. Preparation of bulk galactomannan and sodium caseinate solutions.**

### **3.3.1.2 Preparation of aqueous two-phase binary solutions**

Binary solutions of the Systems 1–4 with various sugar concentrations (Table 3-1) were prepared by mixing carefully weighed amounts of the pairs of bulk solutions,

one containing GM and the other NaCAS. While a wider concentration range of sucrose was used in the experiments, the concentration ranges of other sugars were limited to 30 wt% by the solubility of trehalose at 5°C, which was the lowest experimental temperature.

**Table 3-1. The aqueous two-phase systems investigated on their phase behaviour.**

No.	System	Sugar type	Sugar concentration [wt%]
1	System 1 (LBG)	Sucrose	0, 5, 15, 20, 30, 40, 50, 60
2	System 1 (LBG)	Fructose, glucose, trehalose	0, 15, 30
3	System 2 (TG)	Sucrose	0, 15, 30
4	System 2 (TG)	Fructose, glucose, trehalose	0, 15, 30
5	System 3 (GG)	Sucrose	0, 15, 30, 50
6	System 3 (GG)	Fructose, glucose, trehalose	0, 15, 30
7	System 4 (FG)	Sucrose	0, 15, 30
8	System 4 (FG)	Fructose, glucose, trehalose	0, 15, 30

The content of the macromolecules and sugars is expressed as a percentage of weight of the compound by the total weight of the system. Weight percents (wt%) are also widely used in industrial applications. Molar concentrations, on the other hand, are not used because they require knowledge of the  $M_w$  and  $\rho$  of the compounds. These are difficult to measure, especially in the case of NaCAS and GMs.

Figure 3–2 schematically shows the preparation of the binary solutions and the following paragraphs describe their preparation.

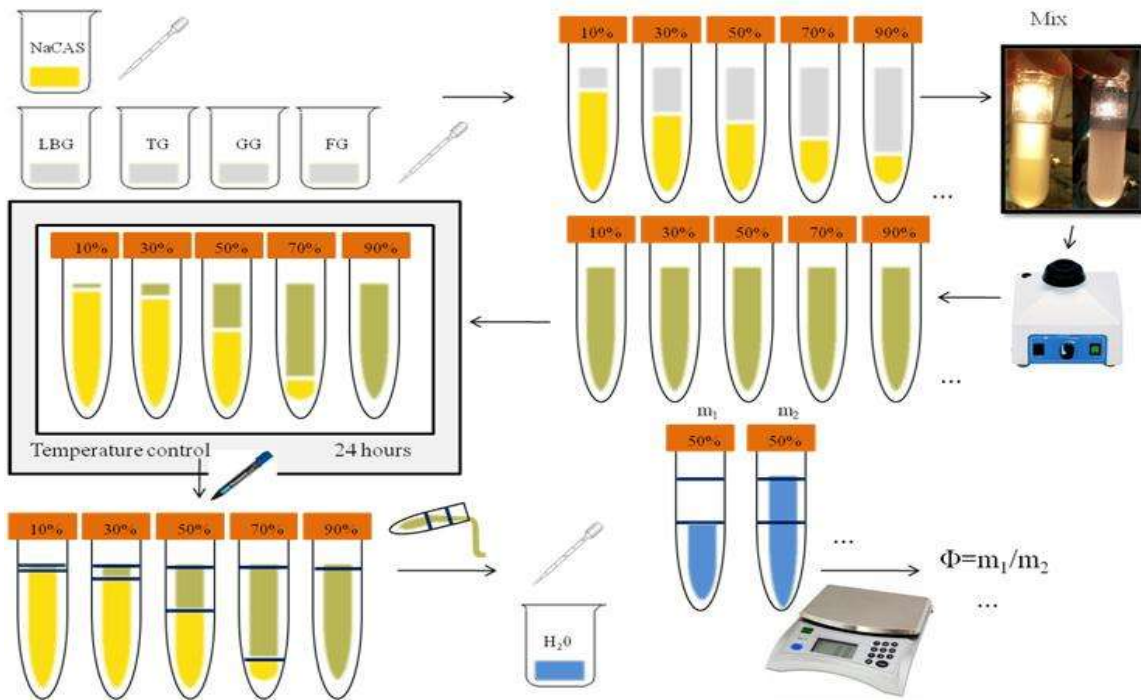


**Figure 3–2. Preparation of aqueous two-phase binary solutions.**

Transparent conical centrifuge tubes (polypropylene Corning® 50 mL, Sigma Aldrich, Gillingham, Dorset, UK) were filled with a total of 30 g of the bulk solution pairs, sealed and mixed using a Chiltern vortex mixer (type VM20 at speed 9 for 2 minutes). The tubes were then incubated for 24 hours in the constant climate chamber ( $20 \pm 0.5^\circ\text{C}$ , Binder-KBF 115 series constant climate chamber, Binder GmbH, Tuttlingen, Germany), fridge ( $5 \pm 2^\circ\text{C}$ ) and oven ( $40 \pm 1^\circ\text{C}$ ).

During incubation the interface formed between the pairs of co-existing equilibrium phases. The time in which the formation of the interface was visible depended on the incubation temperature and the viscosities of the phases. At  $5^\circ\text{C}$  the interface formed faster than at 20 and  $40^\circ\text{C}$ . In less viscous binary solutions ( $< 50\%$  of

the GM phase) the interfaces were formed in 15–30 min and in more viscous binary solutions, in 4–5 h. After 24 hours of incubation and gravity-driven phase separation it was assumed that the equilibrium was reached.

The binary solutions were centrifuged at the required temperature for 15 min to remove air bubbles. Mild rotational speeds were used to avoid centrifuging out the components (namely water). The binary solutions with FG and GG were centrifuged (C4-22 bench top centrifuge, Jouan Inc, Winchester (VA), USA, with capacity of centrifuging  $28 \times 50$  mL conical centrifuge tubes and maximal rotational speed of 3600 g or 4000 rpm) at 500 g and the solutions with LBG and TG were centrifuged at 100 g. After centrifugation new interfaces did not form. Nevertheless,  $< 3\%$  changes<sup>13</sup> in the position of the interfaces were observed in several of the more viscous solutions. These typically contained  $> 50$  wt% of the GM phase. For more concentrated biopolymer solutions a longer period may have been required to reach equilibrium. In any system with  $> 30\%$  sugar a stable foam formed, which gave rise to substantial experimental uncertainties in determining the volume fractions. The occurrence of the stable foam was likely caused by improved self-association of NaCAS in the presence of sugar and high viscosity of the water-continuous phase surrounding the bubbles.

The centrifuge tubes were marked at the interfaces with a permanent marker before and after centrifugation. They were then emptied, cleaned and re-filled with distilled water in order to obtain volume fractions of the GM-rich/top ( $\varphi_{GM}$ ) and NaCAS-

---

<sup>13</sup> 100% is the height from the bottom of the centrifuge tube to an interface before the centrifugation and (100-x)% is the height from the bottom of the tube to the interface after the centrifugation.

rich/bottom ( $\varphi_{NaCAS}$ ). The volume fraction data was used in determination of the phase diagrams—binodals, rectilinear diameter/critical point, tie-lines—and, indirectly, in the determination of the threshold points.

### **3.3.1.3 Phase diagrams and their characteristic points**

Phase diagrams were obtained by application of the phase-volume ratio method. The characteristic points of these phase diagrams were calculated geometrically.

#### **3.3.1.3.1 Phase-volume ratio method**

Koningsveld and Staverman's phase-volume ratio method (1968) was first ascertained as accurate for ATPS by Polyakov et al. (1980; 1985). It was used in this work to determine the phase diagrams of four systems in the absence and presence of sugar (Table 3-1.). The phase diagrams were established at pH 5.8 and at temperatures of 5, 20 and 40°C. The phase diagrams established at 5°C were positioned closest to the x- and y-axes while the phase diagrams established at 40°C were positioned furthest from the axes. Since no other differences were observed and for the sake brevity only phase diagrams obtained at 20°C (easy temperature to work with) are shown in this work. In all cases the best-fit binodals had a high determination coefficient ( $R^2=0.85-0.99$ ).

By this method, the binodal points were obtained by studying the relationships between the compositions (i.e., individual biopolymer concentrations) and the phase-volume ratios of the equilibrium phases in the series of binary solutions that belonged to

a chosen system. For each phase diagram/system, 4–6 sets<sup>14</sup> of experiments were prepared. Each of these sets gave three data points on the phase diagram: two points on the binodal and a point on the rectilinear diameter. The rectilinear diameter represents all systems that separate to produce even fractions of both phases, and is a straight line running through points where volume fractions of both equilibrium phases are equal,  $\varphi_{GM} = \varphi_{NaCAS} = 0.5$ .

Each set was prepared from a pair of bulk solutions with concentrations  $[NaCAS]_i^0$  and  $[GM]_i^0$  ( $i$  = number of set, "0" marks the bulk solution). These were then mixed to give 8–12 binary solutions; among these a sufficient number had to phase separate because only phase separated solutions could provide the data points that could be later used in determination of the binodal and rectilinear points by the method of Polyakov et. al. (1980). The binary solutions were of a constant total biopolymer weight concentration ( $[BP]_i$ , where  $[BP]_i = [NaCAS]_i^0 + [GM]_i^0$ <sup>15</sup>) and of different volume fractions of the equilibrium phases ( $\varphi_{GM}$  and  $\varphi_{NaCAS}$ , where  $\varphi_{GM} + \varphi_{NaCAS} = 1$ ) (Figure 3–3). For example<sup>16</sup>, if  $[BP]_i$  was 10 wt%, mixtures composed of 1–9 wt% of  $[NaCAS]_i^0$  and 9–1 wt% of  $[GM]_i^0$  would be prepared. This corresponds to weight fractions of NaCAS ( $y$ ) between 0.1 and 0.9 and weight fractions of GM ( $1 - y$ ) between

<sup>14</sup> An experimental set involves preparation of a series of binary solutions for the purpose of determining their volume fraction ratios and obtaining binodal points. For each set, the phase-volume ratios of the solutions are plotted against their apparent weight fractions (known from the preparation). A sufficient number of phase-separated systems are required for a confident fit. From each plot/set two binodal points are obtained.

<sup>15</sup> In this work, sugar is assumed to be a solvent, which partitions equally between both phases.

<sup>16</sup> For the sake of brevity, an example is given of an ideal case of equal solubility of both biopolymers where the line connecting  $[NaCAS]_i^0$  with  $[GM]_i^0$  has a slope of -1. In reality, however, NaCAS is ~10 times more soluble than GM; hence the line connecting the bulk biopolymer concentrations is  $< -1$ . In this work the total biopolymer concentrations  $[BP]_i$  prepared for System 1 were between 2 wt% and 10.5 wt% and for other systems between 5.5 wt% and 10.3 wt%.

0.9 and 0.1. The concentrations of the bulk/binary solutions were selected so that both the one-phase and two-phase regions in the 2D Cartesian space were "scanned". As such, binodal points were obtained on both sides of the rectilinear diameter.

The following paragraphs offer a more detailed graphic illustration of the method. Figure 3–3 and Figure 3–4 (see p. 3–85) illustrate the method for the example of NaCAS-LBG ATPS.

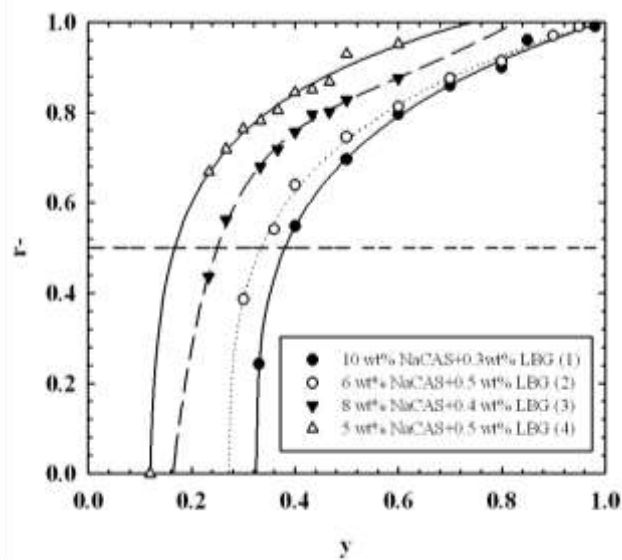


**Figure 3–3.** The first step in the phase-volume ratio approach used for the determination of the phase diagrams; typical dependencies of the phase volume ratio of sodium caseinate-rich equilibrium phase ( $r^-$ ) on the mixture composition ( $y$ ) for sodium caseinate-locust bean gum aqueous two-phase system (used as an example).  $r^-$ =phase volume ratio (i.e., volume fraction [%] of the sodium caseinate equilibrium phase),  $y$ =apparent weight fraction (i.e., ratio of the concentration of the sodium caseinate on the binodal and its concentration in the bulk).

Figure 3–3 shows the volume fractions of NaCAS-rich/bottom phase ( $r^-$ ) against the apparent mass fraction of the NaCAS ( $y$ ). A similar graph can be obtained by plotting the volume fractions of the GM-rich phase/top ( $r^+$ ) against the apparent mass fraction of the GM ( $1-y$ ), but is not shown. The phase volume ratio ( $r$ ) of a binary mix was calculated as follows:

$$r^+ = \frac{m_{top}}{(m_{bot} + m_{top}) \times 100} \Leftrightarrow r^- = \frac{m_{bot}}{(m_{bot} + m_{top}) \times 100} \quad [3-1]$$

where  $r^+$  is a phase volume ratio of the GM-rich/top phase,  $r^-$  the phase volume ratio of the NaCAS-rich/bottom phase,  $m_{top}$  is mass of the top phase and  $m_{bot}$  is mass of the bottom phase. In measuring the masses of the equilibrium phases the densities of both phases are assumed to be equal to water i.e., 1 kg/L.

The apparent weight fractions of the binary mix were calculated as follows:

$$y = \frac{m_{NaCAS} \times [NaCAS]^0}{m_{total}} \times [NaCAS]^0 \Leftrightarrow 1 - y = \frac{m_{GM} \times [GM]^0}{m_{total}} \times [GM]^0 \quad [3-2]$$

where  $y$  is the apparent weight fraction of NaCAS and  $1 - y$  is the apparent volume fraction of the GM in binary solutions;  $m_{NaCAS}$  is a mass of NaCAS bulk solution added to the binary solution,  $m_{GM}$  a mass of GM;  $m_{total}$  a total mass of the binary solution,  $[NaCAS]^0$  = concentration of the NaCAS bulk solution and  $[GM]^0$  = concentration of the GM bulk solution.

The values of  $r^-$  were plotted against  $y$  to establish  $r^- = f(y)$  to obtain binodal and rectilinear points. The binodal points were obtained by extrapolating  $f(y)$  to  $r^- = 1$  and  $r^- = 0$ . The best-fit function was used every time ( $0.97 < R^2 < 0.99$ ). The choice was made between the following three functions: parameter logarithm ( $y = y_0 + a \times \ln|x - x_0|$ ), four parameter sigmoid Weibull function  $y = a \left( 1 - \exp\left(\frac{-|x - x_0 + b \times \ln(2)^{|x - x_0|}}{b}\right)^c \right)$ , and three parameter

power function ( $y = y_0 + a \times x^b$ ). The purpose of the above best-fit functions was only to obtain the most plausible secant points of  $f(y)$  and x-axis ( $r^-$ ), and in that way determine the most likely positions of the binodal points on the secant  $[\text{NaCAS}]^0$   $[\text{GM}]^0$  (Figure 3-4).

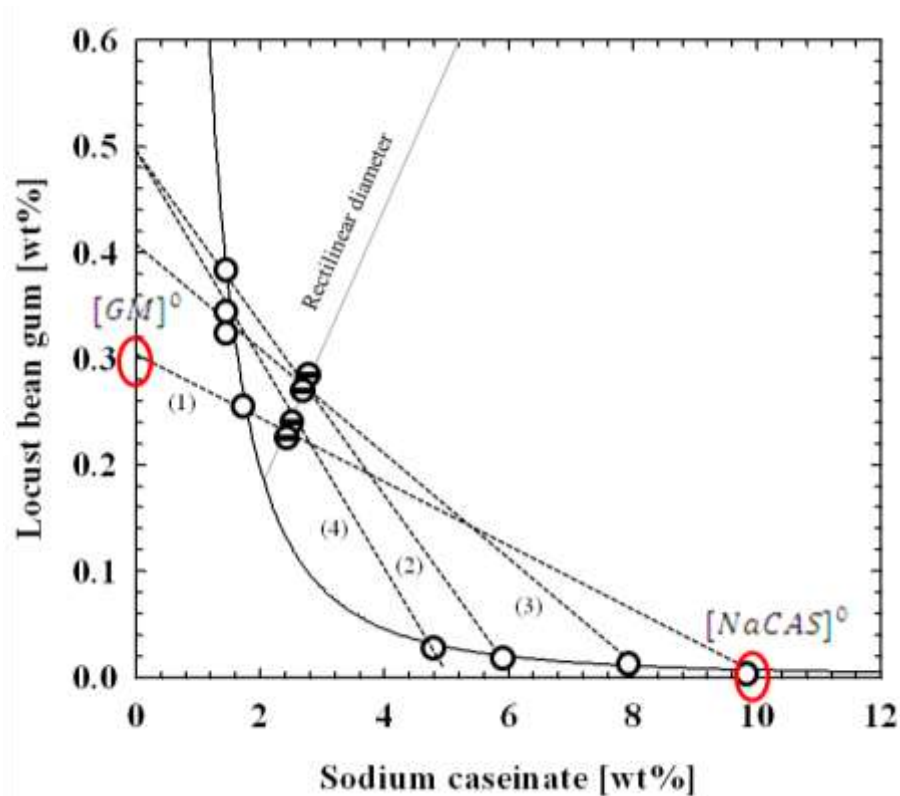


Figure 3-4. The second step in the phase-volume ratio approach used for the determination of the phase diagrams; binodal (the curve), rectilinear diameter and  $[\text{NaCAS}]^0$  (sodium-caseinate bulk concentrations) and  $[\text{GM}]^0$  (galactomannan bulk concentrations) pairs, which are connected with dashed lines; "●" mark binodal points, "⊖" mark rectilinear points.

The secants—each corresponding to a pair of biopolymer bulk solutions—were selected so that they cut the binodal curve in two points and on each side of the rectilinear point/diameter. The rectilinear points—in Figure 3-4 marked with "⊖"—were obtained from  $y$  at  $r^- = 0.5$ . By drawing a straight line through the rectilinear

points a point of contact between the rectilinear diameter and the binodal curve was obtained, so called critical point of the phase diagram.

The binodal curve was obtained as a best-fit curve to the obtained binodal points. For all ATPS a single two-parameter exponential decay function was used to mathematically describe the data:

$$[GM] = a \times [NaCAS]^{-b} \quad [3-3]$$

where [GM] and [NaCAS] are the bulk concentrations of galactomannan and sodium caseinate, and  $a$  and  $b$  are the parameters that describe the binodal curve in 2D Cartesian coordinate space.  $b < 1$  describes the curve further away from the  $x$  and  $y$  axis (a curve with a slower drop) and  $b > 1$  describes a faster dropping curve that runs closer to both axes and frames a smaller two-phase region in the phase diagram. The value  $a$  characterises a contact point between the binodal and  $y$ -axis (i.e., a start of the function); for  $a < 1$  the function touches  $y$ -axis higher then when  $a > 1$ .

In effect, the phase-volume ratio approach provides a “map” of the transition of a given system from the single-phase to the two-phase region of the phase diagram.

### 3.3.1.3.2 *Critical and theoretical points*

Each phase diagram was fitted with characteristic theoretical points, namely a critical point and a threshold point.

The critical point was obtained by drawing a straight line through the points located on the rectilinear diameter (Figure 3-5).

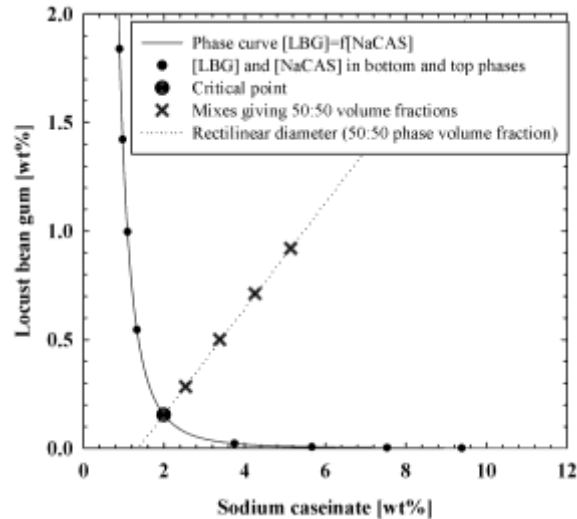


**Figure 3–5. Determination of the critical point in the phase diagram on the example of System 1 (sodium caseinate-locust bean gum) with no added sugar. Critical points for other systems and sugar concentrations were determined in the same way.**

The threshold point was calculated as a tangential point where the straight line—which cuts even sections on both axes of the phase diagram—and the binodal meet (Figure 3–6).

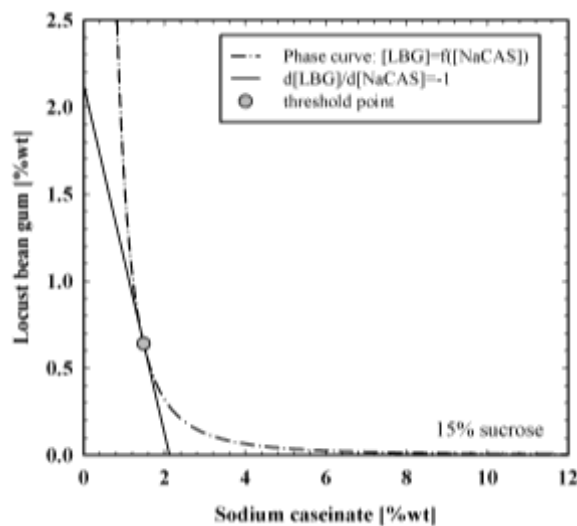


**Figure 3–6. Determination of the threshold point in the phase diagram on the example of System 1 (sodium caseinate-locust bean gum) with 15 wt% added sucrose. Threshold points for other systems and sugar concentrations were determined in the same way.**

The symmetry of the phase diagram was assessed by calculating the distance

( $\lambda_{\text{sym}}$ ) between the two points and the inverse distances of the critical and threshold points from points ( $1/\alpha_{\text{crit}}$  and  $1/\alpha_{\text{thres}}$ ). The distance  $\lambda_{\text{sym}}$  was calculated as follows:

$$\lambda_{\text{sym}} = \sqrt{([GM]_{\text{crit}} - [GM]_{\text{thres}})^2 + ([NaCAS]_{\text{crit}} - [NaCAS]_{\text{thres}})^2} \quad [3-4]$$

where ( $[GM]_{\text{crit}}$ ,  $[NaCAS]_{\text{crit}}$ ) are the coordinates of the critical point and ( $[GM]_{\text{thres}}$ ,  $[NaCAS]_{\text{thres}}$ ) are the coordinates of the threshold point. A bigger distance  $\lambda_{\text{sym}}$  indicates a more asymmetric phase diagram. Further analysis of the symmetry of the phase diagrams included the calculation of the (inverse) distances of the critical and threshold points ( $\alpha_{\text{crit}}$ ,  $\alpha_{\text{thres}}$ ) from the origin of the phase diagram or point (0,0), shown in equations [3-5] and [3-6]:

$$\alpha_{\text{crit}} = \sqrt{[GM]_{\text{crit}}^2 + [NaCAS]_{\text{crit}}^2} \quad [3-5]$$

$$\alpha_{\text{thres}} = \sqrt{[GM]_{\text{thres}}^2 + [NaCAS]_{\text{thres}}^2} \quad [3-6]$$

When the distance  $\alpha$  is small, its inverse value  $1/\alpha$  is large, hence the system separates more readily.

#### 3.3.1.4 Tie-lines determine phase equilibria compositions

For each phase diagram a tie-line was also calculated. Knowing the tie-line, i.e., its slope (STL), and assuming that all tie-lines in a given phase diagram are parallel (Zaslavsky, 1995), enables the determination of the phase equilibria compositions of any given ATPS inside a two-phase region of that phase diagram.

The slopes of the tie-lines were graphically obtained by the method of

Spyropoulos et al. (2010). For each phase diagram an average of at least three tie-lines was calculated. The principle of this method is based on the fact that by knowing the coordinates of the primary ATPS ( $[\text{NaCAS}]$ ,  $[\text{GM}]$ ) and the volume fractions to which it phase separates—lengths of  $\overline{CD}$  and  $\overline{CE}$ —one can calculate the coordinates of the points D and E—the phase equilibria compositions. Figure 3–7 schematically represents the method for the example of NaCAS-LBG ATPS in the absence of sugar. The method is also explained later in this section.

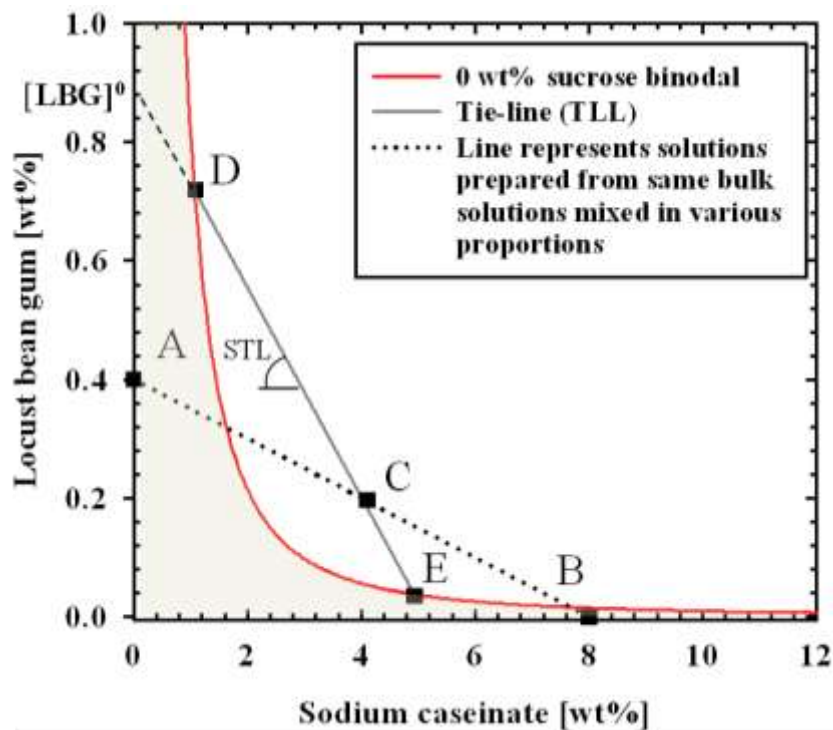


**Figure 3–7.** Tie-line in the phase diagram for a sodium caseinate-locust bean gum aqueous two-phase system (ATPS) without sucrose. A=concentration of locust bean gum bulk solution, B=concentration of sodium caseinate bulk solution, C=concentration of the ATPS, D=concentration of the locust bean gum-rich equilibrium phase, E=concentration of the sodium caseinate-rich equilibrium phase.  $[\text{LBG}]_0$  is the intercept of the tie-line with the y-axis. STL=slope of the tie-line. One phase region of the phase diagram is shaded.

Figure 3–7 shows the tie-line ( $\overline{DE}$ ) that passes through a selected point deep in a two-phase region (point C) of the phase diagram and intersects the binodal at points E and D. Points E and D represent the concentration of the biopolymers (LBG and NaCAS)

in the equilibrium phases that are formed by phase separation of the primary ATPS with concentration  $C$  (marked with "■"). Point  $C$  divides the tie-line  $\overline{DE}$  into segments  $\overline{CD}$  and  $\overline{CE}$ . The lengths of these segments correspond, as shown by Zaslavsky (1995), to the volume fractions to which a chosen ATPS separates (i.e.,  $\overline{CD}$  is the volume fraction of the bottom phase,  $\varphi_{NaCAS}$ , and  $\overline{CE}$  is the volume fraction of the top phase,  $\varphi_{LBG(GM)}$ ).

The rest of this section shows the sequence of equations by which the STL/tie-lines were calculated. The example is given for the tie-line in Figure 3-7.

The coordinates of point  $C$  are the LBG and NaCAS concentrations in the ATPS— $C([NaCAS]_{atps}, [LBG]_{atps})$ —and the coordinates of points  $D$  and  $E$  are their concentrations in the top and bottom equilibrium phases— $D([NaCAS]_{top}, [LBG]_{top}), E([NaCAS]_{bot}, [LBG]_{bot})$ .

The tie-line runs through points  $C$ ,  $D$  and  $E$ , therefore:

$$[LBG]_{atps} = [LBG]_0 + STL \times [NaCAS]_{atps} \quad [3-7]$$

$$[LBG]_{top} = [LBG]_0 + STL \times [NaCAS]_{top} \quad [3-8]$$

$$[LBG]_{bot} = [LBG]_0 + STL \times [NaCAS]_{bot} \quad [3-9]$$

where  $[LBG]_0$  is the intercept between the extended tie-line and the  $y$ -axis of the phase diagram and  $STL$  is slope of the tie-line. First  $[LBG]_0$  is eliminated by subtraction of the equations [3-8] and [3-9] from [3-7]:

$$[LBG]_{top} - [LBG]_{atps} = STL \times ([NaCAS]_{top} - [NaCAS]_{atps}) \quad [3-10]$$

$$[LBG]_{bot} - [LBG]_{atps} = STL \times ([NaCAS]_{bot} - [NaCAS]_{atps}) \quad [3-11]$$

Then STL is eliminated by division of the eq. [3-10] by [3-11] to give eq. [3-12]:

$$\frac{[LBG]_{top} - [LBG]_{atps}}{[LBG]_{bot} - [LBG]_{atps}} = \frac{[NaCAS]_{top} - [NaCAS]_{atps}}{[NaCAS]_{bot} - [NaCAS]_{atps}} \quad [3-12]$$

Points D and E must also lie on the binodal, therefore:

$$[LBG]_{top} = a \times [NaCAS]_{top}^{-b} \quad [3-13]$$

$$[LBG]_{bot} = a \times [NaCAS]_{bot}^{-b} \quad [3-14]$$

where the binodal is described by the best fit exponential decay function shown in eq. [3-3].

Since the ratio of the lengths of each of the segments  $\overline{CD}$  and  $\overline{CE}$  match to the volume fractions of the top ( $\varphi_{top}$ ) and bottom ( $\varphi_{bot}$ ) equilibrium phases and are experimentally obtained, the following two relationships can be established:

$$\frac{\overline{CD}}{\overline{DE}} = \frac{|[NaCAS]_{atps} - [NaCAS]_{top}|}{|[NaCAS]_{bot} - [NaCAS]_{top}|} = \varphi_{bot} \quad [3-15]$$

$$\frac{\overline{CE}}{\overline{DE}} = \frac{|[NaCAS]_{atps} - [NaCAS]_{bot}|}{|[NaCAS]_{bot} - [NaCAS]_{top}|} = \varphi_{top} \quad [3-16]$$

Numerically solving equations [3-12], [3-13] (or [3-14]), and [3-15] (or [3-16]) will give the LBG and NaCAS concentrations in the equilibrium phases ( $[LBG]_{top}$ ,  $[NaCAS]_{top}$ ,  $[LBG]_{bot}$  and  $[NaCAS]_{bot}$ ) and consequently the STL. Equations [3-17] to [3-19] give a possible numeric solution.

$$\frac{\varphi_{bot}}{\varphi_{top}} = \frac{\overline{CD}/\overline{DE}}{\overline{CE}/\overline{DE}} = \frac{\overline{CD}}{\overline{CE}} = \sqrt{\frac{([\text{NaCAS}]_{atps} - [\text{NaCAS}]_{top})^2 + ([\text{LBG}]_{atps} - [\text{LBG}]_{top})^2}{([\text{NaCAS}]_{atps} - [\text{NaCAS}]_{bot})^2 + ([\text{LBG}]_{atps} - [\text{LBG}]_{bot})^2}} \quad [3-17]$$

$$\left(\frac{1 - \varphi_{top}}{\varphi_{top}}\right)^2 = \frac{([\text{NaCAS}]_{atps} - [\text{NaCAS}]_{top})^2 + ([\text{LBG}]_{atps} - [\text{LBG}]_{top})^2}{([\text{NaCAS}]_{atps} - [\text{NaCAS}]_{bot})^2 + ([\text{LBG}]_{atps} - [\text{LBG}]_{bot})^2} \quad [3-18]$$

$$\left. \begin{aligned} &([\text{NaCAS}]_{atps} - [\text{NaCAS}]_{top})^2 + ([\text{LBG}]_{atps} - [\text{LBG}]_{top})^2 - \\ &\left\{ \left(\frac{1 - \varphi_{top}}{\varphi_{top}}\right)^2 \times ([\text{NaCAS}]_{atps} - [\text{NaCAS}]_{bot})^2 + ([\text{LBG}]_{atps} - [\text{LBG}]_{bot})^2 \right\} = 0 \end{aligned} \right\} \quad [3-19]$$

### 3.3.2 Rheology of aqueous two-phase systems, blends and pure biopolymer solutions with and without sugar

#### 3.3.2.1 Preparation of pure biopolymer solutions, aqueous two-phase systems and blends

This section describes the preparation of the systems that were investigated on their flow behaviour. Table 3-2 in this section and Table 3-4 in § 3.3.3.1 (p. 3-100) show the concentrations and types of the investigated systems. The preparation of the pure biopolymer systems and ATPS was similar to the preparation of the bulk solutions and binary solutions/ATPS reviewed in § 3.3.1.1 (p. 3-76) and § 3.3.1.2 (p. 3-77) and will not be repeated here. The slight difference in the preparation and quantities of the investigated ATPS and the preparation of blends, on the other hand, is explained in the following paragraph.

**Table 3–2. Sodium caseinate-galactomannan-sugar ATPS, blends (1–3) and pure solutions (4–6) investigated on flow. [NaCAS], [GM] and [sugar] are the weight concentrations of sodium caseinate, galactomannans (LBG, TG, GG or FG) and sugar, respectively.**

No.	System	[NaCAS] in wt%	[GM] in wt%	Sugar Type	[sugar] in wt%	Fraction of GM-rich phase in the blend in wt%
1	1 (LBG)	4	0.6	Sucrose	0, 5, 15, 20, 40, 60	0, 5, 25, 50, 75, 95, 100
2	2 (GG)	4	0.6	Sucrose	0, 15, 30, 50	0, 5, 25, 50, 75, 95, 100
3	1 (LBG)	4	0.6	Fructose, glucose, trehalose	15	0, 5, 25, 50, 75, 95, 100
4	/	0, 0.6, 1, 2, 4, 6, 8, 10	/	Sucrose	0, 15, 30, 40	/
5	/	0, 0.6, 1, 2, 4, 6, 8, 10	/	Fructose, glucose, trehalose	0, 15, 30	/
6	GM (LBG, TG, GG, FG)	/	0, 0.1, 0.2, 0.3, 0.4, 0.5, 0.6	Sucrose	0, 15, 30	/

The ATPS and blends were prepared as follows.

ATPS were prepared by mixing of (i) NaCAS, (ii) GM and (iii) sugar (sucrose, trehalose, glucose and fructose), all powders, with (iv) citric buffer (pH 5.8) on a hotplate stirrer at 70–80°C until they were dissolved (~2 hours). After cooling, the evaporated water was replaced and the ATPS were further mixed for ~1 min using a Silverson L4RT high-shear mixer at 1000 rpm. The beakers with ATPS (holding total of 500 g each) were sealed and placed in the humidifying cabinet (20°C and 60% moisture, for 24 h). The equilibrium phases were carefully harvested and centrifuged (Juan C4.22, Thermo Fisher Scientific, Loughborough, UK) for 10 min at 500 g at room temperature. The ATPS were prepared so that they separated into equal volume fractions of both of the phases, and in sufficiently large quantities to provide adequate amounts of the equilibrium phases for blend preparation.

Blends were prepared by re-mixing the pairs of the coexisting equilibrium phases. Various amounts of GM-r (where r stands for rich) phase—0, 5, 25, 50, 75 or 95 wt% were mixed with proportional amounts of NaCAS-r phase—100, 95, 75, 50, 25 and 5 wt%. This approach allowed precise control over the composition of each blend. Since all blends were prepared from the same ATPS (i.e., the same pair of coexisting equilibrium phases), they all exist on the same tie-line—the tie-line that goes through the point in the phase diagram that describes the composition of the specific ATPS.

Figure 3–8 shows the ATPS together with the equilibrium phases and blends prepared from it. It also gives the positions of the systems on the phase diagram.

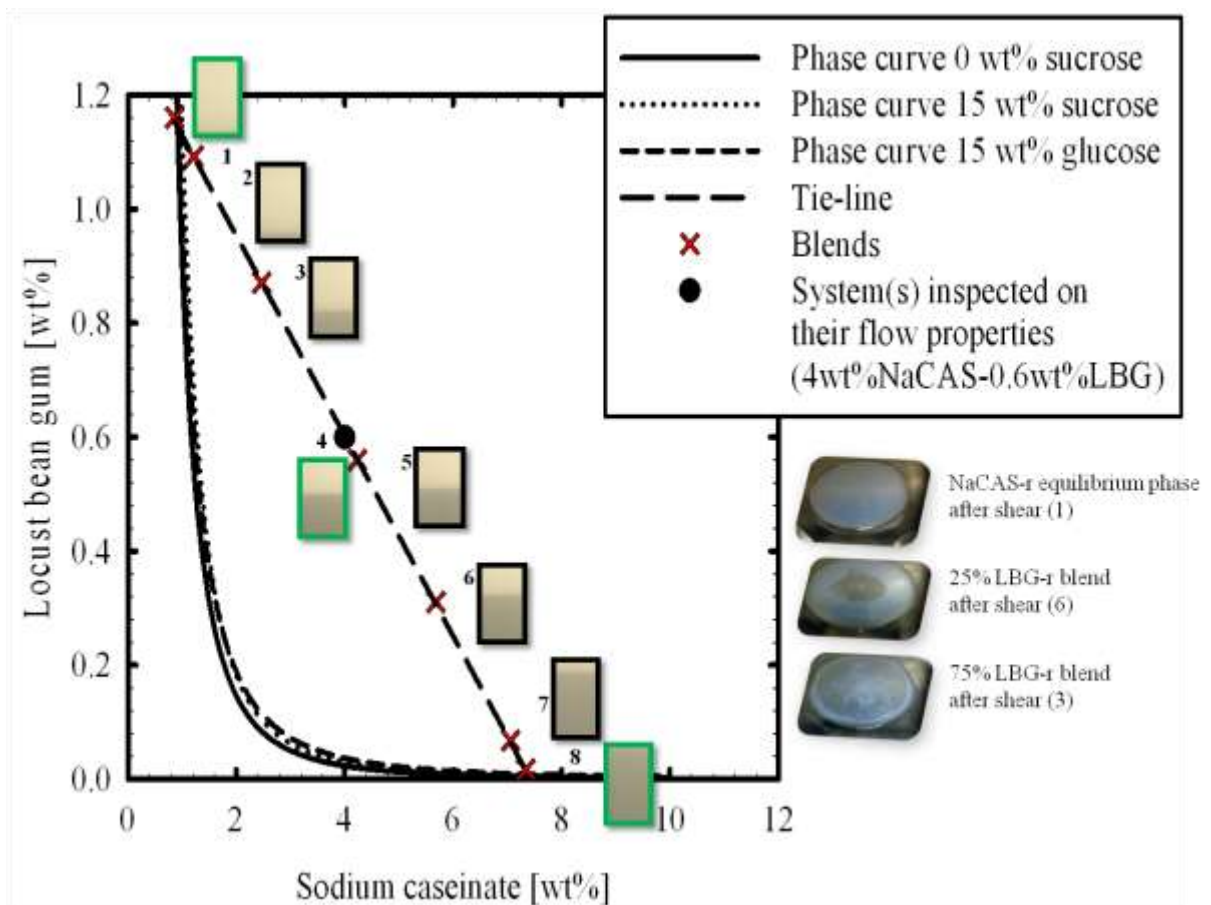


**Figure 3–8.** Preparation of blends from (4) a NaCAS-LBG system that separates into (1) a LBG-rich equilibrium phase and (8) a NaCAS-rich equilibrium phase). The equilibrium phases are then used to prepare blends 2, 3, 5, 6 and 7.

### **3.3.2.2      *Microstructure of aqueous two-phase binary blends in quiescent conditions***

The microstructure of the blends/ATPS, positioned in the phase diagram on the same tie-line, was visualised at 20°C using a confocal scanning laser microscope (Leica DMIRE2, Heidelberg, Germany) equipped with a He-Ne laser lamp operating at a wavelength of 633 nm. Systems 1 and 3 were investigated at various sucrose concentrations (0, 5, 15 and 20 wt%). All images were obtained at 10 times magnification and at 400 scans/min; these were then line-averaged over 8 scans. NaCAS was stained with Nile blue/Rhodamine B (0.01 wt%) 24 hours prior to inspection in order to enhance the contrast in the obtained micrographs. All observations were made directly after gently mixing the blends to ensure representative loading.

### **3.3.2.3      *Viscometry of pure biopolymer solutions and aqueous two-phase blends***

The viscometry measurements of GM-r and NaCAS-r phases, and of their blends, were performed by a Gemini HR nano stress-controlled rheometer (Malvern Instruments, Malvern, UK) using a 4° truncated stainless steel cone-and-plate geometry (40 mm in diameter, truncation of 150 µm), and acrylic plate-and-plate geometry (60 mm in diameter, 500 µm gap), both shown in Figure 3–9. The larger and lighter acrylic geometry with lower inertia was used to measure the viscosity of NaCAS solutions, buffer and sucrose solutions, all with viscosities close to that of the water, 0.001 Pa.s. A larger contact area between the sample and the plate increased measured torque by simultaneously increasing the response of the sample (measured stress) and decreasing the response of the geometry. In this way, the noise in the recorded data was

reduced. For the viscometry of sufficiently viscous equilibrium phases and binary solutions, standard cone-and-plate geometry was used to achieve constant shear rate across the whole sample. A small gap characteristic of this geometry was not considered to be limiting for emulsion-like binary samples because of their inherent instability (sensitivity to time and shear). Smaller gap only resulted in the formation of smaller droplets. It was made certain that the same settings were used to reproduce the same "processing conditions" to make it possible to compare the response of the samples to shear.

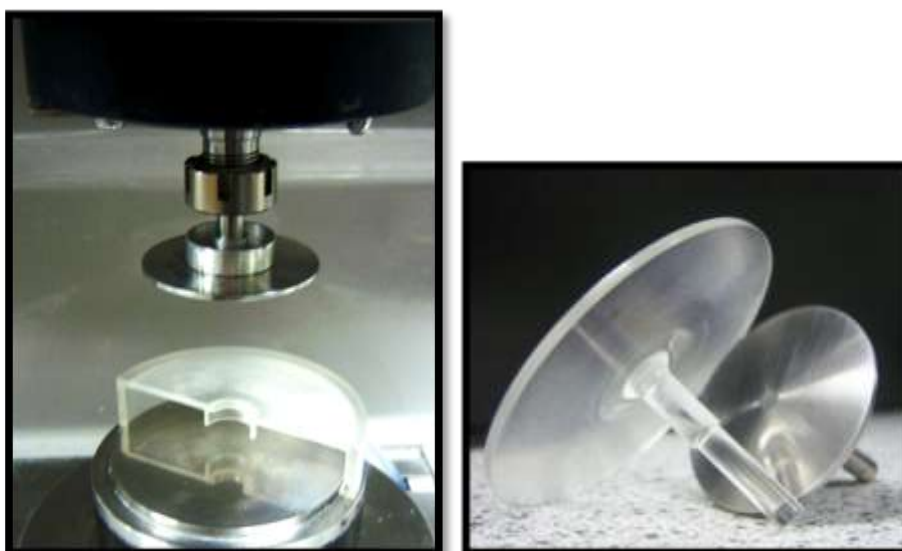


**Figure 3–9.** A 4° 40 mm cone-and-plate geometry (left) and a 60 mm acrylic plate (right) were used for flow experiments.

Steady laminar shear viscosity was measured over the shear rate range from 0.1 to 1000 s<sup>-1</sup> and back to 0.1 s<sup>-1</sup>. The flow curves of the blends were obtained directly after their preparation. Immediately before loading, blends were gently mixed with a spatula 10 times in each direction and loaded on the rheometer plate to achieve representative loading and equal pre-shear. Pure biopolymer solutions were not premixed prior to loading.

### 3.3.2.4 *Microstructure of aqueous two-phase blends in flow*

The microstructure evolution of the blends/ATPS in flow was visualised by an optical rheometer (Bohlin Gemini with Rotonetic drive Z, Malvern Instruments, Malvern, UK) with a glass, 40 mm plate-and-plate geometry (Figure 3–10).



**Figure 3–10. 40mm glass plate-and-plate geometry used in the study of the microstructure and interfacial properties of sodium caseinate-galactomanann ATPS.**

The exact experimental setup of the camera-microscope systems (Olympus SZ-CTV-Dolphin digital interface camera) is explained in more detail in § 3.3.3.2, Figure 3–14, p. 3–103. The flow (in the shear rate range of  $0.1\text{--}1000\text{--}0.1\text{ s}^{-1}$ ) and microstructure characteristics of the blends were observed simultaneously. The microscope-camera system was calibrated with a micrometer-slide for all magnifications achievable with the microscope focus system. Table 3–3 gives the calibration values, however for observation of the microstructure evolution under shear, only maximum (110 times) and minimum (18 times) magnification were used.

**Table 3–3. Calibration of the Olympus CZ-CTV microscope without 10 times magnifying eyepiece at various magnification scales (personal communication with Ourania Gouseti).**

No.	Magnification scale	Pixel size [ $\mu\text{m}/\text{pixel}$ ]
1	1.8	7.790
2	4	3.532
3	8	1.773
4	11	1.329

The images of the system during flow were acquired every 2 s for the duration of the steady state shear viscometry ramp. The images were visually assessed.

### 3.3.2.5 Interfacial rheology

The rheological properties of various interfaces were determined by a biconal  $1^\circ$ , 55 mm stainless steel-ring interfacial geometry attached to a Gemini HR nano stress-controlled rheometer. Figure 3–11 shows the interfacial geometry and the parameters of the oscillation test by which the interfaces between NaCAS-air, GG-air and NaCAS<sub>aq</sub>-GG<sub>aq</sub> were probed.

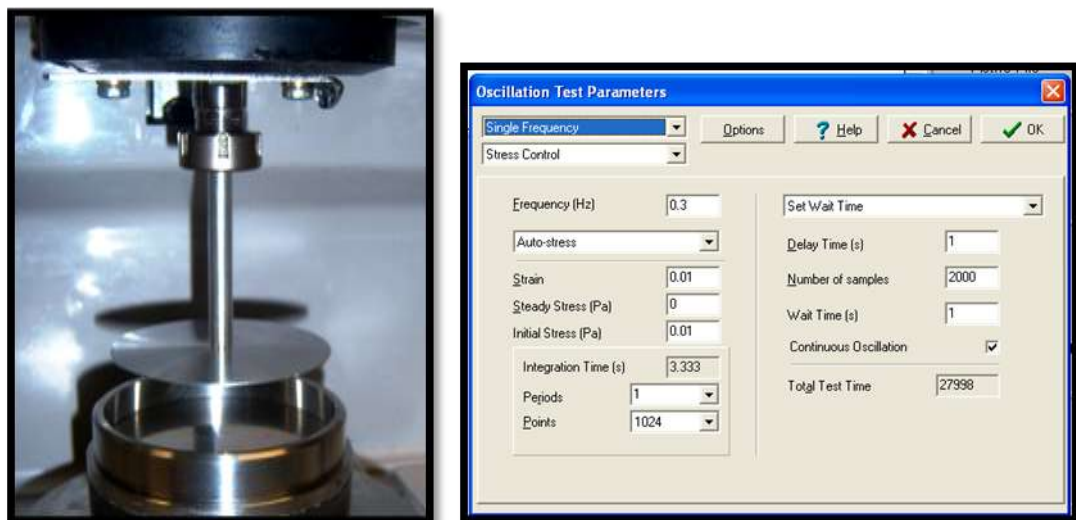


**Figure 3–11. Long shaft  $1^\circ$ , 55 mm biconal-ring geometry used for interfacial rheology (left) and the procedure (right).**

The viscoelastic properties were measured for various interfaces formed in a 2 mm gap between the edge of the biconal geometry and the ring. Air-NaCAS and air-GG interfaces with 0-50% sucrose were probed by pouring 15 ml of a NaCAS/GG-solution in the ring geometry. When NaCAS-GG liquid-liquid interfaces with 0-50% sucrose were probed, NaCAS was, because of its higher density, always poured in the ring geometry first, and then the GG solution was poured over the top of the lowered biconal geometry. The interfaces formed in the 2 mm gap were probed with a single frequency oscillation experiment that gave the measurement of  $G'$  and  $G''$  over time.

### 3.3.3 Interfacial properties of aqueous two-phase blends

The following subsections explain the experimental setup for the study of interfacial properties of NaCAS-GM ATPS using the drop deformation method.

#### 3.3.3.1 Preparation of aqueous two-phase systems and blends

Aqueous two-phase systems and blends (Figure 3–12) were prepared as in § 3.3.2.1, p. 3–92. Table 3–4 shows the ATPS whose interfacial tensions were measured for the effects of composition, phase sense, sugar concentration, sugar type and galactomannan type.

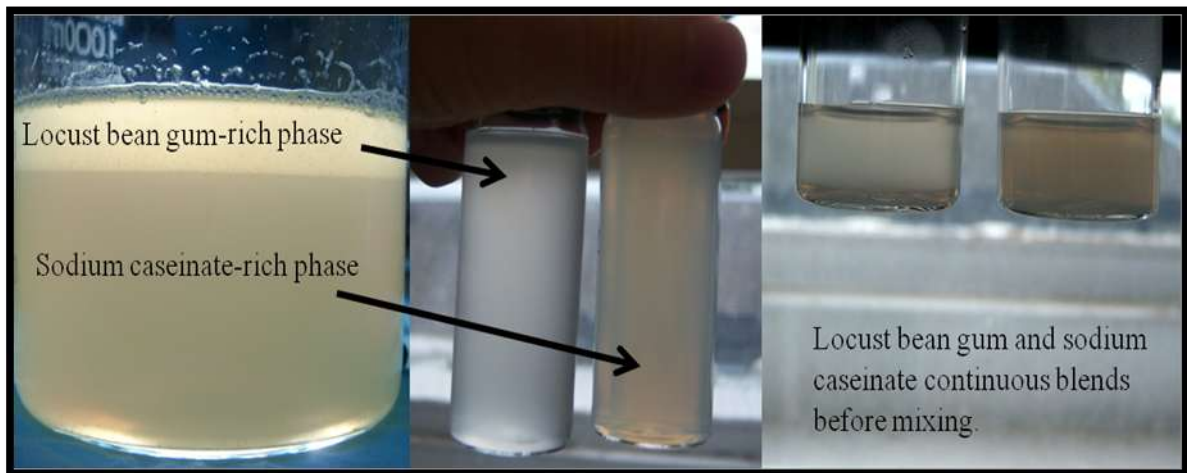
**Table 3–4. Aqueous two-phase systems investigated on their interfacial properties.**

System	Sodium caseinate [wt%]	Galactomannan concentration [wt%]	Galactomannan type	Sugar concentration [wt%]	Sugar type
1 <sup>#</sup>	2	0.25	LBG	0	-
2 <sup>#</sup>	3	0.2	LBG	0	-
3 <sup>#</sup>	4	0.2	LBG	0	-
4	5	0.15	LBG	0	-
5	5	0.2	LBG	0	-
6	6	0.2	LBG	0	-
7	4	0.2	LBG	5	Sucrose
8	4	0.2	LBG	15	Sucrose
9	4	0.2	LBG	20	Sucrose
10 <sup>#</sup>	4	0.2	LBG	30	Sucrose
11	4	0.2	LBG	15	Trehalose
12	4	0.2	LBG	15	Glucose
13	4	0.2	LBG	15	Fructose
14 <sup>#</sup>	4	0.2	TG	0	-
15	4	0.2	GG	0	-
16 <sup>#</sup>	4	0.2	FG	0	-
17	4	0.2	FG	15	Trehalose
18	4	0.2	FG	15	Fructose
19	4	0.2	LBG	30	Trehalose

"#" refers to the systems whose interfacial tensions were measured at various volume fractions of equilibrium phases.

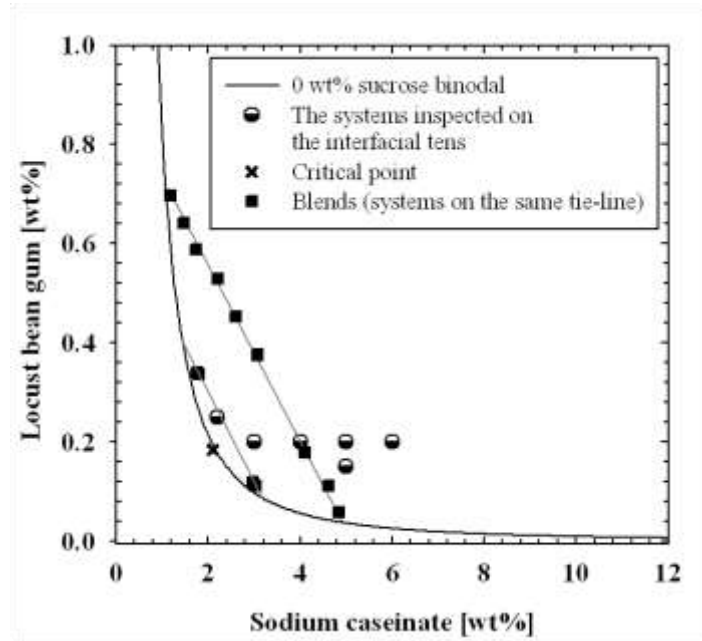
All ATPS from Table 3–4 were chosen within a two-phase regions of the phase diagrams, but still close enough to the binodals (Figure 3–13) to avoid experimental difficulties in retraction experiments, which are described later in § 3.3.3.2 (p. 3–103). The pairs of the equilibrium phases from ATPS were mixed in various wt% to prepare blends. The blends were hence aqueous dispersions of various volume fractions of the two equilibrium phases. It is assumed that the compositions of the phases did not change during blending.

Figure 3–12 shows ATPS (left), separated equilibrium phases (middle) and prepared blends (right).



**Figure 3–12.** 4 wt% sodium caseinate-0.2 wt% locust bean gum system without sugar. Aqueous two-phase system (left), separated equilibrium phases (middle), and blends with 80 wt% and 20 wt% of the locust bean gum-rich phase (right).

Figure 3–12 shows the ATPS, marked with "●", and their blends, marked with "■" for System 1 without sugar in a phase diagram.



**Figure 3–12.** Systems investigated on their interfacial tensions for sodium caseinate-locust bean gum without sugar. "■" refers to blends investigated for interfacial tensions "●" refers to ATPS whose equilibrium phases were used to prepare blends.

Blends (dispersions) of various volume fractions of the equilibrium phases were prepared from the ATPS. Dispersions of 1 wt% of the GM-rich phase in 99 wt% of the NaCAS-rich continuous phase were prepared from all ATPS listed in Table 3–4 so that they could be used in the drop retraction experiments. The last two sections of this chapter explain the experiments in more detail. The low volume fraction and high viscosity of the dispersed phase ( $\eta_d$ ) ensured slow coalescence (fewer droplet-droplet interactions) and fast retraction, and gave good images in these experiments. From ATPS that are marked with "#" in Table 3–4 dispersions of additional volume fractions (that is,  $\varphi_{GM}$  of 10, 20, 60, 80, 90 and 99 wt%, marked with "■" in Figure 3–12) were prepared to test the dependence of the interfacial tension on the phase sense of the system.

### 3.3.3.2 Drop retraction setup and procedure

Digital images of retracting droplets of the dispersions (blends) were recorded and the sizes of droplets were measured to obtain drop shape evolution data with time. The images of the droplets were obtained with the experimental setup shown in Figure 3-13.

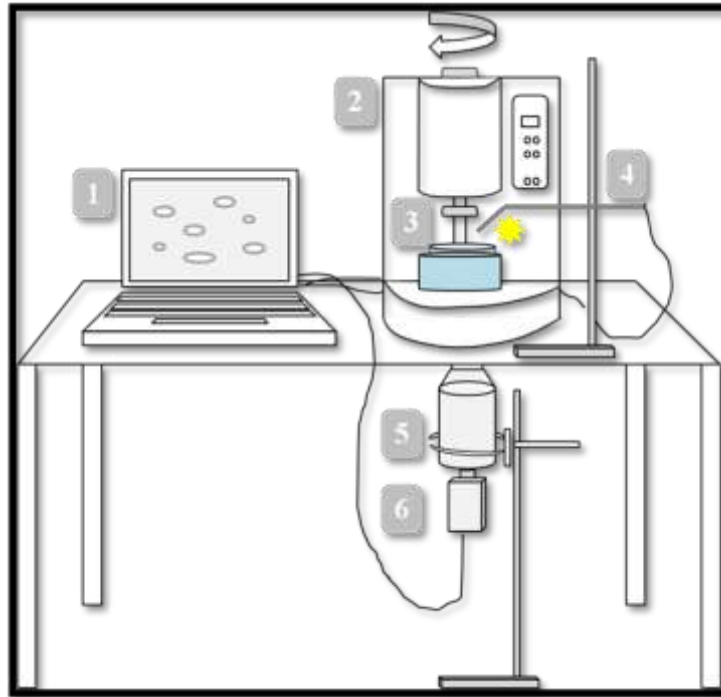


**Figure 3-13.** Experimental setup for the interfacial tension measurement composed of a rotational rheometer with glass plate-and-plate geometry and video-microscope-computer system: 1-video and flow recording, 2-Bohlin Gemini with Rotonetic drive Z stress controlled rotational rheometer (Malvern Instruments), 3-custom made glass plate-and-plate geometry (40 mm diameter), 4-strobe, 5-stereo microscope (110 times magnification), and 6-C-mounted b/w video camera (AVT Dolphin).

An arrangement comprised of a strobe (Strobotach, Metox Ltd., Crowborough, UK), custom-made glass plate-plate geometry (40 mm diameter, 300  $\mu\text{m}$  gap, Figure 3-10), microscope (Olympus SZ-60, with SZ-CTV adapter) and camera (AVT Dolphin F-145B (b/w) with C SXGA mount) enabled visualisation and recording of the evolution of droplet shape under shear and at rest. The strobe light pulsed at the camera's framing

rate and provided sufficient illumination of the sample, which was magnified 110 times and where a pixel corresponded to 1.329  $\mu\text{m}$  length.

The drop retraction experiment was executed as follows. The blends were sheared with a rotational rheometer (Bohlin Gemini with Rotonetic drive Z, Malvern Instruments, Malvern, UK) at room temperature ( $22\pm 2^\circ\text{C}$ ). Prior to being loaded on the rheometer plate, the blends (for preparation see § 3.3.3.1, p. 3–100) were stirred with a spatula 10 times in each direction. Dispersions were then pre-sheared at  $500\text{ s}^{-1}$  for 15 s in order to evenly break up the droplets. The GM-rich continuous systems under shear produced smaller droplets (few  $\mu\text{m}$ ) than NaCAS-rich continuous systems (40–80  $\mu\text{m}$ , 4–5 times smaller than the gap). NaCAS-rich continuous systems were later used exclusively in calculation of the interfacial tensions (see § 3.3.3.3, p. 3–106). The shear was applied stepwise until drop deformation was observed on a real time video monitor display. Drops of a more viscous GM-rich continuous system sufficiently deformed at shear rate of  $\sim 0.5\text{ s}^{-1}$ , but less viscous NaCAS-rich continuous system deformed at a much higher shear rate of  $\sim 800\text{ s}^{-1}$ . When drop retraction from an ellipsoid to a spherical shape was observed, the shear rate was kept constant for at least a minute before the shear was stopped and the head of the rotor was locked to prevent the plate geometry from moving.

The drops in the visual field of the microscope-camera setup were recorded (i) for GM-rich-continuous blends, with a speed of 60 fps, that is every 8 s, for  $\sim 30$  min, and (ii) for NaCAS-rich-continuous blends, with the speed of 15 fps, that is every 2 s, for

~2 min. By analysing different frames, the shape of the droplet was followed with time. The speed of the drop retraction differed with the viscosity of the continuous phase ( $\eta_c$ ). In GM-rich continuous dispersions, droplets of the NaCAS-rich phase retracted in ~20 min, whereas in the NaCAS-rich-continuous dispersions, the GM-rich dispersed droplets retracted significantly faster, ~1 min. The retraction process was finished when spherical droplets were observed across the sample. For each system not every frame was analysed, the total retraction time was divided by 10 as it was found that 10 to 15 frames describe the retraction process with sufficient accuracy.

During observation the drops weren't displaced significantly (on average a maximum displacement of ~3  $\mu\text{m}/\text{min}$  was observed) from the original position, hence the effects of buoyancy were negligible. The deformation parameter,  $D$ , was measured in time with Image J (freeware image analysis programme first developed at National Institute of Health, Bethesda, USA) on the images digitalised with camera software.

A typical example of a retracting drop observed after cessation of shear is shown in Figure 3-14.

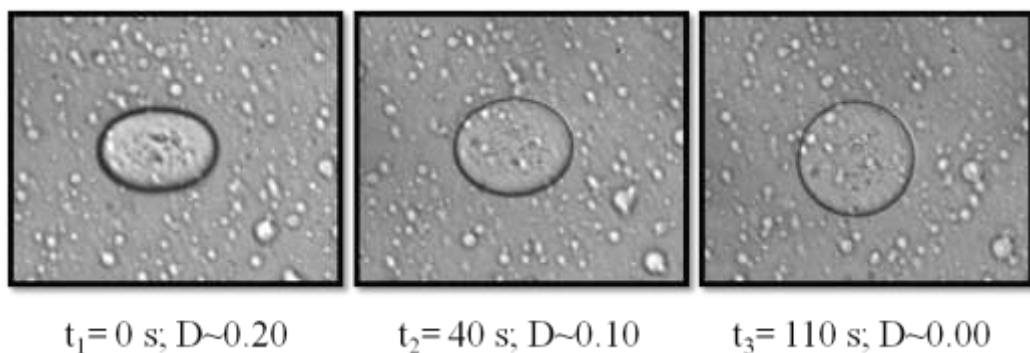


**Figure 3-14. Retracting drop at various times with corresponding drop deformation parameters ( $D$ ) after the cessation of shear. The size of the retracted drop (micrograph on the right) is 60  $\mu\text{m}$ .**

The accuracy of the retraction experiment is limited because the shape of each drop can only be measured once. To improve the accuracy and precision of the measurements the sizes of up to ten drops per blend were analysed. Not all the results, however, were averaged. The evolution of the drop recovering from its deformed ellipsoid shape to a relaxed spherical shape was used to calculate interfacial tensions, described next.

### **3.3.3.3      *Calculation of interfacial tension***

Interfacial tensions in NaCAS-GM-sugar ATPS were calculated by the modified drop deformation method (Guido and Villone, 1999). The principle of the method is to observe the retraction of a droplet after the cessation of shear and relate the rate of change in its shape to the time and viscosities of the continuous and dispersed phases.

The drop retraction method was chosen for three reasons. First, it was not possible to measure interfacial tensions of ATPS with commercial tensiometers/goniometers (of 0.01 mN/m resolution). The ATPS were too opaque and their interfacial tensions (in a  $\mu\text{N}/\text{m}$  range) were too low. Second, the execution of the method was easy. And third, the method was used previously for ATPS (Ding et al., 2002; Guido et al., 2002; Simeone et al., 2004; Scholten et al., 2005; Spyropoulos et al., 2008) and is believed to accurate and precise.

The deformation parameter  $D$  of a chosen droplet was calculated from a digital image. The dimensions of each droplet were measured in triplicate and an average of lengths was taken to calculate the final deformation parameter.

$$D = \frac{(L+W)}{(L-W)} \quad [3-20]$$

as shown in Figure 3-15,  $L$  and  $W$  are major and minor axes of the projection of the drop on the plane in the direction of flow and vorticity. The eq. [3-20] is identical to eq. [2-7] in § 2.4.2.1, p. 2-47 where the parameter  $a$  is  $L$  and the parameter  $b$  is  $W$ .

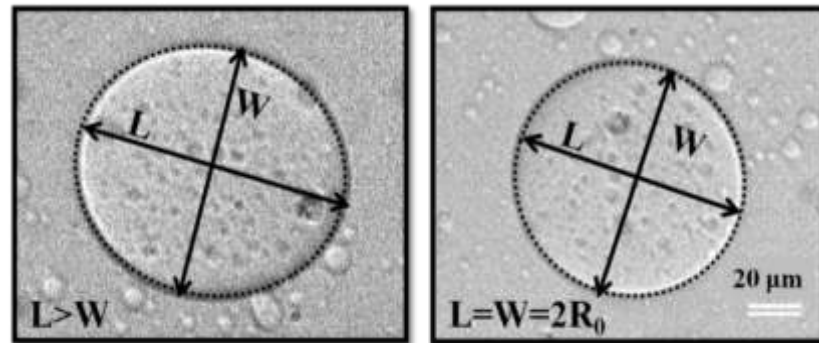


**Figure 3-15.** The calculation of the drop parameters in ellipsoid (left) and spherical (right) droplets.  $L$ =length of the drop,  $W$ =width of the droplet,  $R_0$ =radius of a retracted (spherical) droplet. During the retraction process, the drop rotates round its centre.

For small deformations, the deformation parameter  $D$  changes exponentially with time,

$$D = D_0 \times e^{\left(-\frac{1}{\tau}\right)t} \quad [3-21]$$

$D_0$  is the deformation factor at time  $(t) 0$  and  $\tau$  is characteristic time. Rearranging the eq. [3-21] into the logarithmic form in eq. [3-22]<sup>17</sup> gives a linear relationship between the deformation factor  $D$  and  $t$ .

$$\ln D = \ln D_0 - \left(\frac{1}{\tau}\right)t \Rightarrow y = y_0 - ax \quad [3-22]$$

From the diagram  $\ln D$  vs.  $t$  the rate of change of the deformation  $\tau$  was calculated. A small value of  $\tau$  (less steep slope of the line) meant faster drop retraction.

Factor  $D$  needs to fall in the limits of the small deformation theory for the above

<sup>17</sup> Equations [3-21] and [3-22] are identical to equations [2-12] and [2-13] from § 2.4.2.1, p. 2-47.

equation to be valid, hence only data between certain limits of  $D$  was used to calculate  $\tau$ . The limits were determined experimentally by various authors to be 0.02 and 0.25 (Ding et al., 2002; Scholten et al., 2005; Spyropoulos et al., 2008a), but in this study the values of  $D$  between 0.04 to 0.20 were taken. The limits were established for two reasons. First, at the beginning of the retraction process the droplet was too deformed (it appeared more like a square with round edges than an ellipsoid). And, second, at the end of the retraction highly scattered data was obtained due to the small differences between  $L$  and  $W$  that could not be accurately measured given the resolution of the equipment.

For a single drop in a medium (Guido et al., 1999) or for a dispersion where drops do not touch (Spyropoulos et al., 2008a),  $\tau$  is related to the interfacial tension ( $\sigma$ ), the viscosity of the continuous phase ( $\eta_c$ ), the radius of completely retracted/spherical drop ( $R_0$ ) and the viscosity ratio ( $\lambda$ )—defined as  $\eta_c/\eta_d$  ( $\eta_d$  is the viscosity of the dispersed phase).

$$\tau = \frac{\eta_c R_0}{\sigma} \left( \frac{(19\lambda + 16)(2\lambda + 3)}{40(\lambda + 1)} \right) \quad [3-23]$$

Hence  $\sigma$  can be calculated by measuring  $R_0$  and  $\tau$  of the chosen droplet, as well as  $\eta_c$  and  $\eta_d$  of a chosen system (i.e., viscosities of the equilibrium phases).

# CHAPTER 4: PHASE BEHAVIOUR OF AQUEOUS SODIUM CASEINATE - GALACTOMANNAN - SUGAR MIXTURES

## 4.1 Introduction

The purpose of the study presented here is to better understand the phase equilibria of four model ATPS—System 1 (NaCAS-LBG), System 2 (NaCAS-TG), System 3 (NaCAS-GG) and System 4 (NaCAS-FG)—and how they are affected by solvent properties. The effect of solvent on the systems is tested by varying sugar concentration and sugar type; non-reducing disaccharides, such as: sucrose and trehalose, are compared to open-chain monosaccharides, such as: glucose and fructose. This is done experimentally by establishing the phase diagrams at pH 5.8 and a temperature of 20°C.

The chapter is divided in four parts. In the first part, few general observations inherent to the systems are made. In the second part, the phase diagrams of four reference NaCAS-GM ATPS are established and discussed. In the third part, the effect of sugar concentration is studied by adding various amounts (0–60 wt%) of sucrose<sup>18</sup> to the systems. And in the final part, sucrose is compared with other sugars (trehalose, glucose and fructose) at two concentrations, 15 and 30 wt% (the reasons for selecting these concentrations are explained in § 3.3.1.2, p. 3—77).

---

<sup>18</sup> Sugar concentration is given as the percentage (wt% or %) of weight of sugar over the total weight of the system.

## 4.2 Phase behaviour: a general observation

### 4.2.1 Appearance of the phases

Sodium caseinate and galactomannan associate minimally and readily separate into coexisting phases. One of the determining factors for the occurrence of phase separation is sufficiently large partial concentration of the biopolymers. If the partial concentrations of NaCAS and GM are low enough, their mixtures appear homogenous. These are positioned in a phase diagram (§ 2.3.2, p. 2–35) either below the binodal curve or on the binodal curve. High partial concentrations of the biopolymers result in the formation of coarser and less stable emulsions (e.g., Figure 4–1), where the coalescence of a dispersed phase (e.g., Figure 4–2) concludes in the formation of the separate phases (e.g., Figure 4–3): (i) isotropic polysaccharide-rich (top) and (ii) birefringent protein-rich (bottom) phase. Phase separation is reversible—the equilibrium phases are easily homogenised by shaking/mixing.

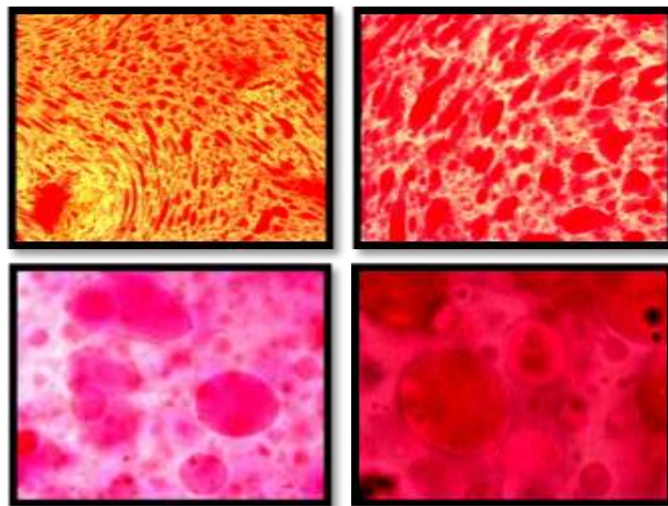


**Figure 4–1. Light micrographs of a 95 wt% locust bean gum-rich blend at 50 times, 100 times, 400 times and 1000 times magnification. The protein-rich phase is dyed with direct red.**

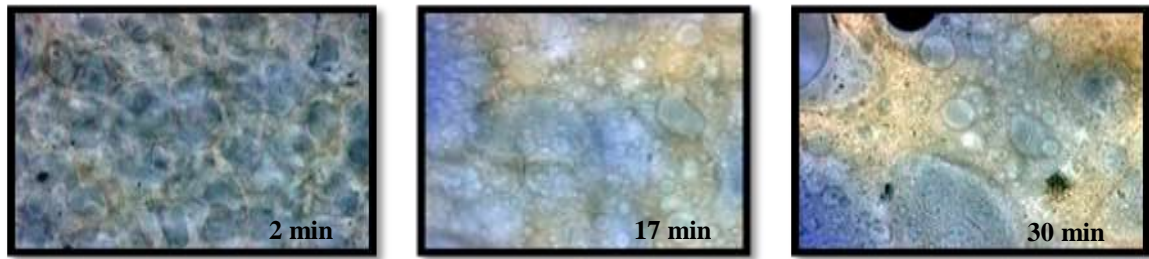


**Figure 4-2.** Phase separation kinetics in 95 wt% locust bean gum-rich blend 100 times magnified. The protein-rich phase is dyed with water blue.

The phase separated systems inside the two-phase region differ in overall composition and microstructure. As shown in Figure 4-3, the volume fractions can be inferred by the position of the ATPS in relation to the rectilinear diameter (see § 3.3.1.3.1, p. 3-81, 82), where ATPS on phase separate into equal volume fractions. In general, a difference in the partial biopolymer concentrations results in an ATPS of a different volume fraction and microstructure (Figure 5-5, p. 5-145). The volume fraction of the equilibrium phases are reported as:  $\varphi_{GM}$ , the volume fraction of GM-rich phase, and  $\varphi_{NaCAS}$ , the volume fraction of the NaCAS-rich phase, which add up to unity.

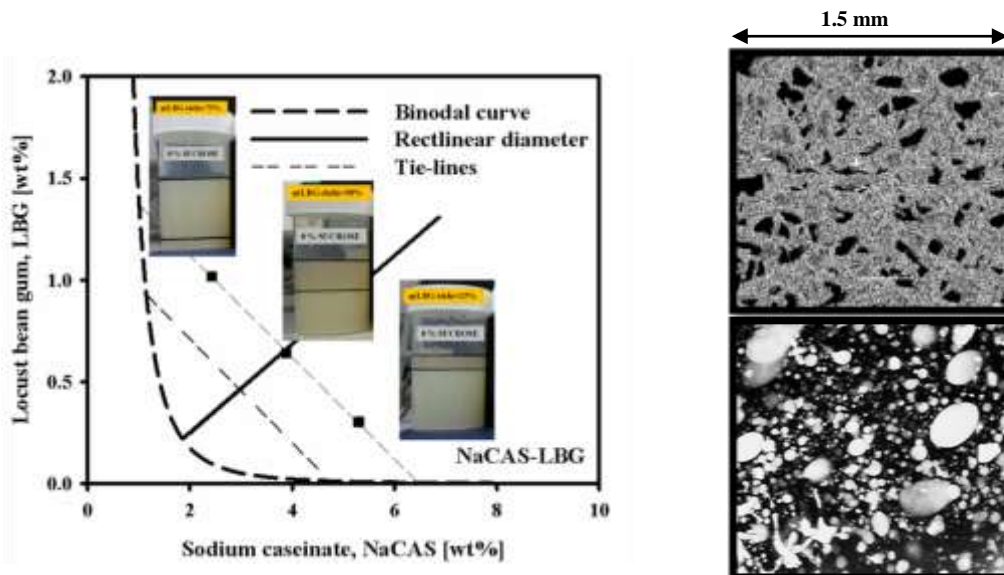


**Figure 4-3.** Phase diagram of sodium caseinate-locust ben gum (NaCAS-LBG) reference system with the images of the systems of three distinct volume fractions: NaCAS-continuous (right), bicontinuous (middle) and LBG-continuous (left). Top phase is rich in LBG and bottom phase is rich in NaCAS. The micrographs are a representation of the GM-rich (top) and NaCAS-rich phases.

Water is the most abundant component of the equilibrium phases and ATPS. Figure 4–4 illustrates its distribution in the protein-rich ATPS (below the rectilinear diameter, image in the left) and polysaccharide-rich ATPS (above the rectilinear diameter, image on the right). Although the microstructure of the ATPS is largely distorted by the formation of ice crystals<sup>19</sup>, the structuring effect—the higher capacity to hold water—of the GMs is still evident.

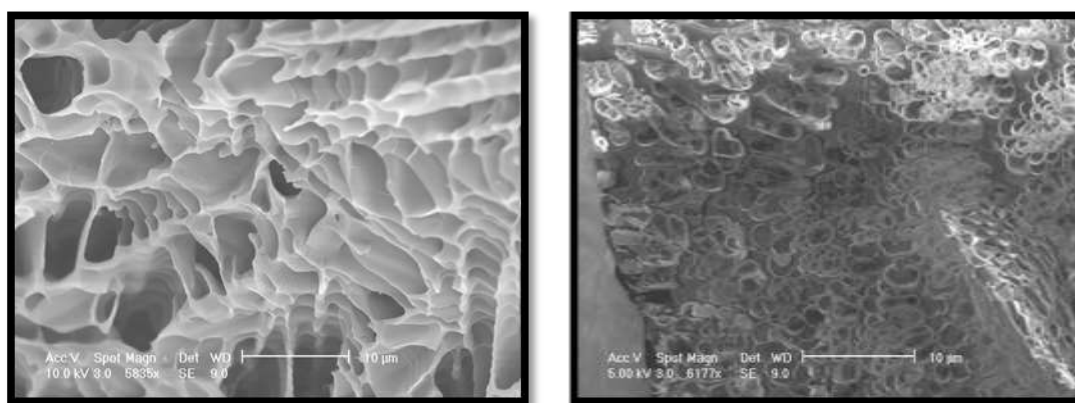


**Figure 4–4. Scanning electron micrographs of the (left) 15 wt% locust bean gum-rich blend, and (right) 75 wt% locust bean gum-rich blend.**

#### 4.2.2 Phase equilibria

The phase equilibria of the systems was assessed in a limited concentration range—4–8 wt% NaCAS and 0.3–0.6 wt% GM, see § 3.3.1.1, p. 3–76. Due to limited practical relevance and experimental difficulties, such as: (i) high viscosities of the mixtures, (ii) limited solubility of the biopolymers—especially GMs, and (iii) longer phase separation times, higher concentrations—GM above 1 wt% and NaCAS above 10 wt%—were only attempted.

<sup>19</sup> Environmental scanning electron microscopy is another technique that could have been used. It allows wet samples to be visualised without freezing and ice sublimation.

The phase equilibria are assessed by establishing phase diagrams. Firstly, the binodals are obtained as best fits to the data points, as described in § 3.3.1.3.1, p. 3–81–86. Secondly, the tie-lines are calculated as described in § 3.3.1.4, p. 3–88, and an average value of the slope (STL) is given for each studied system. Finally, a set of characteristic points is calculated (see § 3.3.1.3.2, p. 3–86) on the basis of which a comparison between the phase diagrams is made. For the reasons of brevity, not all phase diagrams and their characteristic points are presented graphically. Instead, the parameters  $a$  and  $b$  of the best fit function (eq. [3-3], p. 3–86), STL and the characteristic points are listed in tables.

### **4.3 Effect of galactomannan type on the phase behaviour of sodium caseinate-galactomannan mixtures without sugar**

The first set of experiments investigates the phase behaviour of four NaCAS-GM ATPS in citrate buffer. Systems differ in the GM type. Power law function ( $[GM] = a \times [NaCAS]^{-b}$ , eq. [3-3]) was chosen to best describe the theoretical miscibility boundary in the phase separated systems as it approaches both axes asymptotically, which means that the equilibrium phases to which a primary ATPS separates always contain both biopolymers. The choice of a function also makes possible comparison between the systems.

#### **4.3.1 Binodals**

Figure 4–5 shows the phase diagrams for Systems 1–4; binodals on the same phase diagram correspond to a different galactomannan in the system. Critical and

threshold points are also shown. The parameters  $a$  and  $b$  that describe the binodals are given in Table 4–1 together with an average STL, an average of 3–5 tie-lines.

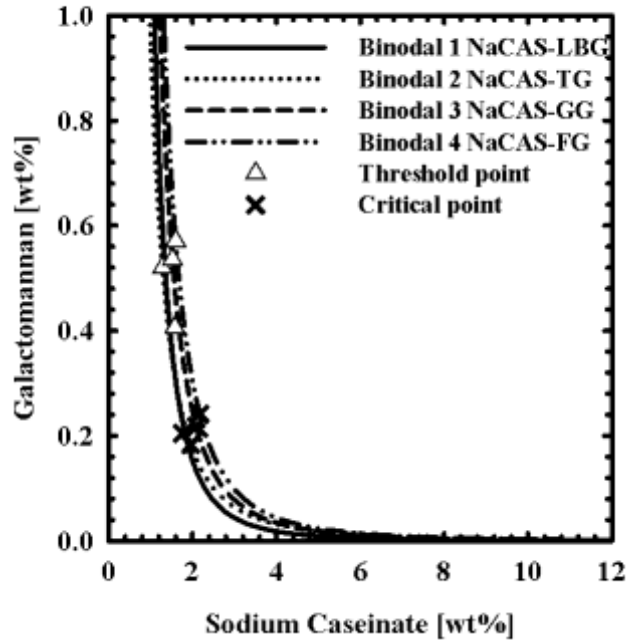


Figure 4–5. Phase diagrams of Systems 1–4 without added sugar.

Table 4–1. Parameters  $a$  and  $b$  in eq. [3-3] and the slopes of the tie-lines (STL) for Systems 1–4. The equation of the phase curve is  $[GM] = a[NaCAS]^{-b}$ .

System	$a$ [wt% <sup>1-b</sup> ]	$b$	$R^2$	STL
1	$0.9111 \pm 0.0166$	$-2.6382 \pm 0.0473$	0.9987	$-0.2453 \pm 0.0357$
2	$1.099 \pm 0.1145$	$-2.5662 \pm 0.1595$	0.9921	$-0.2440 \pm 0.0190$
3	$1.7759 \pm 0.1968$	$-2.8469 \pm 0.2455$	0.9129	$-0.2232 \pm 0.0467$
4	$2.1463 \pm 0.2687$	$-2.8087 \pm 0.5239$	0.8555	$-0.2306 \pm 0.0344$

Figure 4–5 shows low compatibility of NaCAS and GM. Assymetry of the binodals is also observed. The mixing behaviour of the biopolymers remains poor (one-phase region in the phase diagram remains small) regardless of the type of the GM present. Similarly, no apparent changes in the assymetry were observed for these systems. The poor assymmetric mixing behavior of NaCAS and GM is likely caused by a coupling effect of the following two effects: (i)  $M_w$  of the biopolymers—~100 fold difference exists

between the average  $M_w$  of NaCAS and a GM (Belyakova et al., 2003; Wu et al., 2009) and (ii) interaction parameters between each of the biopolymers and the solvent (Hsu and Prausnitz, 1975). Given these observations, the use of molar concentrations would provide for the equal number of molecules in the mix and they are likely to preserve both poor mixing behaviour and asymmetry of the binodals.

### 4.3.2 Asymmetry of the phase diagram: slopes of the tie-lines and characteristic points

Good measures of the incompatibility and symmetry of the phase diagrams are also (i) the critical and threshold points, and (ii) STL. Furthermore, the calculation of (i) the distance between the critical and threshold points ( $\lambda_{\text{sym}}$ ) and (ii) the inverse distances of these points from the origin of the Cartesian coordinate space (0,0) ( $1/\alpha_{\text{crit}}$ ,  $1/\alpha_{\text{thres}}$ , see § 3.3.1.3.2, p. 3–86) enable a detailed assessment of the symmetry and degree of incompatibility between the components. In a perfectly symmetric system, critical and threshold points coincide ( $\lambda_{\text{sym}} = 0$ ) and the STL is -1 (Zaslavsky, 1995). Large inverse distances of systems,  $\ll 1/\alpha$ , characterise mixtures that separate at lower partial concentrations.

Phase diagrams in Figure 4–5 also show that the phase behaviour of the systems differs by the GM present. As seen in Table 4–1 the average values of  $a$  and  $b$  (the parameters describing the binodals) follow the GM related trend:  $\text{LBG} \approx \text{TG} < \text{GG} \approx \text{FG}$ . Given that pH is kept constant—the charge and  $M_w$  of the pH sensitive NaCAS stays

unchanged—NaCAS is assumed not to contribute to the observed differences. The differences must therefore arise from the molecular characteristics of the GMs, such as: the  $M_w$  and the differences in the solubility, which are both related to the G:M ratio of the GM (Wu et al., 2009). Since LBG and TG are less soluble and have slightly lower  $M_w$  than GG and FG (see Table 2–2 in § 2.5.2, p. 2–64), Systems 1 and 2 show lesser cosolubility than Systems 3 and 4.

Galactomannan type also affects the symmetry of Systems 1–4, characterised by parameters, such as: STL,  $\lambda_{\text{sym}}$ ,  $1/\alpha_{\text{crit}}$  and  $1/\alpha_{\text{thres}}$ —shown in Table 4–1, Figure 4–6 and Figure 4–7, respectively. On average, STL reflect high asymmetry of the binodals, which means that the investigated systems separate into equilibrium phases differing greatly in the concentrations of the macromolecular components. More specifically, the asymmetry differs between the systems depending on the GM they contain. Systems 3 and 4 that contain more branched, slightly smaller GM species are ~20% more asymmetric—larger  $\lambda_{\text{sym}}$ —and phase separate less readily (smaller  $1/\alpha_{\text{crit}}$  and  $1/\alpha_{\text{thres}}$ ) than Systems 1 and 2.

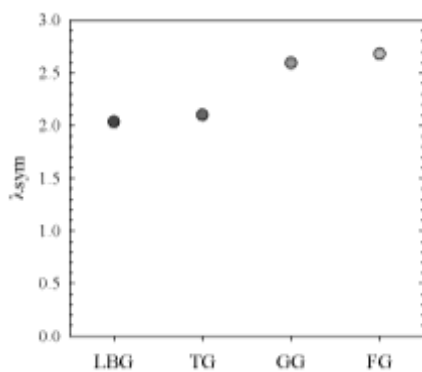


**Figure 4–6. Distances between critical and threshold points ( $\lambda_{\text{sym}}$ ) for Systems 1–4. The degree of branching progresses from System 1 with LBG to System 4 with FG.**

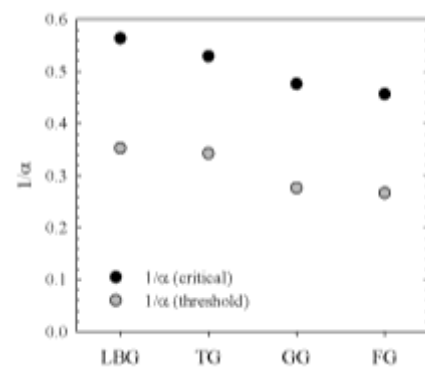


**Figure 4–7. Inverse distances ( $1/\alpha_{\text{crit}}$ ,  $1/\alpha_{\text{thres}}$ ) for Systems 1–4. The degree of branching progresses from System 1 with LBG to System 4 with FG.**

## 4.4 Effect of sugar concentration on the phase behaviour of sodium caseinate-galactomannan mixtures with sucrose

The section reviews the effect of sucrose concentration on the miscibility of Systems 1–4. Slight differences between the GMs were observed in the previous section, where no sugar was added. In this section, the systems containing all four GMs are investigated on the effect of sucrose concentration to determine whether the differences persist. The investigated systems are shown in Table 4–2.

**Table 4–2. Systems investigated on the effect of sucrose concentrations.**

System	Protein	Galactomannan	Sucrose [wt%]
1	NaCAS	LBG	5, 15, 20, 30, 40, 50, 60
2	NaCAS	TG	15, 30
3	NaCAS	GG	15, 30, 50
4	NaCAS	FG	15, 30

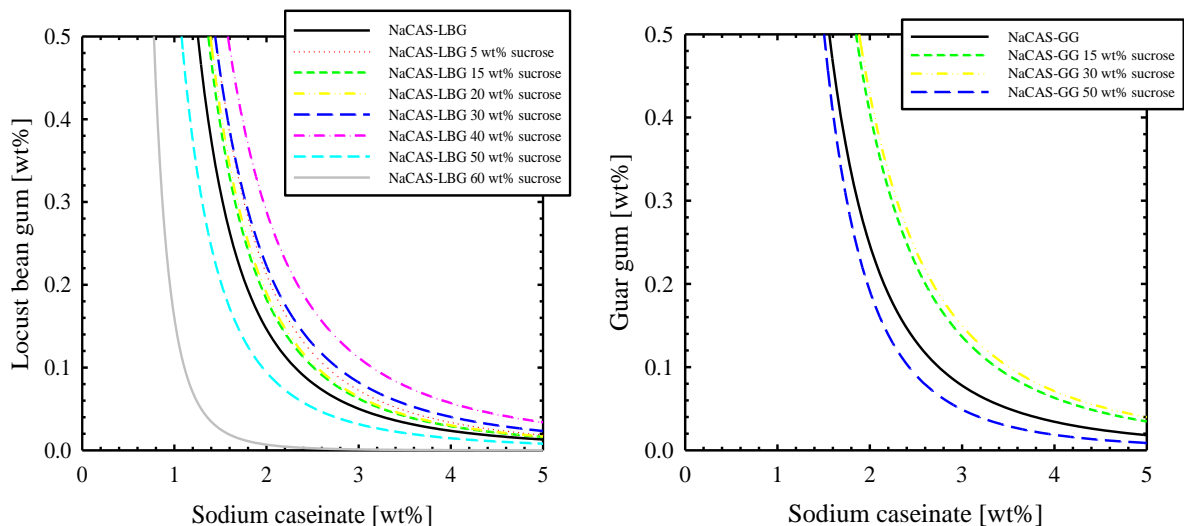
### 4.4.1 Binodals

Table 4–3 shows the parameters  $a$  and  $b$  describing the binodals of the investigated systems.

**Table 4–3. Parameters  $a$  and  $b$  of the phase curves with standard fitting errors for Systems 1-4 with various amounts of sucrose. Coefficients of determination for binodals are  $> 0.92$ . The equation of the phase curve is  $[GM] = a[NaCAS]^{-b}$ .**

Sucrose conc. [wt%]	System 1		System 2		System 3		System 4	
	$a$	$b$	$a$	$b$	$a$	$b$	$a$	$b$
5	$1.2047 \pm 0.021$	$-$ $2.5285 \pm 0.0047$	—	—	—	—	—	—
15	$1.1511 \pm 0.0744$	$-$ $2.6553 \pm 0.1664$	$1.6359 \pm 0.0645$	$2.3077 \pm 0.0876$	$2.5584 \pm 0.0711$	$2.9842 \pm 0.0748$	$2.8756 \pm 0.5071$	$2.3764 \pm 0.1509$
20	$1.2049 \pm 0.104$	$-$ $2.6622 \pm 0.2234$	—	—	—	—	—	—
30	$1.2364 \pm 0.0783$	$-$ $2.4702 \pm 0.1329$	$1.3309 \pm 0.0873$	$2.4241 \pm 0.1617$	$2.6991 \pm 1.2687$	$2.6087 \pm 0.5033$	$3.7954 \pm 0.1564$	$2.5042 \pm 0.0795$
40	$1.4596 \pm 0.11$	$-$ $2.3388 \pm 0.1763$	—	—	—	—	—	—
50	$0.6128 \pm 0.0615$	$-$ $2.7011 \pm 0.2136$	—	—	$1.2963 \pm 0.0402$	$2.65 \pm 0.0707$	—	—
60	$0.16 \pm 0.0315$	$-$ $4.5433 \pm 0.0071$	—	—	—	—	—	—

The binodals for Systems 1 and 3 are also shown graphically in Figure 4–8, where each binodal corresponds to a different sucrose concentration.



**Figure 4–8. Phase diagrams of System 1 (left) and System 3 (right) with various sucrose concentrations.**

The binodals show that sucrose concentration affects the phase behaviour of Systems 1–4. This has been previously shown by the use of a “trial and error” approach on Systems 1 and 3 (Pörtsch, 2007; Spyropoulos et al., 2010). Although the results presented here in principal reconfirm previous findings—i.e., sucrose below the critical value improves the mixing behaviour of NaCAS and GM—the use of the method by Polyakov et al. (1980) establishes a new optimum of sucrose concentration. Previous work by Spyropoulos et al. (2010) states that 15 wt% sucrose results in a maximum increase of the miscibility region and that further increase in its concentration has the opposite effect. This work, however, found that 40 wt% sucrose results in a far greater miscibility region and that a further increase in its concentration  $> 40$  wt% causes a reduction of the cosolubility of the components. The inconsistent results are ascribed to the use of a different method and sample size. In comparison to the phase-volume ratio method the “trial and error” method is less accurate. Its accuracy is greatly limited by the size of an increment in concentration by which the 2D space is scanned for an onset of the phase separation. Given that the differences in the onset of phase separation are small, it is possible that an increment used in the “trial and error method” was too large for the changes to be observed. Another two possible reasons exist that could hamper the accuracy of the method: (i) the absence of centrifugation used for the purpose of degassing the samples completely (e.g., samples with  $< 30\%$  sucrose) or partially (e.g., samples with  $> 30$  wt% sucrose), and (ii) a substantially smaller sample size, i.e., 4 g instead of 30 g.

Although the binodals of System 1 do not seem to follow any trend, they can be classified by the amount of added sucrose as follows:

60 < 50 < 0 < 15 < 20 < 5 < 30 < 40 wt%. The higher a system is in the classification the further its binodal is from x and y axes in the Cartesian coordinate system. As shown in Table 4-3 the increase in the values of the parameter  $a$  and—a less significant—decrease in the values of the parameter  $b$  describes the binodals moving away from the axes. There is, however, a great deal of experimental uncertainty involved with the assessment of the cosolubility in the systems with > 40 wt% sucrose, which leads to possible errors in the determination of these binodals. At high sucrose concentrations (> 40 wt%) the formation of a stable foam<sup>20</sup> and syneresis—expulsion of the solvent (> 60 wt%) surrounding the GM and NaCAS—further decrease the resolution of the method used, hence the positions of these binodals should not be taken at their face value. The latter experimental difficulties also added to a reason why higher sugar concentrations were not attempted for Systems 2 and 4.

The effect of sucrose concentration on the cosolubility of Systems 2–4 shows a similar trend. In all investigated systems 30 wt% sucrose increased the miscibility region further than 15 wt%. The addition of 50 wt% sucrose to System 3 decreased the miscibility region to about the same as that of the reference system without added sucrose. As mentioned earlier, the position of the latter binodal is determined with greater uncertainty than the binodals for systems with < 40 wt% sucrose. Similarly to the observations made for System 1, a change in the position of the binodals is accompanied with the corresponding increase in the parameter  $a$  and a slight decrease of parameter  $b$ .

---

<sup>20</sup> The stable foam forms because of the bipolar nature of NaCAS molecules. The bubbles are stabilised by sucrose and GMs. Sucrose at > 40% causes NaCAS molecules to easily self-associate and easily unfold. Sucrose also structures water. The presence of the GMs lowers the mobility of the molecules in the mix further and adds stability to the foam.

As for the type of GM, the addition of sucrose preserved the differences among Systems 1–4. At a given sucrose concentration (either 15 or 30 wt%) the size of the miscibility region followed the trend: LBG < TG < GG < FG.

#### 4.4.2 Slopes of the tie-lines

Table 4–4 gives average STL values of five randomly selected systems inside a two-phase region of each phase diagram and every system.

**Table 4–4. The slopes of the tie-lines (STL) for Systems 1–4 with sucrose.**

Sucrose concentration [wt%]	System 1	System 2	System 3	System 4
	STL	STL	STL	STL
5	$-0.23445 \pm 0.029347$	—	—	—
15	$-0.22607 \pm 0.014747$	$-0.22382 \pm 0.024268$	$-0.29467 \pm 0.088204$	$-0.22822 \pm 0.061669$
20	$-0.23898 \pm 0.015472$	—	—	—
30	$-0.20477 \pm 0.014613$	$-0.29946 \pm 0.010111$	$-0.25208 \pm 0.033636$	$-0.20237 \pm 0.032048$
40	$-0.2043 \pm 0.02901$	—	—	—
50	$-0.24837 \pm 0.046068$	—	$-0.21994 \pm 0.002816$	—
60	$-0.17387 \pm 0.117259$	—	—	—

Slopes of the tie-lines, in all systems but System 2, decrease with an increase in the [sucrose]. The possible cause for this discrepancy may be system specific; inconclusive data was obtained for System 2 on several occasions (see Table 6–4).

For System 3, another discrepancy is observed; the STL values are higher than that of the reference system, shown in Table 4–1, which breaks the trend (Ref=0>15>30% sucrose) observed for Systems 1, 2 and 4. This discrepancy could result from poor mixing of the macromolecular components at higher total biopolymer

concentrations [BP] caused by their high low-shear viscosity. Poor mixing could subsequently result in a binodal that poorly describes the behaviour of that system.

At sucrose concentrations  $> 40$  wt% the decrease of the STL is masked by large errors that are likely down to a stable foam formation and a diminished miscibility and “clustering” of the macromolecules. Greater errors could be also a result of the fact that the solutions with the help of which the STL were calculated were selected close to the binodal where the errors become significantly more noticeable due to the shorter tie-line lengths (TLL).

The observed changes in STL values are also accompanied by a change in the volume fractions of equilibrium phases, i.e., a decrease in STL relates to an increase in GM-rich phase and subsequent reduction in NaCAS-rich phase (see Table 6–8, § 6.3.2, p. 6–219). The change in STL also shows dilution/concentration effects taking place in the system of the same [BP] and different [sucrose]. For example, the rising [sucrose] in the system of a constant [BP] causes the equilibrium phases to be diluted in GM and concentrated in NaCAS.

#### **4.4.3 Asymmetry of the phase diagrams**

As shown in Figure 4–9, sucrose concentration also affects the symmetry of Systems 1–4.

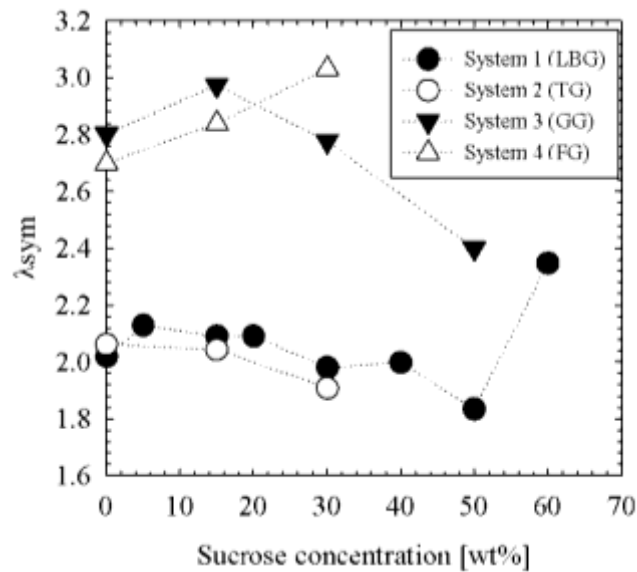


**Figure 4–9.** Distances between the pairs of critical and threshold points ( $\lambda_{sym}$ ) as a function of sucrose concentration. Dotted line is to guide the eye.

Depending on the amount of sucrose present, the asymmetry of the phase diagram can either increase or decrease. Compared to the reference system without sucrose, an increase in asymmetry ( $\lambda_{sym}$ ) is observed: (i) for Systems 3 and 4—up to 15 wt% of sucrose, (ii) for System 1—up to 20 wt% of sucrose, and (iii) for System 4—up to 30 wt% of sucrose. For Systems 1, 2 and 3 a further increase in the sucrose concentration above the optimal value relates to a decrease in the  $\lambda_{sym}$ . The asymmetry changes most likely reflect the effect of sucrose on the solvent quality, and GM molecules (i.e., coil expansion/retraction). Regardless of the amount of sucrose present—and as already shown in Figure 4–6 in § 4.3, p. 4–116—Systems 3 and 4 are more asymmetric than Systems 1 and 2.

Figure 4–10 shows the position of the binodals in the 2D Cartesian space. A clear distinction between the GMs is once again observed. Systems containing moderate

amounts of sucrose separate more readily as compared to the systems where sucrose is either absent or present in a large amount.

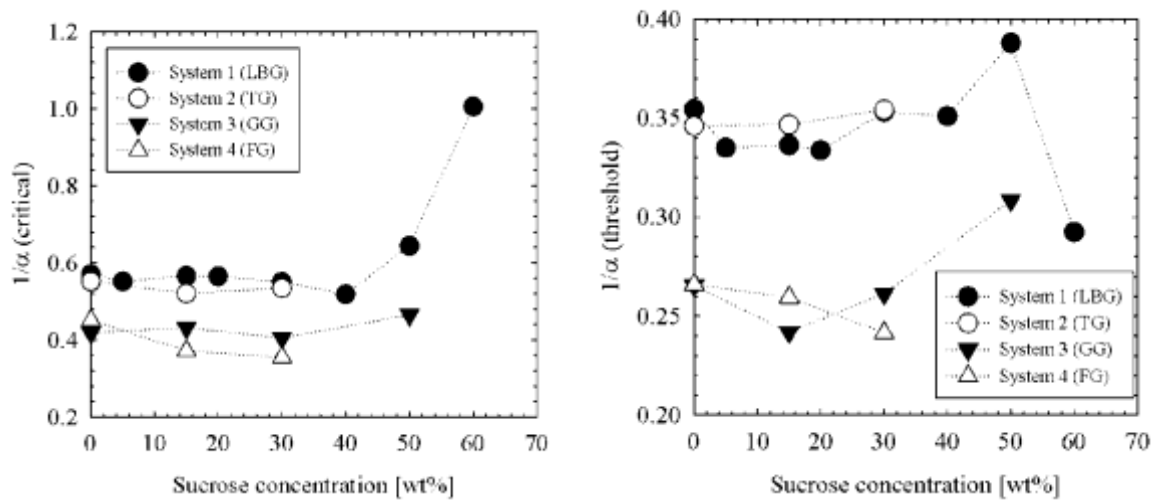


**Figure 4–10.** Inverse distances as a function  $1/\alpha_{crit}$  (left) and  $1/\alpha_{thres}$  (right) as a function of sucrose concentration. Dotted line is to guide the eye.

#### 4.4.4 Discussion

The effect of sucrose on the phase behaviour (equilibria) of various protein-polysaccharide systems was previously linked to the effect of sucrose on the individual macromolecular components (Antipova and Semenova, 1995; Antipova and Semenova, 1997b; Richardson et al., 1998; Antipova et al., 1999; Schorsch et al., 1999b; Schorsch et al., 2000; Belyakova et al., 2003).

In the explanation of the phase equilibria of Systems 1-4 in this work, the study of Richardson et al. (1998) provides a useful insight into solubility of the GMs in sucrose solutions of various concentrations. The authors who studied the properties of dilute GG-sucrose and LBG-sucrose solutions report increased solubility of both biopolymers up to 20 wt% sucrose, which they ascribe to an increase in the solvent quality—

decreased mannan-mannan interactions on the account of preferential formation of sucrose-mannan hydrogen bonds. On the other hand, they report a decrease in  $[\eta]$  of GMs at 5 wt% and 40 wt% sucrose, below that of the  $[\eta]$  of the GMs dissolved in water (see Figure 2-11, § 2.3.1, p. 2-34). They explain the decrease of  $[\eta]$  at 5 wt% of sucrose with a decrease in GM-GM self-association and, at 40 wt%, with a contraction of the GMs chains. Since  $[\eta]$  of the GMs in the presence of 5-20 wt% increase continuously and at 40 wt% abruptly decrease, one can only infer on the  $[\eta]$  at 30 wt% sucrose, i.e.,  $[\eta]$  at 30 wt% could be either larger or smaller than  $[\eta]$  at 20 wt%. Although  $[\eta]$  of the individual GMs respond to sucrose in a similar way, GG has an overall smaller  $[\eta]$  compared to LBG. GG molecules are hence more compact and less soluble in sucrose solution than LBG. Because of that the solvent drainage through GG molecule is reduced, and the impact of sucrose on GG is lesser than on LBG. The findings by Richardson et al. (1998) are indirectly supported by that of Brummer et al. (2003) who state that GG solvated in water is more compact than LBG. A more recent study by Wu et al. (2009), however, provides contradicting data (Table 2-2, § 2.5.2, p. 2-64), by which a greater solubility of GMs in the order of: GG < FG < TG < LBG in water is affirmed. The results in this work provide support to their findings.

The studies of the effect of sucrose on the molecular characteristics of NaCAS/casein by Belyakova et al. (2003), Antipova et al. (1999) and Schorsch et al. (2000) also provide a better understanding of this data. They show that the addition of sucrose controls the hydrophilic-lipophilic properties of NaCAS by the competing

processes of: (i) dissociation of negatively charged NaCAS submicelles, which increases protein's hydrophobicity, and (ii) association of the individual NaCAS molecules into more compact and hydrophilic submicelles. The authors suggest that the dissociation is a result of the formation of the hydrogen bonds between NaCAS and sucrose and leads to a stronger NaCAS-NaCAS repulsion (Belyakova et al., 2003). Association, on the other hand, is most pronounced < 30 wt% sucrose concentration, above which the process is reduced and—by further increment in sugar concentration—ultimately inhibited (Shorsch et al., 2000). More specifically, for the pH of 5.5–6 (pH>pI) relevant to this work, sucrose in the concentrations of 10–60 w/v%<sup>21</sup> causes a marked increase in the affinity of NaCAS for the aqueous solvent (i.e., NaCAS-NaCAS repulsion,  $A_{NaCAS-NaCAS} > 0$ ). In this concentration range, the presence of sucrose decreases:  $M_w$ /excluded volume, effective molecular size ( $R_g/R_h$ ) and polydispersity ( $M_w/M_n$ ) of NaCAS. Furthermore, in this concentration range and at a pH of 6, NaCAS changes shape. The shape of the molecules changes from close to rigid rod behaviour at 0 w/v% to almost sphere like behaviour at 50 w/v% sucrose. Above 60 w/v% surface hydrophobicity of NaCAS molecules increases on the account of a decreased protein hydration due to a marked competition for water between NaCAS and sucrose molecules (Belyakova et al., 2003). The above changes caused by sucrose to NaCAS are a likely cause for the increased cosolubility of the systems between 10 and 40 wt% sucrose in the present study.

Reports also exist on the effect of sucrose on the solubility of biopolymer mixtures (Antipova et al., 1995; Antipova et al., 1997; Schorsch et al., 1999a; Schorsch

---

<sup>21</sup> Sugar concentration is given as the percentage of weight of sugar over the total volume of the system.

et al., 1999b). The reported literature supports findings of the present study as it recognizes a high incompatibility in the polysaccharide-protein ATPS regardless of the amount of added sucrose. When sucrose is added, Antipova and Semenova (1995), at pH 7 and temperature of 22°C, confirm enhanced cosolubility of the following biopolymer aqueous systems: NaCAS-ovalbumin, NaCAS-11S globulin and NaCAS-sodium alginate. They report that an increase in sucrose concentration to 25 w/v% causes most significant increase in the total biopolymer concentration [BP] in the top phase of the ATPS. Further increase of sucrose to 50 w/v% causes —depending on the solubility of the accompanied polysaccharide—either no or only a slight further increase in their cosolubility. Schorsch et al. (1999a, 1999b) report the effect of sucrose on the phase behaviour of skimmed milk protein-LBG and native phosphocaseinate-LBG ATPS at pH 6.8 and temperature of 5°C. The authors find that the addition of 20 wt% sucrose leads to a slight shift of the binodal curve consistent with the increase of the compatibility region. They too attribute the shift to the change in the solvent quality. On the other hand, further increase in the sucrose concentration to 40 wt% does not have a significant effect on the position of the binodal, but instead manifests itself in the decrease of the STL. The latter is also observed in the present study.

Overall, the findings of the present study are consistent with that previously reported. The slight differences in the sucrose concentration, which causes a maximum increase in the cosolubility, can be attributed to either environmental conditions (T, pH, I) or/and different systems studied.

## 4.5 Effect of sugar type on the phase behaviour of sodium caseinate-galactomannan mixtures with sugar

In this section the effect of sugar concentration (15 and 30 wt%) on Systems 1–4 is further reviewed on additional sugar types with the chief intent to determine the differences between them. The effect of nonreducing disaccharides, such as sucrose (see § 4.4) and trehalose is compared to reducing monosaccharides: glucose and fructose. The sugars differ in structure and solubility. While disaccharides are composed of pairs of monosaccharides—sucrose is composed of one glucose and one fructose ring, trehalose consists of two glucose rings—monosaccharides exist in either chain or ring form. Fructose exists largely in open-chain form. Although the above sugars differ in solubility significantly (i.e., fructose > sucrose > glucose > trehalose), they are at 20°C and in concentrations used completely soluble (Nicol, 1979; Okada et al., 1999; Higashiyama, 2002).

### 4.5.1 Binodals

Table 4-5 reviews the parameters  $a$  and  $b$ , describing the position of the binodals in the phase diagrams, for Systems 1–4 with: trehalose, glucose and fructose. A difference in the miscibility boundary between systems is observed as a function of sugar type and concentration. A smaller miscibility region is determined by a combination of a smaller parameter  $a$  and a larger, more negative, parameter  $b$ . While the parameter  $a$  determines the proximity of the binodal to the y-axis the parameter  $b$  determines the steepness of the binodal.

**Table 4–5. Parameters  $a$  and  $b$  with standard fitting errors for the phase curves of Systems 1-4 with various amounts of trehalose, glucose and fructose. Coefficients of determination for binodals are  $> 0.92$ . The equation of the phase curve is  $[GM] = a[NaCAS]^{-b}$ .**

Sugar conc. [wt%]	System 1		System 2		System 3		System 4	
	$a$	$b$	$a$	$b$	$a$	$b$	$a$	$b$
<b>Trehalose</b>								
15	$1.0142 \pm 0.0$ 313	- $2.4119 \pm 0.$ 0674	$1.2402 \pm 0.0$ 531	- $2.3955 \pm 0$ .0939	$2.851 \pm 1.$ 1251	- $2.9856 \pm 0$ .472	$2.3653 \pm 1$ .0084	- $2.5877 \pm 0$ .4849
30	$1.0916 \pm 0.0$ 722	- $2.3959 \pm 0.$ 1469	$1.4968 \pm 0.0$ 742	- $2.4147 \pm 0$ .1355	$3.3574 \pm 0$ .5111	- $2.5082 \pm 0$ .159	$3.0069 \pm 0$ .064	- $2.333 \pm 0.$ 046
<b>Glucose</b>								
15	$0.9777 \pm 0.1$ 064	- $2.3691 \pm 0.$ 2606	$1.2146 \pm 0.0$ 632	- $2.5198 \pm 0$ .1281	$2.4578 \pm 0$ .1125	- $2.8423 \pm 0$ .1565	$2.088 \pm 0.$ 2049	- $2.7186 \pm 0$ .1464
30	$1.4743 \pm 0.4$ 48	- $2.0192 \pm 0.$ 3042	$1.6686 \pm 0.5$ 276	- $2.5581 \pm 0$ .3694	$2.7273 \pm 0$ .374	- $2.3565 \pm 0$ .1165	$4.8201 \pm 0$ .1206	- $2.6086 \pm 0$ .0455
<b>Fructose</b>								
15	$1.0735 \pm 0.1$ 931	- $2.3439 \pm 0.$ 2701	$1.5532 \pm 0.0$ 477	- $2.6255 \pm 0$ .0779	$3.0104 \pm 0$ .0826	- $2.7603 \pm 0$ .0589	$2.8657 \pm 0$ .0965	- $2.5511 \pm 0$ .0672
30	$1.1422 \pm 0.2$ 341	- $1.9752 \pm 0.$ 3131	$1.9076 \pm 0.0$ 659	- $2.7558 \pm 0$ .0891	$3.3721 \pm 1$ .0833	- $2.7131 \pm 0$ .3311	$3.8225 \pm 0$ .1708	- $2.4817 \pm 0$ .0628

Based on the comparison of the parameters the following general observations are made: (i) the presence of 30 wt% sugar, regardless of its type, improves cosolubility of NaCAS and GM more than at 15 wt% sugar, (ii) at 15 wt% of sugar the binodals follow, without exception, the trend: sucrose  $\approx$  glucose  $<$  trehalose  $\approx$  fructose<sup>22</sup>, where the presence of fructose corresponds to the largest miscibility region, (iii) at 30 wt% sugar results are more ambiguous, but—with an exception of System 3—show that at this concentration, monosaccharides increase the cosolubility of the macromolecular components more than disaccharides (trehalose  $\approx$  sucrose  $<$  glucose  $\approx$  fructose)—although, it is unfeasible to sum the results in a general trend, the following trends can

<sup>22</sup> Sign  $\approx$  marks a relationship between systems that cannot be determined conclusively or with sufficient confidence, due to a small difference in the position of the binodal or the inconsistency between various systems.

be deduced for individual systems: (i) Systems 1 and 2 follow: trehalose < sucrose < fructose  $\approx$  glucose, (ii) System 3: sucrose < fructose < glucose < trehalose, and (iii) System 4: sucrose < trehalose < fructose < glucose.

#### 4.5.2 Slopes of the tie-lines

Table 4–6 shows average STL for Systems 1–4 with trehalose, glucose and fructose. Regardless of the type of sugar contained in the system, STL at 30 wt% are always lower than that at 15 wt% sugar. Furthermore—with the exception of System 1—systems containing fructose and glucose show the highest STL values, hence highest degree of symmetry. A decrease in STL between the systems with 0, 15 and 30 wt% of sugar, show no relation to neither the GM type nor the type of sugar.

**Table 4–6. The slopes of the tie-lines (STL) with standard error for Systems 1–4 with trehalose, glucose and fructose.**

Sucrose concentration [wt%]	System 1	System 2	System 3	System 4
	STL	STL	STL	STL
<b>Trehalose</b>				
<b>15</b>	$-0.33371 \pm 0.0618$	$-0.2389 \pm 0.02394$	$-0.2054 \pm 0.012298$	$-0.2114 \pm 0.03271$
<b>30</b>	$-0.1799 \pm 0.0521$	$-0.18432 \pm 0.05977$	$0.1798 \pm 0.0273$	$-0.12715 \pm 0.02431$
<b>Glucose</b>				
<b>15</b>	$-0.25456 \pm 0.026969$	$-0.28016 \pm 0.03041$	$-0.3124 \pm 0.005042$	$-0.25916 \pm 0.015262$
<b>30</b>	$-0.2274 \pm 0.018227$	$-0.21358 \pm 0.013913$	$-0.22259 \pm 0.004163$	$-0.23944 \pm 0.015151$
<b>Fructose</b>				
<b>15</b>	$-0.28369 \pm 0.034427$	$-0.3212 \pm 0.023309$	$-0.33231 \pm 0.024924$	$-0.28247 \pm 0.027907$
<b>30</b>	$-0.26707 \pm 0.037505$	$-0.27491 \pm 0.021053$	$-0.24249 \pm 0.022195$	$-0.23529 \pm 0.022776$

When comparing the STL independently, inside each system, however, a pattern emerges: (i) at 15 wt% systems follow—with the exception of System 3—the trend: glucose  $\approx$  sucrose < fructose  $\approx$  trehalose, and (ii) at 30 wt% STL follows a different

trend: trehalose < sucrose < glucose ≈ fructose. Relatively high average values of the STL data are likely a manifestation of poorly positioned binodals.

Based on the parameters describing the binodals and their STL values, it can be concluded that both type of sugar and its concentration (i.e., number of molecules) are equally important factors affecting the cosolubility of NaCAS and GM.

### 4.5.3 Asymmetry of the phase diagrams

The asymmetry of the systems was assessed further by calculating  $\lambda_{sym}$ . A change in the asymmetry was assessed for an increment of 15 wt% sugar with an attempt to reveal the specificities. The results are shown in Table 4–7.

**Table 4–7. Distances between the correspondent critical and threshold points for the systems of locust bean gum/sodium-caseinate, and guar gum/sodium-caseinate. The following equation was**

**used in their calculation  $\lambda_{sym} = \sqrt{([GM]_{crit} - [GM]_{thres})^2 + ([NaCAS]_{crit} - [NaCAS]_{thres})^2}$ .**

Sugar conc. [wt%]	Sugar type	System 1	System 2	System 3	System 4
		$\lambda_{sym}$	$\lambda_{sym}$	$\lambda_{sym}$	$\lambda_{sym}$
15	Sucrose	2.09	2.04	2.97	2.84
15	Trehalose	1.75	2.36	3.01	2.55
15	Glucose	1.97	2.19	2.80	2.52
15	Fructose	1.97	2.25	2.85	2.80
30	Sucrose	1.98	1.91	2.78	3.03
30	Trehalose	1.80	2.45	3.01	2.94
30	Glucose	1.90	2.25	2.75	3.44
30	Fructose	1.68	2.47	3.07	3.19

On average, an increase in the sugar concentration from 15 to 30 wt% resulted in an increase of the asymmetry of the system—i.e., an increase in  $\lambda_{sym}$ . This is in agreement with the observations made on STL previously, where a reduction of STL

shows greater asymmetry of the system. The data here, however, do not demonstrate the trend consistently.

The positions of the binodals are shown in Table 4–8, by calculating the inverse distances:  $1/\alpha_{crit}$  and  $1/\alpha_{thres}$ . The smallest values characterise systems furthest from the origin of the Cartesian space—the systems with the highest miscibility region.

**Table 4-8. Inverse distances between the critical and threshold points and the origin of the 2D system for Systems 1–4 with trehalose, glucose and fructose. The following two equations were used in their calculation  $\alpha_{crit} = \sqrt{[GM]_{crit}^2 + [NaCAS]_{crit}^2}$  and  $\alpha_{thres} = \sqrt{[GM]_{thres}^2 + [NaCAS]_{thres}^2}$ .**

Sugar conc. [wt%]	Sugar type	System 1		System 2		System 3		System 4	
		$1/\alpha_{crit}$	$1/\alpha_{thres}$	$1/\alpha_{crit}$	$1/\alpha_{thres}$	$1/\alpha_{crit}$	$1/\alpha_{thres}$	$1/\alpha_{crit}$	$1/\alpha_{thres}$
15	Sucrose	0.62	0.39	0.52	0.35	0.43	0.24	0.37	0.26
15	Trehalose	0.62	0.39	0.43	0.32	0.43	0.24	0.45	0.28
15	Glucose	0.52	0.37	0.49	0.33	0.44	0.26	0.48	0.28
15	Fructose	0.52	0.37	0.52	0.31	0.43	0.25	0.39	0.26
30	Sucrose	0.45	0.32	0.53	0.35	0.41	0.26	0.36	0.24
30	Trehalose	0.62	0.36	0.42	0.31	0.36	0.25	0.34	0.26
30	Glucose	0.47	0.38	0.50	0.31	0.37	0.27	0.32	0.22
30	Fructose	0.53	0.43	0.49	0.28	0.38	0.24	0.33	0.24

#### 4.5.4 Discussion

The presence of a sugar changes phase behaviour (i.e., the position of the binodal/ its asymmetry) by reducing the enthalpic interactions between the biopolymers through the changes in their  $M_w$  (size and drainage). Since the  $M_w$  play a direct role on the phase composition of the equilibrium phases—a higher  $M_w$  component will increase in concentration in its enriched phase—it is expected that the changes in the cosolubility are in turn accompanied by the changes in the  $M_w$  of the components. As the addition of sugar causes a dilution of the GM-rich phase and

concentration of the NaCAS-rich phase—shown by a decrease of STL in Tables 4–4 and 4–6 and an increase/decrease in  $\varphi_{LBG} / \varphi_{NaCAS}$  (volume fraction of the LBG-r/NaCAS-r phases) in Tables 6–8 and 6–11 (p. 6–219 and 6–227)—it can be concluded that cosolubility is changed by: a reduction of the size of GM or/and an increase in the size of NaCAS submicelles.

In relation to the  $M_w$ , polydispersity of the components also determines the cosolubility of the components—a low  $M_w$  portion of the same molecular species has a greater tendency to mix with the other species in the solution than a high  $M_w$  portion. A study by Belyakova et al. (2003) shows a reduction of the polydispersity in the presence of sugars, which could also be a contributing factor to the greater cosolubility of the studied systems.

The present study shows that at a constant concentration different sugars affect the cosolubility of NaCAS and GM by a different degree. The cosolubility, for example at 15 wt% sugar, is improved most in the presence of trehalose and fructose. As proposed by the literature this can be attributed to a direct and indirect influence of sugars on water, NaCAS and GM.

Fructose and trehalose—sugars with the highest hydration capacity<sup>23</sup>—are peculiar in the way they structure water and in the way in which the structuring effect is enhanced by the presence of solutes (Nikam et al. 2000; Savaroglu and Ozdemir, 2008).

---

<sup>23</sup> The hydration of a sugar depends on their molecular structure (i.e., "the position of OH(4) in conjunction with its nearest neighbour"), which determines how well they fit to the three dimensional structure of water (Galema and Hoeiland, 1990).

A separate study of Magazù et al. (2004), comparing trehalose and sucrose aqueous solutions, also shows that trehalose affects the solubility of the biopolymers by reacting in a peculiar way with water molecules. Although sucrose also reacts with water in a similar way to trehalose, a higher order and more rigid structure (higher number of hydrogen bonds) is observed in the trehalose solution. Due to its structuring effect, trehalose in solution hinders the water diffusive processes (Magazù et al., 2004), which—as demonstrated in this work—shows in changed phase behaviour.

Furthermore, studies of the effect of sugars on various proteins and galactomannans give a further insight in the mechanisms by which sugars control the phase behaviour.

Antipova and Semenova (1997a) study the effect of sucrose and glucose on proteins and conclude that sucrose causes a greater increase in hydrophilicity of 11S-globulin than glucose. They claim that sugars influence proteins either directly, by the formation of multiple hydrogen bonds between carboxyl groups on the protein, and indirectly, by the formation of the bonds between hydroxyl groups of sucrose and water. A greater cosolubility of NaCAS and GM in the presence of sucrose, compared to glucose, was also observed in the present study. As for the fructose, many medical studies conclude that fructose easily reacts with proteins (Raza and Harding, 1991).

Ptaszek et al. (2007) study the effect of sugar type on GG and observe an increase in the relaxation spectra of in the following order: GG-fructose < pure GG < GG-glucose < GG-glucose + fructose < GG-sucrose. This implies that both glucose and

sucrose make the structure of GG more unified, and that molecules can freely move in the solution, as opposed to when fructose is present in the mix. They propose that fructose delays the relaxation process of GG molecules through the formation of entanglements in the GG network.

The present study also observes a difference between sugar types at 30 wt% sugar concentration. At this concentration, monosaccharides increase the cosolubility of NaCAS and GM to a greater extent than disaccharides. The change in the trend by which the position of the binodals is classified: (i) at 15 wt% and (ii) at 30 wt% sugar, is likely related to a difference in the concentration effects between individual sugars. An existence of a difference in the thermodynamic activity of the proteins (i.e., 11S globulin, pH 7, 25°C) related to a difference in its sugar type and its concentration was previously reported for sucrose and glucose in the concentration range up to  $25 \times 10^{-2}$  g/ml (Antipova and Semenova, 1997a). In this range, larger concentration dependence was observed for sucrose (disaccharide) than glucose (monosaccharide), hence it is not unlikely that at higher concentrations sucrose would peak before glucose, hence the inverse effect of disaccharide on thermodynamic activity of the protein would be observed sooner than that of monosaccharide. This is especially plausible if it is assumed that the concentration effect is enhanced in the presence of other molecules (i.e., GM) in the solution (Magazù et al., 2004).

As for the individual sugars: among disaccharides, a 15 wt% increment in trehalose concentration affects the cosolubility of the systems least. Among monosaccharides, the increment in fructose concentration affects the cosolubility less

than the same increment in glucose concentration. The difference can be explained by different way sugars structure water—by a number of hydrogen bonds formed with water, which is determined by a number of available molecules and/or OH-groups. For example, the 15 wt% reduction in the amount of water ( $M_w=18.02$  g/mol), and a corresponding 15 wt% increase in the number of disaccharides ( $M_w=342.3$  g/mol) or monosaccharides ( $M_w=180.16$  g/mol) causes a significant depletion in the number of water molecules, on one hand, and a significant increase in the number of sugar molecules, on the other hand. It is therefore plausible to think that sugar molecules with a greater capability of binding water sense the effect of depletion significantly more.

#### 4.6 Conclusion

The present study of the effect of: the galactomannan type (LBG, TG, GG, and FG), sugar type (sucrose, trehalose, glucose and fructose) and sugar/sucrose concentration (0–60 wt%) on the phase equilibria of NaCAS-GM APTS, shows at pH 5.8 and temperature of 20°C low cosolubility of its macromolecular components. At sufficiently high macromolecular concentrations—and as previously observed for systems of non interacting random coil biopolymers like the ones studied here—all the investigated systems phase separate into pairs of equilibrium phases. Interactions of the biopolymers with the solvent have a considerable effect on the phase equilibria. Separating the contributions of the interactions of each of the biopolymers with the solvent/sugar is very complicated.

By establishing phase diagrams/binodals, slopes of the tie-lines (STL) and characteristic theoretical points for various APTS, the following conclusions were made.

It has been found that: (i) the cosolubility of the system improves, depending on the type of the GM contained, as follows:  $LBG < TG < GG < FG$ , (ii) the presence of sugar either increases or decreases the cosolubility of the components depending on its concentration (when present  $< 30/40$  wt%, for sucrose/other sugars, the cosolubility increases, and—as shown on the example of the systems containing LBG/GG and sucrose— $> 50$  wt% sucrose the cosolubility of the components decreases, possibly below that determined for the reference system without sugar), (iii) systems, at 15 wt% sugar follow the trend:  $sucrose < glucose < trehalose < fructose$ , and that (iv) systems, at 30 wt% follow a different trend:  $trehalose \approx sucrose < fructose \approx glucose$ . A decrease in STL, at sugar concentrations  $< 30$  wt% was also observed for all investigated systems. STL were used to quantify the asymmetry of the phase diagrams and to assess the way the biopolymers partition between the equilibrium phases.

Although the above results are in good agreement with the available literature on the phase behaviour of similar ATPS and the performance of the individual components of these ATPS, the results bear with it a certain level of experimental uncertainty. The uncertainty could be minimised by reducing the error made within each step of the method used to establish the phase diagrams. This could be done by: (i) measuring and not assuming the densities required to calculate volume fractions of the equilibrium phases and (ii) increasing the number of samples at each of the extremes, which would give a greater confidence to the fits involved in the acquisition of the equilibrium concentrations. It may also be worthwhile to look at other method by which phase diagrams could be established.

# CHAPTER 5: RHEOLOGY AND MICROSTRUCTURE OF THE SODIUM CASEINATE - GALACTOMANNAN - SUGAR AQUEOUS TWO - PHASE SYSTEMS

## 5.1 Introduction

This chapter investigates the flow behaviour of four NaCAS-GM systems: NaCAS-LBG is System 1, NaCAS-TG is System 2, NaCAS-GG is System 3, and NaCAS-FG is System 4. The relationship between the apparent viscosity and microstructure of the systems is assessed with the help of the phase diagrams established in the previous chapter, and by preparing blends composed of various ratios of the equilibrium phases (i.e., NaCAS-rich and GM-rich).

The chapter is divided into five parts. The first introduces the investigated systems, namely equilibrium phases and their blends. The second part reviews their quiescent microstructure by means of optical observation, the third studies the flow of the systems of various microstructures, the fourth explains the observed flow behaviour by additional tests of microstructure evolution under shear, and of the effects of: blend preparation, centrifugation time, solvent type, GM type and temperatures. The fifth part is a short study on the viscoelasticity of the interfaces relevant to this study.

## 5.2 Investigated systems

The microstructure investigation and viscometry are carried on the equilibrium phases and blends of ATPS shown in Table 5-1.

**Table 5-1. Aqueous two-phase systems (ATPS) from which equilibrium phases were harvested and blends were prepared. NaCAS=sodium caseinate; GM=galactomannan; LBG=locust bean gum; TG=tara gum; GG=guar gum; FG=fenugreek gum; r=rich.**

ATPS code	NaCAS [wt%]	GM [wt%]	Sugar [wt%]	Equilibrium phase
<i>1</i>	2	0.25 LBG	0	LBG-r NaCAS-r
<i>2</i>	3	0.2 LBG	0	LBG-r NaCAS-r
<i>3</i>	4	0.2 LBG	0	LBG-r NaCAS-r
<i>4</i>	4	0.6 LBG	0	LBG-r NaCAS-r
<i>5</i>	5	0.15 LBG	0	LBG-r NaCAS-r
<i>6</i>	5	0.2 LBG	0	LBG-r NaCAS-r
<i>7</i>	6	0.2 LBG	0	LBG-r NaCAS-r
<i>8</i>	4	0.6 LBG	5 sucrose	LBG-r NaCAS-r
<i>9</i>	4	0.6 LBG	15 sucrose	LBG-r NaCAS-r
<i>10</i>	4	0.6 GG	15 sucrose	GG-r NaCAS-r
<i>11</i>	4	0.6 LBG	20 sucrose	LBG-r NaCAS-r
<i>12</i>	4	0.6 LBG	40 sucrose	LBG-r NaCAS-r
<i>13</i>	4	0.6 GG	50 sucrose	GG-r NaCAS-r
<i>14</i>	4	0.2 LBG	15 sucrose	LBG-r NaCAS-r
<i>15</i>	4	0.2 LBG	15 trehalose	LBG-r NaCAS-r
<i>16</i>	4	0.2 LBG	15 fructose	LBG-r NaCAS-r
<i>17</i>	4	0.2 LBG	15 glucose	LBG-r NaCAS-r
<i>18</i>	4	0.2 TG	0	TG-r NaCAS-r
<i>19</i>	4	0.2 GG	0	GG-r NaCAS-r
<i>20</i>	4	0.2 FG	0	FG-r NaCAS-r
<i>21</i>	4	0.6 GG	0	GG-r NaCAS-r

A common trait of the systems is that they all, as previously shown in § 4.2.1

(p. 4–110), phase separate into GM-r (less dense, top) and NaCAS-r (more dense, bottom) equilibrium phases. A special attention is paid to the effects of the following parameters: biopolymer concentrations (ATPS 1–7), sugar concentration (sucrose, ATPS 8–11), sugar type (ATPS 12–15), GM type (ATPS 3, 16–18), preparation, impurities, preshear and temperature (ATPS 4) on the flow and the microstructure of ATPS.

### 5.3 Quiescent microstructure

The quiescent microstructures of all systems in Table 5–1 was examined in the optical microscope. System 4, 8–13 and 21, from Table 5–1, were also stained and visualised in the confocal laser microscope, which made possible the determination of the exact location of the separated phases.

A tie-line experiment is performed to investigate the effect of a phase volume fraction on the microstructure of the ATPS. The experiment involves a preparation of primary/starting systems, the concentrations of which are shown in Table 5–1. From these systems pairs of the equilibrium phases are harvested. They are subsequently mixed together in desired volume/mass ratios (see § 3.3.2.1, p. 3–92), and visualised (see § 3.3.2.2, p. 3–95). The blends were composed typically of 5, 25, 50, 75, and 95 wt% GM-r phase added to NaCAS-r phase. The total composition of every equilibrium phase pair amounted to 100%. The individual equilibrium phases blended in that way had the same compositions and differed only in the volume fraction. Because the position of the tie-line can change with starting composition of the primary ATPS preparing a range of different starting concentrations is not recommendable. This is especially true for

polydisperse systems, which are prone to phase separate into phases of different concentrations (Frith, 2010).

### 5.3.1 Individual equilibrium phases

Although the individual equilibrium phases<sup>24</sup> to the naked eye appear homogeneous they are in fact heterogeneous W/W emulsions (Figure 5–1), where one phase adopts a role of a dispersed phase and the other the role of its surrounding matrix or a continuous phase.

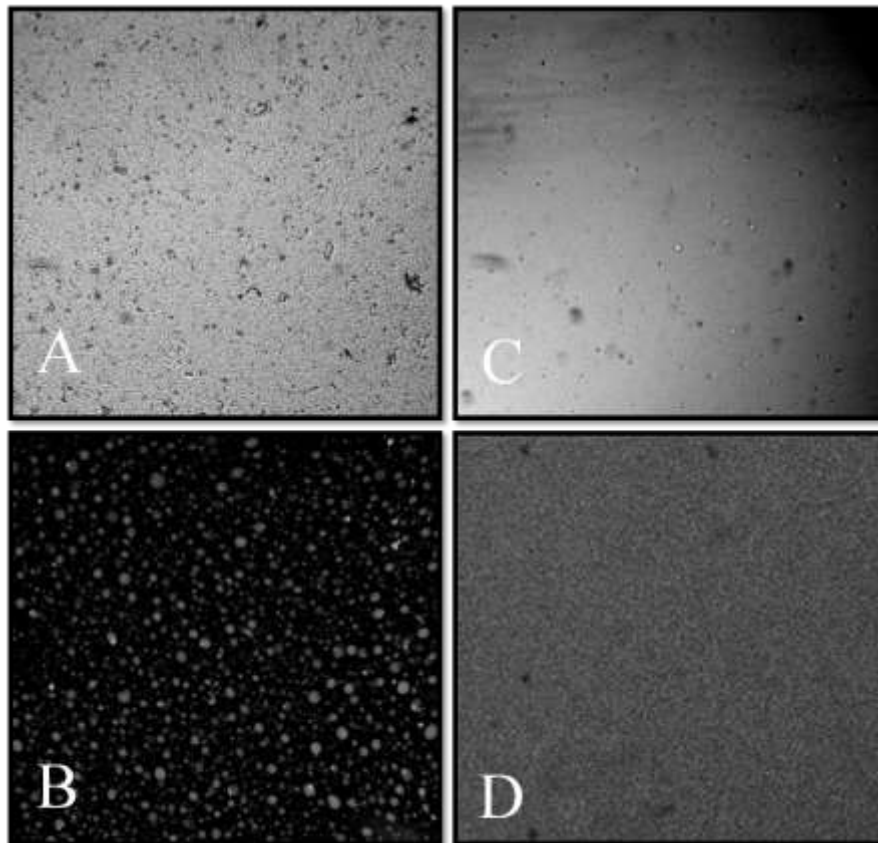


**Figure 5–1.** (A, B) Locust bean gum/LBG-rich and (C, D) sodium caseinate/NaCAS-rich equilibrium phases obtained from 3 wt% NaCAS-0.2 wt% LBG ATPS at 20°C. The width of the light micrographs A and C is 1.3 mm. The width of the confocal micrographs B and D is 0.375 mm. The radius of droplets in micrograph B is < 5  $\mu\text{m}$ .

<sup>24</sup> The equilibrium phases of ATPS are always composed of both biopolymers. Their concentrations can be read from a phase diagram, specifically from the points of contact between a tie-line and a binodal.

It is impossible to separate the equilibrium phases completely. The amount of, for example, NaCAS in GM-rich equilibrium phase depends on many factors, such as: (i) temperature, (ii) physical properties, e.g., GM type, composition, interfacial tension and viscosities, and (iii) physical separation techniques used, e.g., centrifugation and the way the phases are harvested. Experimental work shows that systems of high total biopolymer concentrations form most structured phases that are tedious to phase separate. Furthermore, highly branched galactomannans, such as GG and FG, produce in appearance less structured/less-viscous GM-r equilibrium phases as opposed to weakly gelling, less branched LBG and TG of a higher molecular drainage.

### **5.3.2 Blends**

#### **5.3.2.1 Without sugar**

Similarly to the equilibrium phases that are mentioned in the previous section, blends too are emulsions. For example, GM-r and NaCAS-r equilibrium phases behave much like conventional O/W emulsions, where after mixing one phase adopts the role of a dispersed phase and the other that of the continuous/matrix phase. At low shear and in quiescent conditions, the phase present in a lower volume fraction is dispersed and the phase with a higher volume fraction is continuous. This is true for all GM types. Hence only micrographs of System 1 without sugar are shown in Figure 5–2, Figure 5–3, and Figure 5–4 as an example for all investigated systems.

Figure 5–2 shows a significant change in the microstructure, accompanied by

progressively increasing the volume fraction of the GM-r phase ( $\varphi_{GM}$ , marked black) added to correspondingly decreasing volume of the NaCAS-r equilibrium phase. More specifically, the addition of GM-r phase  $< 50\%$  results in the formation of protein-continuous systems, where an increase in  $\varphi_{GM}$  decreases the size and increases the number of GM-r-droplets and their polydispersity. The addition of GM-r phase  $> 50\%$ , however, causes the GM-r phase to be present in the highest volume fraction and the system to phase invert (micrographs showing a phase inversion are squared).

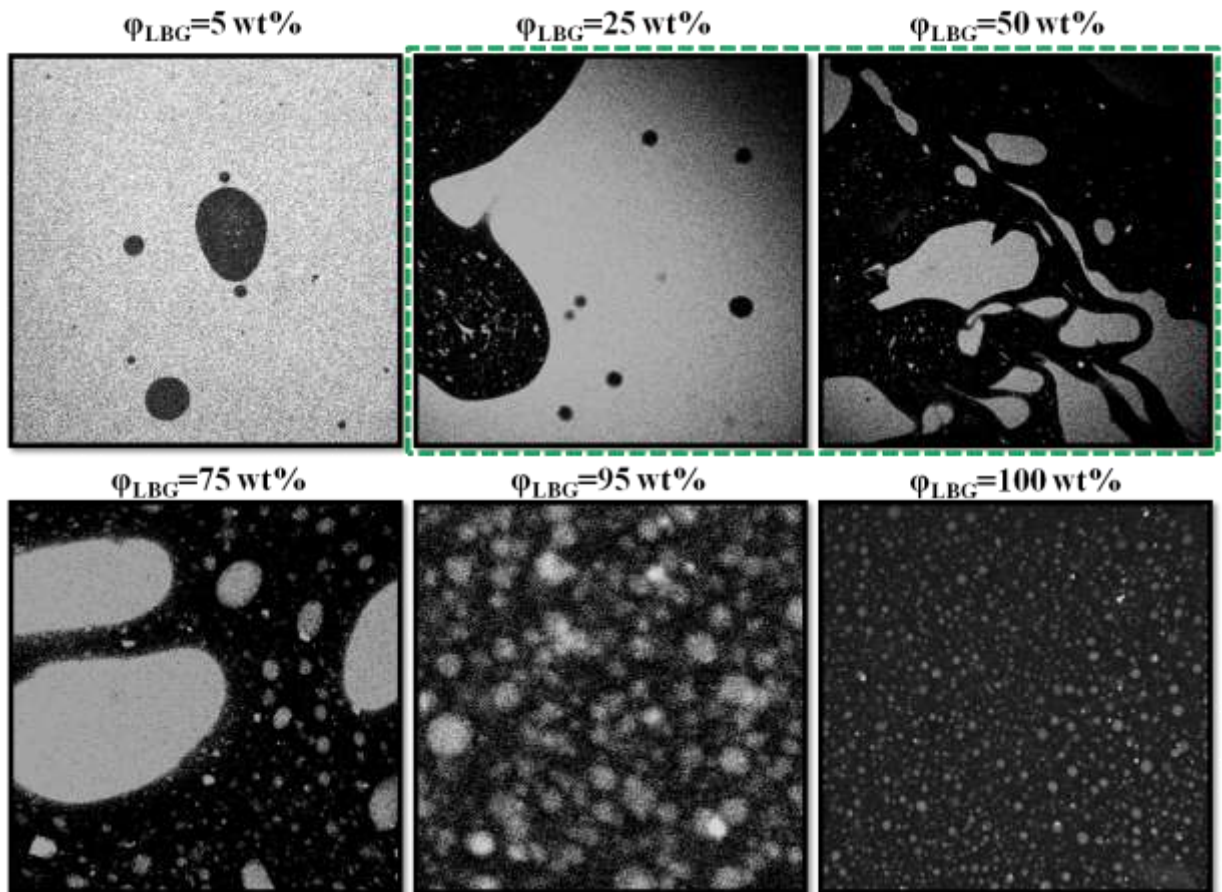


**Figure 5–2.** Confocal micrographs for ATPS 4 (4 wt% NaCAS-0.6 wt% LBG without sugar) at different phase volumes of the LBG-rich phase ( $\varphi_{LBG}$ ) and at quiescent conditions. NaCAS-rich phase is stained and is the lighter phase. Green square marks the bi-continuous systems. The micrographs are 1.5 mm wide.

The phase inversion event occurs over a wide range of the volume fractions. The

micrographs show bi-continuity region between the volume fractions of 25 and 75%. Bi-continuity in W/W emulsions is not a newly discovered phenomenon and has already been reported (Wolf et al., 2000; Pacek et al., 2001; Spyropoulos et al., 2008). At this volume fractions the determination of the continuous and dispersed phases is, due to the similarity of the refractive indices in the absence of staining, virtually impossible.

Figure 5-3 shows 3D micrographs of three distinct microstructures: (i) protein-r-continuous ( $\varphi_{GM} < 25\%$ ), (ii) bi-continuous, where large parts of the system are either protein-r-continuous or polysaccharide-r-continuous microstructure ( $25\% < \varphi_{GM} < 75\%$ ), and (iii) polysaccharide-r-continuous ( $\varphi_{GM} > 75\%$ ).

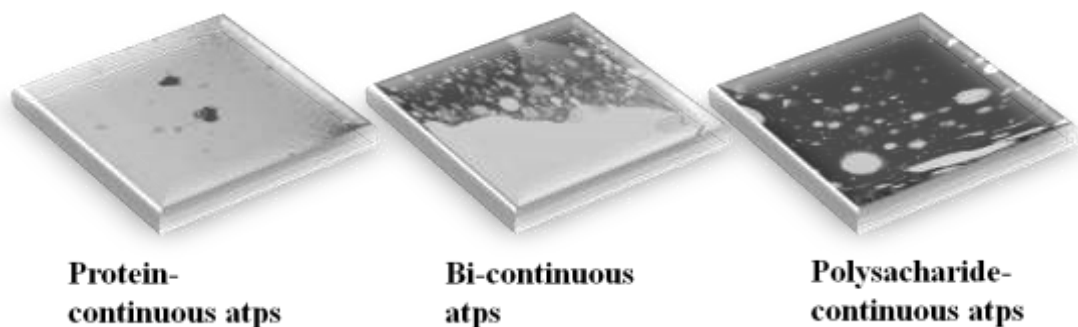


**Figure 5-3.** 3D confocal micrographs for ATPS 4 show three distinct microstructures. The width of the micrographs is 0.882 mm and their depth is 165  $\mu\text{m}$ . Cross sections were scanned in 1.3  $\mu\text{m}$  steps.

As already reported in § 4.2.1 (p. 4-110), W/W emulsions are highly unstable with time, and hence show signs of phase separation minutes after their preparation (Figure 5-4). Moreover, a smaller viscosity of the continuous phase accounts for a greater instability of blends. This is seen from a comparison of confocal images in Figure 5-5 in the next section, where smaller and less polydisperse droplets are observed towards the right bottom side of the group of images.

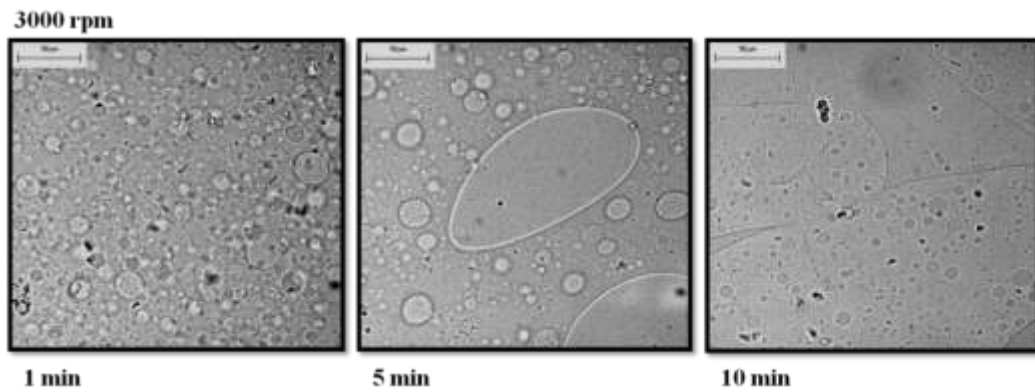


Figure 5–4. Light micrographs illustrate the instability of blends prepared from 4 wt% sodium caseinate-0.6 wt% locust bean gum ATPS with  $\phi_{\text{LBG}}=95\%$  mixed with Silverson (3 min and 3000 rpm).

### 5.3.2.2 With sugar

While no difference in the overall microstructure and phase inversion region is observed between the systems containing different sugar types, a slight change in the droplet size is evident for the systems containing various amounts of sugar. In Figure 5–5 this is shown on the example of System 1 with sucrose.

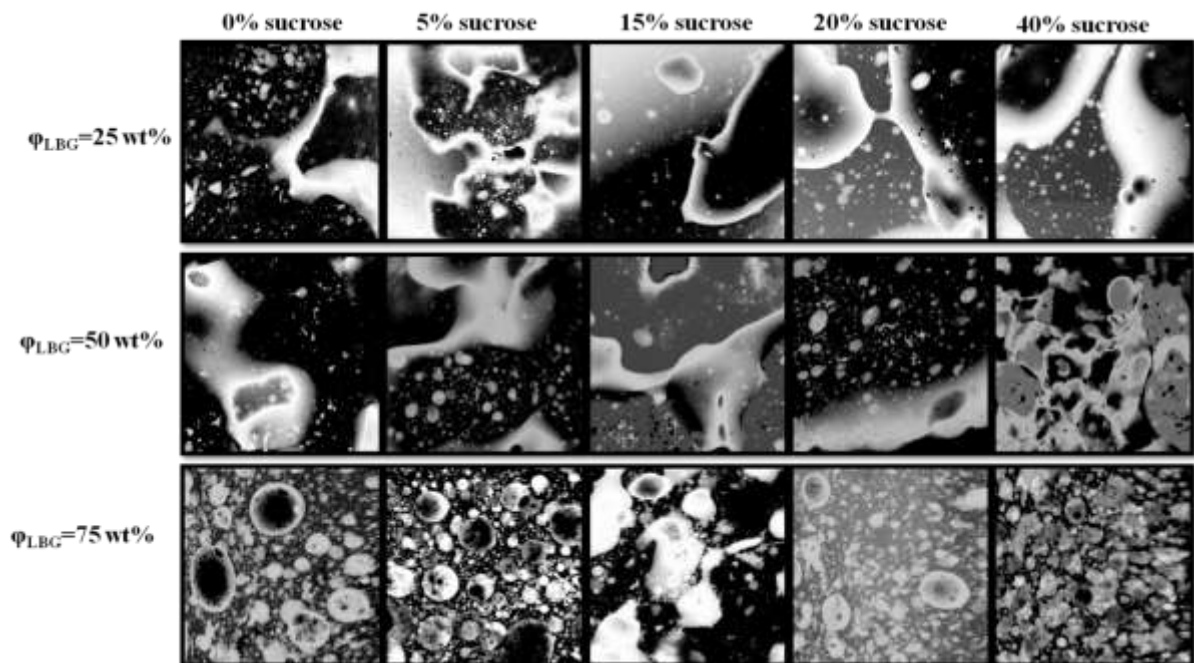
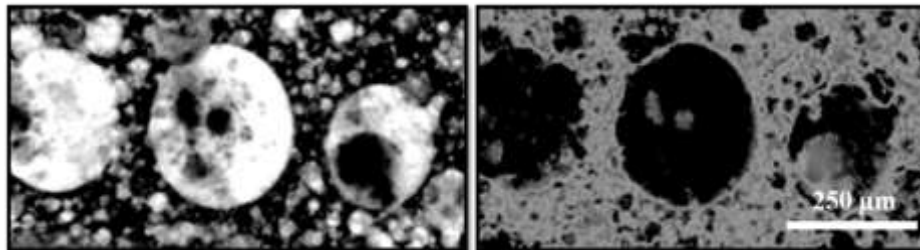


Figure 5–5. Confocal micrographs (sum of 130 scans) of 1.5 mm width for ATPS “4” (4 wt% NaCAS-0.6 wt% LBG with and without sugar) at different phase volumes of the LBG-rich phase ( $\phi_{\text{LBG}}$ ) and at quiescent conditions. NaCAS-rich phase is the lighter phase.

In Figure 5–5 the first and second row of micrographs shows protein-continuous systems, which are unstable with time to a similar degree. Certain parts within the micrographs, however, already show signs of bi-continuity (e.g., micrograph 5 in the second row shows it most clearly). In the third row of the micrographs, greater droplet stability is observed in all polysaccharide-continuous systems. Furthermore, among the latter micrographs a stabilising effect of sucrose on the morphology of the blends also becomes more pronounced. In the presence of > 5% of sucrose the formation of smaller and less polydisperse droplets<sup>25</sup> is observed. The effect is most evident in the systems with 5 and 40% of sucrose. A support to this observation is found in a study by Kiselev et al. (2003), who review the effect of 0–60 wt% sucrose on the stability of unilamellar and multilamellar dimyristoylphosphatidylcholine vesicles, which could be in a broad sense compared to NaCAS-r droplets. The authors report the highest stability for 5-10 wt% of sucrose and minimum polydispersity for 20 wt% sucrose concentrations.



**Figure 5–6. Confocal micrographs of ATPS 8. On left NaCAS-rich phase is shown as lighter. On the right micrograph the marking is inverted.**

Figure 5–6 shows bi-continuity inside larger droplets of a dispersed phase, observed at  $\varphi_{GM} > 75\%$ . Although the latter systems are named polysaccharide-continuous it seems that phase separation perpetuates itself on a smaller scale continuously and as a result produces multiple W/W emulsions. This probably means

<sup>25</sup> The degree of polydispersity within the systems was assessed visually. It was not calculated.

that the system is trying to reach a new equilibrium, the equilibrium prior to the one established by mixing of the equilibrium phases into a blend.

## 5.4 Flow behaviour of the individual equilibrium phases and blends

### 5.4.1 Without sugar

This section reviews the effect of microstructure on flow of the investigated systems: equilibrium phases and blends. The experiment is based on the observations made in the previous section. Systems of different microstructures were subjected to shear and their response is discussed below. The ATPS were exposed to a wide range of shear rates, associated with: (i) the process of levelling and draining ( $< 1 \text{ s}^{-1}$ ), (ii) extruding and chewing ( $1\text{--}100 \text{ s}^{-1}$ ), and (iii) mixing pumping and brushing ( $1000 \text{ s}^{-1}$ ).

The effect of the microstructure on flow of System 1 and System 3 without sugar is studied for the equilibrium phases and blends. The flow curves of these systems are shown in Figure 5–7 a and b, respectively. For both systems the behaviour of the blends is very similar. An increase in the volume fraction of GM-r phase ( $\varphi_{GM}$ ) from 0 wt% (pure NaCAS-r phase) to 75 (System 3) or 95 wt% (System 1), results in (i) an increase in the overall viscosity of the blend (ii) a slight change of the degree of Newtonian behaviour, and in systems with  $\varphi_{GM} > 25 \text{ wt}\%$  (iii) a complex flow behaviour—shear thickening peaks marked with arrows in Figure 5–7.

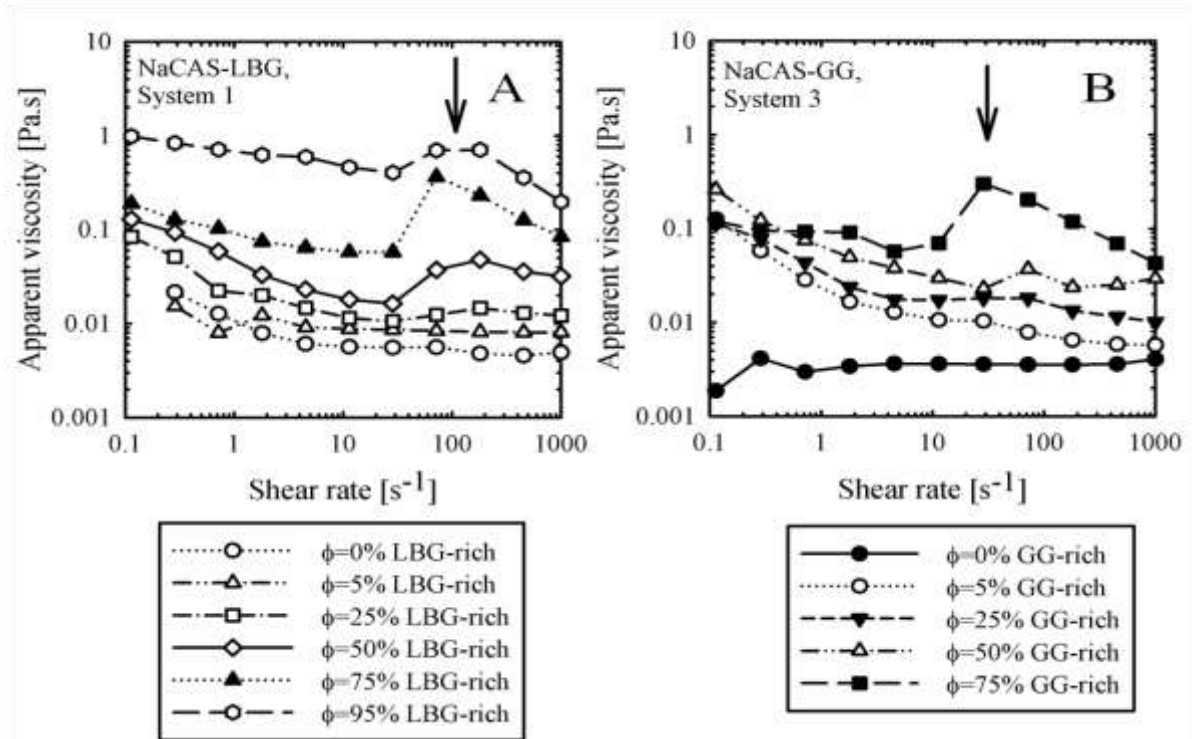


**Figure 5–7.** Ascending flow curves of blends for (A) System 1 and (B) System 3 in the absence of sugar and as the volume fraction of the galactomannan-rich phase ( $\phi = \varphi_{GM}$ , LBG-rich, GG-rich) is progressively increased from 0% (“pure” protein-rich phase) to 95% (System 1) or 75% (System 3).

The shear-thickening peaks occur at the shear rate of  $\sim 100 \text{ s}^{-1}$ . The systems have been measured several times and the peaks were observed each time. When the same system was sheared back and forth (i.e.,  $0.01\text{--}1000\text{--}0.01 \text{ s}^{-1}$ , Figure 5–8) the peaks moved to a lower shear rate. An attempt was made to determine the exact shear rate where the shear thickening occurred, but no clear pattern emerged between the repeats. This was attributed to a significant time and shear instability of the blends, i.e., to the effect of premixing on the blends, which was—as mentioned in § 3.3.2.3, p. 3–95—done by hand and could be hence a potential source of error. It was, however, consistently observed that the highest peak belongs to ATPS with the highest  $\varphi_{GM}$ . An investigations into possible causes for the observed peaks, such as: (i) the flow characteristics of pure

biopolymers, (ii) the effects of blend preparation, (iii) the development of new microstructures under shear and (iv) the effects of composition and temperature, are given later in § 5.5.

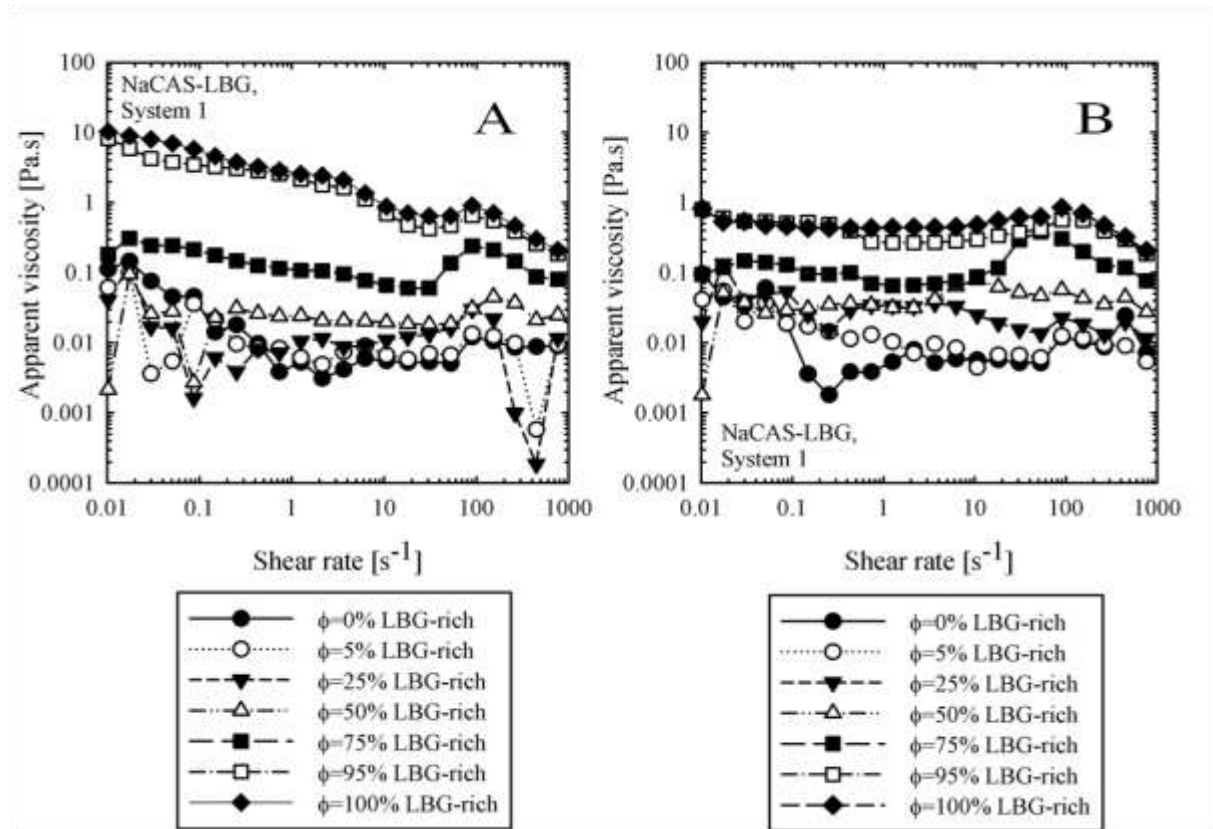


**Figure 5–8. (A) Ascending and (B) descending flow curves of the equilibrium phases and blends for System 1 (4 wt% NaCAS-0.6 wt% LBG) as the volume fractions are progressively increased from 0 (“pure” protein-rich phase) to 100% (“pure” galactomannan-rich phase).**

The systems were also investigated on the effects of preshear. Figure 5–9 shows that presheared systems retain a great deal of structure, which is reduced when ATPS are exposed to more than two shear rate cycles. As already shown in Figure 5–8 and again in Figure 5–9, upon a decrease in the shear rate the peaks consistently shift toward lower shear rates. Since the system and the shear regime remain the same the change is likely related to the time-dependant changes in the structure of these systems.

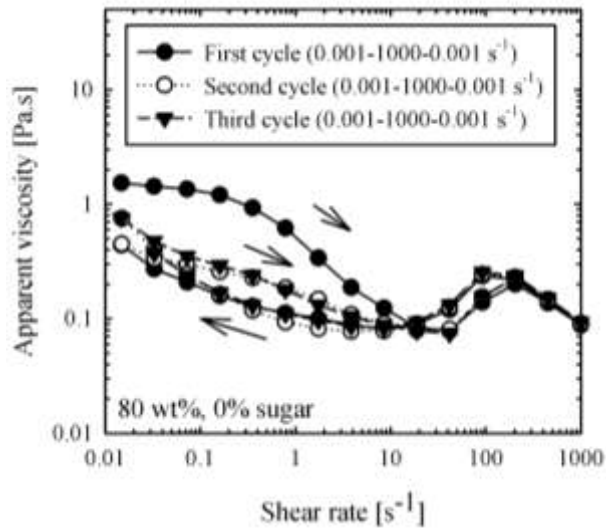


**Figure 5–9.** The effect of shear cycles on ATPS 3 ( $\varphi_{GM}$  =80 wt% blend of 4 wt%NaCAS-0.2 wt% LBG).

#### 5.4.2 With sugar

Figure 5–10 shows flow behaviour of the equilibrium phases and blends at increasing sugar concentration. System 1 with 5, 15, 20 and 40% of sucrose is used as an example and to study the phenomena. The pairs of the equilibrium phases of ATPS 4 (4 wt% NaCAS-0.6 wt% LBG) were used in preparation of the blends of various volume fractions ( $5 \text{ wt\%} < \varphi_{GM} < 95 \text{ wt\%}$ ).

Based on the flow behaviour of these systems it is found that increasing both sugar concentration and  $\varphi_{GM}$  increases the apparent viscosity ( $\eta$ ) and the degree of non-Newtonian behaviour of the equilibrium phases and blends. Furthermore, dependence between the complex flow behaviour and sugar concentration is observed. Shear thickening peaks, similar to those observed in blends without sugar, are observed for GM-r-continuous blends  $< 20 \text{ wt\%}$  of sugar at about the same shear rate as for blends without sugar,  $\sim 100 \text{ s}^{-1}$ . The increase of the sugar content in blends  $> 20 \text{ wt\%}$

(graphs D in Figure 5–10) eliminates the viscosity peaks.

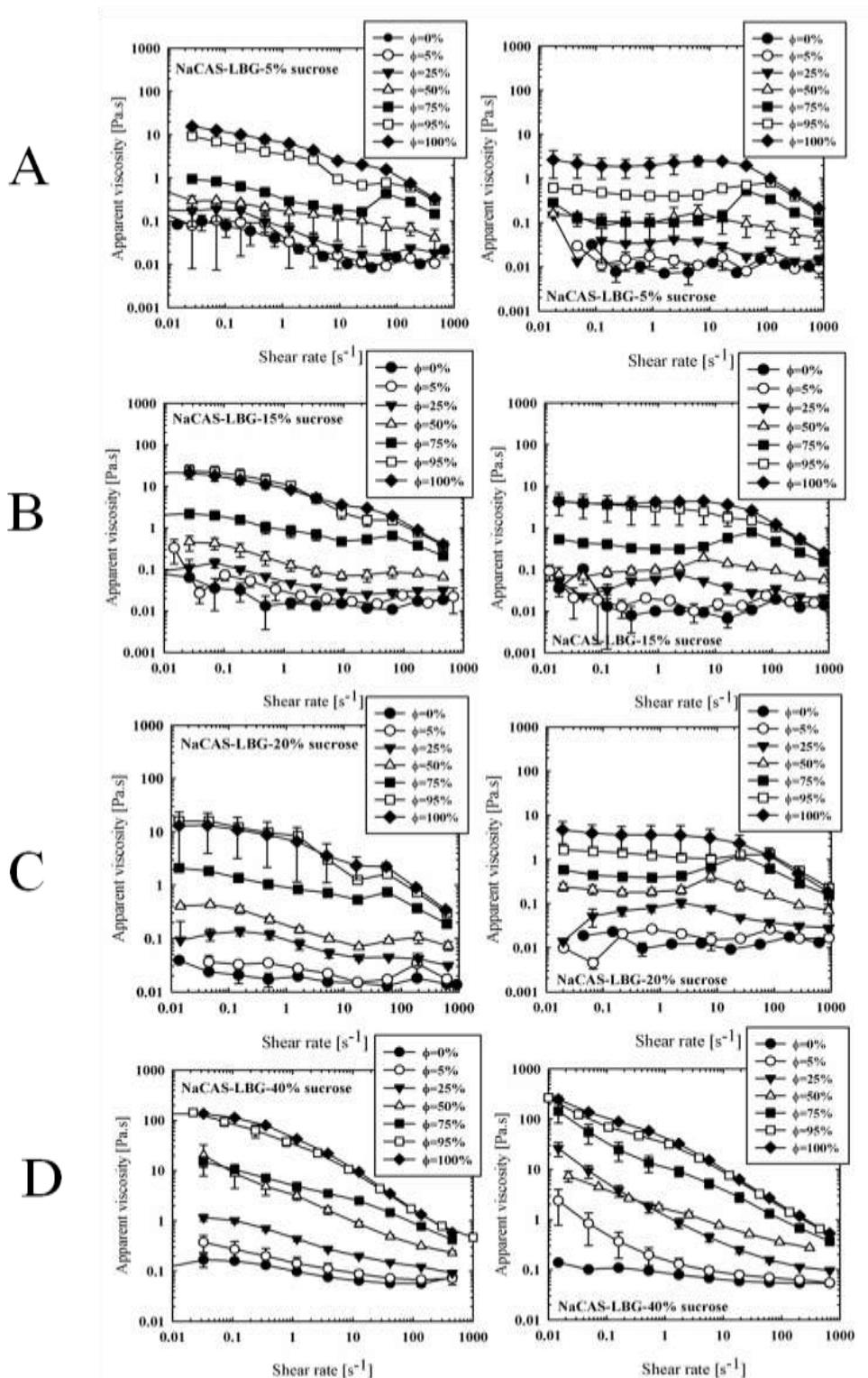


**Figure 5–10.** Ascending (left) and descending (right) flow curves of the equilibrium phases and blends for System 1 (NaCAS-LBG system) at (A) 5, (B) 15, (C) 20, and (D) 40 wt% of sucrose, and as the volume fractions of the LBG-rich phase is progressively increased from 0 (“pure” protein-rich phase) to 100% (“pure” galactomannan-rich phase).

## 5.5 Complex flow behaviour in polysaccharide-continuous blends

This section describes the experiments that were formulated with the aim of explaining the complex flow behaviour (i.e., "peaks") that were observed previously. The ingredients used in the formulation of ATPS (equilibrium phases and blends) and the procedures by which they were prepared are reviewed in the following two subsections.

### 5.5.1 Flow of pure biopolymer solutions and solvents

The section investigates the flow behaviour of solvents, pure protein and pure polysaccharide aqueous solutions that were used to prepare ATPS. The pure components are investigated because they may cause the complex behaviour observed in blends. The aqueous solutions of NaCAS, GM and buffer with and without sugar are tested in the shear rate range of 0.1–1000 s<sup>-1</sup> and the raw data is given in Figures 5–11 and 5–12.

Figure 5–11 shows flow curves of NaCAS at various sucrose concentrations. Although a large difference between NaCAS solutions at < 15% sucrose and at > 30% of sucrose is observed, the flow behaviour of NaCAS solutions is Newtonian.

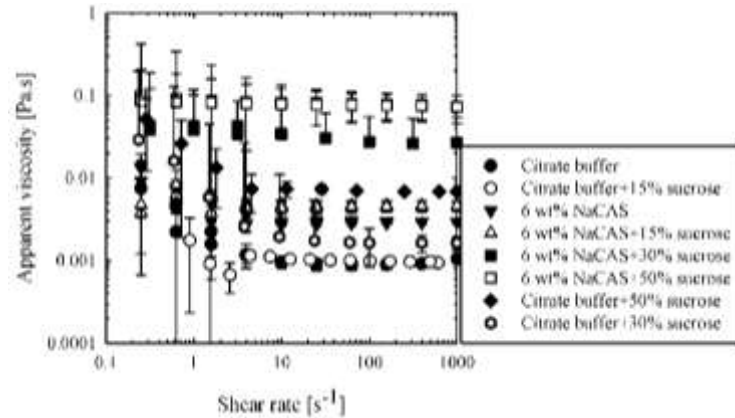


Figure 5–11. Flow curves of the sodium caseinate solutions with various amounts of sucrose.

Similarly, the flow curves in Figure 5–12 confirm (i) the Newtonian behaviour of GM-solutions below  $c^*$  (Figure 5–12 a), and (ii) the non-Newtonian shear-thinning behaviour of the solutions above  $c^*$ , regardless of the type of the GM in the solution (Figure 5–12 a and b).

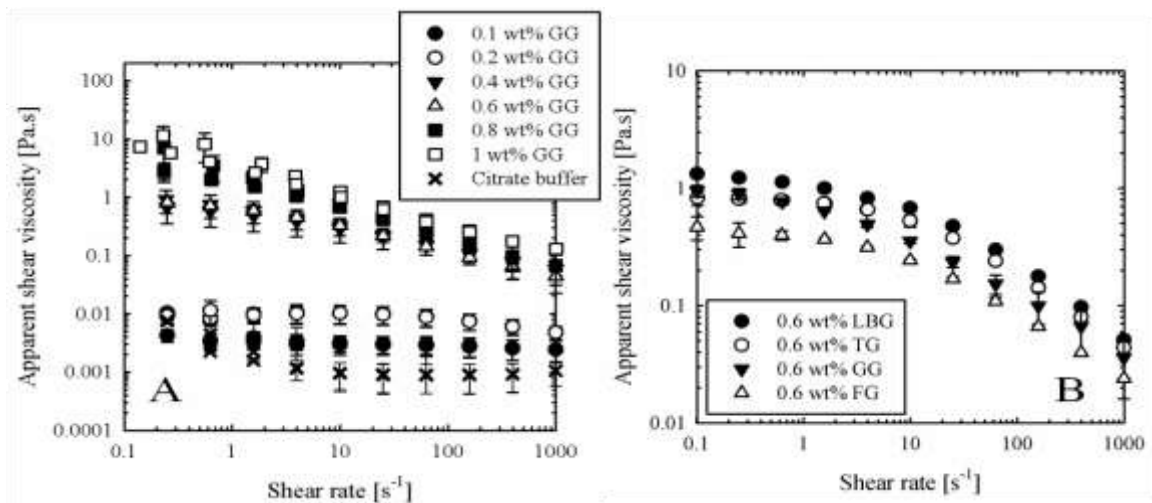


Figure 5–12. Flow curves for (A) various concentrations of guar gum and for (B) various types of galactomannans in the absence of sugar.

In comparison to each other, the individual equilibrium phases that belong to the same ATPS show very different flow behaviours. Less dense polysaccharide-rich phase has a higher overall viscosity and shows shear thinning non-Newtonian behaviour at

concentrations  $< c^*$  as opposed to more dense and less viscous Newtonian protein-rich phase.

Since none of the investigated pure solutions displayed the complex flow behaviour, as first shown in Figure 5-7, the attention is then turned to the preparation procedure.

### **5.5.2 Effect of blend preparation on flow of the equilibrium phases and blends**

The preparation procedure is examined by two tests. The first test studies the effect of centrifugation on flow. And the second test studies the way blends are prepared; blends are prepared from scratch and not from a primary ATPS as before. The results obtained from the experiments are shown in the following two subsections.

#### **5.5.2.1 *Centrifugation affects flow properties of the individual equilibrium phases and their blends***

The centrifugation effects are tested in two ways. First, GM-solution (used in preparation of the ATPS) is centrifuged to remove any insoluble residues (as described in Schorsch et al., 1999b). No difference in the flow behaviour is observed between the centrifuged and non-centrifuged solutions. And second, the equilibrium phases are centrifuged for various lengths. The flow curves of the latter test are given in Figure 5-13 and are explained below.

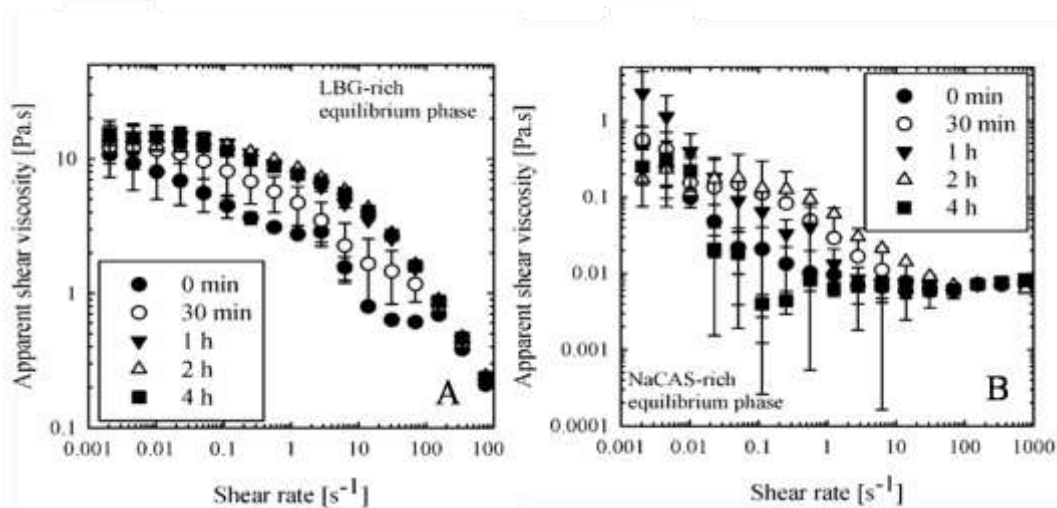


**Figure 5–13.** Flow curves of (A) locust bean gum-rich (LBG-rich) and of (B) sodium caseinate-rich (NaCAS-rich) equilibrium phases for 4 wt% NaCAS-0.6 wt% LBG systems after centrifugation at 4000 RPM and 20°C.

It is observed that regardless of how much care is taken in the separation of the equilibrium phases, the flow behaviour of non-centrifuged polysaccharide-rich phase (Figure 5–13 a) shows a degree of shear-thickening/complex flow behaviour at characteristic shear rates of  $\sim 100 \text{ s}^{-1}$ . Based on these results it is concluded that a multicomponent structure is a likely cause for the complex flow behaviour. Furthermore, it is also shown that centrifugation is required to obtain sufficiently pure equilibrium phases for the preparation of blends. While the centrifugation affects the flow behaviour of the polysaccharide-rich phase, (Figure 5–13 a) it does not affect the flow behaviour of the protein-rich phase (Figure 5–13 b). As GM-rich/top phase is more prone to be “contaminated” with the NaCAS-rich/bottom phase it is no surprise that it is also most affected by the centrifugation time. Longer centrifugation time slightly increases the viscosity of the GM-rich phase and eliminates the complex flow behaviour of these systems.

Figure 5–14 shows the flow behaviour of the presheared polysaccharide-rich

phases centrifuged for different periods. In comparison with the flow curves in Figure 5–13 a, the preshear affects most the uncentrifuged and 30 min centrifuged GM-rich phases and much less purer GM-rich phases (centrifuged for  $\geq 1$  hour). It is hence observed that the presence of a greater volume fraction of NaCAS-rich phase ( $\varphi_{\text{NaCAS}}$ ) increases the sensitivity of the equilibrium phases to preshear, a point to keep in mind when shear is applied to blends.

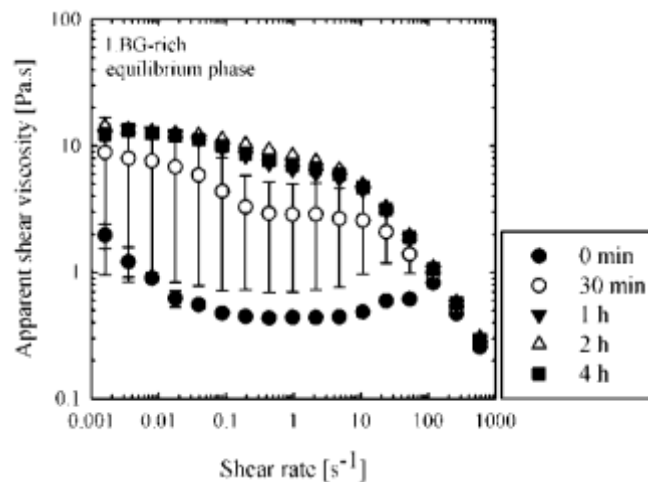


**Figure 5–14.** Flow curves of LBG-rich phases that were centrifuged for various periods and presheared to  $1000 \text{ s}^{-1}$ .

When the centrifuged equilibrium phases are used to prepare blends, similar flow behaviour is observed (see right columns in Figures 5–15 and 5–16) to the one already shown in Figure 5–8 (without sugar), and Figure 5–10 (with sugar, i.e., sucrose).

### 5.5.2.2 *Direct preparation of blends on the same tie-line*

The second experiment is designed to test the procedure of blend preparation directly from powered ingredients and not by blending the equilibrium phases obtained from a primary ATPS as shown in § 5.4, p. 5–147. At the same time systems of various sucrose concentrations are also compared for their flow behaviour. The ATPS are

prepared by mixing NaCAS and GM in concentrations corresponding to the points on the same tie-line in a phase diagram. The ATPS concentrations were selected so that after phase separation the equilibrium phases gave the same volume fractions (25, 50 and 75 wt% of the polysaccharide-rich phase), much like the blends prepared by the procedure in which the equilibrium phases from a primary ATPS were blended together.

Figures 5-15 and 5-16 (on p. 5-159 and p. 5-160) compare the flow behaviour of the systems prepared by the two methods for ascending and descending shear rates, respectively. Although, the approach of preparing blends from solutions of various starting compositions is reported to give disparate results, when compared to the approach where blends are prepared from one starting composition (Frith, 2010), this study shows that both approaches exhibit very similar flow behaviour.

A detailed observation shows only small differences between differently prepared systems. The systems prepared by blending of the equilibrium phases of a single ATPS are slightly more viscous and show more structure than the systems prepared directly (i.e., shear thickening peaks are higher and are observed already for volume fraction of 25 wt%). The slight discrepancy between the systems is likely caused by either of the following two factors: (i) a different time allowed for the structuring within a system to occur before the viscosity is measured (i.e., the systems constructed from a primary ATPS of one starting composition are left undisturbed for ~ 24 hours, and the systems prepared from powders only for ~ 3 hours), and (ii) a different composition of the system pairs (i.e., the same systems prepared by different methods).

Two additional observations can be made from Figures 5-15 and 5-16. First and as observed earlier in the chapter, descending the shear rate moves the shear thickening peaks towards lower shear rates and makes the systems at shears  $< 100 \text{ s}^{-1}$  flow more like Newtonian liquids. Second, a difference in the flow behaviour is observed for systems with 40% of sucrose. The causes for this will be further addressed in § 5.5.3.2 on p. 5-164. Same behaviour is observed regardless of the preparation of the systems.

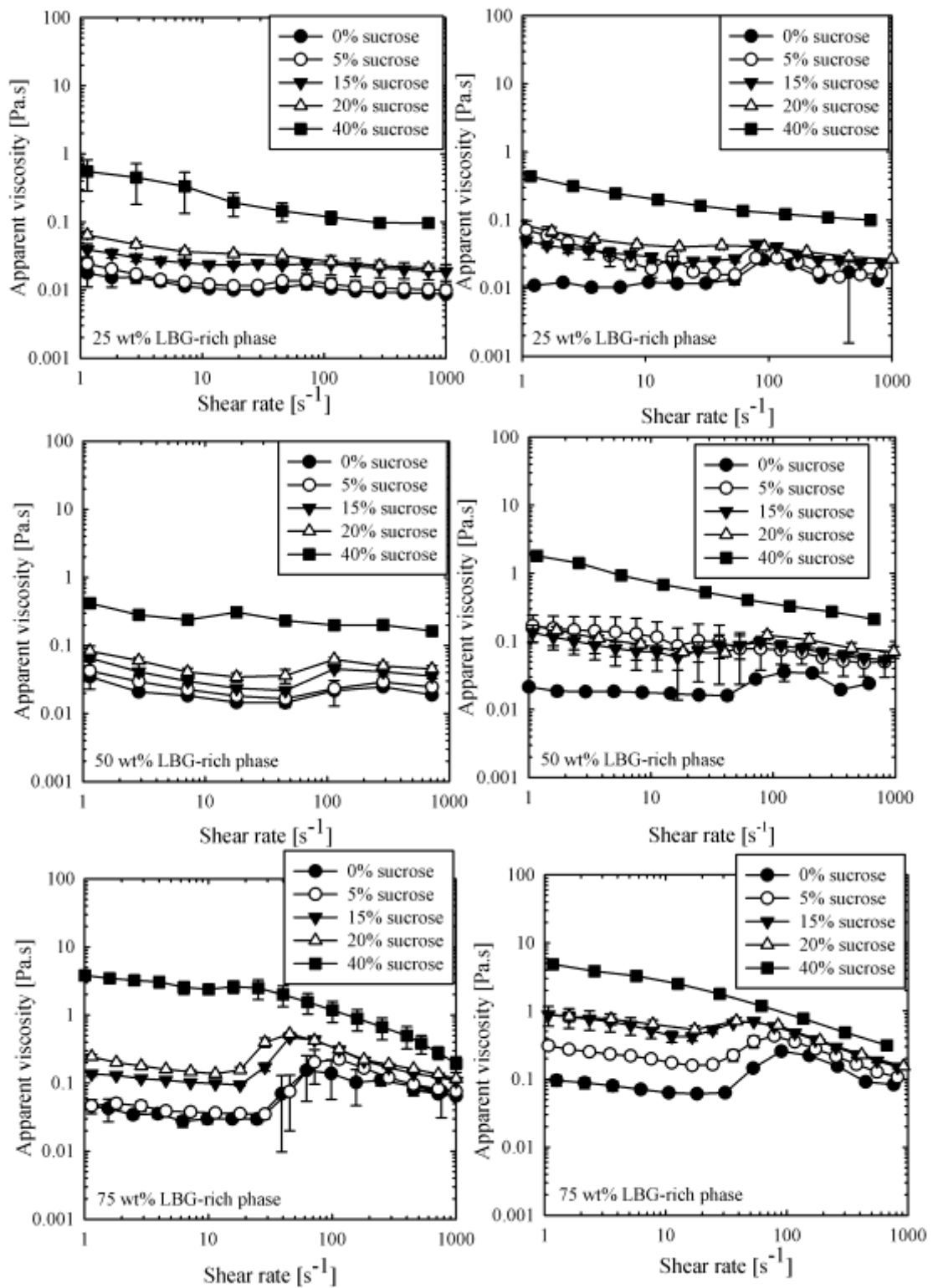


Figure 5-15. Ascending flow curves for blends with 25, 50 and 75 wt% of LBG-rich phase and 0-40 wt% sucrose, prepared by dissolving of the powdered ingredients (left) and by blending of the equilibrium phases from a primary ATPS (right).

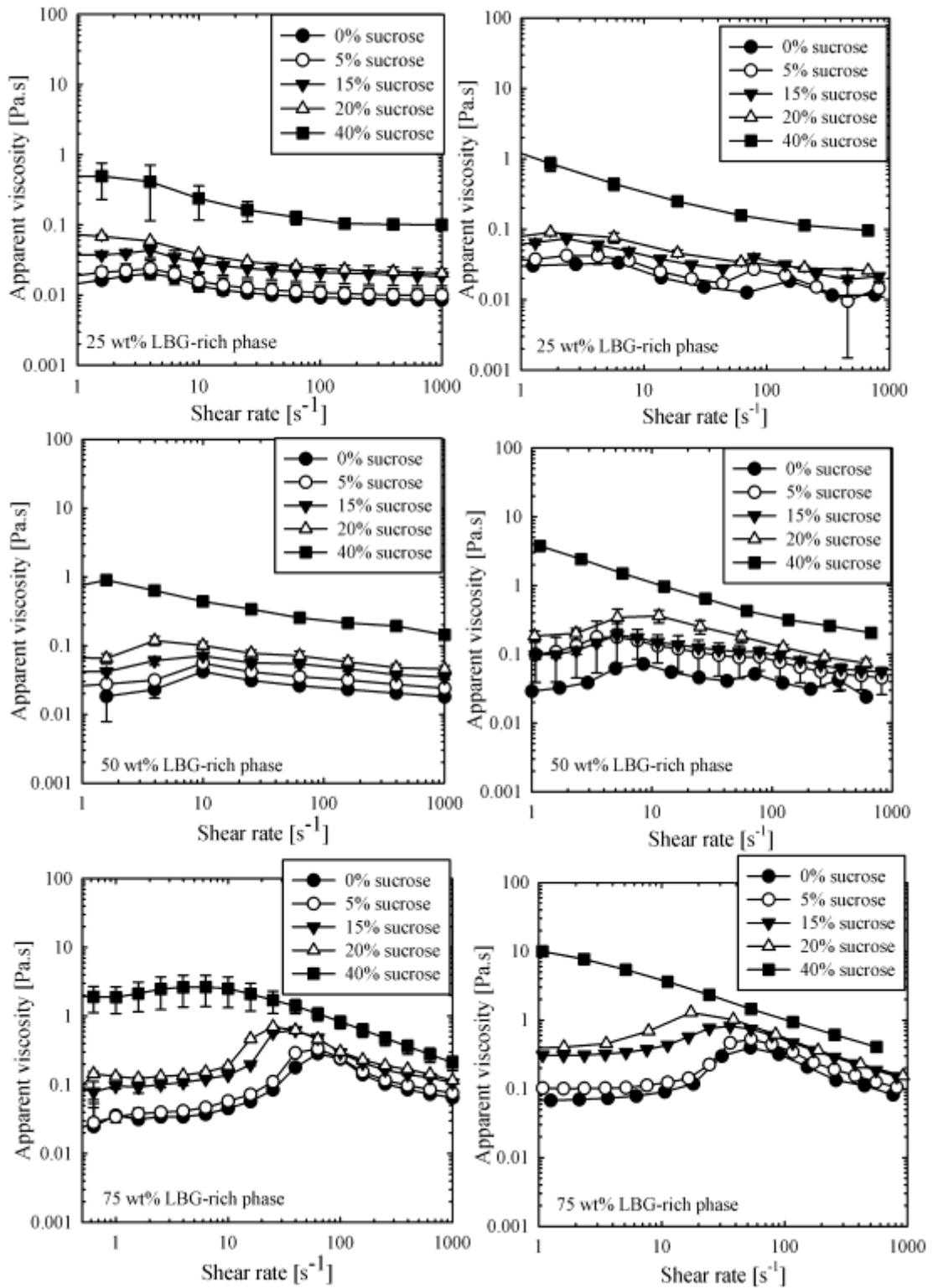


Figure 5-16. Descending flow curves for blends with 25, 50 and 75 wt% of LBG-rich phase and 0-40 wt% sucrose, prepared by dissolving of the powdered ingredients (left) and by blending of the equilibrium phases from a primary ATPS (right).

Since the preparation procedure made no significant difference to the existence of the complex flow in blends, it was concluded that it is indeed related to the multicomponent-emulsion like structure of these blends.

### 5.5.3 Shear induced phase inversion and the microstructure of blends under shear

Our attention was now turned to finding the cause of the presence of the complex flow in initially polysaccharide-rich blends ( $\varphi_{GM} \gg$ ), and its absence in the blends with a high sugar concentration.

#### 5.5.3.1 Complex flow behaviour in polysaccharide-continuous blends

The blends with  $\varphi_{GM} > 50$  wt% flow differently to the blends with  $\varphi_{GM} < 50$  wt%. The major differences between them are their overall viscosity and quiescent microstructure. The blends with  $\varphi_{GM} > 50$  wt% are more viscous and polysaccharide-continuous; and the blends with  $\varphi_{GM} < 50$  wt% are less viscous and protein-continuous. Consequently, keeping in mind the observed changes in the viscosity of the blends during flow, the occurrence of shear thickening peaks in ATPS with  $\varphi_{GM} > 50$  wt% is likely a result of a shear-induced change in the quiescent microstructure/phase sense of the system.

The complex flow behaviour is best explained by a phase inversion event induced by shear. When a polysaccharide-continuous system ( $\varphi_{GM} > 50$  wt%) is subjected to a high enough shear ( $\sim 100$  s<sup>-1</sup>) it phase inverts to a protein-continuous system ( $\varphi_{NaCAS} < 50$  wt%). In such a way a dispersed phase would flip instantly from NaCAS-

rich phase (at a volume fraction of the dispersed phase  $< 50\%$ ) to GM-rich phase (at the volume fraction of the dispersed phase  $> 50\%$ ). The event would cause an increase in the viscosity—observed as a peak. Shear induced phase inversion in mixed biopolymer systems like this one, is not a newly discovered phenomenon. It was previously reported (Brown et al., 1995; Foster et al., 1996; Foster et al., 1997; Wolf et al., 2000) as a way by which an emulsion in flow can lower its energy.

Shear induced phase inversion can be—much like any shear induced change in the microstructure of a multicomponent system—explained by competing processes of droplet breakup and coalescence. In initially polysaccharide-rich blends under low and medium shear, the protein dispersed phase starts to coalesce. When the size of these droplets is sufficiently large and the shear is increased further the droplets deform and in the process engulf and break off the parts of the polysaccharide-continuous phase, which concludes in the formation of a bi-continuous system. Perpetuation of the coalescence transforms an existing bi-continuous system into a protein continuous one and the process of the phase inversion is completed.

In Figure 5–17 an attempt is made to determine shear inversion compositions for the systems of various sucrose concentrations prepared by blending of the equilibrium phases. These were also presented in the previous section. Shear viscosities at the shear rates of  $0.01 \text{ s}^{-1}$  to  $1000 \text{ s}^{-1}$  are plotted as a function of  $\varphi_{GM}$  (0% corresponds to the pure protein-rich phase and 100% to the pure polysaccharide-rich phase). A change from a linear trend in the viscosity plots denotes the phase inversion happening at that particular phase-volume fraction. Where sucrose is added at  $< 20 \text{ wt}\%$  a distinct

change in trend is observed for phase volumes between 25% and 50%. For the system at  $> 20$  wt% of sucrose, on the other hand, the change in trend is not as obvious, which poses a question whether phase inversion in this systems occurs at all. From the relationship between the shear viscosities at various  $\dot{\varphi}_{GM}$  one can also infer on the degree of shear thinning behaviour.

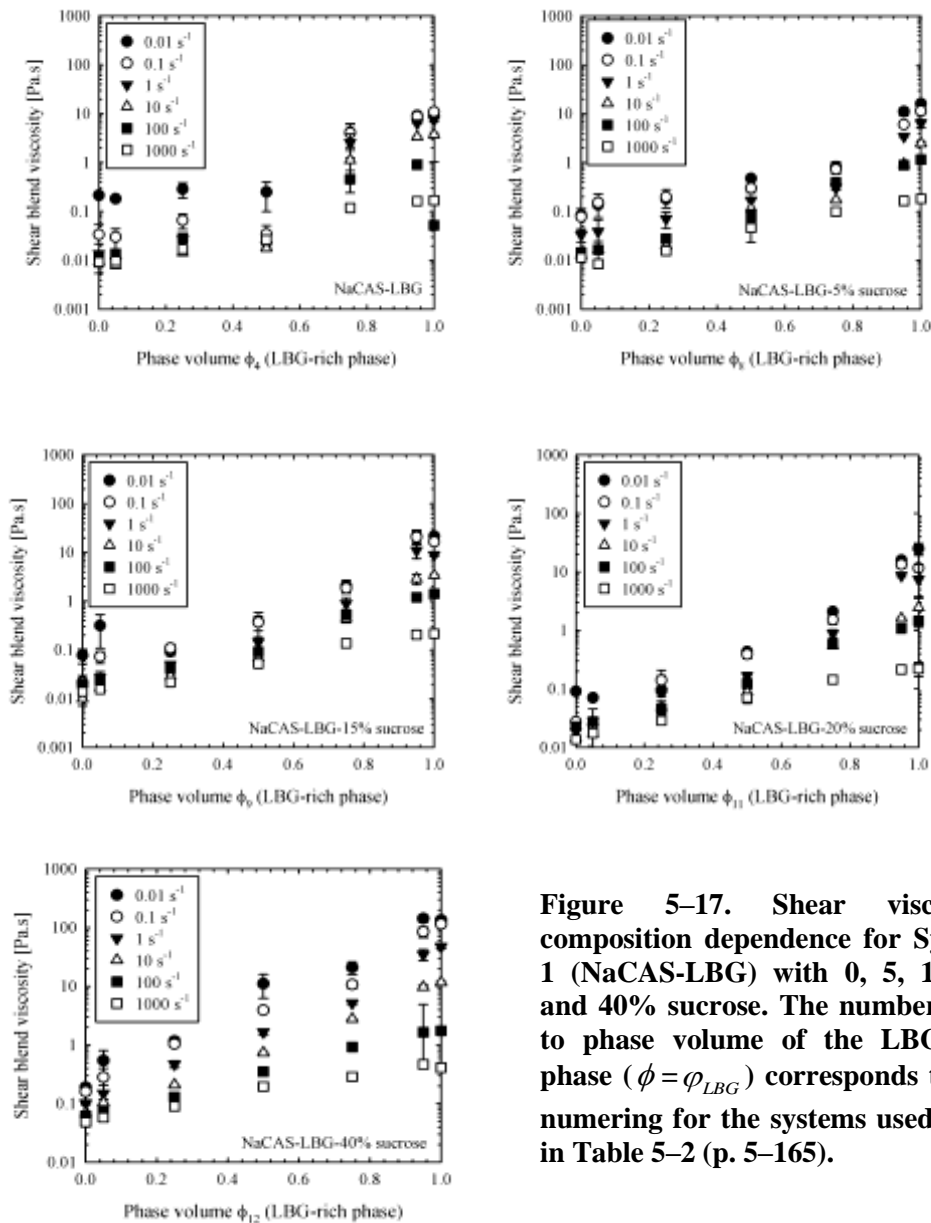


**Figure 5-17.** Shear viscosity-composition dependence for System 1 (NaCAS-LBG) with 0, 5, 15, 20 and 40% sucrose. The number next to phase volume of the LBG-rich phase ( $\phi = \varphi_{LBG}$ ) corresponds to the numbering for the systems used later in Table 5-2 (p. 5-165).

### **5.5.3.2 Complex flow behaviour in protein-continuous blends and polysaccharide-continuous blends at a high sugar concentration**

It was established in the previous sections that the occurrence of the phase inversion event is determined by the following factors: (i) a sufficiently high shear, (ii) an emulsion-like/droplet-like/multicomponent structure, and (iii) a favourable composition (i.e., volume fractions of the equilibrium phases). Furthermore, the studies of the conventional O/W emulsions also show the importance of favourable viscosities, i.e., the viscosity differences between the pairs of the equilibrium phases (Efthimiadu and Moore, 1994), the importance of which is further addressed in this section.

Table 5-2 on the next page shows viscosity values at  $1 \text{ s}^{-1}$ , which offer an insight in the extent of the viscosity differences between the dispersed and continuous phases in the investigated ATPS. A large difference between the viscosities of the equilibrium phases (used to prepare blends) is observed for all systems, especially for those without sugar.

Regardless of the amount and type of sugar, the polysaccharide-rich continuous systems are always more viscous than the protein-rich continuous systems; thus, under shear the polysaccharide-rich continuous systems flow easier if they phase invert. The phase inversion in the polysaccharide-continuous systems offers a solution, as it is a way to lower energy of the system under shear. On the other hand, the blends with less viscous protein-rich phase as a continuous phase and more viscous polysaccharide-rich as a dispersed phase flow better as they are.

**Table 5–2. Aqueous two-phase systems (ATPS) investigated on their microstructure at quiescent conditions and under shear. Absolute viscosities of the equilibrium phases of these systems are also shown.**

ATPS code	NaCAS [wt%]	GM [wt%]	Sugar [wt%]	Equilibrium phase	$\eta$ at 1 s <sup>-1</sup> [Pa.s]
<i>1</i>	2	0.25 LBG	0	LBG-r NaCAS-r	0.15 0.004
<i>2</i>	3	0.2 LBG	0	LBG-r NaCAS-r	0.608 0.003
<i>3</i>	4	0.2 LBG	0	LBG-r NaCAS-r	0.68 0.003
<i>4</i>	4	0.6 LBG	0	LBG-r NaCAS-r	0.416 0.006
<i>5</i>	5	0.15 LBG	0	LBG-r NaCAS-r	4.04 0.004
<i>6</i>	5	0.2 LBG	0	LBG-r NaCAS-r	4.45 0.006
<i>7</i>	6	0.2 LBG	0	LBG-r NaCAS-r	3.63 0.006
<i>8</i>	4	0.6 LBG	5 sucrose	LBG-r NaCAS-r	1.116 0.021
<i>9</i>	4	0.6 LBG	15 sucrose	LBG-r NaCAS-r	1.606 0.022
<i>10</i>	4	0.6 GG	15 sucrose	GG-r NaCAS-r	1.210 0.011
<i>11</i>	4	0.6 LBG	20 sucrose	LBG-r NaCAS-r	2.552 0.022
<i>12</i>	4	0.6 LBG	40 sucrose	LBG-r NaCAS-r	15.202 0.101
<i>13</i>	4	0.6 GG	50 sucrose	GG-r NaCAS-r	27.246 2.375
<i>14</i>	4	0.2 LBG	15 sucrose	LBG-r NaCAS-r	3.3 0.004
<i>15</i>	4	0.2 LBG	15 trehalose	LBG-r NaCAS-r	2.2 0.006
<i>16</i>	4	0.2 LBG	15 fructose	LBG-r NaCAS-r	4.67 0.004
<i>17</i>	4	0.2 LBG	15 glucose	LBG-r NaCAS-r	1.64 0.005
<i>18</i>	4	0.2 TG	0	TG-r NaCAS-r	2.27 0.005
<i>19</i>	4	0.2 GG	0	GG-r NaCAS-r	1.5 0.004
<i>20</i>	4	0.2 FG	0	FG-r NaCAS-r	1.78 0.003
<i>21</i>	4	0.6 GG	0	GG-r NaCAS-r	0.339 0.004

The phase inversion is absent in a high sugar environment despite still very different viscosities of the equilibrium phases (Table 5–2). In the following paragraphs, two possible explanations for the suppression of the phenomenon are offered. The first explanation refers to the suppression of the coalescence and the second refers to the

formation of structures with special flow characteristics.

The shear-induced phase inversion in a high sugar environment is likely repressed by increased viscosity of the polysaccharide-rich continuous phase, which in turn significantly slows down the coalescence of the protein-rich dispersed phase. The coalescence is an important step for the occurrence of the phase inversion and if it is too slow the process of shear-induced phase inversion can not occur for the applied shear rates. Much higher shears (outside the range of our geometry/rheometer setting) might, however, be needed for the phase inversion to take place.

Another event that could conceivably explain the suppression of the phase-inversion event in the polysaccharide-continuous blends at high sugar concentrations is the evolution of anisotropic microstructures (i.e., thread-like structures) under shear. Their existence in ATPS was previously reported (Wolf et al., 2000; Pacek et al., 2001; Spyropoulos et al., 2008). The formation of thread-like structures under shear was characterised by an increase in the shear-thinning behaviour and compared to droplet-like morphologies.

#### 5.5.4 Rheoptical investigation of blends with and without sugar

In the attempt to confirm either of the two hypotheses, explaining the suppression of the phase-inversion event, selected blends were visualised under shear. A series of rheoptical experiments (40 mm glass plate-plate geometry, 300  $\mu\text{m}$  gap, room temperature) was conducted on (i) protein-continuous ATPS with and without sugar, (ii) polysaccharide-continuous ATPS with and without sugar, and (iii) polysaccharide-continuous ATPS in the presence of various types of sugar and GMs. Since the effect of sugar type and GM type shows no significant effect on the microstructure evolution under shear, the data will not be shown.

##### 5.5.4.1 *Protein-continuous blends*

Protein-continuous blends ( $\varphi_{GM} < 50 \text{ wt}\%$ ), regardless of the amount of sugar added, show normal shear-thinning behaviour without shear thickening regions. The microstructure of these systems under shear is shown on the example of the system at 30% of sucrose in Figure 5–18 and the system at 5% sucrose in Figure 5–19. For each of the systems the images that significantly differed from one another were selected to best represent the evolution of microstructures under shear. The flow curves that were obtained simultaneously with the image acquisition are shown next to the images.

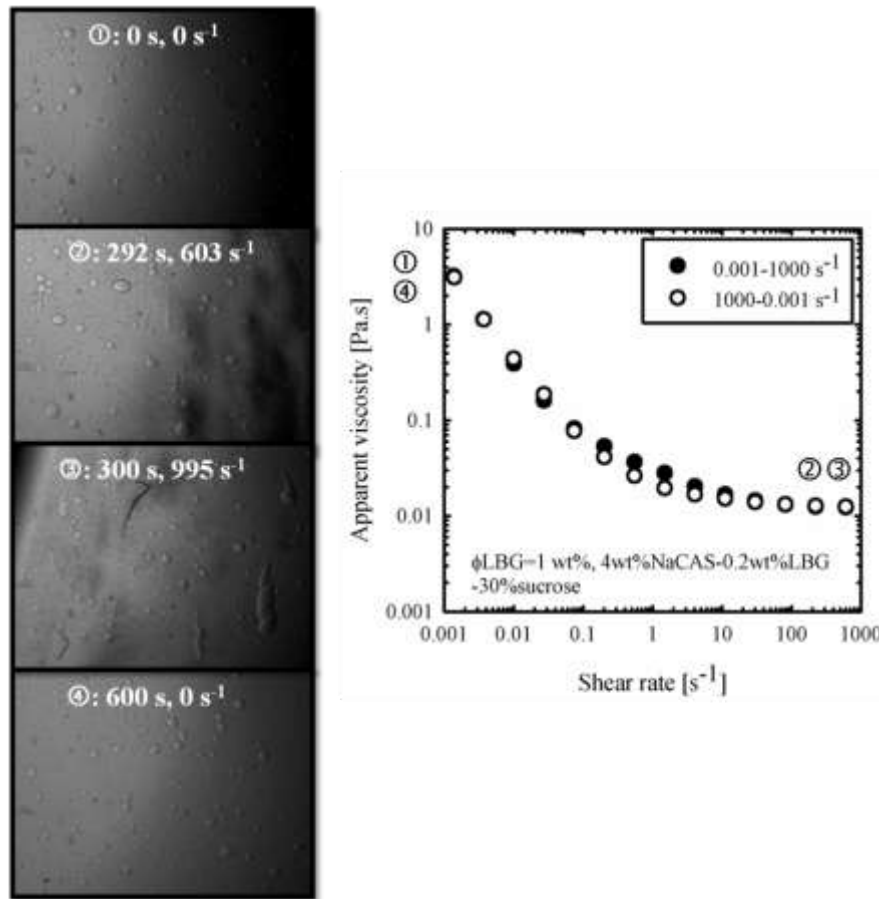


**Figure 5–18. Microstructures under shear and flow curves of ATPS 3 (4 wt% NaCAS-0.2 wt% LBG) at  $\phi_{\text{LBG}}=1 \text{ wt\%}$ . The width of view is 1.7 mm.**

In terms of the microstructure, protein-continuous systems with  $\phi_{GM} < 25 \text{ wt\%}$  undergo few changes and behave much like conventional emulsions. The observed changes are in the number, size and polydispersity of the included droplets. In terms of size, small droplets with the radii  $R, < 2.5 \mu\text{m}$  stay spherical throughout the shear regime, medium sized droplets  $2.5 < R < 30 \mu\text{m}$  assume at rest spherical and under shear ellipsoid shapes, and larger droplets/blobs assume irregular forms, which are broken under high shear environment to smaller, spherical shapes. The shear cycle concludes with the formation of a higher number of evenly sized droplets.

The amount of sugar (e.g., sucrose) added to the protein-continuous blends shows no visible effect on the microstructure evolution events and, hence, the blend with any amount of sugar could be used as an example for the flow behaviour of a protein-continuous system. Slight differences in the degree of deformation of the droplets under shear between systems are briefly referred to in § 6.2.3, p. 6–197.

The microstructuring phenomena in protein-continuous systems are also observed on a larger scale. Images of a lower magnification for the systems with  $\varphi_{GM} = 5$  wt% and  $\varphi_{GM} = 40$  wt% are shown in Figures 5–19 and 5–20, respectively. The microstructure in this blend evolves by a changing balance between the processes of deformation and droplet breakup, on one side, and coalescence, on the other. With the increase in  $\varphi_{GM}$  the interaction between droplets increases and anisotropic structures form.



**Figure 5–19.** Microstructures of ATPS 3 (4 wt% NaCAS-0.2 wt% LBG) at  $\varphi_{GM} = 5$  wt%, 5% sucrose and at 18 times magnification under shear. The width of view per micrograph is 5 mm.

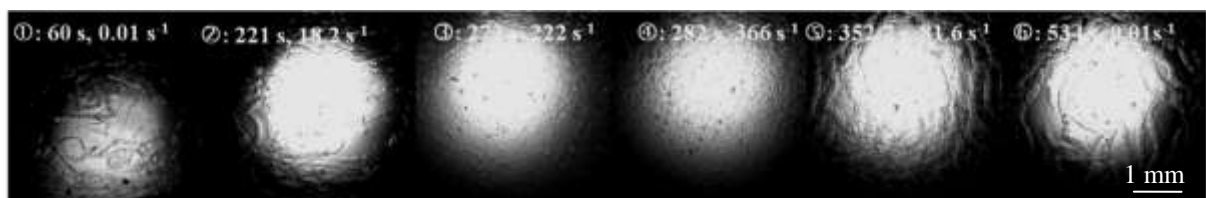


**Figure 5–20.** Microstructures of ATPS 3 (4 wt% NaCAS-0.2 wt% LBG) at  $\varphi_{GM} = 40$  wt%, 5% sucrose and at 18 times magnification under shear. The width of view per micrograph is 5 mm.

The microstructure of the blends under shear evolves as described. The blends are first mixed with spatula, polydisperse systems composed of spherical droplets and bigger blobs of irregular shapes (Figure 5–19, micrograph 1) are obtained. The latter under shear elongate and form threads (Figure 5–19, micrograph 1 and Figure 5–20, micrographs 1–2), which break—by end pinching—into droplets. They, at the average shear rate of  $\sim 250 \text{ s}^{-1}$ , arrange themselves in bands of slightly different shear rates (visible for  $\varphi_{GM} < 25 \text{ wt\%}$ , Figure 5–19, micrograph 3). Upon reduced shear the droplets coalesce (Figure 5–19, micrograph 5 and Figure 5–20, micrographs 5–6) into a new type of highly ordered bi-continuous thread-like or tubular structures (Figure 5–21). They are formed by a lateral coalesce of the droplets and grow in size and complexity with an increase in  $\varphi_{GM}$ .



**Figure 5–21.** A formation of the thread-like or tubular structures from the protein-continuous blends for ATPS 3 at  $\varphi_{GM} = 40 \text{ wt\%}$  after shear. The width of view is 1.186 mm.

Figure 5–22 shows magnified microstructure of ATPS 3 under shear. The relationships among the following are observed: (i) the  $\varphi_{GM}$ , (ii) the initial size of irregular blobs/larger bi-continuity regions (Figure 5–22, micrographs 3 and 4), and (iii) the size and complexity of the tubular structures after shear. Furthermore it is

confirmed that, in the protein-continuous systems, the coalescence of droplets into tubular bi-continuous structures shows itself on the flow diagram as a shear thickening region (arrow in Figure 5-22).

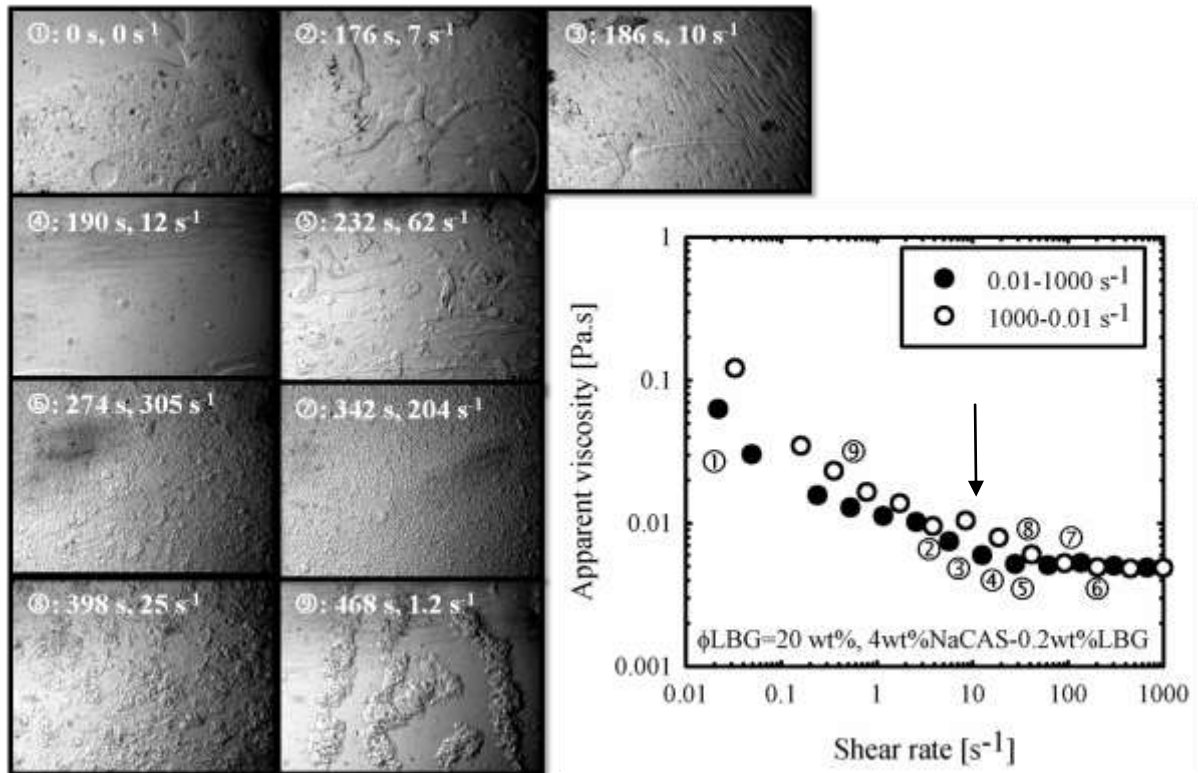


Figure 5-22. Microstructures under shear and flow curves of ATPS 3 (4 wt% NaCAS-0.2 wt% LBG) at  $\phi_{\text{LBG}}=20$  wt%. The width of view is 1.7 mm.

#### 5.5.4.2 Polysaccharide-continuous blends

Polysaccharide-continuous blends flow differently from protein-continuous blends. Figures 5-23 and 5-24 show two distinct cases observed for systems in low sugar environment and high sugar (e.g., sucrose) environment, respectively.

In low sugar environment (Figure 5-23, at  $< 20\%$  sugar), the quiescent microstructure of the polysaccharide-continuous blends is droplet-like. Under low to medium shears ( $1\text{--}200\text{ s}^{-1}$ ) droplets deform, elongate and orientate in flow

(e.g., micrographs 2–4) to the point where they are as thin as capillaries. Under increased shear the threads become thinner and they eventually break (e.g., micrograph 5). The instabilities in the central part and the ends of the threads lead to breakage of the thin structures into many small, evenly sized droplets and some debris. The process of the formation of these structures is instant ( $< 15$  fps) and it is facilitated by a high viscosity difference between the phases. The micron-sized droplets of the polysaccharide-rich phase are now densely packed in the protein-continuous medium and the system phase inverts. The process is seen in the micrograph, as a darkening of the image and a loss of visibility of the structures (e.g., micrographs 6–7).

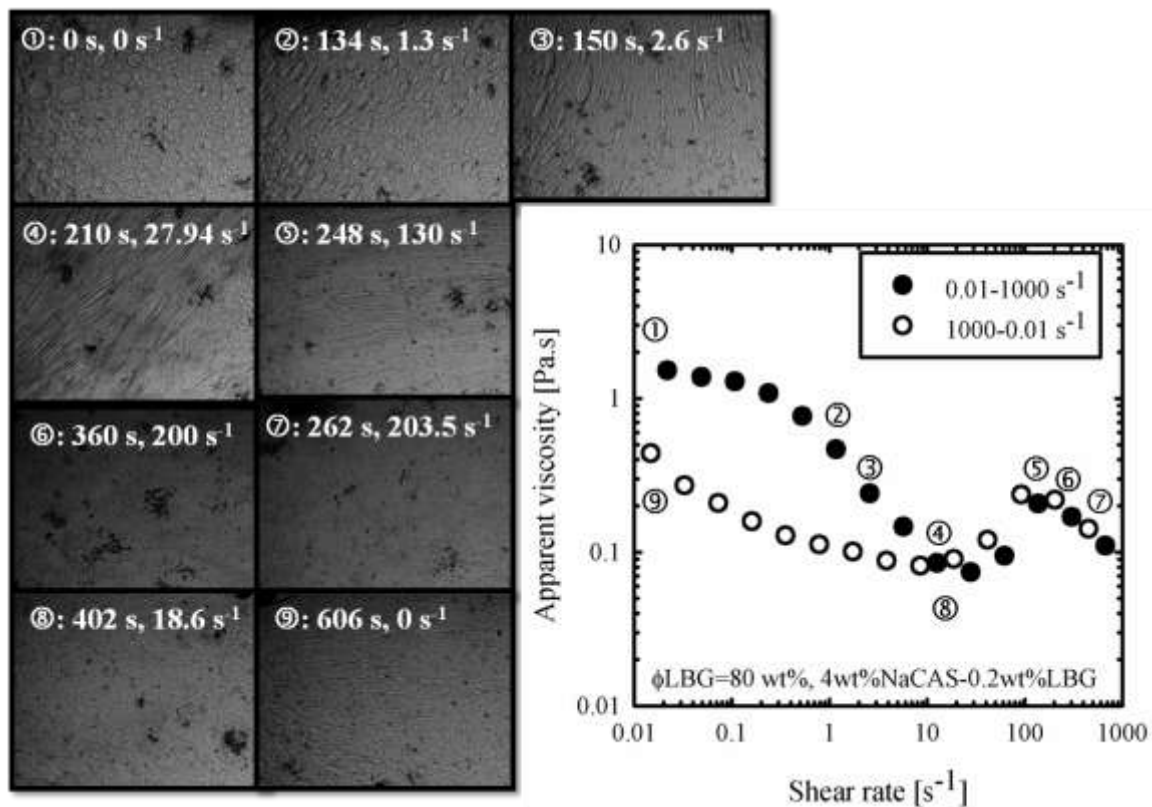


**Figure 5–23.** Microstructures under flow and flow curves for ATPS 3 (4 wt% NaCAS-0.2 wt% LBG) at  $\phi_{GM} = 80$  wt% and 110 times magnification. The width of view per micrographs is 1.7 mm.

When the shear is reduced the blends become unstable again; the polysaccharide-droplets and protein-continuous matrix simultaneously coalesce and

droplet breakup is reduced. Graininess of the images increases when droplets of the polysaccharide-rich phase start to grow (e.g., micrograph 8). With a further reduction of shear the coalescence perpetuates itself and concludes in the formation of protein-rich droplets enclosed in the polysaccharide-rich medium (e.g., micrograph 9). Finally, in the absence of shear and over some time, droplets recover to their original spherical shape (e.g., micrograph 1).

The microstructure evolution in a high sugar environment (at  $> 20\%$ , Figure 6–24) is different as compared to a low sugar environment in two ways. First, due to high  $\lambda$  (higher  $\eta_c$ ) the same energy input produces smaller structures (e.g., micrographs 1–4), and second, the structures coalesce and recover from shear slower because of the elevated  $\eta_{c,d}$ .

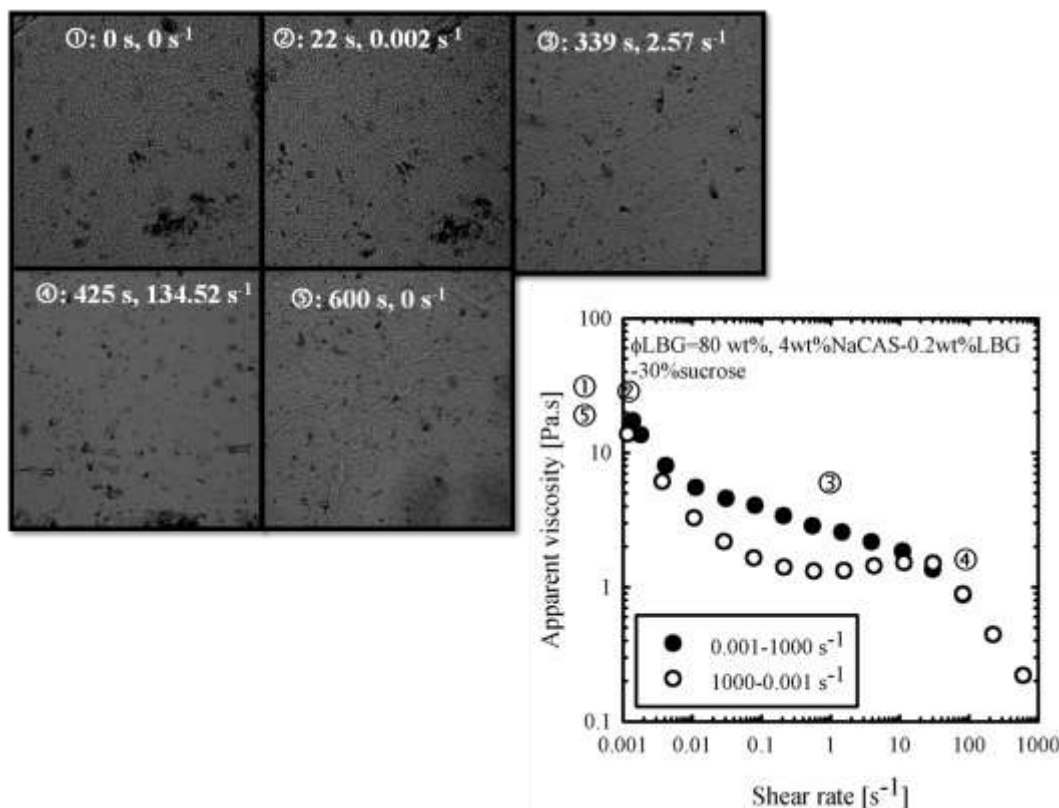


**Figure 5–24.** Microstructures under flow and flow curves for ATPS 3 (4 wt% NaCAS-0.2 wt% LBG) at  $\varphi_{GM}=80$  wt% and 30% sucrose. The width of view per micrographs is 0.85 mm.

The coalescence of the polysaccharide-rich phase during shear is virtually absent, hence the complex flow behaviour is not observed. However, when shear is decreased, medium shear promotes coalescence and concludes in the formation of slightly larger structures/threads, which flow differently (e.g., micrograph 5).

Optical observation of the polysaccharide-rich equilibrium phase that was used to prepare blends (Figure 5–25), reveals the existence of undissolved particles, which show tendency to orient themselves in the flow field. They are, however, very small and are assumed to have very little effect on the flow behaviour of either of the equilibrium phases or their blends.

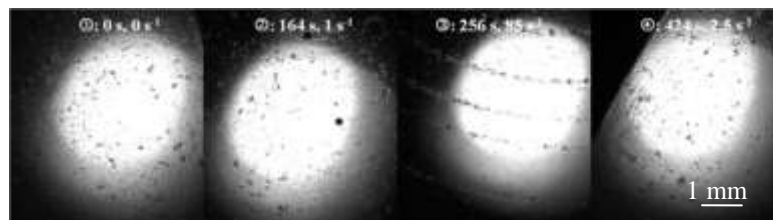


Figure 5–25. Pure LBG-rich phase of ATPS 3 at 18 times magnification. The width of view is 5 mm.

### 5.5.5 Effect of composition and temperature on the viscometry of ATPS: the equilibrium phases and blends

#### 5.5.5.1 *Effect of the biopolymer concentration and galactomannan type on the flow behaviour of individual equilibrium phases*

This subsection reviews the effect of the total biopolymer concentration and the galactomannan type on flow properties of the equilibrium phases. The results of the studies are shown in Figures 5–26 and 5–27, respectively.

Figure 5–26 shows the effect of the total biopolymer concentration

([BP]=[GM]+[NaCAS]) on the apparent viscosities. The findings are based on the investigation of the equilibrium phases of ATPS 1–7 (Table 5–1/5-2). Although different total biopolymer concentration, [BP], shows no effect on the overall flow pattern of the phases, it causes an increase in the apparent shear viscosity,  $\eta$ . The behaviour is shown on the example of NaCAS-LBG system without sugar next.

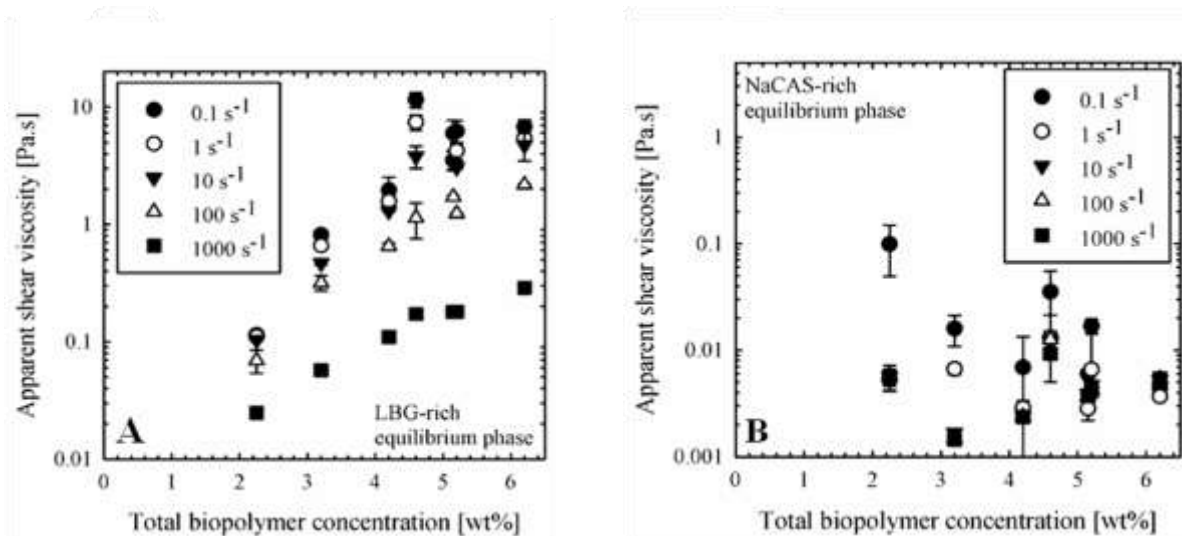


**Figure 5–26.** Effect of the total biopolymer concentration on the viscosity of (A) LBG-rich and (B) NaCAS-rich equilibrium phases for sodium caseinate-locust bean gum (NaCAS-LBG) ATPS.

The effect of the [BP] on the flow behaviour of the phases is described by fitting a power law model to the data shown in Figure 5–26.

**Table 5–3.** Power law parameters for the relationship between the total biopolymer concentrations of the equilibrium phases with their apparent viscosities.

Shear rate [ $s^{-1}$ ] $y=ax^b$	LBG-rich phase				NaCAS-rich phase			
	a	b	R	R <sup>2</sup>	a	b	R	R <sup>2</sup>
<i>0.1</i>	0.0048	4.1555	0.90	0.82	0.1103	-0.0190	0.75	0.56
<i>1</i>	0.0054	3.9236	0.93	0.87	0.0080	-0.5115	0.33	0.11
<i>10</i>	0.0050	3.8816	0.96	0.93	0.0004	1.4755	0.55	0.30
<i>100</i>	0.0049	3.4262	0.98	0.96	0.0002	1.6725	0.58	0.34
<i>1000</i>	0.0035	2.4240	0.99	0.99	0.3853	0.2623	0.62	0.39
<i>Avg</i>	<b>0.0047</b>	<b>3.5622</b>	<b>0.96</b>	<b>0.91</b>	<b>0.1008</b>	<b>0.5760</b>	<b>0.57</b>	<b>0.34</b>
<i>stdevp</i>	<b>0.0006</b>	<b>0.6162</b>	<b>0.03</b>	<b>0.06</b>	<b>0.1482</b>	<b>0.8540</b>	<b>0.14</b>	<b>0.14</b>

While power law equation best describes the relationship between  $\eta$  and [BP] in the

polysaccharide-rich phase, it fits poorly to the data of the protein-rich phase (Table 5-3). Possible reasons behind the poor fit are dubious viscosity measurements at low and high shears, and a large influence of [GM] on the viscosity of the protein-rich equilibrium phases, which is much larger than the effect of [NaCAS] on the viscosity of the polysaccharide-rich phase. A higher [BP] exponentially increases the apparent viscosities of the polysaccharide-rich phase, but has no apparent effect on the viscosities of the protein-rich phase. In relation to the [BP] a similar increase in  $\eta$  is anticipated when working with blend of these equilibrium phases.

The effect of the GM type on the flow behaviour of equilibrium phases is studied on ATPS 3, 16–18 (Table 5-1).

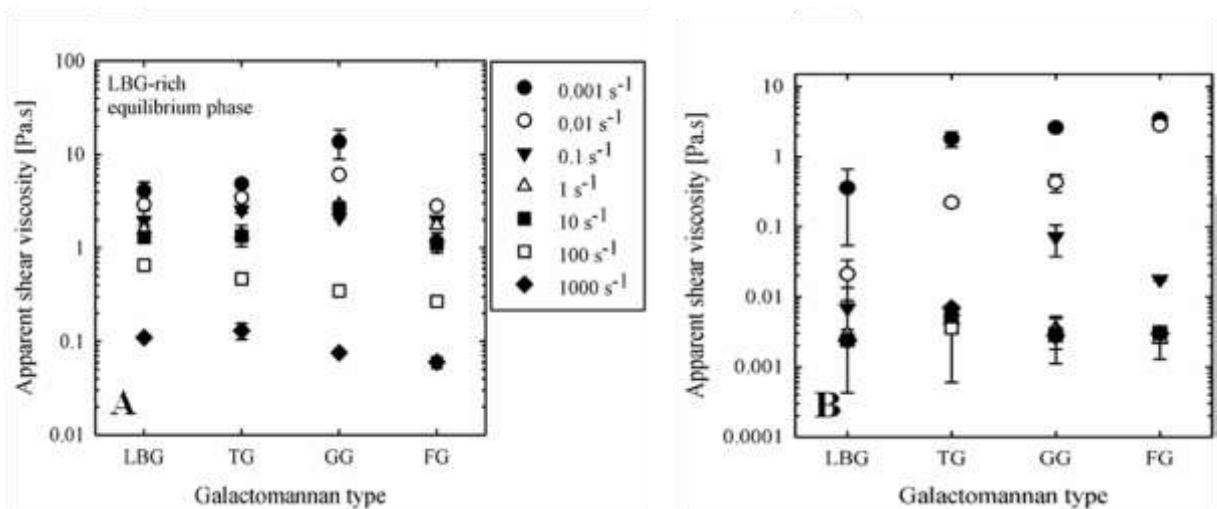


**Figure 5–27.** Effect of the galactomannan type on the viscosity of (A) LBG-rich and (B) NaCAS-rich equilibrium phases for sodium caseinate-locust bean gum (NaCAS-LBG) ATPS.

A clear distinction between the  $\eta$  of the equilibrium phases and GM-type is difficult to make, as it is different at different shears. For medium shear rates (100 s<sup>-1</sup>), however, the dependency in both phases follows the changes related to the M:G ratio of the GM.

### 5.5.5.2 Effect of sugar concentration and type on the flow behaviour of the equilibrium phases and blends

In this subsection the effects of sugar concentration and type are reviewed for the equilibrium phases (Figures 5–28 and 5–29) and for blends (Figures 5–30 and 5–31).

The effect of sugar (i.e., sucrose) concentration is investigated for ATPS 8–11 (Table 5–1/5-2). An exponential increase in  $\eta$  of both equilibrium phases, regardless of shear, is observed for all sugar concentrations. A slight discrepancy from the behaviour at 5% of sugar in the GM-rich phase is likely due to the peculiar effect of moderate amount of sugar on the GM (Richardson et al., 1998).

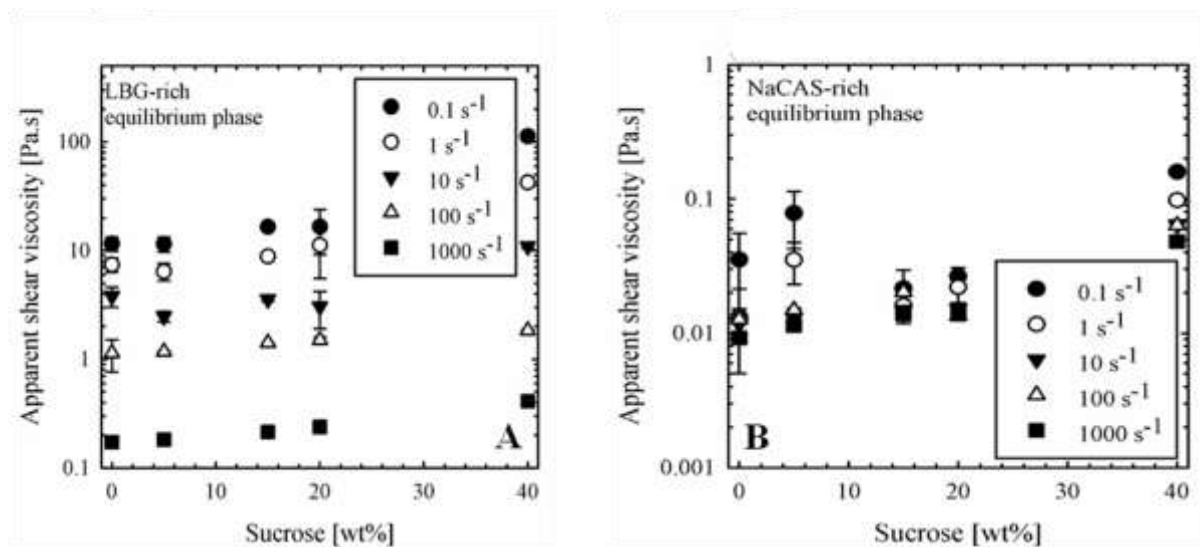
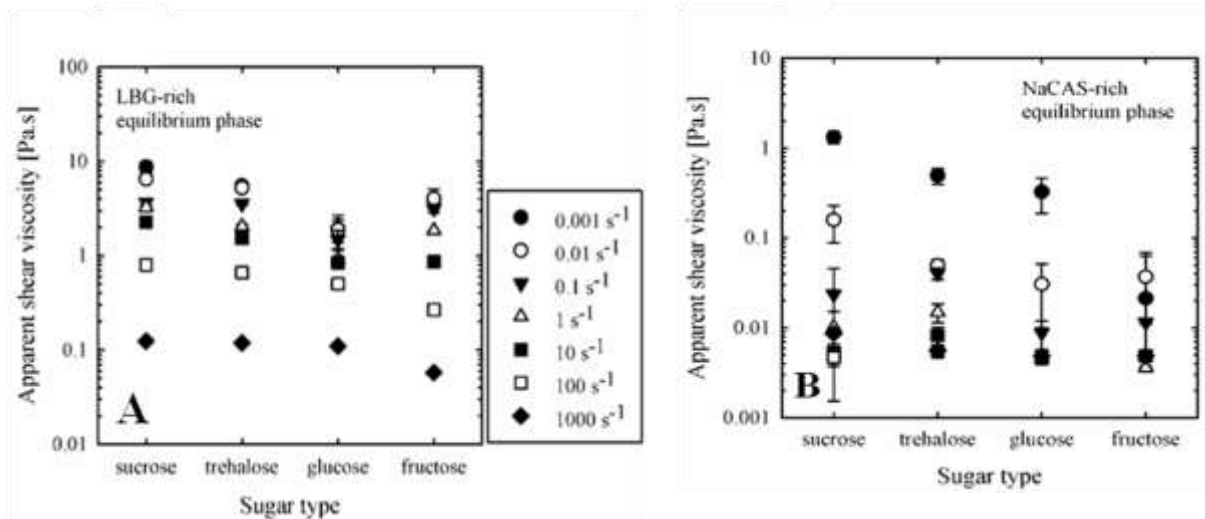


Figure 5–28. Effect of the sucrose concentration on the viscosity of (A) LBG-rich and (B) NaCAS-rich equilibrium phases for sodium caseinate-locust bean gum (NaCAS-LBG) ATPS

The largest shear-rate dependence is observed for the equilibrium phases at 40% of sugar, which implies that more structure exists at the highest sucrose concentration as compared to the systems at < 20% sucrose. The observation supports claims made in the previous chapter, where the highest cosolubility of the macromolecular components at 40% sucrose was contributed to the highest number of the hydrogen bonds formed

between sucrose, water and macromolecules (Magazù et al., 2004). In NaCAS-rich equilibrium phase the latter claim is weakened due to larger errors involved with measurements low viscosity solutions at 0 and 5% of sucrose.

The effect of sugar type is studied on the equilibrium phases of ATPS 12–15 (Table 5–1) and at sugar concentration of 15%. One of the sugars, among: sucrose, trehalose, glucose and fructose, is added to the systems at one time.



**Figure 5–29.** Effect of the sugar type on the viscosity of (A) LBG-rich and (B) NaCAS-rich equilibrium phases for sodium caseinate-locust bean gum (NaCAS-LBG) ATPS

It was found that the type of sugar affects the flow of the equilibrium phases only slightly, and that sucrose gives the highest overall viscosity to the equilibrium phases. The lowest overall viscosity is given by the presence of fructose. The largest shear-rate dependence for GM-rich phase is observed in ATPS with fructose, followed by sucrose, trehalose and glucose. On the other hand, shear dependence in NaCAS-rich phase with fructose phase is the smallest, followed by glucose, trehalose and sucrose. The reasons for the difference in the behaviour possibly lie in a different way sugars react with individual biopolymers and in their purity.

In Figure 5–30 the blends that contain sucrose, glucose, fructose and a reference system without sugar are compared.

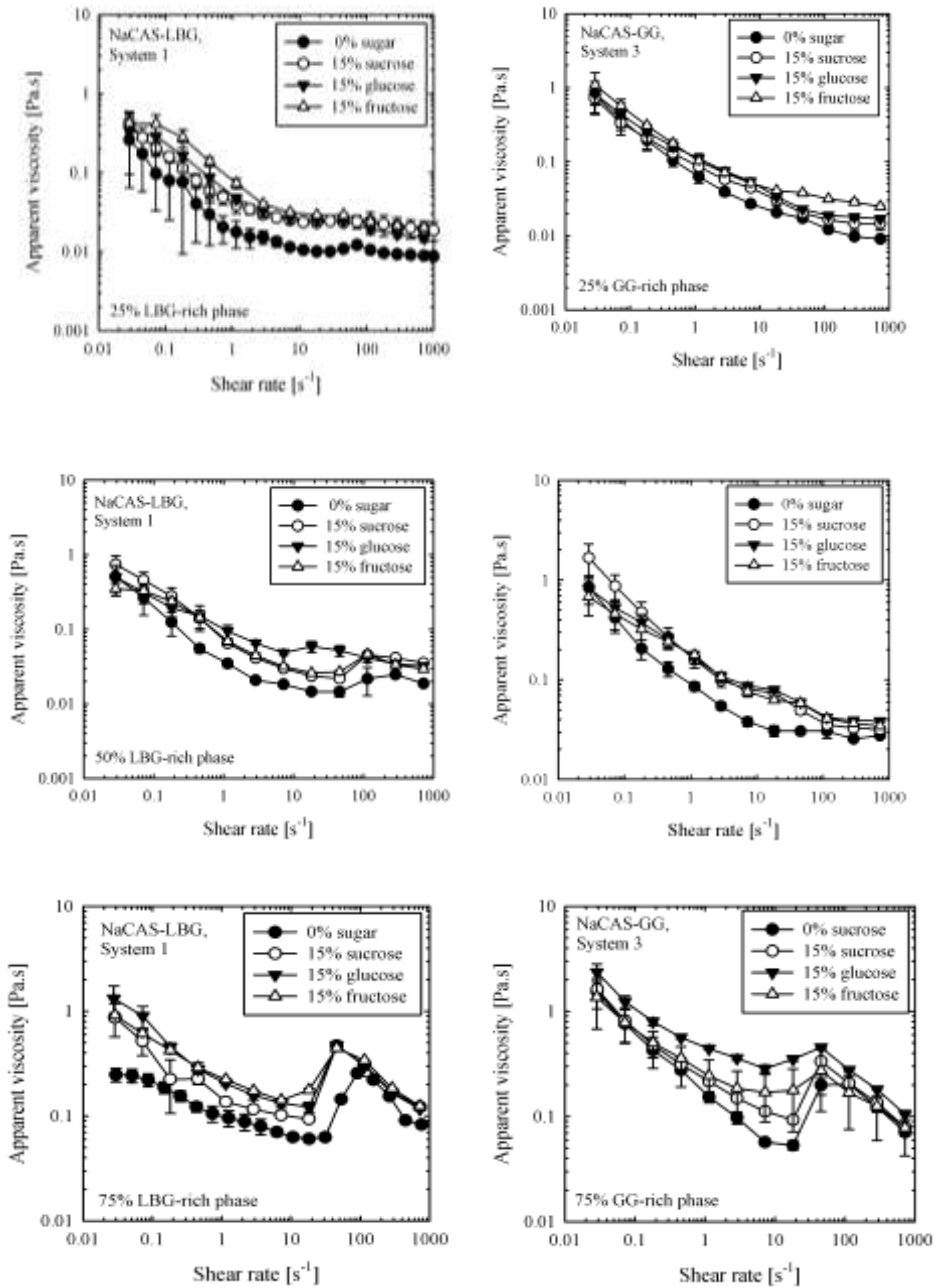


**Figure 5–30.** Comparison of Systems 1 (NaCAS-LBG) and 3 (NaCAS-GG) based on the sugar type.

As shown in Figure 5–30, similarities exist in the flow behaviour of blends with various types of sugar and GM. In the presence of glucose and fructose, similar to

systems with sucrose and without sugar, the complex flow behaviour is clearly observed for blends at  $\varphi_{GM} > 50\%$ . Although the height of the peaks stays roughly the same regardless of the type of sugar, the presence of the different sugar type changes the degree of non-Newtonian behaviour in the shear-rate range between 0.01 and 10 s<sup>-1</sup>. A lower  $\eta$  and a higher degree of non-Newtonian behaviour are also observed for systems containing LBG as compared to GG.

### **5.5.5.3 Effect of temperature on the flow of blends**

This subsection investigates the effect of temperature on the flow behaviour of blends of Systems 1 and 3 at various sugar concentrations and types. An attempt is made to explain a difference in flow behaviour observed in this work and in the previously reported work.

Normal shear thinning flow behaviour was previously observed by Schorsch et al. (1999 a) for a similar ATPS (e.g., phosphocaseinate-LBG-sucrose ATPS) at temperatures of 0, 5, 20°C and at shear rates between 0 and 100 s<sup>-1</sup>. The complex flow behaviour in this ATPS was absent. This could be attributed to the experimental differences between the investigations (Kim et al., 2010), such as: a different protein in the ATPS and the combined effects of the temperature and shear on the processes of droplet break-up and coalescence. It is, however possible that their systems actually did phase invert but at much higher shears. In the attempt to get closer to the explanation for the difference the effect of temperature and shear on the complex flow behaviour of blends relevant to this work were investigated.

Figures 5–31 and 5–32 show the flow of Systems 1 and 3 (NaCAS-GG and NaCAS-LBG) at different  $\varphi_{GM}$  and in the absence and presence of sugars (e.g., fructose and glucose). Monosaccharides are chosen to illustrate the event because of the similar effects on the flow behaviour of blends to sucrose.

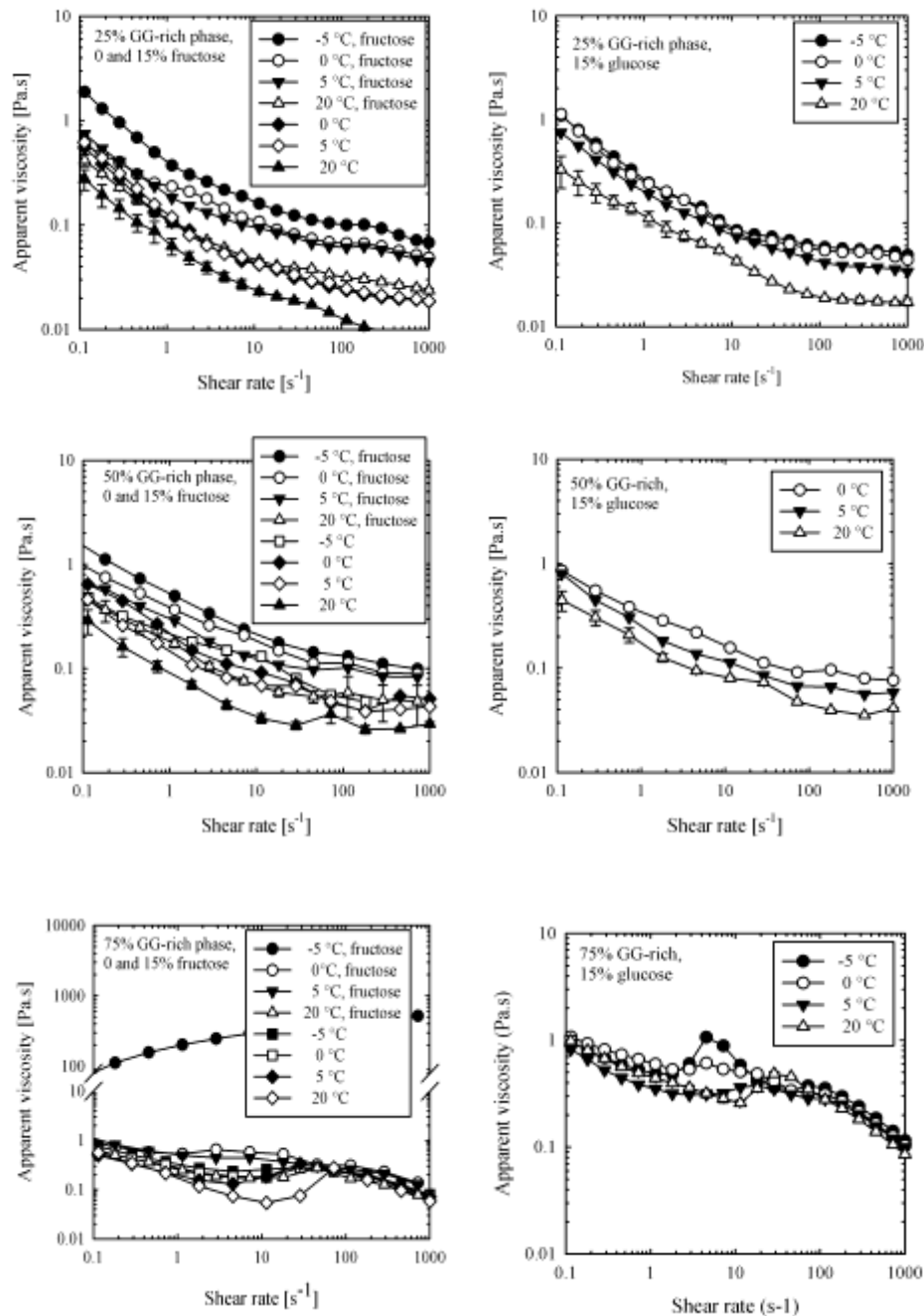


**Figure 5–31.** Effects of shear, temperature and sugar type on blends of System 3 with 25, 50 and 75% of the GG-rich phase. The blends at 0 and 15% of sucrose are positioned on the left hand side, and the blends with 15% glucose on the right hand side.

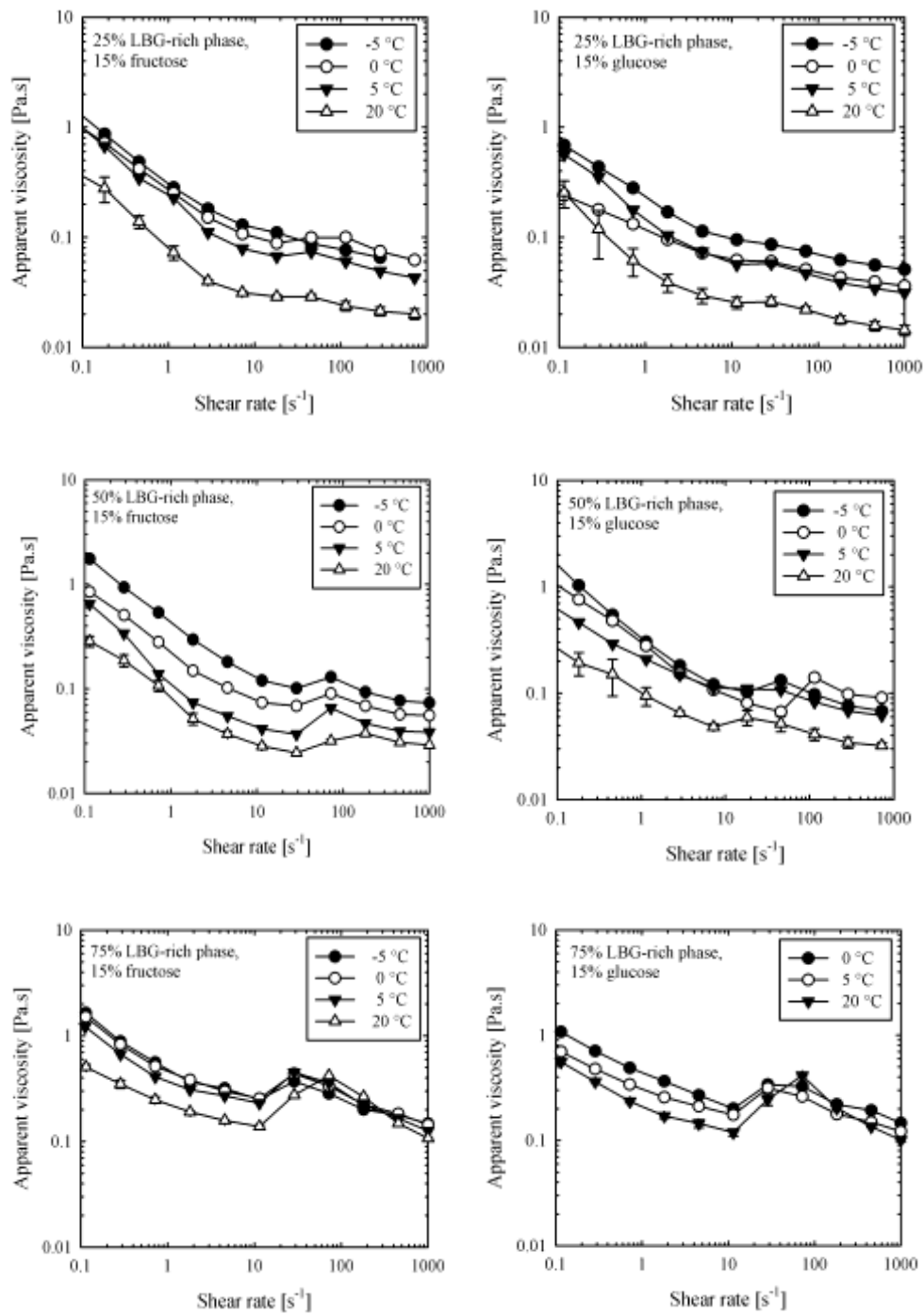


**Figure 5–32.** Effects of shear, temperature and sugar type on blends of System 1 with 25, 50 and 75% of the LBG-rich phase. The blends at 0 and 15% of sucrose are positioned on the left hand side, and the blends with 15% glucose on the right hand side.

The effects of sugar type on the occurrence of the shear induced phase inversion are not pronounced; they are in the range of experimental errors. On the contrary this is not so for the blends of different GMs. For example, the complex flow behaviour in GG-

rich blends (System 3, Figure 5–31) is hardly distinguishable, but this is not the case for the blend with LBG (System 1, Figure 5–32). In order to see a more pronounced viscosity peak in GG-rich systems the temperature needs to be lower than 5°C. The temperature also affects the onset of the shear induced phase inversion event. The peaks are shifted to a lower shear (i.e.,  $\sim 50 \text{ s}^{-1}$ ). Size of the peaks is reduced by an increase in the low and medium shear viscosities (between  $0.1$  and  $10 \text{ s}^{-1}$ ). The above results confirm that temperature affects the shear induced phase inversion (i.e., complex flow behaviour) by changes to the viscosity of the equilibrium phases. After all the shear induced phase inversion is an interplay between the processes of droplet coalescence and droplet breakage, both of which are greatly dependant on the physical characteristics of the phases, such as, drainage (i.e., GM-type), interfacial properties (addressed in terms of viscoelasticity in the following §), as well as densities and viscosities of the individual phases (as affected by temperature and composition).

## **5.6 Interfacial rheology between the pure sodium caseinate and galactomannan solutions with sucrose**

In this subsection, surface viscoelasticity of System 3 (NaCAS-GG ATPS) is investigated in the presence of various amounts of sucrose. The viscoelasticity of a surface/interface is important for the processes of droplet formation, coalescence and stability of an emulsion. The viscoelasticity of the interface is described by  $G'$  or the elastic and  $G''$  the viscous components.

Biconal geometry was used to measure the viscoelastic behaviour of the Air-

NaCAS and NaCAS-GG interfaces as a function of sucrose concentration. The bicone probes the resistance of the interface by dissipating the energy onto the surface which in turn dampens it. The data obtained are shown in Figure 5-33.

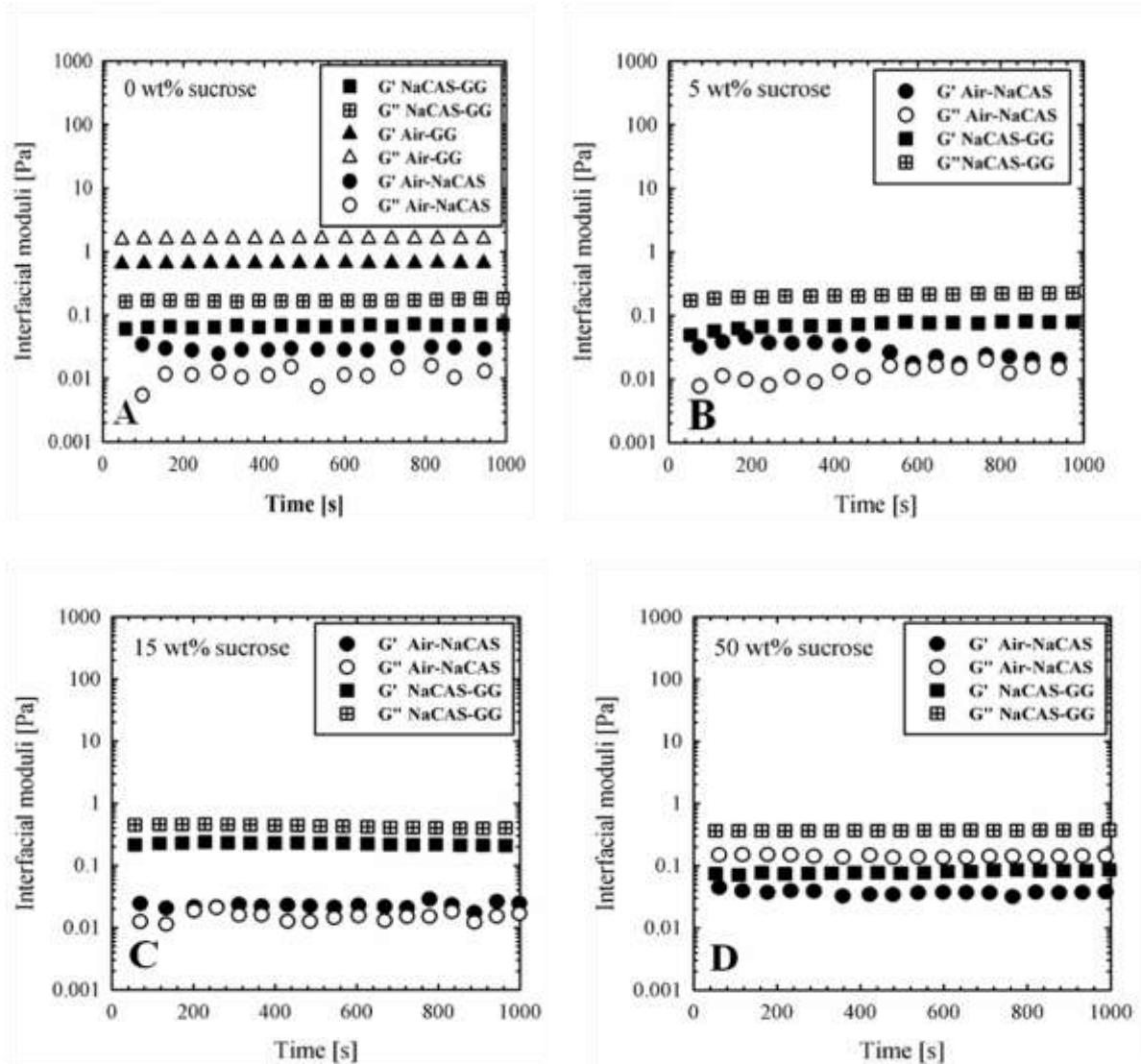


**Figure 5-33.** Log-log plots of the interfacial moduli with time for sodium caseinate, guar gum, and air interfaces, at (A) 0, (B) 5, (C) 15, and (D) 50 wt% of sucrose.

It was observed that the viscoelasticity of the Air-NaCAS/GG interface is always lower than that of the interface between two liquids (NaCAS-GG). Furthermore, a difference in the interface was observed at different sucrose concentrations. The Air-

NaCAS interface at < 15% sucrose shows a higher elastic component as compared to the interface at 50% sucrose, where the interface is more viscous/liquid. The latter could suggest the existence of the syneresis—a layer of water or sucrose solution at the interface. The higher viscoelasticity of Air-NaCAS at the presence of sugars is also a good explanation for the stability of foam formed upon vigorous mixing of the ATPS.

The liquid NaCAS-GG interface is, regardless of the concentration of sucrose in the system, always more viscous than it is elastic. While the viscosity of the interface increases proportionally with sugar concentration, the elasticity peaks at 15% of sucrose. At 50% of sucrose, however, the largest difference between the interfacial moduli is observed, which indicates the largest change of the interface.

Figures 5–33 b-d also show a mild time dependant increase in the complex viscosity of the liquid NaCAS-GG interfaces when sucrose is present. No time dependency, however, is observed for any of the Air-GG/NaCAS interfaces and GG-NaCAS interface without sucrose. There are two possible reasons for the time dependence to be observed in the presence of sucrose within this experiment. First, the formation of the interfaces could occur slowly, within an hour (e.g., at 5% sucrose) or more (e.g., at  $\geq 15\%$  sucrose). Some time may be required for the sucrose molecules to form hydrogen bonds with water and macromolecules. And second, given that the interfaces are created by pouring of the phases with similar densities over one another, mixing of the phases could occur. It is unlikely, however, that further sugar dissolution and water evaporation would have an effect. The solutions used in the experiments were previously completely dissolved and the liquid-liquid interface were studied (i.e. it

would take long for the evaporation to be noticeable).

In the future, it would also be interesting to measure viscoelastic properties of the interfaces over a range of frequencies. Based on the interesting results obtained at the oscillating frequency of 0.3 Hz and delicacy of the interfaces, the new frequency settings should also be kept low (e.g., 0.1-0.4 Hz, or even lower if more time is allowed for the experiment). From the changes in the viscoelasticity (i.e., the values of the individual moduli) it could be seen, for example, if the most elastic interface at 15% sucrose (measured at 0.3 Hz), is still the most elastic among the systems at 0.1 Hz. Based on these findings a definite connection between the phase behaviour and interfacial viscoelasticity for the systems could be made with a greater certainty. Finally, it would also be interesting to test other formulations, with different sugar concentrations and sugar types.

Although the method used is unconventional for determining the interfaces of W/W emulsions, it seems to give promising results.

## **5.7 Conclusions**

This chapter has investigated the effect of sugars on the following properties of NaCAS-GM ATPS: the quiescent microstructure, the microstructure in flow, and the viscoelastic properties of the interfaces.

Analyses of the data show a close link between microstructure and flow behaviour of the investigated ATPS. Optical investigation reveals a droplet-like microstructure and confirms the existence of protein-continuous, bi-continuous and

polysaccharide-continuous systems, which differ in their flow behaviour. Rheo-optical observation confirms that the viscosity is a good predictor for the microstructure of these systems.

Complex flow behaviour and the formation of tubular structures at  $\sim 100 \text{ s}^{-1}$  are observed for the GM-continuous systems (i.e., systems at  $\varphi_{GM} > 25\%$ ) at  $< 20\%$  of sucrose. In GM-continuous systems at  $> 20\%$  sucrose the complex flow behaviour is absent and systems flow similarly to pure NaCAS and GM solutions. Shear induced phase inversion event best explains the phenomena. In the high sucrose environment smaller and more stable structures are produced already at very low shears, hence, phase inversion does not occur.

The rheological analyses of the NaCAS-GM blends with sugar reveals common dependencies of their flow properties on factors, such as: (i) the volume fractions of the dispersed and continuous phases ( $\varphi_d, \varphi_c$ ), (ii) the viscosity of the dispersed and continuous phases ( $\eta_d, \eta_c$ ), the viscosity ratio ( $\lambda$ ), (iii) the temperature, and (vi) the composition (e.g., biopolymer concentration, sugar concentration, sugar type, and galactomannan type).

Interfacial rheology is a useful technique for comparing the interfaces of ATPS. It seems that the degree of viscoelasticity of the interface within the sample can determine how close the system lies to the binodal/critical point in the phase diagram. The viscoelastic properties of the interfaces in the systems of constant [BP] and varying [sucrose] show the highest values of viscous and elastic moduli for the NaCAS-GG interface at  $> 15\%$  sucrose.

# CHAPTER 6: INTERFACIAL TENSIONS OF SODIUM CASEINATE - GALACTOMANNAN - SUGAR AQUEOUS TWO - PHASE SYSTEMS

## 6.1 Introduction

The chapter investigates the interfacial tensions ( $\sigma$ ) of NaCAS-GM-sugar ATPS (listed in Table 3-4, § 3.3.3.1, p. 3-100) measured by a modified droplet retraction method (described in § 3.3.3.2, p. 3-103), by which  $\sigma$  of up to few  $\mu\text{N/m}$  can be determined. In particular, the effects of total biopolymer concentration, [BP], sugar concentration (e.g., at 5-30 wt% sucrose), sugar-type (e.g., sucrose, glucose, fructose and trehalose, 15 wt% added) and GM-type (e.g., FG, GG, TG and LBG, 0.2 wt% added) were studied regarding the interfacial properties of these systems. In this way, the study addressed both the effect of the solvent and that of the biopolymer on interfacial tension.

The investigated systems were phase separated to two-equilibrium phases: (i) the bottom NaCAS-r phase and (ii) the top GM-r phase. Differing equilibrium phase compositions of the ATPS are characterised by 2 to 40 times different viscosities, at the shear rate of  $0.001\text{--}0.5\text{ s}^{-1}$ , and a low density difference (typically  $< 0.01\text{ g/ml}$ ) between them. The modified retraction droplet method used, however, allowed for accurate measurement of the very low  $\sigma$  that are inherent to these systems.

The chapter is divided into two parts. First, studies the effect of the droplet deformation range and the effect of phase sense/microstructure on the  $\sigma$ . And second, correlates  $\sigma$  with the concentrations of (i) NaCAS, (ii) GM (i.e., LBG) and (iii) sugar (i.e., sucrose) by relating the  $\sigma$  with TLL and differences in the individual biopolymer concentrations between the dispersed and continuous phases ( $\Delta[\text{NaCAS}]$  and  $\Delta[\text{LBG}]$ ). In the latter part the  $\sigma$  of the ATPS with different sugar-types and GM-types are calculated and each set of data is discussed.

## **6.2 Effects of the deformation parameter range and microstructure on interfacial tension**

Preliminary tests were carried out to assess the accuracy of the measurements and to determine the limitations of the modified droplet retraction method. The method assumes (i) small droplet deformations, (ii) ellipsoid/spherical shapes of deformed/retracted droplets and (iii) Newtonian behaviour of the liquid phases in contact —at very low shear rates and at short shear rate intervals (see § 2.4.2.2.2, p. 2–51).  $\sigma$  values were calculated within a limited deformation parameter range.

### **6.2.1 The limits of the deformation parameter range**

Plots of  $\ln D$  against time that follow linear behaviour are taken within the limits of the droplet deformation range ( $0.15 < D < 0.04$ , see § 3.3.3.3, p. 3–106) to ensure the accuracy of the interfacial tension measurements. The lower limit ( $D_{\min}=0.04$ ) is established by the resolution of the digital image, camera and human eye, which restrict

the accuracy of the measurements of the droplet to a pixel size  $\sim 2 \mu\text{m}$ . Hence, measurements at  $D < 0.04$  result in more scattered data. The upper limit ( $D_{\text{max}}=0.15$ ) is determined by the assumptions of the small deformation theory. One of the assumptions of the method is that  $\ln D$  changes linearly with time (eq. [3-19], § 3.3.3.3, p. 3-106) only at very small deformations, i.e., that only for sufficiently small deformations, the deformation parameter  $D$  changes exponentially with time (eq. [3-18], § 3.3.3.3, p. 3-106) (Figure 6-1).

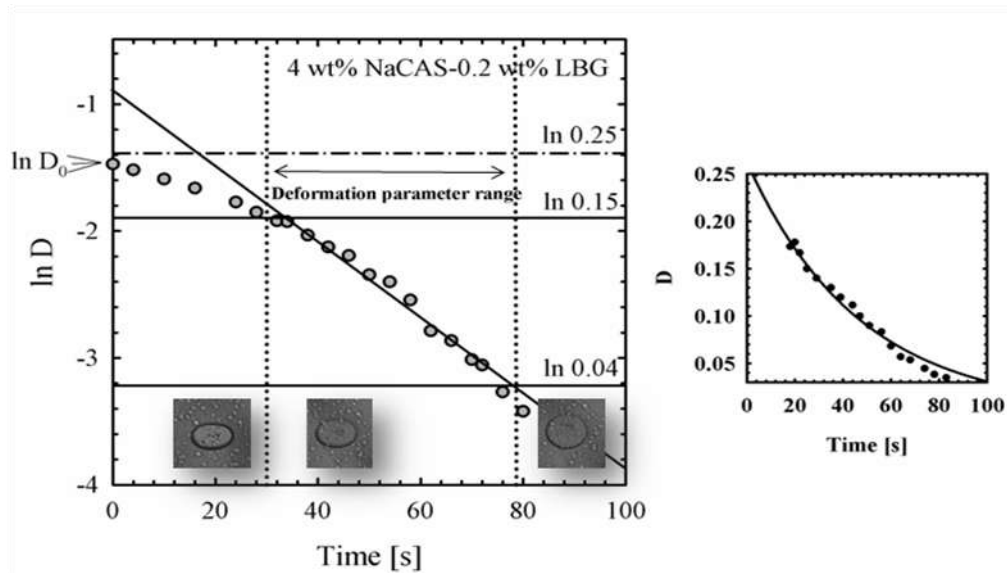


**Figure 6-1.** Droplet deformation parameter ( $D$ ) against time for a 4 %wt sodium caseinate-0.2 %wt locust bean gum aqueous-two-phase system with  $\lambda$  ( $0.001 \text{ s}^{-1}$ )=15.3. Three stages in the droplet retraction methods are shown with three light micrographs, The radius of the retracted droplet,  $R_0 = 54 \mu\text{m}$ . The left graph ( $R^2=0.98$ ) shows linear and the right graph ( $R^2=0.95$ ) exponential decay change of  $D$  vs. time.

Spyropoulos et al. and Ding et al. (2008a; 2002) used this method for SDS-pulullan and gelatin-dextran aqueous systems and for the range of  $0.25 < D < 0.04$ . In the present work and as mentioned earlier, however, the  $D_{\text{max}}$  is lower. Even if the linearity of the droplet retraction process extends to higher  $D$  values, finding the right flow conditions to obtain highly deformed droplets ( $D > 0.15$ ) by dispersing the droplets

is not always easy. In the case where droplets are obtained by dispersion, the optimum shear is sought by the trial and error method and can therefore be easily incremented for a value that can cause droplets to break instantly. Consequently, larger numbers of smaller droplets are produced. These are more rigid and hence deform to a lesser extent.

### 6.2.2 Effect of phase sense on interfacial tensions

The subsection reviews the interfacial tension of the systems positioned in the phase diagram on the same tie-line. These systems are mixtures of a disparate bulk concentration that separate into pairs of equilibrium phases of the same composition, i.e., a NaCAS-r/GM-r phase in each mixture has the same composition as the NaCAS-r/GM-r phase of the next mixture that is positioned on the same tie-line. Previous research on the interfacial tensions of aqueous systems much like this one (Guido et al., 2002; Spyropoulos et al., 2008a) has shown that systems with the same compositions of the equilibrium phases, regardless of their phase sense, have the same  $\sigma$ . The abovementioned finding will also be tested in this work.

The effect of microstructure was tested on two systems of different sugar concentrations. As shown in § 5.3.2 (Figures 5-2 and 5-5, p. 5-143 and p. 5-145, respectively), the phase sense of Systems 1-4, regardless of the amount and type of sugar and below the critical shear rate (i.e., also at quiescent conditions), depends solely on the volume fractions of the equilibrium phases ( $\phi$ ). With this in mind, various blends of the equilibrium phases with volume fractions of the GM-rich phase (i.e.,  $\phi_{GM} = 1, 20, 60, 80$  and  $99$  wt% dispersed in  $100 - \phi_{GM}$  wt% of the NaCAS-rich phase)

were prepared for the experiments. The equilibrium phases discussed below were prepared from two ATPS: (i) 4 wt% NaCAS-0.2 wt% LBG and (ii) 4 wt% NaCAS-0.2 wt% LBG-30% sucrose. Figure 6-2 shows the microstructures of the blends without sucrose (a-c) and at 30 wt% sucrose (d) on the basis of which  $\sigma$  were assessed on the effects of phase sense.

Based on the raw images, it was observed that certain microstructures performed better under the experimental conditions. They gave more consistent results, i.e., droplets were easily deformed and of the right size (big enough to be visible and small enough not to interact with the glass plates or the borders of the measuring cell). The GM-r-continuous emulsions ( $\varphi_{GM} > 80$  wt%, shown in Figure 6-2 d) were easily over-mixed, hence they readily formed a disperse phase with very small droplets ( $\sim 5$   $\mu\text{m}$  in diameter), too small to be sufficiently deformed and useful for the calculation of the interfacial tensions. Furthermore, the emulsions at  $20 < \varphi_{GM} < 60$  wt% produced bi-continuous systems. In such systems, given the absence of staining and the use of a b/w camera in image acquisition, it was not always clear which phase was continuous and which was dispersed. Besides, at  $\varphi_{GM} > 20$  wt%, droplet-droplet interactions were more likely to occur. In NaCAS-r-continuous emulsions of higher  $\varphi_{GM}$ , the continuous phase contained micron-sized GM-r-droplets (Figure 6-2 a), which readily coalesced with the bigger droplets during the retraction process. The droplets in the latter emulsions/blends also did not significantly increase in number as they did in size and polydispersity. Finally, by comparing images (b) and (c) in Figure 6-2, we could observe that at the same mixing condition, the systems with sugar appear to form

comparably smaller droplets. The formation of small droplets is likely a manifestation of higher viscosities and a difference in interfacial tension.

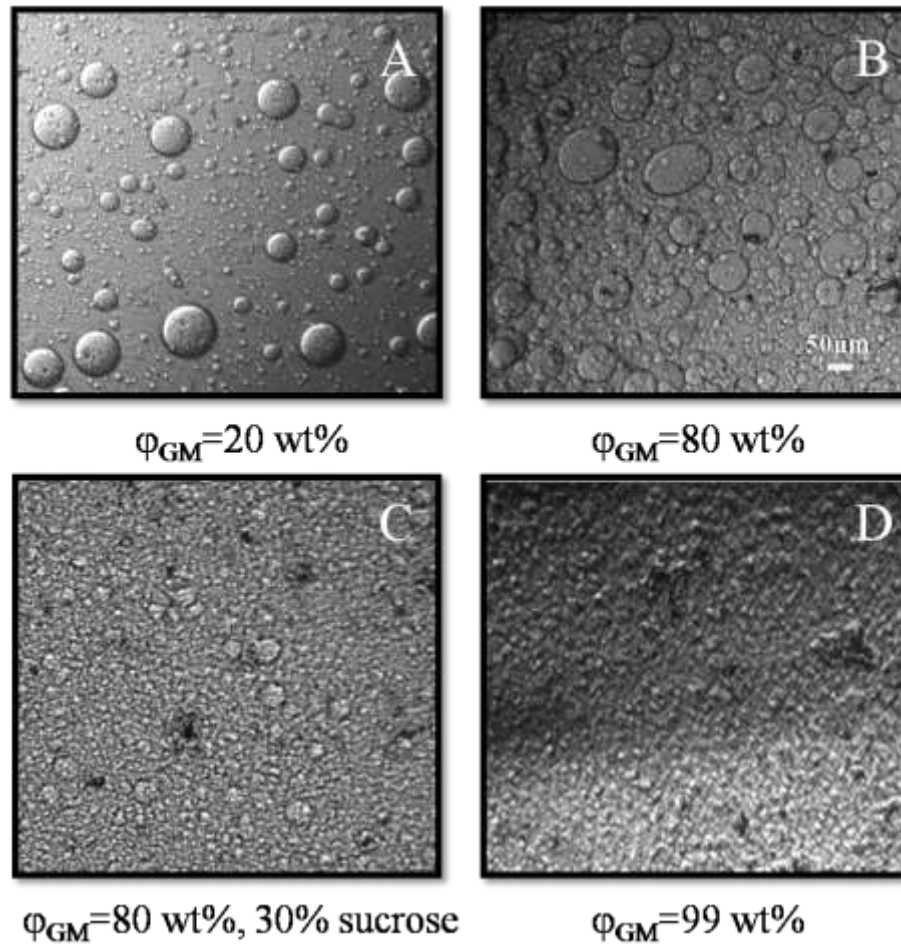


**Figure 6–2.** Light micrographs for (A) a sodium caseinate-continuous and (B–D) a locust bean gum-continuous systems after shear. Systems shown in micrographs A–C were prepared from the equilibrium phases of a 4 wt% sodium caseinate-0.2 wt% locust bean gum ATPS, and system shown in micrograph D were prepared from the equilibrium phases of a 4 wt% sodium caseinate-0.2 wt% locust bean gum-30% sucrose.

From a series of images, the time evolution of a droplet shape  $D$  was measured and the characteristic droplet deformation times  $\tau$  were calculated. The graphs in Figure 6–3 show semi-logarithmic droplet deformation plots ( $\ln D$  vs. time) for two disparate ATPS/blends fitted with linear regression. A difference in the kinetics of droplet retraction between the two microstructures, NaCAS-r-continuous

( $\varphi_{GM} = 20$  wt%) and GM-continuous ( $\varphi_{GM} = 80$  wt%), was observed for two different ATPS: (a) without sucrose and (b) with 30% sucrose. Figure 6–4 on the next page shows the blends of the ATPS without sucrose on the phase diagram.

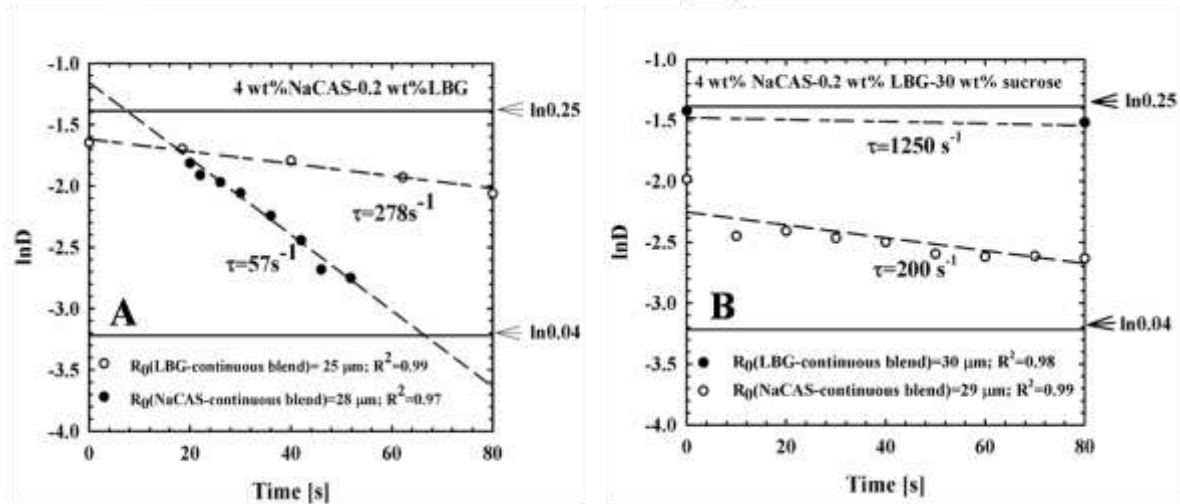


**Figure 6–3.** Differences in characteristic retraction times ( $\tau$ ) for two distinct microstructures. Graph (A) shows a system without sucrose, and graph (B) shows a system at 30 wt% sucrose. For each system, two drops were chosen: one droplet was chosen to show retraction in a sodium caseinate-continuous blend ( $\varphi_{GM} = 20$  wt%) and the other in a locust bean gum-continuous blend ( $\varphi_{GM} = 80$  wt%).

The retraction was  $\sim 5$ – $6$  times faster in the less viscous NaCAS-r-continuous systems than in the corresponding GM-r-continuous system. The exact value depended on the amount of sugar present. Regardless of the phase sense of the system, the retraction process occurred  $\sim 4$  times faster in the ATPS/blends without sugar and with a lower bulk viscosity. The characteristic droplet retraction times as shown in Figure 6–3 were used to calculate the  $\sigma$  of the blends (see § 3.3.3.3, eq. [3-20], p. 3–107).

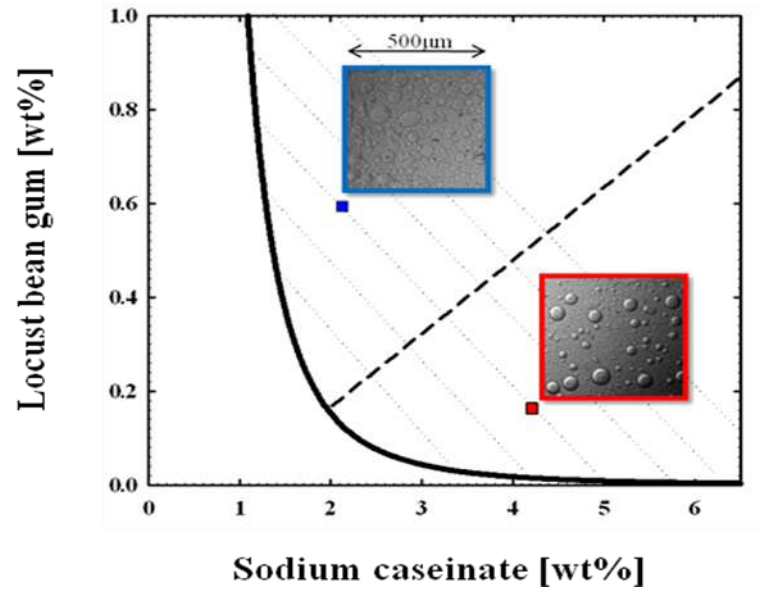


**Figure 6–4.** Two distinct microstructures shown on the phase diagram of a sodium caseinate-locust bean gum system without sugar.

Table 6–1 summarizes the calculated interfacial tensions of the NaCAS-LBG ATPS/blends (i) without sugar and (ii) at 30 wt% sucrose, and of two distinctly different morphologies, (i) NaCAS-r-continuous ( $\varphi_{GM}=20$  wt%) and (ii) LBG-r-continuous ( $\varphi_{GM}=60$  and 80 wt%). Although the execution of the droplet deformation method allows us to observe many droplets at the same time, it makes the recognition of the same droplet for the second or third time difficult, if not impossible. Hence, each  $\sigma$  value in Table 6–1 represents a measurement of a single droplet. A minimum of five different droplets per system were chosen to assess the reproducibility of the measurements. The apparent viscosities of the equilibrium phases taken in the calculation of  $\sigma$  are based on the actual apparent viscosity values at the shear rate of  $0.001\text{ s}^{-1}$ , rather than on theoretical extrapolated zero shear viscosities, due to the considerable error involved (Holdsworth, 1993).

**Table 6-1. Interfacial tensions of different blends ( $\varphi_{GM} = \varphi = 20, 60$  and  $80\%$ ) for a 4 wt% sodium caseinate-0.2 wt% locust bean gum system at 0% and 30% of sucrose. The table shows the viscosities of the equilibrium phases at the shear rate of  $0.001 \text{ s}^{-1}$  and their viscosity ratios ( $\lambda$ ).  $\eta_c$ = viscosity of the continuous phase,  $\eta_d$ =viscosity of the dispersed phase,  $R_0$ =radius of a retracted drop,  $\sigma$ =interfacial tension, and  $\tau$ =average retraction time.**

	NaCAS-continuous system				LBG-continuous system							
	0% sucrose		30% sucrose		0% sucrose				30% sucrose			
$\eta_c$	0.25		0.34		3.8				12.7			
$\eta_d$	3.8		12.7		0.25				0.34			
$\lambda$	15.3		37.4		0.07				0.03			
<i>i</i>	$\varphi=20\%$		$\varphi=20\%$		$\varphi=60\%$		$\varphi=80\%$		$\varphi=60\%$		$\varphi=80\%$	
	$R_0$ [ $\mu\text{m}$ ]	$\sigma$ [ $\mu\text{N/m}$ ]										
<i>1</i>	56	1,727.4	44	1120.2	45	1.2	38	0.63	46	0.3	29	1.4
<i>2</i>	56	1,409.6	45	976.4	24	1.0	29	0.57	41	0.6	26	1.4
<i>3</i>	65	1,862.0	45	1092.9	18	1.0	25	0.68	28	0.3	26	1.2
<i>4</i>	56	1,166.6	33	1113.7	18	1.0	27	0.55	30	0.4	24	0.8
<i>5</i>	64	1,064.8	46	1050.5	23	1.0	23	0.58	37	0.6	27	0.7
<i>6</i>					26	1.3	25	0.53			28	0.9
Avg	59 $\pm$ 4	1,446.1 $\pm$ 308.9	42 $\pm$ 5	1070.7 $\pm$ 53.1	26 $\pm$ 9	1.1 $\pm$ 0.2	28 $\pm$ 5	0.5 $\pm$ 0.9	37 $\pm$ 7	0.4 $\pm$ 0.1	26 $\pm$ 2	1.1 $\pm$ 0.3
$\tau_{avg}$	44 $\pm$ 10		561 $\pm$ 102		220 $\pm$ 48		260 $\pm$ 42		1480 $\pm$ 523		519 $\pm$ 93	

For both ATPS (one without sucrose and the other with 30% sucrose), the average  $\sigma$  observed for the blends on the same tie-line showed inconsistent results. The  $\sigma$  values of the NaCAS-r-continuous and LBG-r-continuous blends were expected to be the same, but instead the values for the blends in Table 6–1 vary by a factor of 1000. Although, as shown in Figure 6–3, the  $\tau$  for the systems differ (Figure 6–3), the difference is not sufficient for equal results. Furthermore, the  $\sigma$  values for the LBG-r-continuous blends ( $\varphi_{GM} = 60$  and  $80 \text{ wt}\%$ ) for both ATPS are too low to be true. The difference in interfacial tensions, however, was clearly manifested when the data for the blends of lower volume fractions ( $\varphi_{GM} = 1 \text{ wt}\%$ ) were reviewed (the results are given later in this chapter). There was no discrepancy between the results in NaCAS-r-continuous blends with  $\varphi_{GM} = 1 \text{ wt}\%$  and  $\varphi_{GM} = 20 \text{ wt}\%$  at 0% sucrose. However, a small

difference was found between the 30% sucrose blends, which could be the result of the formation of larger droplets and debris (i.e., small micron-sized droplets) during shear, or merely a reflection of poor dissolution.

There are various possible explanations of the above results. First, there could be droplet-droplet interaction due to dense packaging and limited space; the retraction of an observed droplet is thus controlled by the retractions of neighbouring droplets by a sort of a “chain reaction” and is indirectly controlled by the borders of the 1.5 ml measuring cell (i.e., parallel glass plates separated by a gap of 300  $\mu\text{m}$ ). Second, it is also possible that the blends are not GM/LBG-r-continuous and what was seen are densely packed GM/LBG-r droplets dispersed in a NaCAS-r-continuous phase.

Even though it could not be confirmed by the use of the modified droplet deformation method that  $\sigma$  in NaCAS-LBG systems is independent of its morphology, it was decided that the method provides satisfactory results for NaCAS-r-continuous blends at  $\varphi_{GM} < 20$  wt%. Hence, the results given later in this chapter were all obtained from blends at  $\varphi_{GM} = 1$  wt%, chosen to avoid droplet-droplet interactions.

### 6.2.3 Droplet shapes, sizes and shear

The drop retraction method assumes that the maximum shear rates to which ATPS are exposed do not affect the retraction process of the dispersed droplets and, as such, do not affect  $\sigma$ . The flow field, however, affects the droplet sizes and/or the extent of their deformation in flow, conditioned by their size. Because of the ultralow

$\sigma$  inherent to our systems, a variety of droplet shapes, by which droplets optimise their flow, was observed during shear (Figure 6–5). Tubular, biconcave, elliptical, spherical, triangular and other shapes were observed.

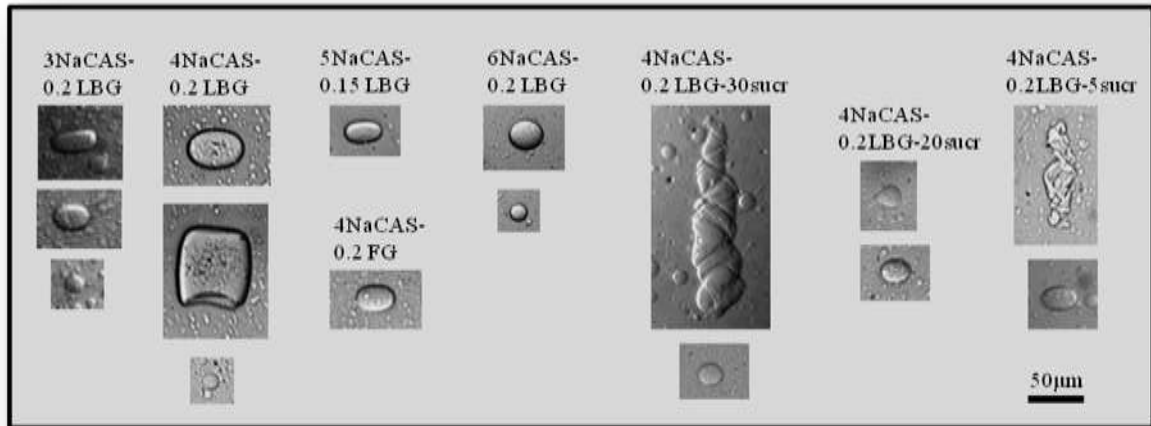


**Figure 6–5. Droplet shapes observed in shear for various aqueous two-phase systems. The concentration of the biopolymers is in weight percent.**

The shapes of the droplets depend on their size. Small ( $< 10 \mu\text{m}$ ) droplets stay in a stable spherical form, whereas larger ( $30\text{--}50 \mu\text{m}$ ) droplets assume ellipsoidal shapes under shear. At lower shears, larger ( $> 100 \mu\text{m}$ ) tubular formations were observed, but when sheared sufficiently, they were soon broken into either spherical or ellipsoid droplets. Various droplet shapes are stable under constant shear, where viscous forces are balanced with the interfacial forces and permeability of the interface (Scholten et al., 2005), but after the cessation of shear, in their relaxed state, all droplets are spherical. Molecules of one kind because of cohesive forces (i.e., surface/interfacial tension) between them tend to minimise surface area and hence form an interface of a spherical shape.

Regardless of the composition or phase sense of the blend, the average size of the droplets produced and used in measurements was approximately between 20 and

60  $\mu\text{m}$ , which is roughly 5–10 times smaller than the 300  $\mu\text{m}$  gap size used in the experiments. Droplet sizes were measured with the help of ImageJ program from micrographs obtained by means of optical reometry. The initial shear rates sufficient to produce and deform these droplets were  $\sim 700\text{--}900\text{ s}^{-1}$  for blends at  $\varphi_{GM} = 1\text{ wt}\%$ .

### **6.3 Interfacial tension in the sodium caseinate-galactomannan aqueous two-phase systems with sugar**

The following paragraphs review the interfacial tensions of NaCAS-GM ATPS on the effects of changing (i) NaCAS and GM concentrations, (ii) sugar concentrations, (iii) sugar type and (iv) GM type.

#### **6.3.1 Effect of the concentration of sodium caseinate and locust bean gum on the interfacial tension**

The effect of [NaCAS] and [GM] (concentration of NaCAS and GM), thus changing the [BP], is investigated for six different NaCAS-LBG ATPS in the absence of sugar. The concentrations of the studied systems are shown on a NaCAS-LBG phase diagram in terms of the percent total weight of the solution (Vossoughi, 1999) in Figure 6–6. Two of the ATPS were used to study the effects of a change in the [LBG] and other four to study the effects of a change in the [NaCAS].

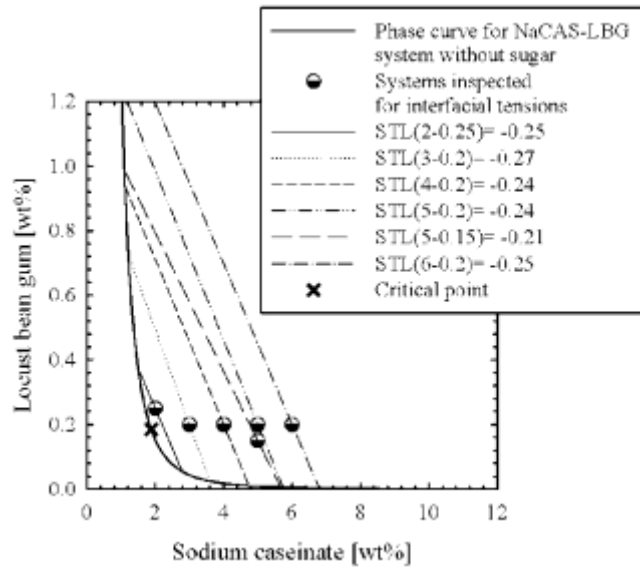


Figure 6–6. Phase diagram for a sodium caseinate-locust bean gum systems. Systems inspected for interfacial tensions are marked with "●". A critical point is marked with "x", a tie-line and its slope (STL) is given for each of the systems. The average slope of the tie-line is  $0.25 \pm 0.02$ .

The ATPS were selected so that each of them were on a different tie-line, thus both the compositions of the equilibrium phases and their volume fraction changed. The slopes of the tie-lines (STL) in Figure 6–6 were calculated from the experimental volume fractions ( $\phi$ ) of the investigated ATPS, which are listed in Table 6–2.

#### Physical properties of the equilibrium phases

The exact compositions of the ATPS and the volume fractions ( $\phi$ ), average viscosities ( $\eta_{\text{avg}}$ ) and densities ( $\rho$ ) of their equilibrium phases are given in Table 6–2.

Table 6–2. Compositions of the systems investigated at 20°C on the effects of individual biopolymer concentrations on interfacial tensions. The table also shows: volume fractions ( $\phi$ ), densities ( $\rho$ ), consistency constants (K), power law index (n), and average viscosities ( $\eta_{\text{avg}}$ ) of the individual equilibrium phases of investigated ATPS.

<i>i</i>	NaCAS [wt%]	LBG [wt%]	Equilibrium phases	$\phi$ [wt%]	$\rho$ [g/ml]	K	n	R <sup>2</sup>	$\eta_{\text{avg}}$ [Pa.s]	$\eta$ stdevp [Pa.s]
1	3	0.2	NaCAS-rich	75.08	0.9944	0.0053	1.06	0.50	0.0057	0.0007
			LBG-rich	24.92	0.9865	0.1101	0.99	0.80	0.110	0.003
2	4	0.2	NaCAS-rich	79.60	0.9999	0.0058	0.49	0.99	0.0074	0.0048
			LBG-rich	20.40	0.9912	0.6443	0.92	0.88	0.80	0.17
3	5	0.2	NaCAS-rich	84.30	1.0004	0.0016	1.22	0.34	0.0029	0.0022
			LBG-rich	15.70	0.9986	1.6039	0.88	0.95	2.65	1.05
4	6	0.2	NaCAS-rich	86.45	1.0046	0.0045	0.83	0.64	0.0049	0.0017
			LBG-rich	13.55	0.9998	4.4556	0.85	0.77	7.36	3.50
5	5	0.15	NaCAS-rich	85.35	1.0019	0.0072	0.74	0.94	0.0075	0.0027
			LBG-rich	14.65	0.9872	4.3908	0.84	0.98	5.66	2.01
6	2	0.25	NaCAS-rich	38.91	0.9920	0.0054	0.97	0.70	0.0054	0.0003
			LBG-rich	61.09	0.9838	5.488	0.84	0.76	7.13	2.84

Table 6–2 shows that increasing [NaCAS] or [LBG] in the ATPS increases the volume of the corresponding equilibrium phase. Hence, an increase in [NaCAS] in the system results in a larger and denser NaCAS-r phase, and a smaller and less dense LBG-r phase. On the other hand, an increase in [LBG] (conclusion is made based on the measurement of only two different systems) reduces the volume fraction and density of the NaCAS-r phase and increases both parameters in the LBG-r phase. Although both equilibrium phases contain mainly water and have very similar densities the NaCAS-r phase is always denser.

The viscosities of the equilibrium phases, the most influential physical parameter determining the interfacial properties of an ATPS, are given in their raw form in Figure 6–7. NaCAS gives solutions with very low viscosities, whereas LBG gives much more viscous solutions. The viscosity ratio ( $\lambda$ ) is high. The average viscosity values ( $\eta_{\text{avg}}$ ) were calculated for the shear rate range of 0.001–10 s<sup>-1</sup> and are given in Table 6–2. The selection of the shear rates for the calculation was based on the first Newtonian plateau observed for the LBG-r (GM-r/top) equilibrium phases as this was most viscous phase.

A power law model in eq. [6-1], a popular two-parameter model used to describe the flow of time-independent foodstuffs (i.e., milk and other hydrocolloids) (Holdsworth, 1993), was also fitted to the viscosity data in this shear rate range.

$$\eta = K \dot{\gamma}^{n-1} \Rightarrow \log_{10} \eta = \log_{10} K + (n-1) \log_{10} \dot{\gamma} \quad [6-1]$$

where  $\eta$  is the apparent viscosity in Pa.s, K is the consistency factor in  $\frac{Ns^n}{m^2}$  (for n=1, K= $\eta$ ) and n is a flow behaviour index that enables us to classify the equilibrium phases

in terms of the degree of Newtonian behaviour ( $n=0.95-1.05$  is Newtonian).  $K$  is the viscosity (or stress) at shear rate of  $1 \text{ s}^{-1}$ . The values  $K$  and  $n$  are dependent upon each other. They also depend on the temperature and concentration of the system.

For the LBG-r/top phase, the  $K$  vs.  $n$  plots show an exponential decay relationship; i.e., larger  $[\text{NaCAS}]$  or  $[\text{LBG}]$  led to a reduction in the values of  $K$  and  $n$ . For the NaCAS-r/bottom phase, the relationship was likely to be linear (the poor fit is a result of unreliable data for the shear rate range  $< 0.5 \text{ s}^{-1}$ ), following the same concentration-related pattern. The same procedure was also followed for other systems described later in this chapter.

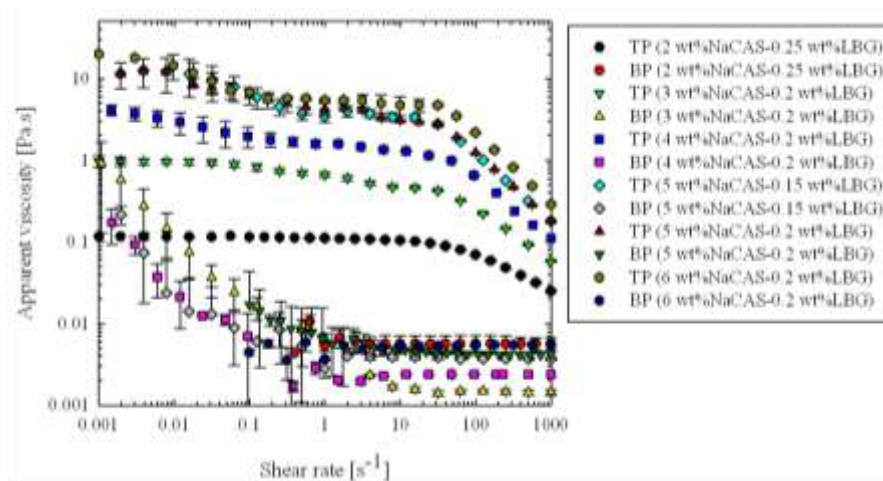


**Figure 6–7. Log-log apparent viscosities of the top (TP) and bottom (BP) equilibrium phases for sodium caseinate-locust bean gum (NaCAS-LBG) ATPS investigated for the effect of the concentration of biopolymers on the interfacial tension.**

Although the biopolymers are known to be non-Newtonian shear thinning, for the selected and limited shear rate range, they can be regarded as Newtonian to weakly non-Newtonian. As seen in Table 6–2, the flow behaviour index ( $n$ ) for the LBG-r/top phase varied from 0.84–0.99; the small deviations from ideal behaviour ( $n=1$ ) in the range were possibly due to its high structure, i.e., the intrinsic molecular microstructure and the emulsion like microstructure. While the NaCAS-r/bottom phases in the

investigated concentrations expected to be Newtonian, the flow behaviour index showed inconsistent results:  $n=0.49-1.22$ . Larger deviations in the  $n$  values for the bottom phases could be attributed to the low  $\eta$  of these samples, which were close to the resolution of the instrument (1 nNm torque resolution). Overall, the high average values of  $n$  sufficiently justify the choice of the modified droplet deformation method that assumes Newtonian behaviour of both phases. Due to the abovementioned inconsistencies in the degree of Newtonian behaviour, though, the  $\sigma$  were calculated at apparent viscosities at the shear rates of  $0.001 \text{ s}^{-1}$  and  $0.5 \text{ s}^{-1}$ .

#### Calculation of interfacial tensions

After establishing the physical properties of the phases, the interfacial tensions  $\sigma$  were calculated from the deformation parameter  $D$ , as described in § 3.3.3.3 (p. 3–106). An example of the raw data from which the characteristic retraction times ( $\tau$ ) were calculated by fitting linear regression in semi-log coordinates is given in Figure 6–8 for the 4 wt%NaCAS-0.2 wt% LBG ATPS. The experimental data fit the straight lines well ( $R^2>0.94$ ).

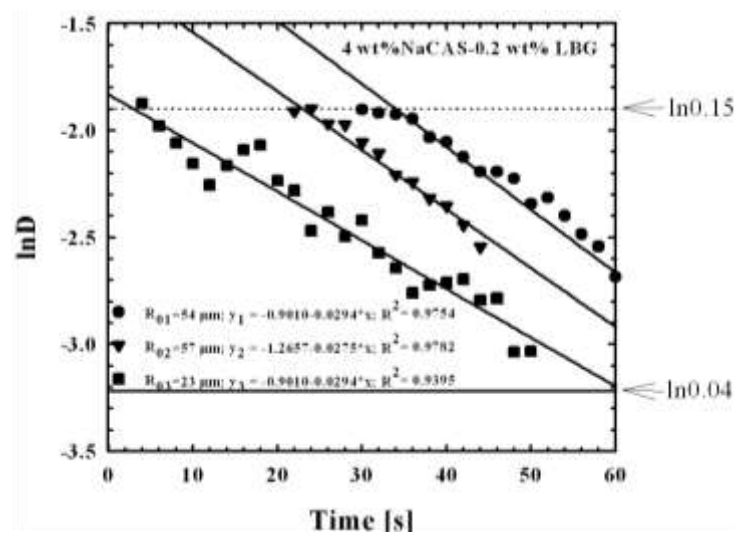
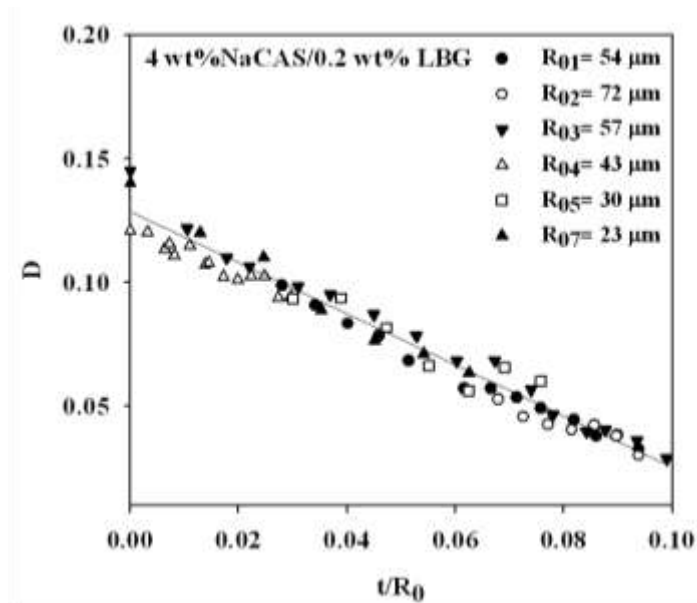


Figure 6–8. Semi logarithmic plot of the deformation parameter ( $D$ ) as a function of time with linear regression for a 4 wt% sodium caseinate-0.2 wt% locust bean gum ATPS at  $\phi=1 \text{ wt}\%$ .  $R_0$ =radius of a retracted droplet.  $\phi$ = volume fraction of the locust bean gum-rich phase.

As mentioned earlier in § 6.2.2 (p. 6–191) here and for the rest of this chapter,  $\tau$  was calculated for each droplet. In each system, at least five different droplets were taken to calculate the corresponding values of  $\tau$ . If the linear regressions fitted to the data ( $\ln D$  vs. time) for each drop are close to parallel, the standard deviation error of  $\tau$  will be small (Figure 6–8).

Although the relaxation time of differently sized droplets is different, i.e., at the same point in time, differently sized droplets are deformed to a different extent, the normalisation of the  $D$  values for  $R_0$  ( $R$  of the retracted droplet) and time brings all data points to the same line (Figure 6–9). The slope of this line is  $-\frac{1}{\tau}$  and, for small deformations, is not affected by droplet size.



**Figure 6–9.** Deformation parameter ( $D$ ) as a function of  $t/R_0$  for a 4 wt% sodium caseinate-0.2 wt% locust bean gum ATPS.

#### Effect of total biopolymer concentration on the interfacial tension: results

Table 6–3 and Table 6–4 summarise the apparent shear viscosities of the equilibrium phases, droplet radii ( $R_0$ ) and calculated  $\sigma$  for six different ATPS, which

differ in the total amount of the biopolymer they contain and are hence positioned on the phase diagram on different tie-lines.

**Table 6–3.** Calculated interfacial tensions ( $\sigma$ ) and their averaged values for the sodium caseinate-locust bean gum (NaCAS-LBG) ATPS of various concentrations. The table also gives the radii of the droplets ( $R_0$ ) from which the interfacial tensions were calculated, the apparent viscosities ( $\eta$ ) of the equilibrium phases given for a shear rate of  $0.001 \text{ s}^{-1}$  and a temperature of  $20^\circ\text{C}$ , as well as the corresponding viscosity ratios ( $\lambda$ ).

	2 wt% NaCAS/ 0.25 wt% LBG		3 wt% NaCAS/ 0.2 wt% LBG		4 wt% NaCAS/ 0.2 wt% LBG		5 wt% NaCAS/ 0.15 wt% LBG		5 wt% NaCAS/ 0.2 wt% LBG		6 wt% NaCAS/ 0.2 wt% LBG	
$\eta(\text{NaCAS})$	0.07 Pa.s		0.86 Pa.s		0.25 Pa.s		0.56 Pa.s		0.86 Pa.s		1 Pa.s	
$\eta(\text{LBG})$	0.17 Pa.s		1.02 Pa.s		3.8 Pa.s		13 Pa.s		16 Pa.s		20 Pa.s	
$\lambda$	2.37		1.2		15.3		23.2		18.6		20	
$i$	$R_{0i}$ [ $\mu\text{m}$ ]	$\sigma_i$ [ $\mu\text{N/m}$ ]										
1	125	1.2	22	3.0	54	1,720	21	584	26	2,975	40	2,251
2	80	0.9	25	4.2	72	1,657	19	834	24	1,638	41	2,417
3	86	0.8	25	3.4	57	2,077	21	1323	37	3,448	42	4,165
4	22	1.4	27	3.2	43	1,190	19	695	28	2,659	28	6,120
5	22	1.4	28	5.5	30	646	18	1185	26	2,189	23	3,895
6	24	1.7	30	3.1					20	2,015		
7	38	1.9	25	4.0					23	2,166		
8	26	1.9										
$\sigma_{\text{avg}}$	1.4 $\pm$ 0.4		3.8 $\pm$ 0.8		1,458 $\pm$ 495		924 $\pm$ 284		2,441 $\pm$ 575		3,769 $\pm$ 1402	

**Table 6-4.** Calculated interfacial tensions ( $\sigma$ ) and their averaged values for the sodium caseinate-locust bean gum (NaCAS-LBG) ATPS of various concentrations. The table also gives the radii of the droplets ( $R_0$ ) from which the interfacial tensions were calculated, the apparent viscosities ( $\eta$ ) of the equilibrium phases given for a shear rate of  $0.5 \text{ s}^{-1}$  and a temperature of  $20^\circ\text{C}$ , as well as the corresponding viscosity ratios ( $\lambda$ ).

	2 wt% NaCAS/ 0.25 wt% LBG		3 wt% NaCAS/ 0.2 wt% LBG		4 wt% NaCAS/ 0.2 wt% LBG		5 wt% NaCAS/ 0.15 wt% LBG		5 wt% NaCAS/ 0.2 wt% LBG		6 wt% NaCAS/ 0.2 wt% LBG	
$\eta(\text{NaCAS})$	0.012 Pa.s		0.01 Pa.s		0.006 Pa.s		0.008 Pa.s		0.0086 Pa.s		0.009 Pa.s	
$\eta(\text{LBG})$	0.113 Pa.s		0.713 Pa.s		1.7 Pa.s		3.9 Pa.s		4.5 Pa.s		6 Pa.s	
$\lambda$	9.42		71.3		283.3		487.5		523.3		666.7	
$i$	$R_{0i}$ [ $\mu\text{m}$ ]	$\sigma_i$ [ $\mu\text{N/m}$ ]	$R_{0i}$ [ $\mu\text{m}$ ]	$\sigma_i$ [ $\mu\text{N/m}$ ]	$R_{0i}$ [ $\mu\text{m}$ ]	$\sigma_i$ [ $\mu\text{N/m}$ ]	$R_{0i}$ [ $\mu\text{m}$ ]	$\sigma_i$ [ $\mu\text{N/m}$ ]	$R_{0i}$ [ $\mu\text{m}$ ]	$\sigma_i$ [ $\mu\text{N/m}$ ]	$R_{0i}$ [ $\mu\text{m}$ ]	$\sigma_i$ [ $\mu\text{N/m}$ ]
1	125	5.3	22	939	54	870,335	21	67,628	26	671,571	40	641,120
2	80	4.3	25	1,329	72	838,496	19	96,521	24	369,818	41	688,453
3	86	3.6	25	1,070	57	1,051,288	21	153,179	37	778,252	42	1,186,115
4	22	6.2	27	1,008	43	602,148	19	80,480	28	600,157	28	1,742,871
5	22	6.5	28	1,731	30	327,051	18	137,132	26	494,235	23	1,109,153
6	24	7.8	30	961					20	454,883		
7	38	8.5	25	1,243					23	488,960		
8	26	8.5										
$\sigma_{\text{avg}}$	6.3 $\pm$ 1.8		1,183 $\pm$ 261		737,864 $\pm$ 298,501		106,988 $\pm$ 32,874		551,125 $\pm$ 129,688		1,073,543 $\pm$ 399,305	

Regardless of the apparent shear viscosities used to calculate the  $\sigma$ , the increase in the [BP] ([NaCAS] and [LBG]) brings about an increase in the  $\sigma$  of the systems. The use of different shear viscosities in the calculation of  $\sigma$  clearly changes its absolute values, but by no means changes the relationships between  $\sigma$  of the investigated systems. From the phase diagram (Figure 6–6) and  $\sigma$  vs. TLL plot (Figure 6–10), it can be observed that systems positioned in a phase diagram, further from its critical point, have higher  $\sigma$  and lie on a longer tie-line than the systems that are closer to the critical point. The distance of the ATPS from the critical point relates well with the TLL; in fact, it is almost identical (data not shown).

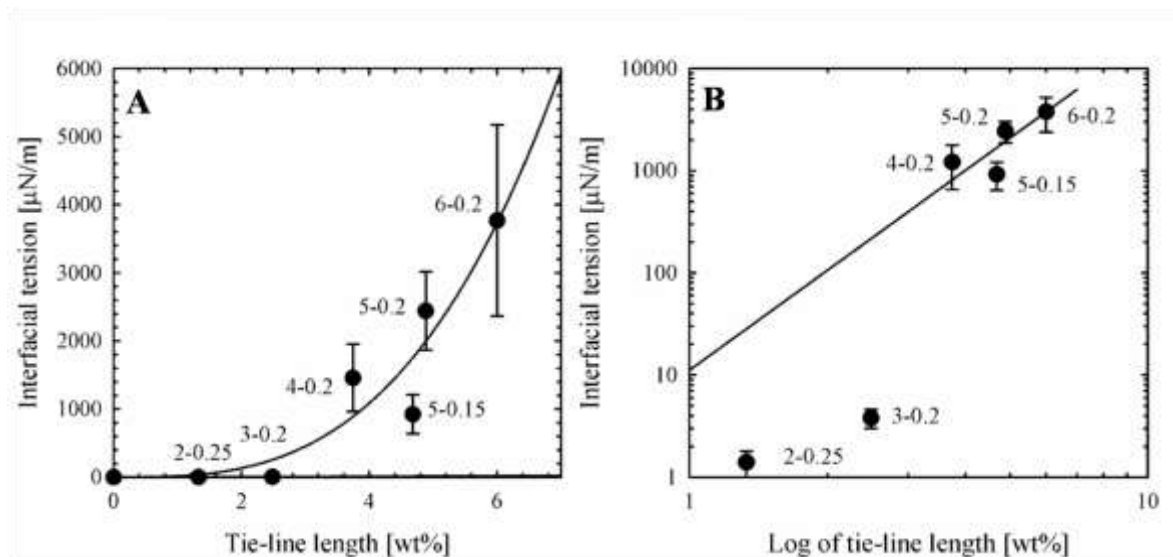


**Figure 6–10.** Interfacial tensions in sodium caseinate-locust bean gum ATPS as a function of the tie-line length (A). The log-log plot (B) gives a straight line.

Figure 6–11 plots the  $\sigma$  as a function of  $\Delta[\text{NaCAS}]$ , and  $\Delta[\text{LBG}]$ . The error bars are a fair representation of the experimental difficulties encountered with more concentrated systems, where the interfaces were less elastic and harder to deform in flow.

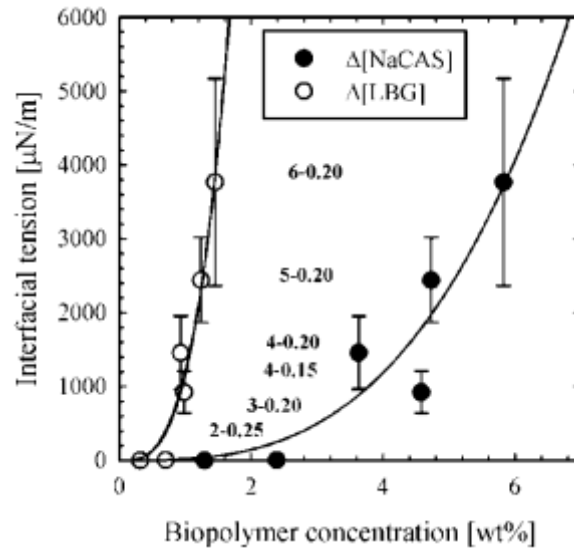


**Figure 6–11.** Interfacial tensions in sodium-caseinate and locust bean gum (NaCAS-LBG) ATPS of varied concentrations as a function of NaCAS ( $\Delta[\text{NaCAS}]$ , marked with "●") and LBG ( $\Delta[\text{LBG}]$ , marked with "○") concentration differences between the phases. The concentrations of the ATPS are given in weight %.

The interfacial tension data  $\sigma$  were fitted with a two-parameter power law equation (Figure 6–10 a and Figure 6–11), which in log-log coordinates gives a linear line of best fit (Figure 6–10 b). The power law function ( $y = ax^b$ ) was used, because it best fits the data ( $R^2 > 0.90$ ), and because the function goes through a critical point (0,0) where both the TLL and the interfacial tension are 0. Furthermore, this equation is universally used to describe natural phenomena and is easy to work with, in both the exponential and linear forms. For the above data, the following mathematical functions were obtained:

$$\sigma = 16.0412 \times TLL^{3.0414}; R^2 = 0.8987; R = 0.9480 \quad [6-2]$$

$$\sigma = 1233.9421 \times \Delta[\text{LBG}]^{3.0428}; R^2 = 0.9565; R = 0.9780 \quad [6-3]$$

$$\sigma = 17.9117 \times \Delta[\text{NaCAS}]^{3.0281}; R^2 = 0.8743; R = 0.9350 \quad [6-4]$$

where  $\sigma$  is the interfacial tension, TLL is the tie-line length, and  $\Delta[\text{NaCAS}]$  and  $\Delta[\text{LBG}]$

are the differences in the concentrations of NaCAS and LBG between the equilibrium phases, respectively.

Any of the abovementioned parameters (TLL,  $\Delta[\text{NaCAS}]$  and  $\Delta[\text{LBG}]$ ) can be used to mathematically describe the relationship between  $\sigma$  and the composition of the system. In the above equations, the exponent (constant  $b$  and also the slope of the linear log-log function) characterises the dependency of the parameters on  $\sigma$ , which seems to be inherent to these systems. In addition, constant  $b$  indicates how flat the curve describing the relationship is, i.e., how parallel to the x-axis it is. The constant  $a$  shows how close the function is to the y-axis (i.e., the point from which the curve “hangs”) and differs between the equations.

The constants  $a$  describing the relationship of  $\sigma$  with TLL and  $\Delta[\text{NaCAS}]$  were similar, but there was a 100-fold difference between the constant  $a$  and the parameters describing the relationship of  $\sigma$  with  $\Delta[\text{LBG}]$ . Smaller changes in  $\Delta[\text{LBG}]$ , therefore, affect  $\sigma$  more, i.e., they are reflected in a steeper change. The effect of [LBG] on  $\sigma$  is also seen graphically in Figures 6-10 a and 6-11, where the data point for system 4-0.15 is somewhat out of line and might be better left out when fitting a curve. Further inspection of, for example, systems: "2-0.15", "5-0.15", etc., would, however, confirm that for certain. Support for the above claim that LBG has a significant effect on the  $\sigma$  of a NaCAS-GM ATPS has been provided by a study on the effect of high molecular weight neutral carbohydrates, such as dextran and maltodextrin, on the surface activity of a globular protein (11S globulin) by Antipova and Semenova (1997). They showed that

neutral polysaccharides (much like LBG and other GMs) influence the surface/interfacial activity of proteins by means of excluded volume. Thermodynamic studies ( $A_{23} > 0$ ) of the systems show that the volume of the aqueous medium occupied by a neutral biopolymer cannot be occupied by the protein; hence, more protein molecules are pushed into the adsorbing layer where they increase the interfacial pressure, which causes an increase in the protein surface activity. The larger the  $M_w$  of the polysaccharide, the greater the effect. Furthermore, a greater concentration of protein amounts to a greater number of the molecules at the interface and hence an increase in  $\sigma$ . To conclude, the difference in the constant  $a$  refers in eq. [6-3] to the difference in thermodynamic incompatibility between NaCAS and LBG, whereas the similarity of constants  $a$  and  $b$  in equations [6-2] and [6-4] exposes a close connection between  $\sigma$  and (i) the phase behaviour of the systems as well as (ii) the important role that NaCAS plays on it.

### **6.3.2 Effect of sucrose concentration on the interfacial tension**

In this section the effect of sucrose concentration on  $\sigma$  is investigated for four NaCAS-LBG ATPS. The ATPS have the same biopolymer composition, but differ in the amount of sucrose (i.e., 5, 15, 20 and 30%, as shown in Figure 6-12).

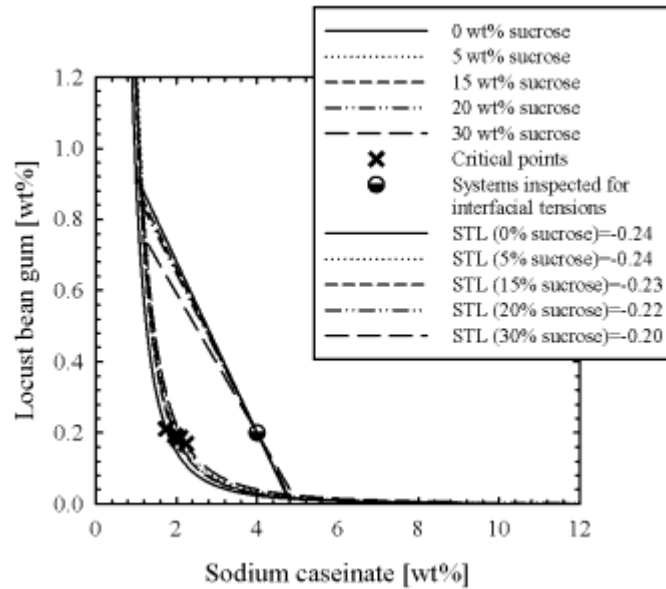


Figure 6–12. Phase diagrams of sodium caseinate-locust bean gum-sucrose systems. Systems inspected for interfacial tensions are marked with "●" and critical points with "X", a tie-line as well as its slope (STL) is calculated for each of the ATPS.  $STL_{avg} = -0.24 \pm 0.02$ .

### Physical properties of the equilibrium phases

The physical properties of the equilibrium phases of the systems are reviewed in Table 6–5. The raw viscosity data, on the basis of which the viscosities of the separated equilibrium phases were chosen and power law parameters calculated, are shown in Figure 6–13.

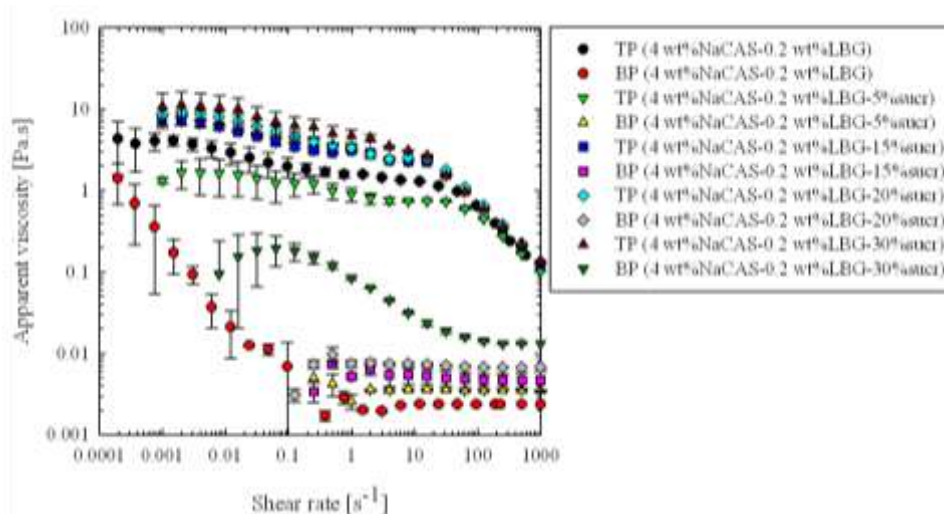


Figure 6–13. Log-log plots of apparent viscosities of the top (TP, LBG-rich=locust bean gum-rich) and bottom (BP, NaCAS-rich=sodium caseinate-rich) phases of the ATPS investigated for the effects of sucrose concentration.

Besides providing the relevant physical properties of the equilibrium phases, Figure 6–13 also demonstrates the difference in flow between low sucrose (< 20%) and high sucrose (> 20%) equilibrium phases. The effect of a large amount of sucrose is especially evident in the flow pattern of the NaCAS-r (bottom) phases and manifests itself as an obvious increase in viscosity. It is evident, however, that the increase in sucrose concentration also elevates the viscosities of both phases. The only exception is the LBG-r phase of the 5 wt% sucrose ATPS, where the measured viscosity of the phase appears to be smaller than that of the reference ATPS. As shown by Richardson et al. (1998), this is most likely a manifestation of a reduced level of biopolymer-biopolymer association (especially noticeable for LBG) due to improved solvent quality.

In Table 6–5, the viscosity of these ATPS is assessed on the degree of Newtonian behaviour. The results are summarised together with other physical properties of the equilibrium phases. In the shear rate range of  $10\text{--}0.001\text{ s}^{-1}$  (a shear rate range where the data are fitted with the power law equation), the equilibrium phases exhibit weakly Newtonian behaviour.

**Table 6–5. Compositions of a 4 wt% sodium caseinate-0.2 wt% locust bean gum-sucrose ATPS investigated at 20°C for the effects of sucrose concentrations on the interfacial tension. The table shows: volume fractions ( $\phi$ ), densities ( $\rho$ ), consistency constants ( $K$ ), the power law index ( $n$ ) and average viscosities ( $\eta_{\text{avg}}$ ) of the individual equilibrium phases of the investigated ATPS.**

<i>i</i>	NaCAS [wt%]	LBG [wt%]	Sucrose [wt%]	Equilibrium phases	$\phi$ [%]	$\rho$ [g/ml]	$k$	$n$	$R^2$	$\eta_{\text{avg}}$ [Pa.s]	$\eta_{\text{stdevp}}$ [Pa.s]
1	4	0.2	0	NaCAS-rich	79.60	1.000±0.032	0.0024	0.89	0.27	0.1775	0.3676
				LBG-rich	20.40	0.991±0.030	1.6039	0.88	0.95	2.6494	1.0506
2	4	0.2	5	NaCAS-rich	79.76	0.9731±0.0027	0.0039	0.94	0.72	0.1951	0.3713
				LBG-rich	20.24	0.9678±0.0029	0.9485	0.91	0.82	1.2201	0.3261
3	4	0.2	15	NaCAS-rich	78.57	1.060±0.034	0.0062	0.92	0.33	0.1976	0.3680
				LBG-rich	21.43	1.054±0.034	2.8347	0.86	0.97	4.3869	1.7691
4	4	0.2	20	NaCAS-rich	77.95	1.06995±0.0001	0.0083	0.92	0.49	0.1950	0.3609
				LBG-rich	22.05	1.0324±0.0004	3.365	0.84	0.96	5.4298	2.3410
5	4	0.2	30	NaCAS-rich	75.18	1.119±0.045	0.0777	0.85	0.51	0.1417	0.0947
				LBG-rich	24.82	1.116±0.045	4.7159	0.86	0.95	7.5559	2.7072

An increased sucrose concentration increases the densities of the phases and slightly increases the density differences between them.

The phase behaviour is also altered by the sucrose concentration. An increase in the sucrose concentration caused a decrease in the  $\varphi_{NaCAS}$ , as opposed to an increase in the  $\varphi_{GM}$ .

#### Calculation of interfacial tensions

As previously described in § 6.3.1 (p. 3–199), a droplet deformation parameter in each of the ATPS as a function of time was plotted for a number of droplets. Figure 6–14 gives an example of the retraction of three droplets in a system with 5 wt% sucrose. For each system, a minimum of five approximately parallel plots was chosen for the calculation of the characteristic droplet retraction times ( $\tau$ ) and, consequently,  $\sigma$ .

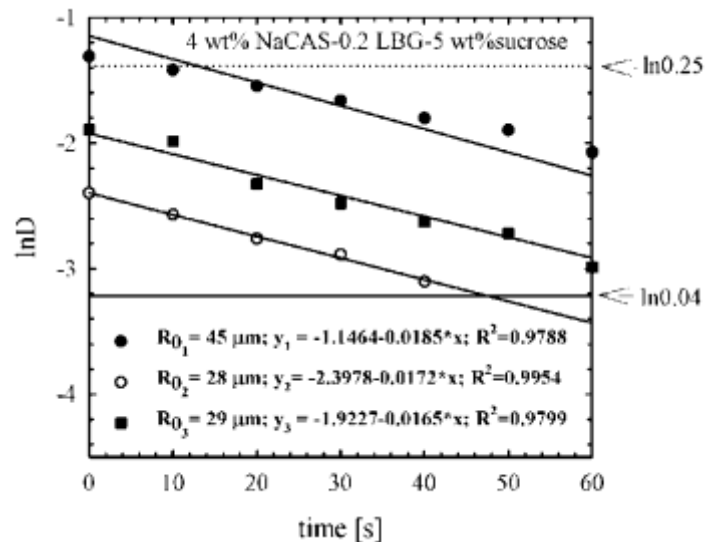


**Figure 6–14.** Semi-logarithmic plot of the deformation parameter ( $D$ ) as a function of time with linear regression for a 4 wt% sodium-caseinate-0.2 wt% locust bean gum-5% sucrose ATPS at  $\varphi=1$  wt%.  $R_0$ =radius of a retracted droplet;  $\varphi$ =volume fraction of the locust bean gum-rich phase.

The calculated  $\sigma$  values of the ATPS with sucrose are compared with those of the reference ATPS without sucrose in Table 6-6 and Table 6-7. The results differed due to different viscosities taken in the calculation. Because droplets at rest are not exposed to substantial shear, an optimal viscosity was, as mentioned in 6.2.2 (p. 6-191) and 6.3.1 (p. 6-199), chosen at the lowest shear rate, where the viscosity data of both of the phases could still be trusted and deduced with some confidence ( $0.001 \text{ s}^{-1}$ ). In this way, an extrapolation to a theoretical zero shear, a possible source of large error, to obtain zero shear viscosities ( $\eta_0$ ) is avoided. For comparison, as previously discussed in this chapter,  $\sigma$  is also reported when the viscosity at a shear rate of  $0.5 \text{ s}^{-1}$  was considered in the calculation. Although  $\sigma$  calculated from different viscosities differed, their average values followed the same pattern.

**Table 6–6.** Calculated interfacial tensions for the 4 wt% sodium caseinate-0.2 wt% locust bean gum (NaCAS-LBG) ATPS at different sucrose concentrations. The table also gives the radii of the droplets ( $R_0$ ) from which the interfacial tensions were calculated, the apparent viscosity of the equilibrium phases at the shear rate of  $0.001 \text{ s}^{-1}$  and  $20^\circ\text{C}(\eta)$ , as well as the viscosity ratio ( $\lambda$ ).

	0 wt% sucrose		5 wt% sucrose		15 wt% sucrose		20 wt% sucrose		30 wt% sucrose	
$\eta(\text{NaCAS})$	0.25 Pa.s		0.26 Pa.s		0.275 Pa.s		0.35 Pa.s		1 Pa.s	
$\eta(\text{LBG})$	3.8 Pa.s		3.1 Pa.s		7.4 Pa.s		8 Pa.s		10 Pa.s	
$\lambda$	15.2		11.9		26.9		22.9		10	
$I$	$R_{0i}$ [ $\mu\text{m}$ ]	$\sigma_i$ [ $\mu\text{N/m}$ ]								
1	54	1,720	30	123	29	699	16	629	27	115
2	72	1,657	29	221	27	630	18	539	20	82
3	57	2,077	30	80	22	591	27	572	21	29
4	43	1,190	29	81	21	644	29	566	21	73
5	30	646	30	184	26	529	29	617	22	52
6			38	202	22	627	27	631	33	121
7									29	226
$\sigma_{\text{avg}}$	1,458 $\pm$ 459		148 $\pm$ 57		620 $\pm$ 52		592 $\pm$ 35		100 $\pm$ 60	

**Table 6-7.** Calculated interfacial tensions for the 4 wt% sodium caseinate-0.2 wt% locust bean gum (NaCAS-LBG) ATPS with different sucrose concentrations. The table also gives the radii of the droplets ( $R_0$ ) from which the interfacial tensions were calculated, the apparent viscosity of the equilibrium phases at the shear rate of  $0.5 \text{ s}^{-1}$  and  $20^\circ\text{C}(\eta)$ , as well as the viscosity ratio ( $\lambda$ ).

	0 wt% sucrose		5 wt% sucrose		15 wt% sucrose		20 wt% sucrose		30 wt% sucrose	
$\eta(\text{NaCAS})$	0.003 Pa.s		0.005 Pa.s		0.006 Pa.s		0.01 Pa.s		0.13 Pa.s	
$\eta(\text{LBG})$	1.7 Pa.s		1.1 Pa.s		2.9 Pa.s		3.6 Pa.s		5.25 Pa.s	
$\lambda$	566.7		220		483.3		360		40.4	
$i$	$R_{0i}$ [ $\mu\text{m}$ ]	$\sigma_i$ [ $\mu\text{N/m}$ ]								
1	54	870,335	30	11,538	29	78,773	16	61,495	27	803
2	72	838,496	29	20,706	27	71,032	18	52,647	20	1,086
3	57	1,051,288	30	7,470	22	66,578	27	55,891	21	748
4	43	602,148	29	7,591	21	72,640	29	55,292	21	154
5	30	327,051	30	17,266	26	59,590	29	60,270	22	823
6			38	18,974	22	70,715	27	61,665	33	1,473
7									29	1,259
$\sigma_{\text{avg}}$	737,864 $\pm$ 298,501		13,924 $\pm$ 5,325		69,888 $\pm$ 5,852		57,877 $\pm$ 3,443		1,105 $\pm$ 304	

When compared to the reference system without sucrose,  $\sigma$  in the presence of sucrose decreased. More specifically, the decrease followed a trend: ref=0% > 15% > 20% > 5% > 30% sucrose.

Similar to the previous section, a mathematical description of the relationship

between  $\sigma$  TLL and the compositions of the equilibrium phases of ATPS with varied sucrose concentrations was assessed using nonlinear regression. Figure 6–15 plots the interfacial tensions  $\sigma$  for the ATPS TLL on a linear scale (right) and a log-log scale (left), and Figure 6–16 shows the relationships of  $\sigma$  with the compositions of the equilibrium phases.

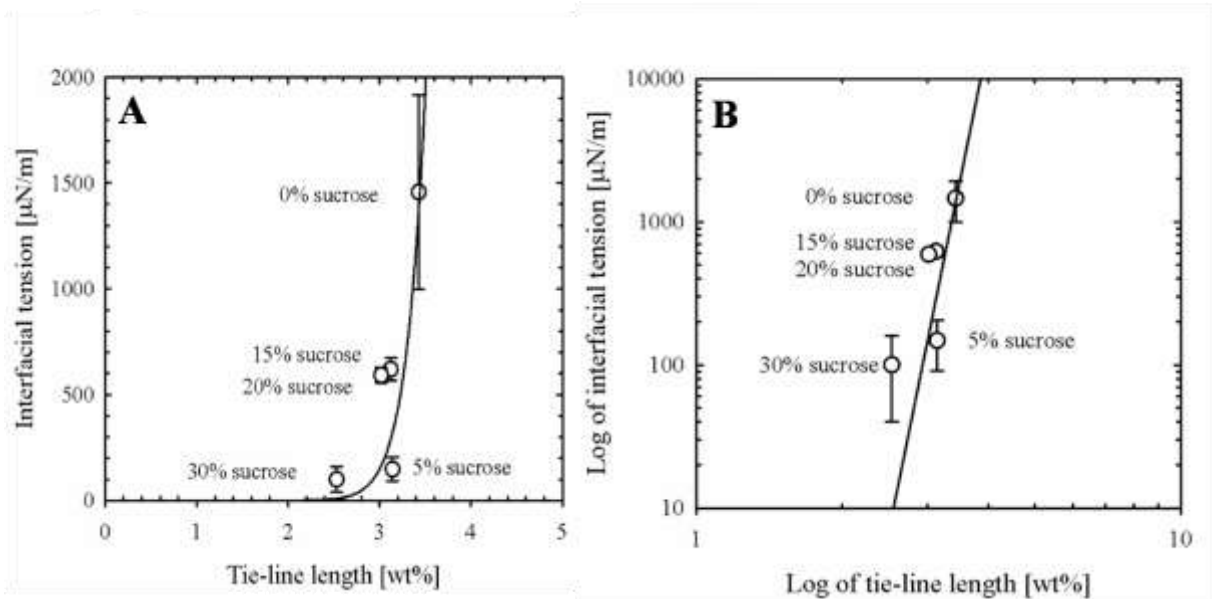


Figure 6–15. Interfacial tension for a sodium caseinate-locust bean gum-sucrose ATPS as a function of the tie-line length (A). The log-log plot (B) gives a straight line.

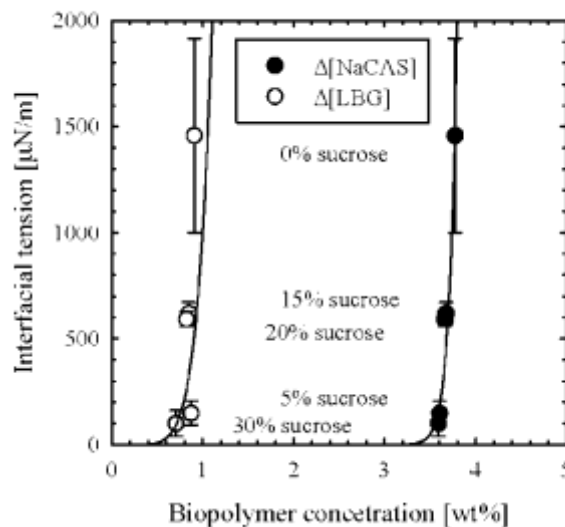


Figure 6–16. Interfacial tension for a 4 wt% sodium caseinate-0.2 wt% locust bean gum-sucrose (NaCAS-LBG-sucrose) ATPS as a function of the NaCAS ( $\Delta[\text{NaCAS}]$ , marked with "●") and LBG ( $\Delta[\text{LBG}]$ , marked with "○") concentration difference between the phases.

The following best fit equations were obtained:

$$\sigma = 1.6E - 6 \times TLL^{16.6721}; R^2 = 0.5487; R=0.7408 \quad [6-5]$$

$$\sigma = 1012.074 \times \Delta[LBG]^{6.8834}; R^2 = 0.2292; R=0.4788 \quad [6-6]$$

$$\sigma = 7E - 24 \times \Delta[NaCAS]^{45.6591}; R^2 = 0.9069; R=0.9523 \quad [6-7]$$

where  $\sigma$  is the interfacial tension, TLL is the tie-line length,  $\Delta[NaCAS]$  is the change in the concentration of NaCAS between the equilibrium phases and  $\Delta[LBG]$  is the difference in the concentration of LBG between the equilibrium phases.

In contrast to the findings in the previous section, the data give a poorer fit (see equations [6-5]–[6-6]). This is likely caused by the significantly different  $\sigma$  of the system with 5 wt% sucrose and the relative uncertainty of the position of the miscibility boundary in relation to the systems with 15 and 20 wt% sucrose. The reason why this system behaved differently compared to the others can be attributed to a significant effect of moderate amounts of sucrose on LBG, previously acknowledged by Richardson et al. (1998). These authors claim that a moderate amount of sucrose (< 10%) changes the solubility of LBG due to a decrease in the biopolymer-biopolymer association. A poor power law dependence of  $\sigma$  with  $\Delta[LBG]$  (eq. [6-6]) could be explained in the same manner, i.e., a non-power law dependence of the behaviour of LBG when in solution with sucrose.

On the other hand, as shown in eq. [6-7], a power law dependence of  $\sigma$  with  $\Delta[NaCAS]$  was observed. A good fit with the data shows that the effect of sucrose on  $\sigma$

of the ATPS relates closely to the effect of sucrose on NaCAS. Belyakova et al. (2003) observe in dilute solutions of NaCAS at pH 6 and in the presence of sucrose concentrations up to 60% an increase in the thermodynamic affinity of the NaCAS micelles for the aqueous medium, i.e., an increase in their hydrophilicity, water composition and hence a decrease in their surface/interfacial activity.

Compared to equations [6-2] to [6-4] (p. 6-207) in the previous section, the parameters  $a$  and  $b$  in equations [6-5] to [6-7] (p. 6-216) differ. The constant  $b$ , previously  $b \approx 3$ , increased to  $b > 7$ . The constant  $a$  in equations [6-2] and [6-4], on the other hand, decreased significantly ( $a \approx 10^{-6} - 10^{-24} \ll 16 - 17$ ). This could infer that the increment of sucrose caused a steeper change in  $\sigma$  than an increment in [BP]. The different constants show that the sucrose concentration affects  $\sigma$  in a more complex way than the biopolymer composition. Although both NaCAS and LBG are random coiled biopolymers, they are affected by sucrose to a different extent.

### 6.3.3 Effect of sugar type on the interfacial tension

The effect of sugar type on  $\sigma$  of four NaCAS-LBG systems with the same biopolymer composition (4 wt% NaCAS-0.2 wt% LBG) was investigated. 15 wt% of sucrose, trehalose, glucose and fructose was added to the systems. The investigated systems are shown on a 2D phase diagram in Figure 6–17. As previously indicated, a critical point and a tie-line were calculated for each of the systems on the basis of the experimental volume fractions, shown with other physical characteristics in Table 6–8, as well as the binodal.

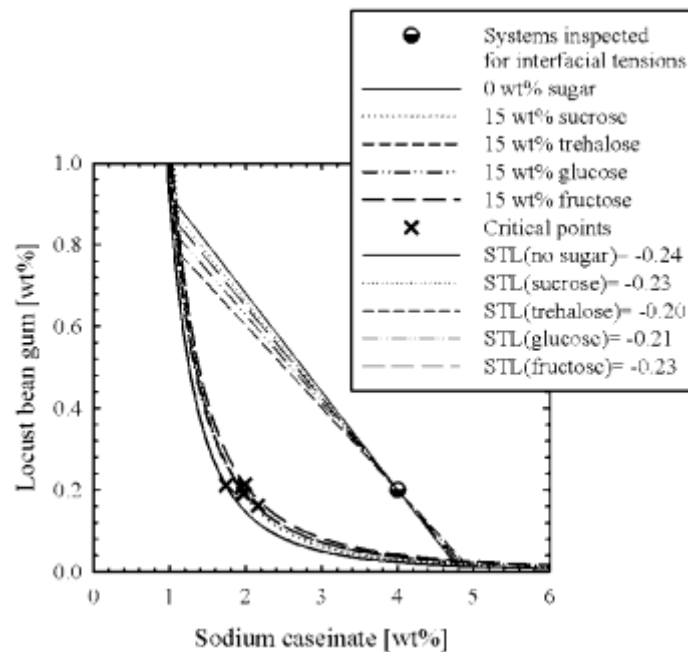


**Figure 6–17.** Phase diagram of a sodium caseinate-locust bean gum ATPS at 15 wt% of sucrose, trehalose, glucose and fructose. Systems inspected for interfacial tensions are marked with "●" and a critical point "x", a tie-line, as well as its slope (STL) is given for each of the systems. The curves for glucose and trehalose almost overlap.  $STL_{avg} = -0.22 \pm 0.02$ .

To calculate  $\sigma$ , the equilibrium phases were evaluated for their viscosities. The raw viscosity data are given in graphical form in Figure 6–18 and in numerical form in Table 6–8.

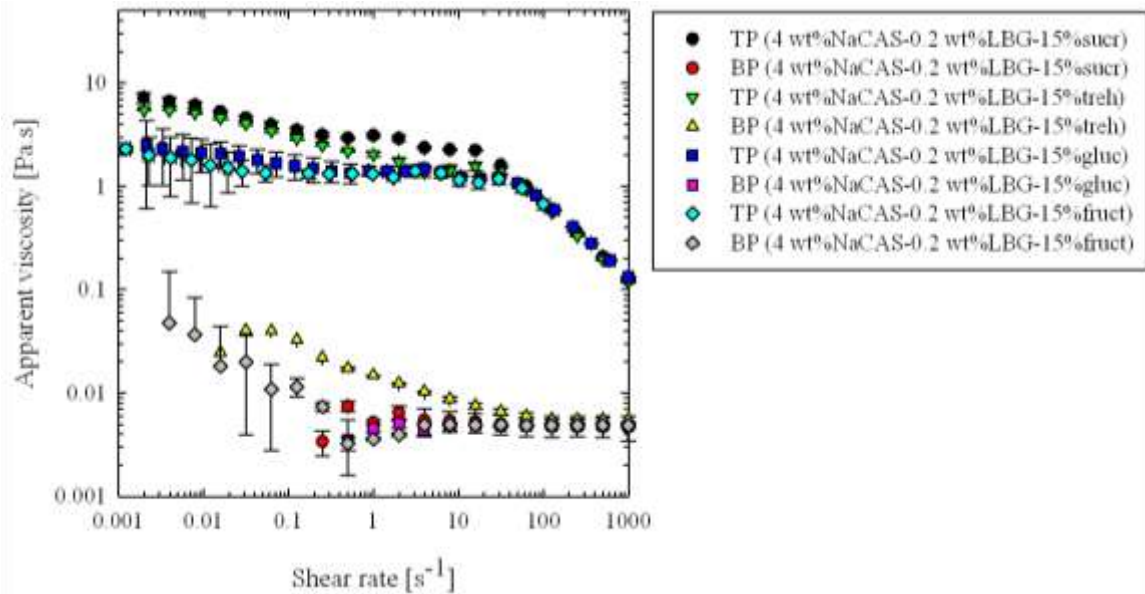


Figure 6–18. Log-log apparent viscosities of top (TP) and bottom (BP) phases of a sodium caseinate-locust bean gum (NaCAS-LBG) ATPS investigated for the effects of sugar-type (sucrose, trehalose, glucose and fructose) on interfacial tensions.

Table 6–8. Compositions of systems investigated at 20°C on the effects of sugar type on interfacial tension. The table also shows: volume fractions ( $\phi$ ), densities ( $\rho$ ), consistency constants ( $K$ ), power law index ( $n$ ) and average viscosities ( $\eta_{\text{avg}}$ ) of the individual equilibrium phases.

$i$	NaCAS [wt%]	LBG [wt%]	Sugar type	Equilibrium phases	$\phi$ [wt%]	$\rho$ [g/ml]	$k$	$n$	$R^2$	$\eta_{\text{avg}}$ [Pa.s]	$\eta_{\text{stdevp}}$ [Pa.s]
1	4	0.2	Glucose 15%	NaCAS-rich	78.04	1.028±0.019	0.0047	1	0.04	0.0050	0.0013
				LBG-rich	21.96	1.024±0.019	1.2664	0.93	0.76	1.5946	0.3611
2	4	0.2	Fructose 15%	NaCAS-rich	79.09	1.056±0.040	0.0049	0.90	0.14	0.0047	0.0003
				LBG-rich	20.91	1.051±0.038	1.4169	0.92	0.90	1.7724	0.3691
3	4	0.2	Sucrose 15%	NaCAS-rich	78.57	1.060±0.034	0.0062	0.92	0.33	0.0060	0.0008
				LBG-rich	21.43	1.054±0.034	2.8347	0.86	0.97	4.3869	1.7691
4	4	0.2	Trehalose 15%	NaCAS-rich	76.58	1.048±0.042	0.0157	0.80	0.72	0.0223	0.0112
				LBG-rich	23.42	1.044±0.042	2.07	0.85	0.92	3.3515	1.4665
5	4	0.2	Trehalose 30%	NaCAS-rich	74.02	1.108±0.045	0.0172	0.69	0.87	0.0259	0.0149
				LBG-rich	25.98	1.106±0.045	3.326	0.87	0.67	5.2404	2.1851

The above data show that sugars differ in their effect on the phase behaviour. While, on one hand, trehalose produced systems with the largest LBG-r phase and the smallest NaCAS-r phase, on the other hand, the ATPS with fructose separated into the

smallest NaCAS-r phase and largest LBG-r phase. In Table 6–8, data for a fifth system, not mentioned previously, is also given. The system is not mentioned elsewhere because  $\sigma$  for the ATPS was not calculated due to the experimental difficulties, as sufficiently retracted droplets for the system could not be obtained by dispersion. As also shown in Table 6–8, the average viscosities of the equilibrium phases containing glucose were slightly lower than those with fructose. With the exception of trehalose, the effect of sugar type on the average viscosity of the NaCAS-r phase was not pronounced. On the other hand, sucrose had the greatest effect on the average viscosity of the LBG-r or top phase and also the greatest effect on the density difference of the equilibrium phases among the sugars. This could also be the result of impurities in the sugar.

The interfacial data of Systems 1–4 in Table 6–8 were calculated from  $\tau$  and two apparent viscosities. The  $\sigma$  values calculated with the viscosity at a shear rate  $0.001 \text{ s}^{-1}$  are summarized in Table 6–9 and  $\sigma$  calculated with the viscosity at  $0.5 \text{ s}^{-1}$  are shown in Table 6–10. As previously indicated, the use of different viscosities caused a difference in the calculated  $\sigma$ .

**Table 6–9.** Calculated interfacial tensions ( $\sigma$ ) and their averages for the sodium caseinate-locust bean gum (NaCAS-LBG) ATPS with various sugars. The table also gives the radii of the droplets ( $R_0$ ), the apparent viscosities ( $\eta$ ) of the equilibrium phases at the shear rate of  $0.001 \text{ s}^{-1}$  and temperature of  $20^\circ\text{C}$ , as well as the viscosity ratios ( $\lambda$ ).

	15 wt% trehalose		15 wt% sucrose		15 wt% glucose		15 wt% fructose	
$\eta(\text{NaCAS})$	0.3 Pa.s		0.275 Pa.s		0.07 Pa.s		0.06 Pa.s	
$\eta(\text{LBG})$	4.8 Pa.s		7.4 Pa.s		2.1 Pa.s		1.9 Pa.s	
$\lambda$	16		26.9		30		31.7	
$i$	$R_{0i}$ [ $\mu\text{m}$ ]	$\sigma_i$ [ $\mu\text{N/m}$ ]	$R_{0i}$ [ $\mu\text{m}$ ]	$\sigma_i$ [ $\mu\text{N/m}$ ]	$R_{0i}$ [ $\mu\text{m}$ ]	$\sigma_i$ [ $\mu\text{N/m}$ ]	$R_{0i}$ [ $\mu\text{m}$ ]	$\sigma_i$ [ $\mu\text{N/m}$ ]
1	29	250	29	699	27	491	37	408
2	22	255	27	630	26	452	35	531
3	24	271	22	591	25	411	30	279
4	23	193	21	644	25	426	29	447
5	41	230	26	529	33	467	29	237
6	28	174	22	627	29	640	44	248
7	31	176			28	445		
$\sigma_{\text{avg}}$	221 $\pm$ 37		620 $\pm$ 52		476 $\pm$ 71		358 $\pm$ 111	

**Table 6–10.** Calculated interfacial tensions ( $\sigma$ ) and their averages for the sodium caseinate-locust bean gum (NaCAS-LBG) ATPS with various sugars. The table also gives the radii of the droplets ( $R_0$ ), the apparent viscosities ( $\eta$ ) of the equilibrium phases at the shear rate of  $0.5 \text{ s}^{-1}$  and temperature of  $20^\circ\text{C}$ , as well as the viscosity ratios ( $\lambda$ ).

	15 wt% trehalose		15 wt% sucrose		15 wt% glucose		15 wt% fructose	
$\eta(\text{NaCAS})$	0.02 Pa.s		0.006 Pa.s		0.0052 Pa.s		0.004 Pa.s	
$\eta(\text{LBG})$	2.3 Pa.s		2.9 Pa.s		1.42 Pa.s		1.34 Pa.s	
$\lambda$	115.0		483.3		273.1		335.0	
$i$	$R_{0i}$ [ $\mu\text{m}$ ]	$\sigma_i$ [ $\mu\text{N/m}$ ]	$R_{0i}$ [ $\mu\text{m}$ ]	$\sigma_i$ [ $\mu\text{N/m}$ ]	$R_{0i}$ [ $\mu\text{m}$ ]	$\sigma_i$ [ $\mu\text{N/m}$ ]	$R_{0i}$ [ $\mu\text{m}$ ]	$\sigma_i$ [ $\mu\text{N/m}$ ]
1	29	5,216.7	29	78,773	27	24,957.9	37	18,821
2	22	5,310.4	27	71,032	26	22,992.4	35	34,285
3	24	5,651.1	22	66,578	25	20,875.5	30	12,850
4	23	4,010.3	21	72,640	25	21,682.3	29	20,622
5	41	4,792.5	26	59,590	33	23,768.1	29	10,911
6	28	3,627.0	22	70,715	29	32,528.9	44	11,443
7	31	3,660.5			28	22,601.8		
$\sigma_{\text{avg}}$	4,610 $\pm$ 775		69,888 $\pm$ 5,852		24,201 $\pm$ 3,617		18,155 $\pm$ 8,087	

Based on the average interfacial tensions  $\sigma_{\text{avg}}$  in Tables 6–9 and 6–10, ATPS could be classified for the effect of a sugar type as follows: sucrose > glucose > fructose > trehalose. A possible explanation of this behaviour is given in § 4.5 (p. 4–128) for the effect of sugars on the cosolubility of NaCAS and GM in the bulk. Because the bulk and surface properties of the systems are intertwined, the interfacial activity of the systems was affected most by sugars that imparted the most structure in the solvent, such as

fructose and trehalose, which indirectly affect the mobility of the macromolecular components to the interface. A difference in the number of molecules and their structure, i.e., the number of reactive OH groups, could as well enhance the difference in the way they indirectly affect the surface activity in these systems. The reason why the difference between disaccharides and monosaccharides was not observed for systems with sucrose and glucose could have been due to impurities present in the sucrose.

The interfacial tensions from Table 6-9 were plotted against TLL,  $\Delta[\text{NaCAS}]$  and  $\Delta[\text{LBG}]$ . The plots are shown in Figure 6-19 and Figure 6-20.

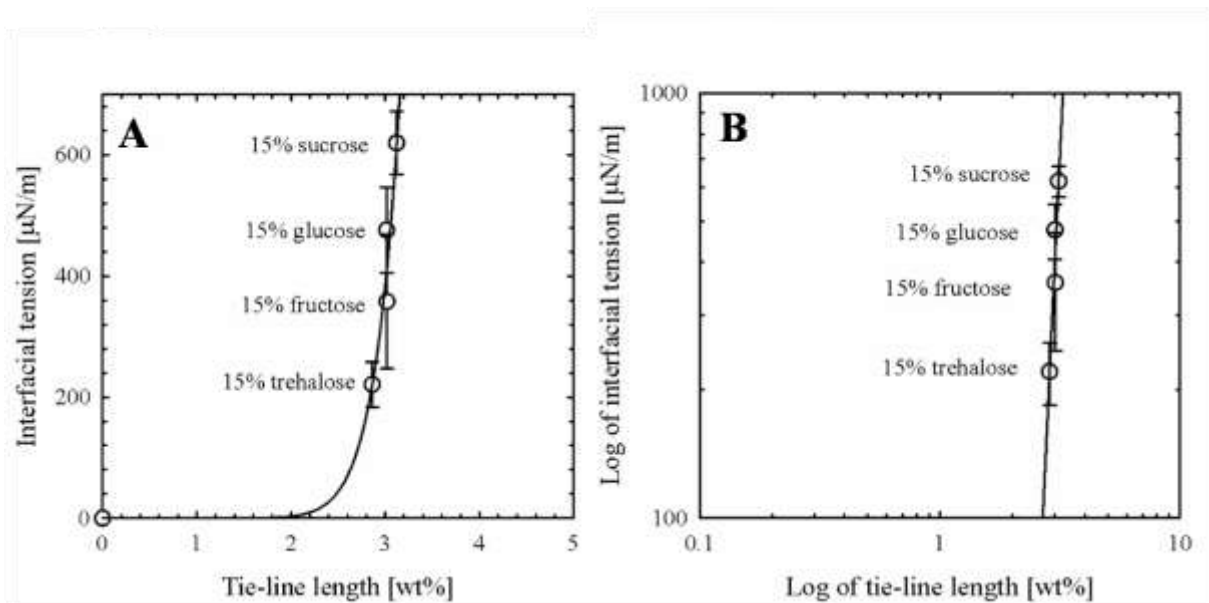


**Figure 6-19.** Interfacial tension for sodium caseinate-locust bean gum ATPS for various sugar types as a function of the tie-line length (A). The log-log plot (B) gives a straight line.

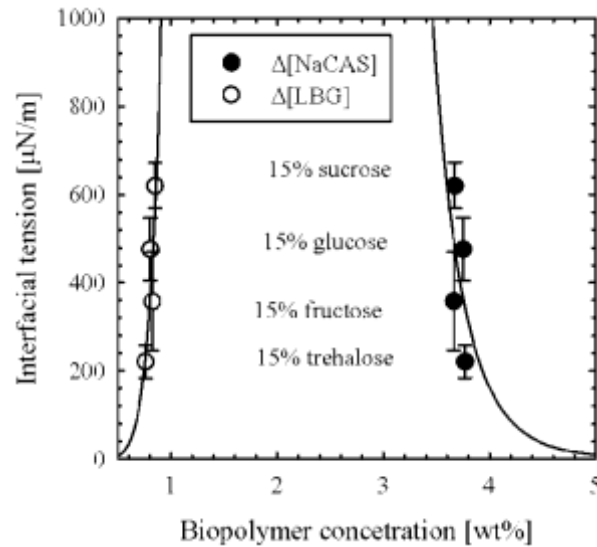


**Figure 6–20.** Interfacial tensions for sodium-caseinate and locust bean gum (NaCAS-LBG) ATPS with different sugar types as a function of NaCAS ( $\Delta[\text{NaCAS}]$ , marked with "●") and LBG ( $\Delta[\text{LBG}]$ , marked with "○") concentration differences between the phases.

The interfacial tension data show a power law dependence with the parameters TLL and  $\Delta[\text{LBG}]$ . A poor fit was observed for the relationship between  $\sigma$  and  $\Delta[\text{NaCAS}]$ . The coefficients of the best fit power law equations for the data in the above figures are given in the following equations:

$$\sigma = 0.0008 \times \text{TLL}^{11.8728}; R^2 = 0.9156; R = 0.9569 \quad [6-8]$$

$$\sigma = 2167.212 \times \Delta[\text{LBG}]^{8.1333}; R^2 = 0.7642; R = 0.8742 \quad [6-9]$$

$$\sigma = 7.3\text{E}9 \times \Delta[\text{NaCAS}]^{-12.7163}; R^2 = 0.4681; R = 0.2191 \quad [6-10]$$

The eq. [6-8] shows good agreement between  $\sigma$  and TLL. The system that lies on the longest tie-line, furthest from the critical point in the phase diagram, had the largest  $\sigma$ . A fair fit between  $\sigma$  and  $\Delta[\text{LBG}]$  observed in eq. [6-9] suggests that a change in sugar type follows a  $\Delta[\text{LBG}]$  in a power law fashion. This is not the case for

the relationship between  $\sigma$  and  $\Delta[\text{NaCAS}]$ . There are two possible explanations for this discrepancy. First, there is a possibility that trehalose affects NaCAS in a distinctly different way compared to the other sugar types. Second, the binodal, which determines the equilibrium phase compositions of the system, could be incorrectly positioned in the 2D space.

The coefficients describing the dependence of sugar-type on  $\sigma$  are similar to the coefficients given by equations [6-5] to [6-7] (p. 6-216) in the previous section describing the effect of sucrose concentration on  $\sigma$ . In both cases, the constant  $b$  is  $> 10$ . Constants  $a$  in eq. [6-8] and [6-9], too, are similar, with the exception of constant  $a$  in equation [6-10]. Because of the similarity of the coefficients, it can be concluded that sugar type and sugar concentration affect  $\sigma$  in a similar way and perhaps a power law relationship does not describe them best.

### 6.3.4 Effect of galactomannan type on the interfacial tension

In this section, four ATPS, each composed of 4 wt% NaCAS and 0.2 wt% GM, are investigated for the effect of the GM type on  $\sigma$ . Figure 6–21 shows the investigated systems on a 2D phase diagram. A critical point and a tie-line are given for each of the Systems 1–4: NaCAS-LBG, NaCAS-TG, NaCAS-GG and NaCAS-FG.

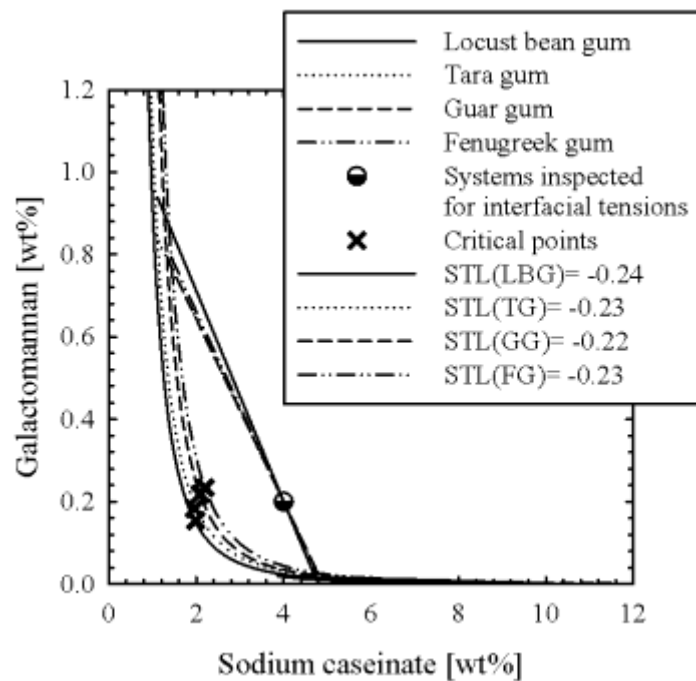


**Figure 6–21.** Phase diagram of sodium caseinate-galactomannan systems without sugar. The same amounts of sodium caseinate and galactomannans: locust bean gum (LBG), tara gum (TG), guar gum (GG) and fenugreek gum (FG) were added to make the ATPS. Systems inspected for interfacial tensions are marked with "●" and a critical point marked with "x", a tie-line, as well as its slope (STL) is given for each of the ATPS.  $STL_{avg} = -0.23 \pm 0.01$ .

As in previous sections the viscosities of the equilibrium phases were measured and the raw data are shown (Figure 6–22).

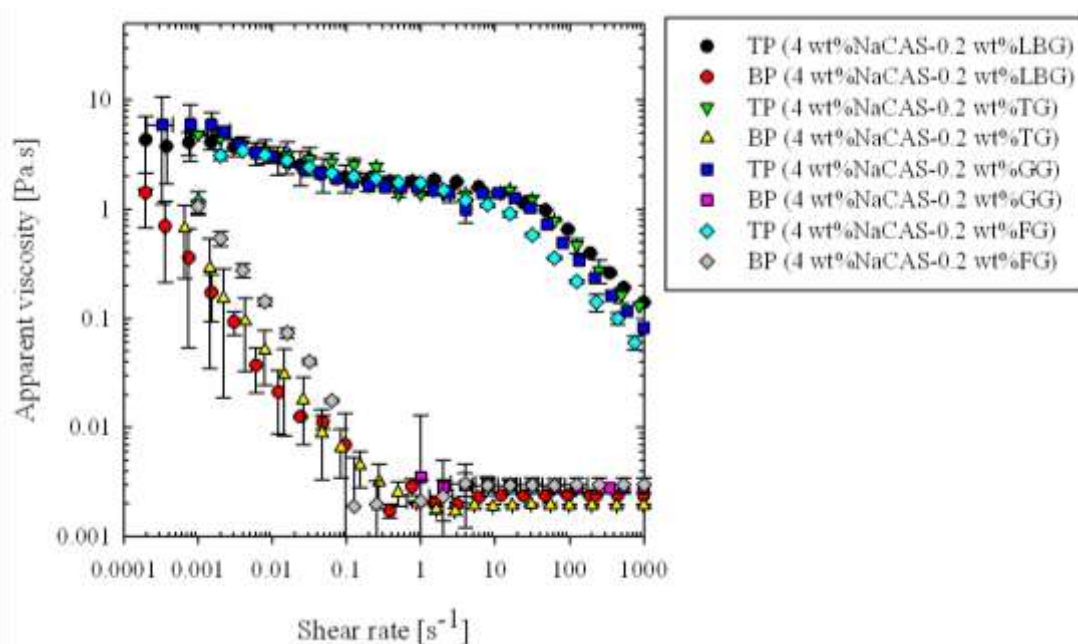


**Figure 6–22.** Log-log plots of apparent viscosities for the top (TP) and bottom (BP) phases of a sodium caseinate-galactomannan (NaCAS-GM) ATPS investigated for the effect of galactomannan type on interfacial tension. GM=galactomannan, LBG=locust bean gum, GG=guar gum, FG=fenugreek gum.

The physical properties of the equilibrium phases for the investigated ATPS in terms of the effect of GM type are summarized in Table 6–11. The data show that the type of GM in ATPS changes the phase behaviour of the systems. Less branched GM, such as LBG and TG, produced a smaller GM-r phase and respectively a larger NaCAS-r phase, possibly due to larger molecular drainage, compared to more branched GM. The degree of branching, a major structural difference between the GM also affected the density of the equilibrium phases. Less branched LBG and TG produced denser equilibrium phases than more branched GG and FG. The differences in the viscosities between the GM are less pronounced, i.e., a different relationship between them could be found at different shear rates. Table 6–11 also gives data for an additional fifth system composed of FG with 15 wt% of trehalose, which will be referred to in the next section.

**Table 6–11. Compositions of systems investigated at 20°C on the effects of galactomannan-type on interfacial tensions. The table shows: volume fractions ( $\phi$ ), densities ( $\rho$ ), consistency constants (K), power law index (n) and average viscosities ( $\eta_{\text{avg}}$ ) of the individual equilibrium phases. LBG=locust bean gum, TG=tara gum, GG=guar gum and FG=fenugreek gum.**

<i>i</i>	NaCAS [wt%]	LBG [wt%]	GM type	Equilibrium phases	$\phi$ [wt%]	$\rho$ [g/ml]	K	n	R <sup>2</sup>	$\eta_{\text{avg}}$ [Pa.s]	$\eta_{\text{stdev}}$ [Pa.s]
1	4	0.2	LBG	NaCAS-rich	79.60	1.000±0.032	0.0021	1.04	0.04	0.0022	0.0004
				LBG-rich	20.40	0.991±0.030	1.7526	0.89	0.92	2.7238	0.9734
2	4	0.2	TG	NaCAS-rich	78.34	0.986±0.040	0.0022	0.71	0.82	0.0025	0.0009
				TG-rich	21.66	0.993±0.040	1.6135	0.84	0.95	2.6603	1.1651
3	4	0.2	GG	NaCAS-rich	76.75	0.973±0.016	0.0033	0.93	0.35	0.0031	0.0003
				GG-rich	23.25	0.967±0.015	1.3401	0.81	0.93	2.7951	1.6325
4	4	0.2	FG	NaCAS-rich	77.44	0.992±0.040	0.0023	1.12	0.85	0.0024	0.0005
				FG-rich	22.56	0.976±0.036	1.5539	0.86	0.97	1.9807	0.6040
5	4	0.2	FG 15% Trehalose	NaCAS-rich	81.22	1.027±0.016	0.0056	0.74	0.84	0.0064	0.0027
				FG-rich	18.78	1.023±0.016	2.7741	0.81	0.99	5.1462	2.7202

The  $\sigma$  of four ATPS containing different GM were calculated from the drop retraction data as mentioned in earlier sections. The results are given in Table 6–12 and Table 6–13.

**Table 6–12. Calculated interfacial tensions ( $\sigma$ ) and their averages ( $\sigma_{\text{avg}}$ ) for the sodium caseinate-galactomannan (NaCAS-GM) ATPS. The table also gives radii of droplets ( $R^0$ ), apparent viscosities ( $\eta$ ) of the equilibrium phases at the shear rate of 0.001 s<sup>-1</sup> and temperature of 20°C and viscosity ratios ( $\lambda$ ). LBG=locust bean gum, TG=tara gum, GG=guar gum; FG=fenugreek gum.**

	4 wt% NaCAS- 0.2 wt% LBG	4 wt% NaCAS- 0.2 wt% TG	4 wt% NaCAS- 0.2 wt% GG	4 wt% NaCAS- 0.2 wt% FG				
$\eta(\text{NaCAS})$	0.25 Pa.s	0.35 Pa.s	0.8 Pa.s	0.83 Pa.s				
$\eta(\text{LBG})$	3.8 Pa.s	4.9 Pa.s	3.4 Pa.s	3.6 Pa.s				
$\lambda$	15.2	14	4.25	4.3				
<i>i</i>	$R_{0i}$ [ $\mu\text{m}$ ]	$\sigma_i$ [ $\mu\text{N/m}$ ]						
1	54	1,720	47	378.8	56	81.8	52	31.3
2	72	1,657	49	685.9	54	95.9	46	36.3
3	57	2,077	64	954.9	57	56.0	54	43.4
4	43	1,190	55	590.3	44	23.7	58	43.6
5	30	646	50	842.8	51	19.6	57	35.5
6			53	405.8	54	51.4	41	23.1
7			48	684.0	82	115.6	41	21.5
$\sigma_{\text{avg}}$	1,458±495		649±196		55±28		33.5±8.2	

**Table 6–13.** Calculated interfacial tensions ( $\sigma$ ) and their averages ( $\sigma_{\text{avg}}$ ) for the sodium caseinate-galactomannan (NaCAS-GM) ATPS. The table also gives radii of droplets ( $R^0$ ), apparent viscosities ( $\eta$ ) of the equilibrium phases at the shear rate of  $0.5 \text{ s}^{-1}$  and temperature of  $20^\circ\text{C}$  and viscosity ratios ( $\lambda$ ). LBG=locust bean gum, TG=tara gum, GG=guar gum; FG=fenugreek gum.

	4 wt% NaCAS- 0.2 wt% LBG		4 wt% NaCAS- 0.2 wt% TG		4 wt% NaCAS- 0.2 wt% GG		4 wt% NaCAS- 0.2 wt% FG	
$\eta(\text{NaCAS})$	0.003 Pa.s		0.0026 Pa.s		0.005 Pa.s		0.0052 Pa.s	
$\eta(\text{LBG})$	1.7 Pa.s		1.5 Pa.s		1.6 Pa.s		1.5 Pa.s	
$\lambda$	566.7		750		320		288.5	
$i$	$R_{0i}$ [ $\mu\text{m}$ ]	$\sigma_i$ [ $\mu\text{N/m}$ ]	$R_{0i}$ [ $\mu\text{m}$ ]	$\sigma_i$ [ $\mu\text{N/m}$ ]	$R_{0i}$ [ $\mu\text{m}$ ]	$\sigma_i$ [ $\mu\text{N/m}$ ]	$R_{0i}$ [ $\mu\text{m}$ ]	$\sigma_i$ [ $\mu\text{N/m}$ ]
<b>1</b>	54	870,335	47	265,777	56	110,101.2	52	29,540.3
<b>2</b>	72	838,496	49	481,316	54	129,154.7	46	34,222
<b>3</b>	57	1,051,288	64	670,057	57	75,334.57	54	40,866.3
<b>4</b>	43	602,148	55	414,209	44	31,883.26	58	41,129.9
<b>5</b>	30	327,051	50	591,416	51	26,389.32	57	33,447.5
<b>6</b>			53	284,739	54	69,214.3	41	21,738.5
<b>7</b>			48	510,952	82	155,605.3	41	20,256.4
$\sigma_{\text{avg}}$	737,864 $\pm$ 298,501		459,781 $\pm$ 138,863		73,680 $\pm$ 37,439		31,600 $\pm$ 7,720	

The data in the above tables differ according to the viscosities taken to calculate them. Although  $\sigma$  differ in their absolute values, they still show the same trend. The systems can be, according to  $\sigma$  and the GM type, classified as follows: LBG>TG>GG>FG. The relationship shows that the molecular characteristics of the GM, their  $M_w$  and the degree of branching influence  $\sigma$ . More branched GM or a larger  $M_w$  resulted in smaller interfacial tensions than less branched ones. The surface/interfacial activity of the investigated GM was recently confirmed by Wu et al. (2009). The authors studied pure GM solutions and related the difference in their activity to the difference in the concentration, molecular structure, the solubility and water binding capacity of the GM. They, however, reported a slightly different relationship between the GM: TG>LBG>GG>FG, which could be attributed to one of the following factors: (i) different concentrations used in the experiment, (ii) the presence of NaCAS and (iii) a difference in the source of the GM used (namely GG and LBG). In the same study, the authors also

reported the emulsion capacity, a property closely related to the interfacial activity of the GM in the following order: GG>FG>TG>LBG. The highest interfacial activity was, once more, attributed to highly branched GM, where a higher proportion of the galactose branches increases the hydrophilicity of the GM.

In this work, the interfacial properties are shown by plotting  $\sigma$  against the parameters TLL (Figure 6-23),  $\Delta[\text{GM}]$  and  $\Delta[\text{NaCAS}]$  (Figure 6-24).

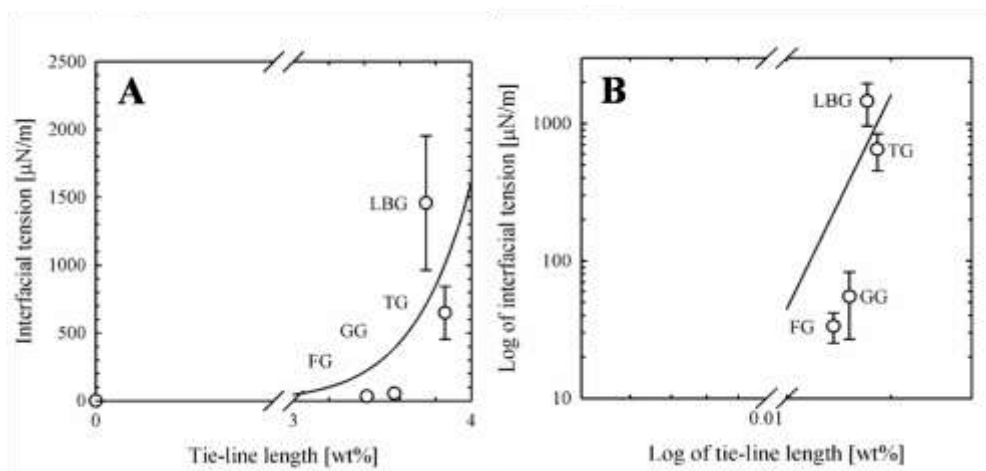


**Figure 6-23.** Interfacial tension for the sodium caseinate-galactomannan ATPS as a function of the tie-line length (A). The log-log plot (B) gives a straight line. LBG=locust bean gum, TG=tara gum, GG=guar gum, and FG=fenugreek gum.

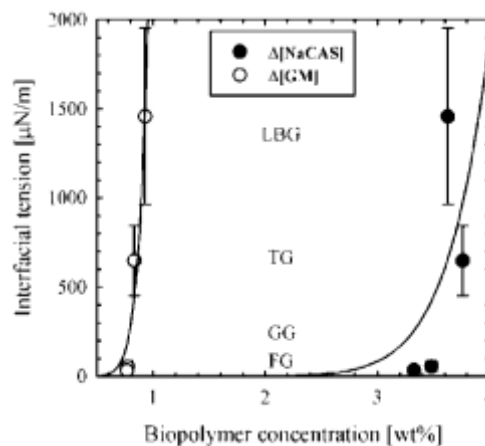


**Figure 6-24.** Interfacial tensions in the 4 wt% sodium caseinate-0.2 wt% galactomannan (NaCAS-GM) ATPS as a function of NaCAS ( $\Delta[\text{NaCAS}]$ , marked with "●") and GM ( $\Delta[\text{GM}]$ , marked with "○") concentration differences between the equilibrium phases.

A clear power law dependence of  $\sigma$  with the TLL,  $\Delta[\text{GM}]$  and  $\Delta[\text{NaCAS}]$  was observed. The coefficients of best fit equations are given below:

$$\sigma = 0.0174 \times TLL^{9.2155}; R^2 = 0.9813; R = 0.9906 \quad [6-11]$$

$$\sigma = 5271.88 \times \Delta[\text{GM}]^{13.1289}; R^2 = 0.9767; R = 0.9539 \quad [6-12]$$

$$\sigma = 6.64\text{E-}20 \times \Delta[\text{NaCAS}]^{38.727}; R^2 = 0.998; R = 0.9996 \quad [6-13]$$

Although the power law dependence for the interfacial tensions holds for all these relationships ( $R^2 > 0.98$ ), the coefficients calculated in this section differ from those calculated for the ATPS investigated in terms of the effect of [BP] in § 6.3.1 (p. 6–199). The above constants are, however, most similar with the constants in § 6.3.2 (p. 6–209), that describe the effect of sucrose concentration on  $\sigma$ . This could imply similarities in the mechanisms involved in the change of  $\sigma$ , i.e., a determining effect of the excluded volume which may be changed by a different GM or sugar.

#### **6.3.4.1 Effect of galactomannan type on the interfacial tension of ATPS with 15% trehalose**

In this subsection the effect of the GM type is further investigated in the presence of 15% trehalose. Two systems, NaCAS-LBG-15% trehalose and NaCAS-FG-15% trehalose, are compared to each other and the reference systems—NaCAS-LBG and NaCAS-FG ATPS. Figure 6–25 shows the systems on the phase diagram. LBG and FG were selected as GM with molecular properties that were most differed—two ends of the spectra. For that reason TG and GG were not investigated.

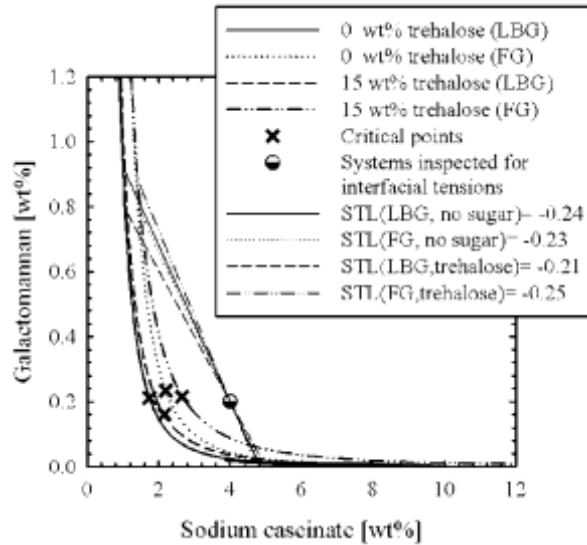


**Figure 6–25.** Phase diagram of the sodium caseinate-locust bean gum (NaCAS-LBG) and sodium caseinate-fenugreek gum (NaCAS-FG) ATPS with 15% trehalose and without trehalose. Systems investigated on interfacial tensions are marked with "●". Critical points are marked with "x". A tie-line and its slope (STL) is given for each of the investigated systems.  $STL_{avg} = -0.23 \pm 0.02$ .

The physical characteristics of the systems used to calculate  $\sigma$  and provide a better understanding of the systems are shown in Table 6–8 and Table 6–11. Furthermore, Figure 6–26 gives the raw data of the viscosities of the equilibrium phases of the investigated systems.

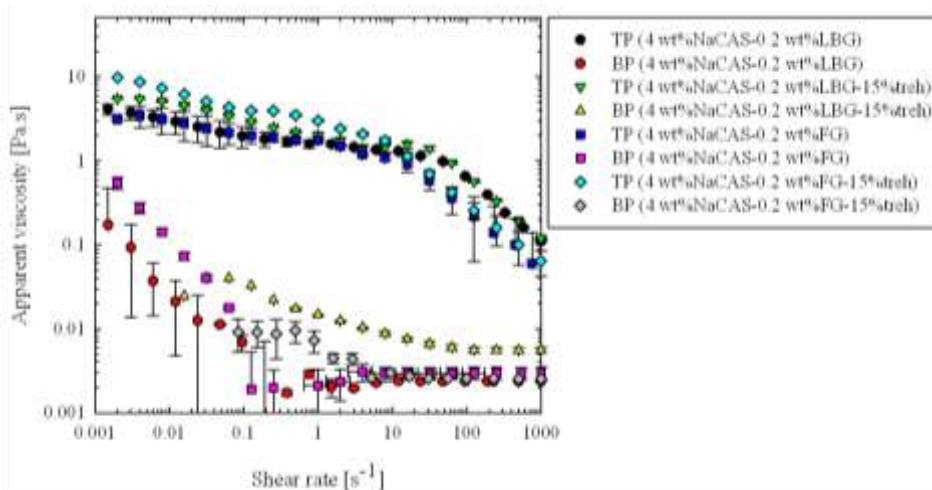


**Figure 6–26.** Log-log apparent viscosities of the top (TP) and bottom (BP) phases of the sodium caseinate-galactomannan (NaCAS-GM) ATPS investigated for the effects of galactomannan type and sugar type on the interfacial tension. LBG=locust bean gum, FG=fenugreek gum.

The calculated interfacial tensions with the apparent viscosity data at two shear rates, 0.001 and 0.5 s<sup>-1</sup> are shown in Table 6–14 and Table 6–15, respectively.

**Table 6–14.** Calculated interfacial tensions for the 4 wt% sodium caseinate-0.2 wt% locust bean gum/fenugreek gum ATPS without sugar and at 15% trehalose. The table also gives the radii of the retracted droplets ( $R_0$ ), the apparent viscosities ( $\eta$ ) of the equilibrium phases for the shear rate of 0.001s<sup>-1</sup> and 20°C, as well as the viscosity ratios ( $\lambda$ ).

	LBG system with 15 wt% trehalose		FG system with 15 wt% trehalose		LBG system without sugar		FG system without sugar	
$\eta(\text{NaCAS})$	0.3 Pa.s		0.37 Pa.s		0.25 Pa.s		0.83 Pa.s	
$\eta(\text{LBG})$	4.8 Pa.s		2.5 Pa.s		3.8 Pa.s		3.6 Pa.s	
$\lambda$	16		6.8		15.2		4.3	
$i$	$R_{0i}$ [ $\mu\text{m}$ ]	$\sigma_i$ [ $\mu\text{N/m}$ ]	$R_{0i}$ [ $\mu\text{m}$ ]	$\sigma_i$ [ $\mu\text{N/m}$ ]	$R_{0i}$ [ $\mu\text{m}$ ]	$\sigma_i$ [ $\mu\text{N/m}$ ]	$R_{0i}$ [ $\mu\text{m}$ ]	$\sigma_i$ [ $\mu\text{N/m}$ ]
1	29	250	33	44.0	54	1,720	52	31.3
2	22	255	33	34.9	72	1,657	46	36.3
3	24	271	43	28.2	57	2,077	54	43.4
4	23	193	27	13.4	43	1,190	58	43.6
5	41	230	25	12.4	30	646	57	35.5
6	28	174					41	23.1
7	31	176					41	21.5
$\sigma_{\text{avg}}$	221±37		26.6±12.3		1458±495		33.5±8.2	

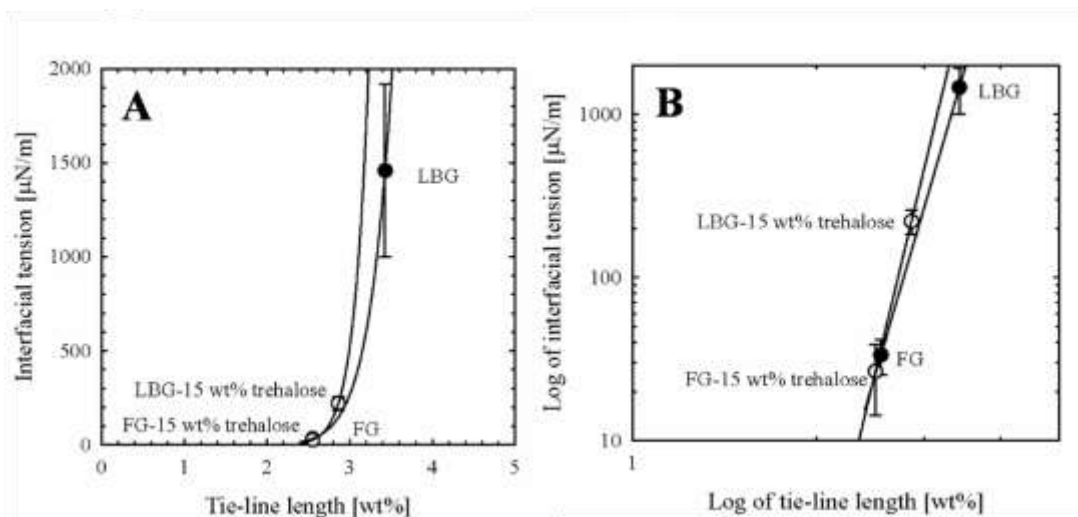
**Table 6–15.** Calculated interfacial tensions for the 4 wt% sodium caseinate-0.2 wt% locust bean gum/fenugreek gum ATPS without and with 15% trehalose. The table also gives the radii of the retracted droplets ( $R_0$ ), the apparent viscosities ( $\eta$ ) of the equilibrium phases for the shear rate of 0.5 s<sup>-1</sup> and 20°C, as well as the viscosity ratios ( $\lambda$ ).

	LBG system with 15 wt% trehalose		FG system with 15 wt% trehalose		LBG system without sugar		FG system without sugar	
$\eta(\text{NaCAS})$	0.02 Pa.s		0.02 Pa.s		0.003 Pa.s		0.0052 Pa.s	
$\eta(\text{LBG})$	2.3 Pa.s		3.5 Pa.s		1.7 Pa.s		1.5 Pa.s	
$\lambda$	115		175		566.7		288.5	
$i$	$R_{0i}$ [ $\mu\text{m}$ ]	$\sigma_i$ [ $\mu\text{N/m}$ ]	$R_{0i}$ [ $\mu\text{m}$ ]	$\sigma_i$ [ $\mu\text{N/m}$ ]	$R_{0i}$ [ $\mu\text{m}$ ]	$\sigma_i$ [ $\mu\text{N/m}$ ]	$R_{0i}$ [ $\mu\text{m}$ ]	$\sigma_i$ [ $\mu\text{N/m}$ ]
1	29	5,217	45	26,709	54	870,335	52	29,540
2	22	5,310	43	21,159	72	838,496	46	34,222
3	24	5,651	43	17,091	57	1,051,288	54	40,866
4	23	4,010	45	8,109	43	602,148	58	41,130
5	41	4,793	45	7,520	30	327,051	57	33,448
6	28	3,627					41	21,739
7	31	3,661						
$\sigma_{\text{avg}}$	4,610±775		16,118±7,438		737,864±298,501		31,600±7,720	

The above data reveals the dependence of  $\sigma$  on the GM and sugar. It shows that  $\sigma$  decreases most at the moderate amounts of sugar and in the presence of more soluble GM. The solubility of the GM is related to its degree of branching, i.e., the G:M ratio.

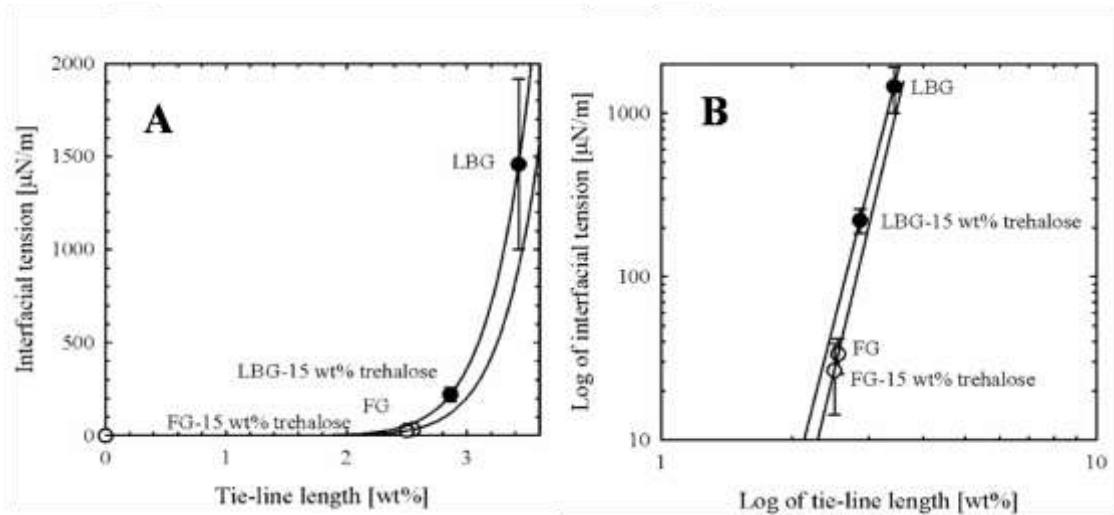
In an attempt to assess: (i) the effect of the GM-type (i.e., LBG and FG) in the presence and absence of trehalose, and to assess (ii) the effect of trehalose concentration (0 and 15 wt%) on the GM types, the relationships between  $\sigma$ , on one hand, and parameters such as TLL,  $\Delta[\text{GM}]$  and  $\Delta[\text{NaCAS}]$  on the other hand, were established. The interfacial tensions  $\sigma$  from Table 6-14 were plotted against the TLL in Figures 2-27 and 6-28.

Figure 6-27 compares the relationship  $\sigma$  vs. TLL as a function of the GM type in the presence and absence of trehalose.



**Figure 6-27.** Interfacial tension for the sodium caseinate-locust bean gum/fenugreek gum (NaCAS-LBG/FG) ATPS with and without trehalose as a function of the tie-line length (A). The log-log plot gives a straight line (B). Galactomannans are compared at the same trehalose concentration.

Figure 6–28 compares, in systems differing by the GM-type, the relationship  $\sigma$  vs. TLL as a function of the trehalose concentration.



**Figure 6–28.** Interfacial tension for the sodium caseinate-locust bean gum/fenugreek gum ATPS (NaCAS-LBG/FG) with and without trehalose as a function of the tie-line length (A). The log-log plot (B) gives a straight line. ATPS are compared by the individual galactomannan type at different trehalose concentrations.

Given the scarcity of the data, as only two data points at a time are compared, a linear regression would also give a perfect fit ( $R=R^2=1$ ). Regardless, a power law function was used to enable the comparison with the mathematical relationships obtained in previously in this chapter. The relationships plotted in Figures 6–27 to 6–29 are given in the following equations:

$$\sigma = 1.7134E-5 \times TLL^{15.5706}, \text{ for ATPS at 15\% trehalose} \quad [6-14]$$

$$\sigma = 0.0002 \times TLL^{12.7644}, \text{ for ATPS at 0\% trehalose} \quad [6-15]$$

$$\sigma = 0.0037 \times TLL^{10.4626}, \text{ for ATPS with LBG at different [trehalose]} \quad [6-16]$$

$$\sigma = 0.0010 \times TLL^{11.1464}, \text{ for ATPS with FG at different [trehalose]} \quad [6-17]$$

A similarity in the relationship was observed by comparing constants  $a$  and  $b$  in equations [6-14] to [6-17]. Constant  $b$  determines the degree of change of  $\sigma$  with the

change in the composition of the system/position in the phase diagram. The constant is slightly larger in the case where the effect of GM-type on  $\sigma$  (eq. [6-14] and [6-15]) is compared to the effect of trehalose concentrations on  $\sigma$  (eq. [6-16] and [6-17]). The difference in  $b$  is small, hence it can be reconfirmed (as § 6.3.4, p. 6-225) that the GM-type and the concentration of trehalose affect the relationship between  $\sigma$  and the TLL to a similar extent.

Figures 6-29 and 6-30 show the relationship between  $\sigma$  and  $\Delta[\text{GM}]$  and  $\Delta[\text{NaCAS}]$ . Figure 6-29 compares the abovementioned relationship for the effect of trehalose concentration (i.e., 0 and 15%), and Figure 6-30 compares the relationship of the systems containing different GM (i.e., LBG and FG).

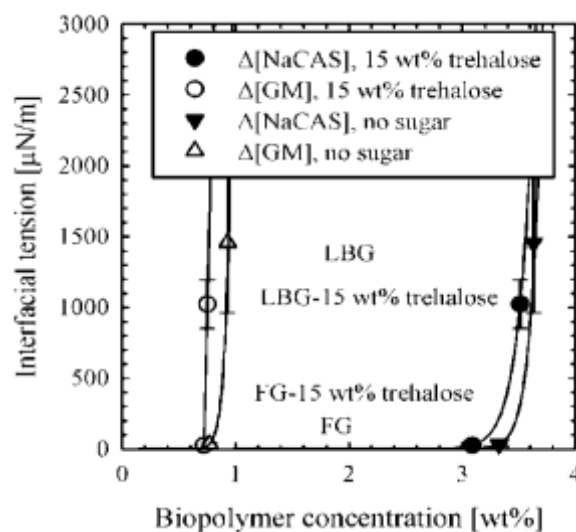


**Figure 6-29.** Interfacial tensions in the sodium caseinate-locust bean gum/fenugreek gum (NaCAS-LBG/FG) ATPS as a function of a NaCAS and LBG/FG concentration differences in the equilibrium phases. ATPS are compared at different trehalose concentrations.

The eq. [6-18] gives the mathematical relationship of  $\sigma$  vs.  $\Delta[\text{NaCAS}]$  and  $\Delta[\text{GM}]$  in the 0 wt% sugar environment and equation [6-19] in the 15 wt% trehalose environment.

$$\sigma = 12616.5484 \times \Delta[GM]^{22.3528} \quad \text{no sugar} \quad [6-18]$$

$$\sigma = 9.9310E-15 \times \Delta[NaCAS]^{29.7568}$$

$$\sigma = 32933.5075 \times \Delta[GM]^{-27.5943} \quad 15\% \text{ trehalose} \quad [6-19]$$

$$\sigma = 9.9500E-5 \times \Delta[NaCAS]^{11.0151}$$

Eq. [6-18] is in agreement with the relationships obtained in equations [6-12] and [6-13] (p. 6-230) which is not surprising since it attempts to describe the same effect. Eq. [6-21] shows a disparate outcome, which is likely the result of the contradictory phase separation data reported in Tables 6-8 (p. 6-219) and 6-11 (p. 6-227). The data show that an increment in the trehalose concentration in the ATPS with LBG caused an increase in the volume fraction of the LBG-r phase ( $\varphi_{LBG}$ ); the opposite was true for ATPS with FG.

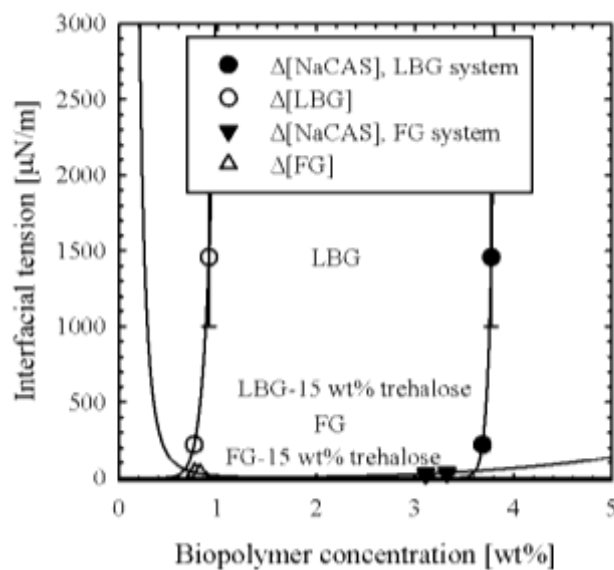


**Figure 6-30.** Interfacial tensions in the sodium caseinate-locust bean/fenugreek gum (NaCAS-LBG/FG) ATPS as a function of a NaCAS and LBG/FG concentration differences in the equilibrium phases. The ATPS are compared for the galactomannan types.

Equations [6-20] and [6-21] describe the relationship between interfacial tension  $\sigma$  and  $\Delta[NaCAS]$  or  $\Delta[LBG]$  for ATPS with LBG and ATPS with FG, respectively:

$$\begin{aligned} \sigma &= 4041.7210 \times \Delta[\text{LBG}]^{10.5615} \\ \sigma &= 8.603E - 43 \times \Delta[\text{NaCAS}]^{78.3998} \end{aligned} \quad \begin{array}{l} \text{for ATPS with LBG} \\ \text{for ATPS with LBG} \end{array} \quad [6-20]$$

$$\begin{aligned} \sigma &= 13.4200 \times \Delta[\text{FG}]^{-3.4476} \\ \sigma &= 0.5387 \times \Delta[\text{NaCAS}]^{3.4373} \end{aligned} \quad \begin{array}{l} \text{for ATPS with FG} \\ \text{for ATPS with FG} \end{array} \quad [6-21]$$

The relationship in eq. [6-20] attempts to describe the effect of trehalose concentration on the interfacial properties of ATPS with LBG, and is in agreement with the relationship describing the effect of sucrose on the same system, reported in equations on p. 6-216. Hence, it could be assumed that sucrose and trehalose affect on  $\sigma$  to the same extent. A rather different relationship, however, was observed in eq. [6-21] for ATPS with FG. The difference in the relationship is likely a manifestation of the abovementioned difference in the phase behaviour between the systems with LBG and FG, which could be explained by (i) a real difference in the way LBG and FG ATPS are influenced by trehalose or (ii) an experimental error.

## 6.4 Conclusion

The droplet deformation method was successfully used to measure interfacial tensions ( $\sigma$ ) of dilute NaCAS-GM ATPS ( $\varphi_{GM} < 20$  wt%). The effects of the total biopolymer concentration, sucrose concentration, sugar type and galactomannan type were investigated. The present study confirms that the concentration, molecular characteristics, and sugar, play an important role in the interfacial properties of the investigated systems. Based on the results reported in this chapter, the following claims can be made: (i) an increase in the total biopolymer concentration results in an

exponential increase in  $\sigma$ ; (ii) an increase in the sucrose concentration causes a decrease in  $\sigma$  such that based on the amount of sucrose added to the ATPS, the following trend was observed: 0% > 15% > 20% > 5% > 30%; (iii) a change in the  $M_w$  and M:G ratio of the GM has a pronounced effect on  $\sigma$  such that based on the type of GM, the ATPS follow trend: LBG > TG > GG > FG; and (iv) the effect of GM type on  $\sigma$  is preserved in the presence of 15% of trehalose such that the systems at LBG-15% trehalose have a higher  $\sigma$  than systems at FG-15% trehalose.

The interfacial tension measurements support the phase behaviour. A power law increase in  $\sigma$  was confirmed for all investigated systems when the  $\sigma$  was related to an increase in the tie-line length (TLL) and the distance of the investigated ATPS from the critical point in the phase diagram. Furthermore, the power law constants  $a$  and  $b$  consistently described the relationship between  $\sigma$  and the compositions of the equilibrium phases, characterised by  $\Delta[\text{NaCAS}]$  and  $\Delta[\text{GM}]$ . Inconsistencies in the latter relationship were observed for systems containing 15% trehalose.

## CHAPTER 7: CONCLUSIONS AND FUTURE WORK

This work is an experimental study of the effect of sugar on sodium caseinate-galactomannan aqueous two-phase systems (NaCAS-GM-sugar ATPS). The systems were prepared by dissolving GM (LBG, TG, GG and FG), NaCAS and sugar (commercially available sucrose, trehalose, D-glucose and D-fructose) in a citrate buffer (pH 5.8) with potassium sorbate as a preservative. The investigated systems have been named Systems 1-4, depending on the GM they contain. The work has been performed, to better understand these systems, by focusing on the following objectives:

- (i) determine the phase equilibria at the temperature of 20°C;
- (ii) evaluate the microstructure and flow behaviour of these systems in the shear rate range of 0-1000-0 s<sup>-1</sup> and various temperatures; and
- (iii) calculate the interfacial properties of these systems at room temperature.

### 7.1 Phase equilibria

The phase volume-ratio method by Polyakov et al. (1980) was used to draw phase diagrams, by which the miscibility of the systems was determined for every investigated system. Low compatibility and asymmetry of the phase diagrams is observed for all systems. The results of this study show that the solvent quality, altered by added sugar, plays a role in the phase separation—caused largely by the thermodynamic incompatibility between NaCAS and GM.

The study shows a good correlation between the measured interfacial tensions of the systems that differ by GM type, sugar type and sugar concentration, on one hand, and the established phase diagrams of these systems, on the other hand. It was found that:

- a GM with the lowest M:G ratio and the highest  $M_w$  (i.e., FG, M:G  $\approx$  1) increases the cosolubility of the systems more than GMs of higher M:G ratios and lower  $M_w$  (i.e., GG < TG < LBG, M:G  $\approx$  2, 3 4, respectively).
- Depending on the sugar type—by comparing 32 NaCAS-GM-sugar ATPS, half of which contained 15% sugar and the other half 30% sugar—the systems are classified: (i) at 15 wt% sugar, glucose < sucrose < trehalose < fructose, and (ii) at 30 wt%, trehalose  $\approx$  sucrose < fructose  $\approx$  glucose. The second classification is done with a lower confidence (shown by  $\approx$ ) due to greater inconsistencies among the data belonging to the different systems.
- The results show that < 40% sucrose/< 30% of other sugars—30% is the highest investigated concentration for sugars other than sucrose—improves the cosolubility of the systems, and that >50% sucrose decreases the cosolubility of the systems, possibly to less than that observed for the reference systems, without sugar. Above 50% sugar, a stable foam formation increased the experimental uncertainty, the binodals—deduced for NaCAS-LBG and NaCAS-GG systems—should not be taken at their face value. The impact of the increased sugar concentration on the cosolubility of the components is also reflected in the changes of the STL, which correspond to the changes in partitioning/fractionation of the components between the top and bottom phases, i.e., GM-r phase, on one hand, is diluted and NaCAS-r phase is concentrated on the biopolymers.

## 7.2 Microstructure and rheological behaviour

Gemini HR Nano and Gemini Rotonetic rheometers with cone and plate (steel, 40 mm diameter, 4° truncation, 150  $\mu\text{m}$  gap) and plate and plate geometry (glass, 40 mm diameter, 300  $\mu\text{m}$  gap) were used to measure viscosities of Systems 1-4 and visualise their microstructure under flow, respectively.

The data show that:

- At static conditions, low shears and sufficient concentrations of the macromolecular components, the microstructure of ATPS was emulsion-like. Three distinct microstructures (protein-continuous, bi-continuous and polysaccharide-continuous systems) were observed. Bi-continuous systems existed over a wide range of volume fractions (i.e.,  $25 \text{ wt}\% < \varphi_{GM} < 75 \text{ wt}\%$ ).
- Under shear a close link between composition, microstructure and flow behaviour was confirmed. The microstructure and related flow behaviour of the investigated systems differed by: (i) the volume fractions of the dispersed and continuous phases ( $\varphi_d, \varphi_c$ ), (ii) the viscosity of the dispersed and continuous phases ( $\eta_d, \eta_c$ ), the viscosity ratio ( $\lambda$ ), and (iii) other factors, which in turn altered the latter parameters; for example, shear, composition (biopolymer concentration, sugar concentration, sugar type and galactomannan type) and temperature. While sugar type and temperature did not significantly affect the flow behaviour of the systems, a high sugar concentration notably increased the overall viscosity of the equilibrium phases and enhanced the non-Newtonian behaviour of the model systems. At the critical shear rate ( $\sim 100 \text{ s}^{-1}$ ), galactomannan-continuous systems at  $< 20 \text{ wt}\%$  sugar

phase inverted. The event was facilitated by a favourable viscosity ratio between the coexisting phases. The galactomannan-continuous systems at >20 wt% sugar and protein-continuous systems at any sugar concentration, behaved similarly to pure NaCAS and GM aqueous solutions. In the latter two systems, the formations of either thread-like structures or non-interacting droplets in flow are observed. The existence and absence of the phase inversion event were confirmed by the rheoptical observation.

- Viscoelasticity of the Air-NaCAS and GG-NaCAS interfaces  $\leq$  15% sugar differs from that at 50% sugar. Higher differences between average values of  $G'$  and  $G''$  are observed in both interfaces. Furthermore,  $G''$  dominates over  $G'$  in Air-NaCAS-50% sugar interfaces.

### 7.3 Interfacial properties

The interfacial tensions of the systems were measured with a modified droplet retraction method by Guido et al. (1999a). A setup of a light microscope and a Gemini Rotonetic rheometer with a glass plate and plate geometry (40 mm diameter) were used in the experimental investigation of flow-induced droplet deformation and consequent droplet retraction. Systems of different total biopolymer concentration, sugar/sucrose concentration, sugar type (sucrose, trehalose, glucose and fructose) and GM type (LBG and FG) instigated the changes in the cosolubility of these systems, which in turn lead to the changes in droplet size, viscosity ratio, droplet retraction and interfacial tensions of these systems.

The interfacial tensions were—depending on the system and a shear viscosity

used to calculate them—in the range of  $1.4 \pm 0.4$  to  $3.769 \pm 1.402$   $\mu\text{N}/\text{m}$  (for viscosity at  $0.001 \text{ s}^{-1}$ ) and  $6.3 \pm 1.8$  to  $1.073.543 \pm 399.305$   $\mu\text{N}/\text{m}$  (for viscosity at  $0.5 \text{ s}^{-1}$ ). The comparison of the data revealed the following relationships between the investigated systems:

- The interfacial tensions for System 1 at constant GM concentration showed a power law increase with increasing NaCAS concentration. On the contrary, a decrease in the galactomannan concentration at the constant protein concentration decreased the interfacial tension.
- The interfacial tensions of System 1 compared at various amounts of sugar/sucrose are classified as follows:  $30\% < 5\% < 20\% < 15\% < 0\%$ .
- The interfacial tensions of the systems compared for sugar type, at 15% sugar concentration, are classified as follows: trehalose  $<$  fructose  $<$  glucose  $<$  sucrose.
- As for the GM type, the interfacial tensions followed the following trend:  $\text{FG} < \text{GG} \ll \text{TG} < \text{LBG}$ .
- Comparison of Systems 1 and 4 with trehalose showed that the interfacial tension of System 1 at 15% trehalose is lower than that of System 4 at 15% trehalose.

The calculated interfacial tensions show a power law relationship with parameters, such as: the tie-line length (TLL) and compositions of the equilibrium phases ( $\Delta[\text{NaCAS}]$  and  $\Delta[\text{GM}]$ ). The power law exponent  $b$  consistently described dependency of the investigated parameters with the interfacial tension, but power law constant  $a$  differed among the investigated parameters.

## 7.4 Future work

Based on the findings from this research, some further work could be undertaken.

- In this research, the approach by Polyakov et al. (1980) and Guido et al. (1999a) was used to compare the effects of common sugars (i.e., sucrose, trehalose, glucose and fructose, and of their concentrations) on the cosolubility of the biopolymers (i.e., proteins and polysaccharides) and the interfacial properties in the ATPS. There is, however, need for additional systematic fundamental studies on the effects of other sugars of industrial relevance—such as sugar alcohols (a popular replacement of the cariogenic sugars studied here)—on protein-polysaccharide aqueous systems. A similar comparative study based on the structural characteristics of these sugars could also be performed. For example, the effects of sugar alcohols such as, erythritol (4-carbon), xylitol (5-carbon), sorbitol (6-carbon), and maltitol (12-carbon), could be compared for their effects on the solvent and ATPS. A comparison with the results of the current study could be made. The latter cosolutes were researched within a different context and for gelling ATPS by Tsoga et al. (2004a; 2004b).
- Since the execution of the phase-volume-ratio method is labour intensive, and at higher sugar concentrations inaccurate, it would be interesting to assess its accuracy by either (i) a chemical experimental technique where the compositions of the equilibrium phases (i.e., binodal points) are obtained, for example, by spectrophotometric determination, or (ii) theoretically by modelling, i.e., thermodynamic approach. In addition, Hansen's approach to the molecular solubility could be applied to the investigations to see how well the experimental and

theoretical data match (Hanson, 2007).

- This research addressed the effect of sugars on the cosolubility of NaCAS and GM cumulatively. To improve understanding of the underlying molecular mechanisms between the individual sugars and individual macromolecular species (i.e., GMs), light scattering and rheological studies (e.g., determination of the intrinsic viscosities) could be performed.
- Apart from the need for more fundamental research, the future task will be also to handle more complex systems used in technical applications, such as biphasic systems with a gelling component (e.g.,  $\kappa$ -carrageenan and  $\iota$ -carrageenan), ternary systems with a gelling polysaccharides, and, eventually, real food formulations. Understanding of the phase equilibria compositions and interfacial tension in such systems is important for predicting the flow-induced morphologies, stability of the systems, and to improve a design of extraction equipment used in food manufacture. Mechanical interactions between the components could be assessed by mathematical models, such as Palierne model (1990), fitted to the rheological data under oscillatory flow. A prediction of the smallest size and average size of droplets in the mixture could also be made based on the interfacial tensions and with the help of the model.
- The results of this research could be analysed further; the experimental phase inversion compositions of the investigated systems (determined by optical investigation) could be compared with the phase inversion compositions obtained by models (e.g., the model by Utracki, 1991, Wolf and Firth, 2003).
- Finally, based on the work performed by Scholten et al. (2004a, 2005), the effects of the composition and temperature on the interfacial permeability and interfacial thickness of ATPS could also be studied.

## CHAPTER 8: REFERENCES

1. Aarts DGAL, Dullens RPA, Lekkerkerker HNW (2005) Interfacial dynamics in demixing systems with ultralow interfacial tension. *New Journal of Physics* 7(1), 40:1-12
2. Albertsson P, Frick G (1960) Partition of virus particles in a liquid two-phase system. *Biochimica et Biophysica Acta* 37:230-237
3. Antipova AS, Semenova MG (1995) Effect of sucrose on the thermodynamic incompatibility of different biopolymers. *Carbohydrate Polymers* 28:359-365
4. Antipova AS, Semenova MG (1997a) Effect of neutral carbohydrate structure in the set glucose/sucrose/maltodextrin/dextran on protein surface activity at the air/water interface. *Food Hydrocolloids* 11:71-77
5. Antipova AS, Semenova MG (1997b) Influence of sucrose on the thermodynamic properties of the 11S globulin of *Vicia faba*-dextran-aqueous solvent system. *Food Hydrocolloids* 11:415-421
6. Antipova AS, Semenova MG, Belyakova LE (1999) The effect of sucrose on the thermodynamic properties of ovalbumin and sodium caseinate in bulk solution and at air-water interface. *Colloids and Surfaces B: Biointerfaces* 12:261-270
7. Antonov YA, Grinberg VY, Zhuravskaya NA, Tolstoguzov VB (1980) Liquid two-phase water-protein-polysaccharide systems and their processing into textured protein products. *Journal of Texture Studies* 11:199-215
8. Antonov YA, Van Puyvelde P, Moldenaers P Flow-induced phase behaviour and structure development in aqueous emulsion of associative biopolymers. *Food Hydrocolloids*
9. Antonov YA, Van Puyvelde P, Moldenaers P (2004) Interfacial tension of aqueous biopolymer mixtures close to the critical point. *International Journal of Biological Macromolecules* 34:29-35
10. Antonov YA, Van Puyvelde P, Moldenaers P (2009) Solvent quality as a key factor for shear-induced mixing in biopolymer emulsions. *Food Hydrocolloids* 23:262-270
11. Antonov YA, Van Puyvelde P, Moldenaers P, Leuven KU (2003) Effect of shear flow on the phase behavior of an aqueous gelatin/dextran emulsion. *Biomacromolecules* 5:276-283
12. Antonov Y, Grinberg VY, Tolstoguzov VB (1977) Phase equilibria in water-protein-polysaccharide systems. *Colloid and Polymer Science* 255:937-947

13. Antonov Y, Grinberg VY, Zhuravskaya NA, Tolstoguzov VB (1982) Concentration of the proteins of skimmed milk by membraneless, isobaric osmosis. *Carbohydrate Polymers* 2:81-90
14. Bamberger S, Seaman GVF, Sharp KA, Brooks DE (1984) The effects of salts on the interfacial tension of aqueous dextran poly(ethylene glycol) phase systems. *Journal of Colloid and Interface Science* 99:194-200
15. Beijerink MW (1910) The formation of an emulsion by mixing solutions of some gell forming colloids. *Kolloid Zeitschrift* 7:16-20
16. Belyakova LE, Antipova AS, Semenova MG, Dickinson E, Matia Merino L, Tsapkina EN (2003) Effect of sucrose on molecular and interaction parameters of sodium caseinate in aqueous solution: relationship to protein gelation. *Colloids and Surfaces B: Biointerfaces* 31:31-46
17. BeMiller J, Whistler L (1996) Carbohydrates. In: Fennema OD (ed) *Food chemistry*, 3<sup>rd</sup> edn. Marcel Dekker, New York, pp 207-208
18. Bourriot S, Garnier C, Doublier JL (1999) Phase separation, rheology and structure of micellar casein-galactomannan mixtures. *International Dairy Journal* 9:353-357
19. Brown C, Foster TJ, Norton IT, Underdown J (1995) Influence of shear on the microstructure of mixed biopolymer systems. In: Harding SE and Mitchell JR (eds) *Biopolymer Mixtures*. University Press, Nottingham, pp 65-83
20. Brummer Y, Cui W, Wang Q (2003) Extraction, purification and physicochemical characterization of fenugreek gum. *Food Hydrocolloids* 17:229-236
21. Capron I, Costeux SP, Djabourov M (2001). Water in water emulsions: phase separation and rheology of biopolymer solutions. *Rheologica Acta*, 40:441-456
22. Caserta S, Sabetta L, Simeone M, Guido S (2005) Shear-induced coalescence in aqueous biopolymer mixtures. *Chemical Engineering Science* 60:1019-1027
23. Çengel YA, Boles MA (2007) *Thermodynamics: An engineering approach* 6<sup>th</sup> edn. (SI units). McGraw Hill, London
24. Clark AH (2006) Mixed biopolymer gelation: a route to versatile soft solids and complex gel microstructure. In: *Gums and stabilisers for the food industry* 13. The Royal Society of Chemistry Publishing, Cambridge, pp 170-184
25. de Hoog EHA, Lekkerkerker HNW (1999) Measurement of the interfacial tension of a phase-separated colloid/polymer suspension. *The Journal of Physical Chemistry B* 103:5274-5279

26. de Kruif CG, Tuinier R (2000) Casein micelles and their interaction with exopolysaccharides; turbidity and viscosity. In: Williams PA and Phyllips GO (eds) *Gums and stabilisers for the food industry* 10. The Royal Society of Chemistry Publishing, Cambridge, pp 196-202
27. Dea ICM, Clark AH, McCleary BV (1986a) Effect of galactose-substitution-patterns on the interaction properties of galactomannans. *Carbohydrate Research* 147:275-294
28. Dea ICM, Clark AH, McCleary BV (1986b) Effect of the molecular fine structure of galactomannans on their interaction properties-the role of unsubstituted sides. *Food Hydrocolloids* 1:129-140
29. Dickinson E, Woskett CM (1988) Effect of alcohol on adsorption of casein at the oil-water interface. *Food Hydrocolloids* 2:187-194
30. Dickinson E (1982) Thermodynamic aspects of emulsion phase inversion. *Journal of Colloid and Interface Science* 87:416-423
31. Dickinson E (2008) Interfacial structure and stability of food emulsions as affected by protein-polysaccharide interactions. *Soft Matter* 4:932-942
32. Dickinson E (2010) Mixed biopolymers at interfaces: Competitive adsorption and multilayer structures. *Food Hydrocolloids* In Press, Corrected Proof
33. Dickinson E, Casanova H (1999) A thermoreversible emulsion gel based on sodium caseinate, *Food Hydrocolloids*, 13 (4):285-289
34. Ding P, Pacek AW, Frith WJ, Norton IT, Wolf B (2005) The effect of temperature and composition on the interfacial tension and rheology of separated phases in gelatin/pullulan mixtures. *Food Hydrocolloids* 19:567-574
35. Ding P, Wolf B, Frith WJ, Clark AH, Norton IT, Pacek AW (2002) Interfacial tension in phase-separated gelatin/dextran aqueous mixtures. *Journal of Colloid and Interface Science* 253:367-376
36. Doyle JP, Giannouli P, Martin EJ, Brooks M, Morris ER (2006) Effect of sugars, galactose content and chainlength on freeze-thaw gelation of galactomannans. *Carbohydrate Polymers* 64:391-401
37. Doyle JP, Lyons G, Morris ER (2009) New proposals on "hyperentanglement" of galactomannans: Solution viscosity of fenugreek gum under neutral and alkaline conditions. *Food Hydrocolloids* 23:1501-1510
38. Efthimiadu I, Moore IPT (1994) Phase inversion of liquid-liquid dispersions produced between parallel shearing plates. *Chemical Engineering Science* 49:1439-1449

39. Fang Y, Li L, Inoue C, Lundin L, Appelqvist I (2006) Associative and segregative phase separations of gelatin/ $\kappa$ -carrageenan aqueous mixtures. *Langmuir* 22:9532-9537
40. Flory PJ (1953) Principles of polymer chemistry. Cornell University Press, Ithaca and London
41. Forciniti D, Hall CK, Kula MR (1990) Interfacial tension of polyethyleneglycol-dextran-water systems: influence of temperature and polymer molecular weight. *Journal of Biotechnology* 16:279-296
42. Foster T, Brown C, Norton I (1996) Phase inversion of water-in-water emulsions. In: Gums and stabilisers for the food industry. Oxford University Press., pp 297-309
43. Foster TJ, Underdown J, Brown CRT, Ferdinando DP, Norton IT (1997) Emulsion behaviour of non-gelled biopolymer mixtures. In: Dickinson E and Bergenstal B (eds) Food colloids: Proteins, lipids and polysaccharides. The Royal Society of Chemistry Publishing, Cambridge, p 346
44. Frith WJ (2010) Mixed biopolymer aqueous solutions-phase behaviour and rheology. *Advances in Colloid and Interface Science* 161:48-60
45. Galema SA, Hoeiland H (1991) Stereochemical aspects of hydration of carbohydrates in aqueous solutions. 3. Density and ultrasound measurements. *The Journal of Physical Chemistry* 199195 (13), 5321-5326
46. German ML, Blumenfeld AL, Yuryev VP, Tolstoguzov VB (1989) An NMR study of structure formation in maltodextrin systems. *Carbohydrate Polymers* 11:139-146
47. Goff HD, Ferdinando D, Schorsch C (1999) Fluorescence microscopy to study galactomannan structure in frozen sucrose and milk protein solutions. *Food Hydrocolloids* 13:353-362
48. Granger C, Leger A, Barey P, Langendorff V, Cansell M (2005) Influence of formulation on the structural networks in ice cream. *International Dairy Journal* 15:255-262
49. Guido S, Villone M (1998) Three-dimensional shape of a drop under simple shear flow. *Journal of Rheology* 42:395-416
50. Guido S, Greco F, Villone M (1999a) Experimental determination of drop shape in slow steady shear flow. *Journal of Colloid and Interface Science* 219:298-309
51. Guido S, Simeone M, Alfani A (2002) Interfacial tension of aqueous mixtures of Na-caseinate and Na-alginate by drop deformation in shear flow. *Carbohydrate Polymers* 48:143-152

52. Guido S, Simeone M, Villone M (1999b) Diffusion effects on the interfacial tension of immiscible polymer blends. *Rheologica Acta* 38:287-296
53. Guido S, Villone M (1999) Measurement of interfacial tension by drop retraction analysis. *Journal of Colloid and Interface Science* 209:247-250
54. Goff HD (2002) Formation and stabilisation of structure in ice-cream and related products, *Current Opinion in Colloid & Interface Science*, 7, (5-6):432-437
55. Hansen C M (2007) *Hansen Solubility Parameters: A User's Handbook*, Second Edition, CRC Press
56. Higashiyama T (2002) Novel functions and applications of trehalose. *Pure Applied Chemistry* 74:1263-1269
57. Holdsworth SD (1993) Rheological models used for the prediction of the flow properties of food products: a literature review. In: *Food and bioproducts processing: Transactions of the institution of chemical engineers, Part C*. Institution of Chemical Engineers, pp 139-179
58. Holmberg K (2001) *Handbook of Applied Surface and Colloid Chemistry*, Volumes 1-2. John Wiley and Sons
59. Hoskins R, Robb ID, Williams PA, Warren P (1996) Phase separation in mixtures of polysaccharides and proteins. *Journal of the Chemical Society, Faraday Transactions* 92:4515-4520
60. Hsu CC, Prausnitz JM (1974) Thermodynamics of polymer compatibility in ternary systems. *Macromolecules* 7:320-324
61. Jenkins P, Snowden M (1996) Depletion flocculation in colloidal dispersions. *Advances in Colloid and Interface Science* 68:57-96
62. Jeon HS, Hobbie EK (2001a) Shear viscosity of phase-separating polymer blends with viscous asymmetry. *Physical Review E* 63:061403
63. Jeon HS, Hobbie EK (2001b) Shear viscosity of phase-separating polymer blends with viscous asymmetry. *Physical Review E* 63:061403-1-061403-5
64. Jeon HS, Nakatani AI, Hobbie EK, Han CC (2001) Phase inversion of polybutadiene/polyisoprene blends under quiescent and shear conditions. *Langmuir* 17:3087-3095
65. Jourdain L, Leser ME, Schmitt C, Michel M, Dickinson E (2008) Stability of emulsions containing sodium caseinate and dextran sulfate: Relationship to complexation in solution. *Food Hydrocolloids* 22:647-659

66. Kasapis S, Al-Marhoobi MA (2000) Glass transitions in high sugar biopolymer mixtures-some recent developments. In: Williams PA and Phillips GO (eds) *Gums and stabilisers for the food industry* 10. The Royal Society of Chemistry Publishing, Cambridge, UK, pp 303-312
67. Kasapis S, Al-Marhoobi IMA, Khan AJ (2000) Viscous solutions, networks and the glass transition in high sugar galactomannan and  $\kappa$ -carrageenan mixtures. *International Journal of Biological Macromolecules* 27:13-20
68. Kaushik J, Bhat R (2003) Why is trehalose an exceptional protein stabilizer? An analysis of the thermal stability of proteins in the presence of the compatible osmolyte trehalose. *Journal of Biological Chemistry* 278:26458-26465
69. Kim DY, Shin WS, Hong WS (2010) The unique behaviors of biopolymers, BSA and fucoidan, in a model emulsion system under different pH circumstances. *Macromolecular Research* 18:1103-1108
70. Kiselev MA, Wartewig S, Janich M, Lesieur P, Kiselev AM, Ollivon M, Neubert R (2003) Does sucrose influence the properties of DMPC vesicles? *Chemistry and Physics of Lipids* 123:31-44
71. Kök MS, Hill SE, Mitchell JR (1999) Viscosity of galactomannans during high temperature processing: influence of degradation and solubilisation. *Food Hydrocolloids* 13:535-542
72. Koningsveld R, Stockmayer WH, Nies E (2001) *Polymer phase diagrams-A textbook*. Oxford university press, Oxford
73. Koningsveld R, Staverman AJ (1968) Liquid-liquid phase separation in multicomponent polymer solutions. I. Statement of the problem and description of methods of calculation. *Journal of Polymer Science A-2 Polymer Physics* 6:305-323
74. Lorén N (2001) *Structure evolution during phase separation and gelation of biopolymer mixtures*. Göteborg, Sweden, Department of Food Science, Chalmers University of Technology. Ref Type: Thesis/Dissertation
75. Lucey JA, Srinivasan M, Singh H, Munro PA (2000) Characterization of commercial and experimental sodium caseinates by multiangle laser light scattering and size-exclusion chromatography. *Journal of Agricultural and Food Chemistry* 48:1610-1616
76. Magazù S, Branca C, Migliardo F, Romeo G, Mangione A (2004) Scattering findings on disaccharide/water mixtures. *Journal of Molecular Structure* 700:211-215
77. McClements DJ (2000) Comments on viscosity enhancement and depletion flocculation by polysaccharides. *Food Hydrocolloids* 14:173-177

78. Miquelim JN, Lannes SCS, Mezzenga R (2010) pH Influence on the stability of foams with protein-polysaccharide complexes at their interfaces. *Food Hydrocolloids* 24:398-405
79. Mandala I, Karabela I, Kostaropoulos A (2007) Physical properties of breads containing hydrocolloids stored at low temperature I. Effect of chilling. *Food Hydrocolloids*, 21:1397–1406
80. Morris ER, Cutler AN, Ross-Murphy SB, Rees DA, Price J (1981) Concentration and shear rate dependence of viscosity in random coil polysaccharide solutions. *Carbohydrate Polymers* 1:5-21
81. Mulvihill DM, Murphy PC (1991) Surface active and emulsifying properties of caseins/caseinates as influenced by state of aggregation. *International Dairy Journal* 1:13-37
82. Nan YQ, Liu HL, Hu Y (2006) Interfacial tension in phase-separated aqueous cationic/anionic surfactant mixtures. *Journal of Colloid and Interface Science* 293:464-474
83. Nash W, Pinder DN, Hemar Y, Singh H (2002) Dynamic light scattering investigation of sodium caseinate and xanthan mixtures. *International Journal of Biological Macromolecules* 30:269-271
84. Nikam PS, Ansari HR, Hasan M (2000) Acoustical properties of fructose and maltose solutions in water and in aqueous 0.5 M NH<sub>4</sub>Cl. *Journal of Molecular Liquids* 84:169-178
85. Nicol WM (1979) Sucrose and food technology. In: Birch GG and Parker KJ (eds) *Sugar, Science and Technology*. Applied Science Publishers, London, UK, pp 211-230
86. Norton IT, Frith WJ (2001) Microstructure design in mixed biopolymer composites. *Food Hydrocolloids* 15:543-553
87. Okada, K., Miyake, T, and hibuya, T. High Trehalose content syrup. (5916881). 6-4-1999. US patent. Ref Type: Patent
88. Palierne JF (1990) Linear rheology of viscoelastic emulsions with interfacial tension. *Rheologica Acta* 29:204-214
89. Pacek AW, Ding P, Nienow AW (2001) The effect of volume fraction and impeller speed on the structure and drop size in aqueous/aqueous dispersions. *Chemical Engineering Science* 56:3247-3255
90. Pacek AW, Moore IPT, Nienow AW, Calabrese RV (1994a) Video technique for measuring dynamics of liquid-liquid dispersion during phase inversion. *AIChE Journal* 40:1940-1949

91. Pacek AW, Nienow AW, Moore IPT (1994b) On the structure of turbulent liquid-liquid dispersed flows in an agitated vessel. *Chemical Engineering Science* 49:3485-3498
92. Perrechil FA, Cunha RL (2011) Development of multiple emulsions based on the repulsive interaction between sodium caseinate and LBG. *Food Hydrocolloids* In Press, Corrected Proof
93. Petkowicz CLO, Reicher F, Mazeau K (1998) Conformational analysis of galactomannans: from oligomeric segments to polymeric chains. *Carbohydrate Polymers* 37:25-39
94. Piculell L, Lindman Br (1992) Association and segregation in aqueous polymer/polymer, polymer/surfactant, and surfactant/surfactant mixtures: similarities and differences. *Advances in Colloid and Interface Science* 41:149-178
95. Pitkowski A, Durand D, Nicolai T (2008) Structure and dynamical mechanical properties of suspensions of sodium caseinate. *Journal of Colloid and Interface Science* 326:96-102
96. Polyakov VI, Grinberg VY, Tolstoguzov VB (1980) Application of phase-volume-ratio method for determining the phase diagram of water-casein-soybean globulins system. *Polymer Bulletin* 2:757-760
97. Polyakov VI, Kireyeva OK, Grinberg VY, Tolstoguzov VB (1985a) Thermodynamic compatibility of proteins in aqueous media. Part. I. Phase diagrams of some water-protein A -protein B systems. *Nahrung* 29:153-160
98. Polyakov VI, Popello IA, Grinberg VY, Tolstoguzov VB (1985b) Thermodynamic compatibility of proteins in aqueous media. Part 2. The effect of some physicochemical factors on thermodynamic compatibility of casein and soybean globulin fraction. *Nahrung* 29:323-333
99. Polyakov VI, Popello IA, Grinberg VY, Tolstoguzov VB (1986) Thermodynamic compatibility of proteins in aqueous medium. *Nahrung* 30:365-368
100. Portschi A (2007) Designing the structure of the water-matrix phase in ice-cream. The University of Birmingham, School of Engineering, Department of Chemical Engineering. Ref Type: Thesis/Dissertation
101. Ptaszek P, Lukasiewicz M, Achremowicz B, Grzesik M (2007) Interaction of hydrocolloid networks with mono- and oligosaccharides. *Polymer Bulletin* 58:295-303
102. Raza K, Harding JJ (1991) Non-enzymic modification of lens proteins by glucose and fructose: Effects of ibuprofen. *Experimental Eye Research* 52:205-212

103. Richardson PH, Norton IT (1998) Gelation behavior of concentrated locust bean gum solutions. *Macromolecules* 31:1575-1583
104. Richardson PH, Willmer J, Foster TJ (1998) Dilute solution properties of guar and locust bean gum in sucrose solutions. *Food Hydrocolloids* 12:339-348
105. Rivas G, Ferrone F, Herzfeld J (2004) Life in a crowded world. *EMBO Rep* 5:23-27
106. Rodríguez Patino JM, Pilosof AMR (2011) Protein-polysaccharide interactions at fluid interfaces. *Food Hydrocolloids* 25:1925-1937
107. Sakane Y, Inomata K, Morita H, Kawakatsu T, Doi M, Nose T (2001) Effects of low-molecular-weight additives on interfacial tension of polymer blends: experiments for poly (dimethylsiloxane) / poly (tetramethyldisiloxanyethylene) + oligo (dimethylsiloxane), and comparison with mean-field calculations. *Polymer* 42:3883-3891
108. Savaroglu G, Ozdemir M (2008) Apparent molar volume and apparent molar isentropic compressibility of glycerol in fructose-water at different temperatures. *Journal of Molecular Liquids* 137:51-57
109. Scholten E, Sagis LMC, van der Linden E (2004) Bending rigidity of interfaces in aqueous phase-separated biopolymer mixtures. *The Journal of Physical Chemistry B* 108:12164-12169
110. Scholten E, Sagis LMC, van der Linden E (2006a) Effect of permeability on aqueous biopolymer interfaces in spinning drop experiments. *Biomacromolecules* 7:2224-2229
111. Scholten E, Sagis LMC, van der Linden E (2006b) Effect of bending rigidity and interfacial permeability on the dynamical behavior of water-in-water emulsions. *The Journal of Physical Chemistry B* 110:3250-3256
112. Scholten E, Sprakel J, Sagis LMC, van der Linden E (2005) Effect of interfacial permeability on droplet relaxation in biopolymer-based water-in-water emulsions. *Biomacromolecules* 7:339-346
113. Schorsch C, Clark AH, Jones MG, Norton IT (1999a) Behaviour of milk protein/polysaccharide systems in high sucrose. *Colloids and Surfaces B: Biointerfaces* 12:317-329
114. Schorsch C, Jones MG, Norton IT (1999b) Thermodynamic incompatibility and microstructure of milk protein/locust bean gum/sucrose systems. *Food Hydrocolloids* 13:89-99
115. Schorsch C, Jones MG, Norton IT (2000a) Effect of sucrose on milk protein, LBG and their interactions. In: Williams, P. A. and Phyllips, G. O (eds) *Gums and stabilisers for the food industry* 10. The Royal Society of Chemistry, Cambridge, pp 292-302

116. Schorsch C, Jones MG, Norton IT (2000b) Phase behaviour of pure micellar casein/ $\kappa$ -carrageenan systems in milk salt ultrafiltrate. *Food Hydrocolloids* 14:347-358
117. Semenova M, Dickinson E (2010) *Biopolymers in Food Colloids: Thermodynamics and Molecular Interactions*. Brill, Leiden, Boston
118. Semenova MG (2007a) Thermodynamic analysis of the impact of molecular interactions on the functionality of food biopolymers in solution and in colloidal systems. *Food Hydrocolloids* 21:23-45
119. Semenova MG (2007b) Thermodynamic analysis of the impact of molecular interactions on the functionality of food biopolymers in solution and in colloidal systems. *Food Hydrocolloids* 21:23-45
120. Semenova MG, Antipova AS, Belyakova LE (2002) Food protein interactions in sugar solutions. *Current Opinion in Colloid and Interface Science* 7:438-444
121. Shi T, Ziegler VE, Welge IC, An L, Wolf BA (2004) Evolution of the interfacial tension between polydisperse immiscible polymers in the absence and in the presence of a compatibilizer. *Macromolecules* 37:1591-1599
122. Sigillo I, Di Santo L, Guido S, and Grizzutti N. (1997) Comparative measurements of the interfacial tension in a model biopolymer blend. *Polymer Engineering and Science* 37, 1540-1549. 1997. Ref Type: Patent
123. Simeone M, Alfani A, Guido S (2004) Phase diagram, rheology and interfacial tension of aqueous mixtures of Na-caseinate and Na-alginate. *Food Hydrocolloids* 18:463-470
124. Son Y, Migler KB (2002) Interfacial tension measurement between immiscible polymers: improved deformed drop retraction method. *Polymer* 43:3001-3006
125. Spyropoulos F (2006) *Biopolymer-surfactant aqueous two phase systems: equilibria, rheology and interfacial properties*. Birmingham, Department of Chemical Engineering, The University of Birmingham. Ref Type: Thesis/Dissertation
126. Spyropoulos F, Ding P, Frith WJ, Norton IT, Wolf B, Pacek AW (2008a) Interfacial tension in aqueous biopolymer-surfactant mixtures. *Journal of Colloid and Interface Science* 317:604-610
127. Spyropoulos F, Frith WJ, Norton IT, Wolf B, Pacek AW (2008b) Sheared aqueous two-phase biopolymer-surfactant mixtures. *Food Hydrocolloids* 22:121-129
128. Spyropoulos F, Portscht A, Norton IT (2010) Effect of sucrose on the phase and flow behaviour of polysaccharide/protein aqueous two-phase systems. *Food Hydrocolloids* 24:217-226

129. Srivastava M, Kapoor V (2005) Seed Galactomannans: An Overview. *Chemistry and Biodiversity* 2:295-317
130. Stokes JR, Wolf B, Frith WJ (2001) Phase-separated biopolymer mixture rheology: Prediction using a viscoelastic emulsion model volume. *Journal of Rheology* 45:1173-1191
131. Taylor GI (1934) The formation of emulsions in definable fields of flow. *Proceedings of the Royal Society of London Series A* 146:501-523
132. Tolstoguzov VB (1988) Concentration and purification of proteins by means of two-phase systems: membraneless osmosis process. *Food Hydrocolloids* 2:195-207
133. Tolstoguzov VB (1991) Functional properties of food macromolecules. In: Phillips, GO, Wedlock DY and Williams PA (eds) *Gums and stabilisers for the food industry* 6. Oxford: IBL Press, pp 241-266
134. Tolstoguzov VB (1998) Functional properties of protein-polysaccharide mixtures. In: Hill SE, Ledward DA and Mitchel JR (eds) *Functional properties of food molecules*. Aspen Publishing, Gaithersburg, pp 252-277
135. Tolstoguzov V (1996) Protein functionality in food systems (IFT basic symposium series 9). *Trends in Food Science and Technology* 7:31-32
136. Tolstoguzov V (1999) Compositions and phase diagrams for aqueous systems based on proteins and polysaccharides. In: Walter H, Donald E and Brooks P (eds) *International Review of Cytology: Microcompartmentation and Phase Separation in Cytoplasm*, Volume 192 edn. Academic Press, pp 3-31
137. Tolstoguzov V (2002) Thermodynamic aspects of biopolymer functionality in biological systems, Foods, and Beverages. *Critical Reviews in Biotechnology* 22:89-174
138. Tolstoguzov V (2003) Some thermodynamic considerations in food formulation. *Food Hydrocolloids* 17:1-23
139. Tolstoguzov V (2006) Texturising by phase separation. *Biotechnology Advances* 24:626-628
140. Torza S, Cox RG, Mason SG (1972) Particle motions in sheared suspensions XXVII. Transient and steady deformation and burst of liquid drops. *Journal of Colloid and Interface Science* 38:395-411
141. Tromp HR, van de Velde F, van Riel J, Paques M (2001) Confocal scanning light microscopy (CSLM) on mixtures of gelatine and polysaccharides. *Food Research International* 34:931-938

142. Tromp RH, Rennie AR, Jones RAL (1995) Kinetics of the Simultaneous Phase Separation and Gelation in Solutions of Dextran and Gelatin. *Macromolecules* 28:4129-4138
143. Tromp RH, de Hoog EHA (2008) Band formation on shearing in phase-separated polymer solutions. *Physical Review Letters* E 77:031503
144. Tsoga A, Richardson RK, Morris ER (2004 a) Role of cosolutes in gelation of high-methoxy pectin. Part 1. Comparison of sugars and polyols, *Food Hydrocolloids*, 18 (6): 907-919
145. Tsoga A, Richardson RK, Morris ER (2004 b) Role of cosolutes in gelation of high-methoxy pectin. Part 2. Anomalous behaviour of fructose: calorimetric evidence of site-binding, *Food Hydrocolloids*, 18 (6), 921-932
146. Tuinier R, Rieger J, de Kruif CG (2003) Depletion-induced phase separation in colloid-polymer mixtures. *Advances in Colloid and Interface Science* 103:1-31
147. Turgeon SL, Laneuville SI (2009) Protein-polysaccharide coacervates and complexes: from scientific background to their application as functional ingredients in food products. In: Kasapis S, Norton IT, and Ubbink JB (eds) *Modern Biopolymer Science*. Academic Press, San Diego, pp 327-363
148. Utracki LA (1991) On the viscosity-concentration dependence of immiscible polymer mixtures. *Journal of Rheology* 35:1615-1637
149. van Heukelum A, Barkema GT, Edelman MW, van der Linden E, de Hoog EHA, Tromp RH (2003) Fractionation in a phase-separated polydisperse polymer mixture. *Macromolecules* 36:6662-6667
150. Van Puyvelde P, Antonov YA, Moldenaers P (2002) Rheo-optical measurement of the interfacial tension of aqueous biopolymer mixtures. *Food Hydrocolloids* 16:395-402
151. Vossoughi S (1999) Flow of non-newtonian fluids in porous media. In: Siginer DA (ed) *Rheology Series: Advances in the Flow and Rheology of Non-Newtonian Fluids*, Volume 8<sup>th</sup> edn. Elsevier, pp 1183-1235
152. Wang S, van Dijk JAPP, Odijk T, Smit JAM (2001) Depletion-induced demixing in aqueous protein-polysaccharide solutions. *Biomacromolecules* 2:1080-1088
153. Williams PA (2006) An overview of the structure-function relationships of hydrocolloids. In: Williams PA and Phillips OG (eds) *Gums and Stabilisers for the Food Industry* 13. RCS Publishing, pp 15-29
154. Wolf B, Frith WJ (2003) String phase formation in biopolymer aqueous solution blends. *Journal of Rheology* 47:1151-1170

155. Wolf B, Scirocco R, Frith WJ, Norton IT (2000) Shear-induced anisotropic microstructure in phase-separated biopolymer mixtures. *Food Hydrocolloids* 14:217-225
156. Wu Y, Cui W, Eskin NAM, Goff HD (2009) An investigation of four commercial galactomannans on their emulsion and rheological properties. *Food Research International* 42:1141-1146
157. Wu Y, Li W, Cui W, Eskin NAM, Goff HD A molecular modeling approach to understand conformation-functionality relationships of galactomannans with different mannose/galactose ratios. *Food Hydrocolloids* In Press, Corrected Proof
158. Yeo YL, Matar OK, Perez de Ortiz ES, Hewitt G (2000) Phase inversion and associated phenomena. *Multiphase Science and Technology* 12(1):51–116
159. Zaslavsky BY (1995) *Aqueous Two-Phase Partitioning: Physical Chemistry and Bioanalytical Applications*, 9<sup>th</sup> edn. Marcel Dekker, Inc., New York, Basel, Oxford
160. Zeman L, Patterson D (1972) Effect of the solvent on polymer incompatibility in solution. *Macromolecules* 5:513-516